Effect of hemin and baicalein on heme oxygenase-1 accumulation and function in *Xenopus laevis* cultured cells

by

James Campbell

A thesis

presented to the University of Waterloo

in fulfillment of the

thesis requirement for the degree of

Doctor of Philosophy

in

Biology

Waterloo, Ontario, Canada, 2018

Examining Committee Membership
The following served on the Examining Committee for this thesis. The decision of the Examining Committee is by majority vote.

External Examiner	Dr. Sashko Damjanovski Associate Professor University of Western Ontario Canada
Internal-external Member	Dr. Joe Quadrilatero Associate Professor
Supervisor	Dr. John J. Heikkila Professor
Internal Member	Dr. Brian Dixon Professor
Internal Member	Dr. Mungo Marsden Associate Professor

Author's Declaration

I hereby declare that I am the sole author of this thesis. This is a true copy of the thesis, including any required final revisions, as accepted by my examiners. I understand that my thesis may be made electronically available to the public

Abstract

Heme oxygenase-1 (HO-1) is a stress-inducible enzyme that catalyzes the rate-limiting step in the hemin degradation pathway. Studies in mammalian systems determined that HO-1 promoted cell survival by reducing oxidative damage in cells exposed to heavy metal toxicants. While most of the knowledge regarding HO-1 synthesis and function was derived from mammals, less is known about this stress-inducible protein in poikilothermic vertebrates such as amphibians and fish. The aim of the present study is to investigate stress-induced accumulation of HO-1 and its potential cytoprotective effects in A6 kidney epithelial cells derived from the aquatic frog, *Xenopus laevis*. Treatment of A6 cells with hemin, baicalein (a plant flavinoid) or $CdCl_2$ induced HO-1 accumulation in a concentration- and time-dependent manner. While $CdCl_2$ treatment also induced the accumulation of the heat shock proteins (HSPs), HSP70 and HSP30, their accumulation was not detectable in cells treated with baicalein or hemin. Immunocytochemical analysis revealed that hemin, baicalein and $CdCl_2$ treatment induced the accumulation of HO-1 primarily in the perinuclear region in a granular pattern with some localization in the nucleus. While treatment of cells with 25 μM hemin or 200 μM baicalein induced slight disorganization of actin filaments, exposure of cells to higher concentrations of $CdCl_2$ (e.g. 200 μM) produced pronounced actin cytoskeletal disorganization and membrane ruffling. Stress-induced accumulation of HO-1 was the result of *de novo* synthesis since upregulated HO-1 levels were inhibited by the transcriptional and translational inhibitors, actinomycin D and cycloheximide, respectively. Furthermore, the heat shock factor 1 (HSF1) inhibitor, KNK437, suppressed hemin-, baicalein-, and $CdCl_2$-induced HO-1 accumulation. Since previous studies reported that stress-induced HO-1 accumulation may be associated with oxidative stress, the levels of the ROS-responsive transcription factor, Nrf2, were measured and

found to increase in cells treated with baicalein and $CdCl_2$ but not with hemin. However, levels of the antioxidant enzyme, peroxiredoxin 5 (PRDX5), were elevated in response to all three stressors. Finally, analysis of reactive oxygen species (ROS) production using a fluorescent probe detected enhanced ROS amounts in A6 cells treated with baicalein and $CdCl_2$ but not with hemin. In another approach, A6 cells, which were incubated with buthionine sulfoximine (BSO), an inhibitor of glutathione synthesis and a known inducer of ROS, enhanced HO1 accumulation in cells treated with $CdCl_2$ but with either hemin or baicalein. This study also determined that HO-1 accumulation was required for cytoprotection of A6 cells to $CdCl_2$ since cotreatment with the HO-1 enzyme activity inhibitors, tin protoporphyrin (SnPP) and zinc protoporphyrin (ZnPP), enhanced cadmium-induced actin cytoskeleton dysregulation and the formation of aggregated protein and aggresome-like structures. Finally, this study examined whether treatment of A6 cells with hemin or baicalein could ameliorate the toxic effects of 275 μM of $CdCl_2$. Hemin and baicalein both inhibited the effect of cadmium on the dysregulation of actin cytoskeleton and the accumulation of aggregated protein and aggresome-like structures. Furthermore, this protective effect was suppressed with the addition of SnPP. In summary, this study has shown that HO-1 accumulation may play a vital role in regulating the stress response against cadmium treatment in *Xenopus laevis*. Additionally, the present research has revealed, for the first time, that cotreatment of cells with low concentrations of either hemin or baicalein inhibited the formation of cadmium-induced aggregated protein and aggresome-like structures whereas cotreatment with HO-1 enzyme activity inhibitors suppressed this phenomenon.

Acknowledgements

I'd like to thank my supervisor Dr. John Heikkila, for his help, support and patience, and to wish him luck in whatever he does. I would also like to thank my committee members Dr. Mungo Marsden and Brian Dixon. I am greatly indebted to Dr. Imran Khamis and Cody Shirriff for their friendship and their exceptional ability to endure my eccentricity. I also must express my appreciation for Dr. Justin Knapp, Dr. Marc Gibson, and my old supervisor Dr. Matthew Smith. Finally, thank you to my family - especially my father and my mother.

Table of Contents

List of Figures ix

List of Tables xii

List of Abbreviations xiii

1.0 Introduction 1
1.1 Heme oxygenase 1
1.2 Regulation of *ho-1* gene expression 2
1.3 Mechanisms of HO-1 mediated cytoprotection 6
1.4 Inducers of heme oxygenase accumulation 7
1.5 Hemin 9
1.6 Baicalein 10
1.7 Cadmium 11
1.8 Oxidative stress 12
1.9 Oxidative stress and unfolded proteins 14
1.10 Proteostasis 16
1.11 Heat shock proteins and the heat shock response 18
1.12 *Xenopus laevis* 19
1.12.1 Stress-induced HSP accumulation in *Xenopus* cultured cells 22
1.12.2 Stress-induced HO-1 accumulation in *X. laevis* 23
1.13 Hypothesis and objectives 24

2.0 Materials and methods 26
2.1 Chemicals 26
2.2 Culture of *Xenopus laevis* A6 kidney epithelial cells 26
2.3 Cell treatments 27
2.4 Protein isolation and quantification 28
2.5 SDS-PAGE and immunoblot analysis 28
2.6 Densitometry 29
2.7 Immunocytochemistry and laser scanning confocal microscopy (LSCM) 30
2.8 CellRox Green oxidative stress detection assay 31
2.9 Proteostat aggregation assay 32
2.10 Bioinformatic analysis 32

3.0 Results 34
3.1 Characterization of the heme oxygenase-1 (HO-1) amino acid sequence in *X. laevis* 34
3.2 Pattern of HO-1 accumulation in cells treated with hemin, baicalein or $CdCl_2$ exposure 38
3.3 Immunocytochemical analysis of HO-1 and HSP30 localization and actin and tubulin cytoskeletal structure in hemin-, baicalein- and $CdCl_2$-treated cells. 54
3.4. Effect of transcriptional and translational inhibitors on hemin- and baicalein-induced HO-1 accumulation. 71
3.5. Identification of Nrf2 and HSF1 transcription factor binding sites in the 5' regulatory region of the *X. laevis ho-1* gene 78
3.6 Effect of hemin, baicalein and $CdCl_2$ on Nrf-2 levels in A6 cells 78
3.7 Effect of an HSF1 inhibitor, KNK437, on hemin-, baicalein- and $CdCl_2$-induced HO-1 accumulation. 84
3.8 Effect of hemin, baicalein and $CdCl_2$ on PRDX5 accumulation 84
3.9 Detection of ROS generation in hemin, baicalein and $CdCl_2$ treated cells 91
3.10 Effect of buthionine sulfoxamine (BSO) treatment on hemin, baicalein and $CdCl_2$-induced HO-1 accumulation 91
3.11 Effect of hemin, baicalein and $CdCl_2$ on the accumulation of aggregated protein and aggresome-like structures 94
3.12 Effect of HO-1 enzyme activity inhibitors, SnPP and ZnPP, on the accumulation HO-1 in $CdCl_2$-treated A6 cells. 101
3.13 Effect of HO-1 enzyme activity inhibitors on $CdCl_2$-induced HO-1 localization, actin and tubulin cytoskeletal structure and the presence of aggregated protein. 108
3.14 Effect of hemin and baicalein treatment on $CdCl_2$-induced changes to actin cytoskeletal structure and the accumulation of aggregated protein. 118
3.15 Effect of hemin, baicalein and SnPP treatment on the localization of $CdCl_2$-induced HSP30 and aggregated protein accumulation. 132

4.0 Discussion 138

References 157

List of Figures

Figure 1. Activation of *ho-1* gene transcription. 3
Figure 2: Activation of the heat shock response. 20
Figure 3. Alignment of *Xenopus laevis, Xenopus tropicalis* and *Homo sapiens* HO-1 amino acid sequences. 36
Figure 4. Comparison of *X. laevis* and *H. sapiens* HO-1 structure. 39
Figure 5. Effect of different concentrations of hemin on HO-1 accumulation. 41
Figure 6. Concentration-dependent accumulation of HO-1 in response to baicalein treatment. 43
Figure 7. Effect of different concentrations of $CdCl_2$ on HO-1, HSP70 and HSP30 accumulation. 45
Figure 8. Time course of HO-1 accumulation in response to hemin. 48
Figure 9. Temporal pattern of HO-1 accumulation in response to 100 μM baicalein. 50
Figure 10. Time course of $CdCl_2$-induced HO-1, HSP70 and HSP30 accumulation. 52
Figure 11. HO-1 accumulation during recovery from hemin treatment. 55
Figure 12. Temporal pattern of HO-1 accumulation during recovery from baicalein treatment. 57
Figure 13. Localization of HO-1 in cells treated with hemin. 59
Figure 14. Accumulation and distribution of HO-1 in baicalein-treated cells. 61
Figure 15. HO-1 localization in cells treated with $CdCl_2$. 63
Figure 16. Time course of HO-1 localization in cells treated with hemin. 65
Figure 17. Temporal pattern of HO-1 localization in cells treated with baicalein. 67
Figure 18. Time course of HO-1 localization in cells treated with $CdCl_2$. 69
Figure 19. Effect of hemin, baicalein or $CdCl_2$ on HSP30 localization of HSP30. 72
Figure 20. Effect of hemin, baicalein or $CdCl_2$ treatment on the actin and tubulin cytoskeleton. 74
Figure 21. Effect of actinomycin D and cycloheximide on hemin- and baicalein-induced HO-1 accumulation. 76
Figure 22. Nrf-2 and HSF1 transcription factor binding sites in the *Xenopus laevis ho-1* gene promoter region. 79
Figure 23. Effect of hemin, baicalein, and $CdCl_2$ on Nrf-2 accumulation. 81
Figure 24. Effect of HSF1 inhibitor, KNK437, on hemin-, baicalein- or $CdCl_2$-induced HO-1 accumulation. 85
Figure 25. Effect of hemin, baicalein, and $CdCl_2$ on PRDX-5 accumulation. 87
Figure 26. Effect of hemin, baicalein and $CdCl_2$ on ROS accumulation in A6 cells. 92
Figure 27. Effect of BSO treatment on hemin-induced HO-1 and SOD1 accumulation. 95
Figure 28. Influence of BSO treatment on baicalein-induced HO-1 and SOD1 accumulation. 97
Figure 29. Effect of BSO treatment on $CdCl_2$-induced HO-1 and SOD1 accumulation. 99

Figure 30. Effect of hemin, baicalein and $CdCl_2$ on the accumulation of aggregated protein and aggresome-like structures. 102
Figure 31. Effect of ZnPP and SnPP on HO-1 accumulation. 104
Figure 32. Effect of ZnPP or SnPP treatment on 50 µM $CdCl_2$-induced HO-1 and HSP70 accumulation. 106
Figure 33. Effect of ZnPP or SnPP treatment on $CdCl_2$-induced HO-1 localization. 109
Figure 34. Effect of ZnPP or SnPP treatment on actin and tubulin organization. 112
Figure 35. Effect of ZnPP or SnPP treatment on $CdCl_2$-induced aggregated protein and aggresome-like structure formation. 115
Figure 36. Effect of treatment with hemin and/or SnPP on Cd-induced HO-1 localization and actin organization. 119
Figure 37. Effect of treatment with baicalein and/or SnPP on Cd-induced HO-1 localization and actin organization. 122
Figure 38. Effect of treatment with hemin and/or SnPP on Cd-induced aggregated protein and microtubular network. 126
Figure 39. Effect of treatment with baicalein and/or SnPP on Cd-induced aggregated protein and microtubular network. 129
Figure 40. Effect of treatment with hemin and SnPP on Cd-induced HSP30 and aggregated protein and aggresome-like structures. 133
Figure 41. Effect of treatment with baicalein and SnPP on Cd-induced HSP30 and aggregated protein and aggresome-like structure accumulation. 135
Figure 42. Schematic of HO-1 induction by various agents. 142

List of Tables

Table I. A comparison of *Xenopus laevis* HO-1 with selected HO-1 and HO-2 from other organisms. 35

List of Abbreviations

ANOVA	analysis of variance
ARE	antioxidant response element
ATP	adenosine triphosphate
Bach-1	bric-a-brac and CNC homology
BC	Baicalein
BCA	bicinchoninic acid
BCIP	5-bromo-4-chloro-3-indolyl phosphate
BiP	binding immunoglobulin protein
BSA	bovine serum albumin
BSO	buthionine sulfoximine
C	control
Cd	cadmium chloride
CdRE	cadmium response element
CoA	coenzyme A
DAPI	4,6-diamidino-2-phenylindole
DMSO	dimethylsulphoxide
DNA	deoxyribonucleic acid
DTT	dithiothreitol
EDTA	ethylene-diamine-tetraacetic acid
ER	endoplasmic reticulum
FBS	fetal bovine serum
GFP	green fluorescent protein
GMP	guanosine monophosphate
GSH	glutathione
GSSH	glutathione disulphide
HBSS	Hank's balanced salt solution
HDAC6	histone deacetylase 6
HeLa	Henrietta Lacks
Hemin	heme chloride
HEPES	4-(2-hydroxyethyl)-1-piperazineethanesulfonic acid
HM	Hemin
HO	Heme oxgenase
HO-1	heme oxygenase-1
HSE	heat shock element
HSF	heat shock factor
HSP	heat shock protein
HSR	heat shock response
IL	interleukin
Keap-1	Kelch-like ECH associated protein
KNK437	N-formyl-3,4-methylenedioxy-benzylidene-gamma-

	butyrolactam
L-15	Leibovitz-15
LSCM	laser scanning confocal microscopy
MAF	musculoaponeurotic fibrosarcoma
MAPK	mitogen activated protein kinase
MARE	MAF recognition element
MDA	malondialdehyde
MG132	carbobenzoxy-L-leucyl-L-leucyl-L-leucinal
MHC	major histocompatibility complex
MTOC	microtubule organizing complex
NADPH	nicotinamide adenine dinucleotide
NBT	4-nitro blue tetrazolium
Nrf-2	nuclear factor (erythroid-derived 2)-like 2
PBS	phosphate buffered saline
PDI	protein disulphide isomerase
PEST	proline-glutamic acid-serine-threonine
PRDX	peroxiredoxin
ROS	reactive oxygen species
RNA	ribonucleic acid
SDS-PAGE	sodium dodecyl sulfate-polyacrylamide gel electrophoresis
sHSP	small heat shock protein
SOD	superoxide dismutase
SnPP	tin protoporphyrin-IX
TBS-T	tris buffered saline solution – Tween20
TNF	tumour necrosis factor
Tris	tris(hydroxymethyl)aminomethane
TRITC	rhodamine-tetramethylrhodamine-5-isothiocyanate phalloidin
TX-100	triton-x 100
UPR	unfolded protein response
UPS	ubiquitin proteome system
ZIP	zinc transport protein
ZnPP	zinc protoporphyrin-IX

1.0 Introduction

1.1 Heme oxygenase

Heme oxygenase was first described in 1968 after it was determined that the degradation of heme was an enzymatically-catalyzed process (Tenhunen et al., 1968). Heme oxygenase-1 (HO-1), the stress inducible isozyme of heme oxygenase that catalyzes the first step of the heme degradation pathway (Müller et al., 1988). This enzyme is also known as heat shock protein 32 (HSP32) given the discovery of an enhancer, the heat shock element (HSE), upstream of the coding region of the rat *ho-1* gene as well as its induction by heat shock in a few but not all experimental systems (Müller et al., 1987; Taketani et al., 1988; Ryter and Choi, 2016). In addition to the stress-inducible HO-1, two constitutive heme oxygenase isozyme genes exist, namely, *ho-2* and a pseudogene *ho-3* (Lee et al., 1996; Platt and Nath, 1998; McCoubrey et al., 1997; Hayashi et al 2004). HO-1, which acts as an oligomer, catalyzed the breakdown of heme into CO, free iron and biliverdin (Platt and Nath, 1998; Hwang et al., 2009). This process required the presence of NADPH and oxygen (Ortiz de Montellano, 2000). Biliverdin was then converted to bilirubin by biliverdin reductase whereas free iron was sequestered by the iron-binding protein ferritin (Platt and Nath, 1998; Ferris et al., 199). Free iron was also removed from the cell by an iron-pumping ATPase, which was shown to co-localize with HO-1 (Ferris et al., 1999). While HO-1 is an ER protein, it lacks a signal peptide and a KDEL retention sequence (Gottlieb et al., 2012). However, HO-1 is posttranslationally inserted into the ER membrane via its C-terminal end (Yoshida and Sato, 1989). This was demonstrated using *in vitro* translated rat HO-1, which spontaneously inserted into microsomes in the absence of the signal recognition particle (Yoshida and Sato, 1989). Analysis of transiently expressed HO-1-GFP fusion gene constructs in mouse monocytes by a fluorescence protease protection assay suggested that HO-1

anchored in the ER faces the cytosol (Gottlieb et al., 2012). This implied that the breakdown products of heme were released into the cytosol. This may not hold true for biliverdin and bilirubin as they were amphipathic when conjugated and could insert into lipid membranes (Tazuma and Holzbach, 1987). Additionally, palmitoylated HO-1 was targeted to portions of the ER membrane proximal to the mitochondria, also known as the mitochondrial-associated membrane (Lynes et al, 2012). The proximity of HO-1 to mitochondria could facilitate the breakdown of mitochondrial heme proteins. These findings suggest that heme breakdown products are proximal to three subcellular locations: the ER membrane, the mitochondrial membrane and the cytosol.

1.2 Regulation of *ho-1* gene expression

Several regulatory *cis*-acting elements are located upstream of the human and mouse *ho-1* genes, including the musculoaponeurotic fibrosarcoma (MAF; also named the antioxidant response element, ARE)) recognition element, the cadmium response element (CdRE) and the heat shock element (HSE) as indicated in Figure 1 (Alam et al., 2000; Alam and Cook, 2007; Macleod et al., 2009). In terms of *trans*-acting factors, nuclear factor (erythroid-derived 2)-like 2 (Nrf2), a basic leucine zipper transcription factor, was determined to be primarily responsible for controlling transcription of the *ho-1* gene (Alam and Cook, 2007; Ryter et al., 2006). During basal conditions, Nrf-2 is situated in the cytosol and bound to Kelch-like enoyl CoA hydratase associated protein (Keap1). The Keap1-Nrf2 complex undergoes continuous ubiquitination and proteasomal degradation by the Keap1-mediated recruitment of an E3 ubiquitin ligase (Ryter et al., 2006). During stress, Keap1-Nrf2 binding is suppressed resulting in the translocation of Nrf2 to the nucleus and its heterodimerization with small MAF proteins and association with MARE

Figure 1. Activation of *ho-1* gene transcription. Under non-stressed conditions, Nrf2 is associated with Keap1, which has been shown to facilitate Nrf2 degradation, while Bach1 blocks Nrf2 binding at the MARE (inset, lower right). Activation of HO-1 gene transcription is dependent on dissociation of Keap1 from Nrf2, which is mediated by stressor modification of Keap1 or the action of p38 MAPK. Bach1 dissociation from the MARE is prompted by binding of heme to Bach1. Pescadillo has been shown to interact with the CdRE adjacent to the MARE. HSR involvement may be through interactions with pescadillo at the CdRE

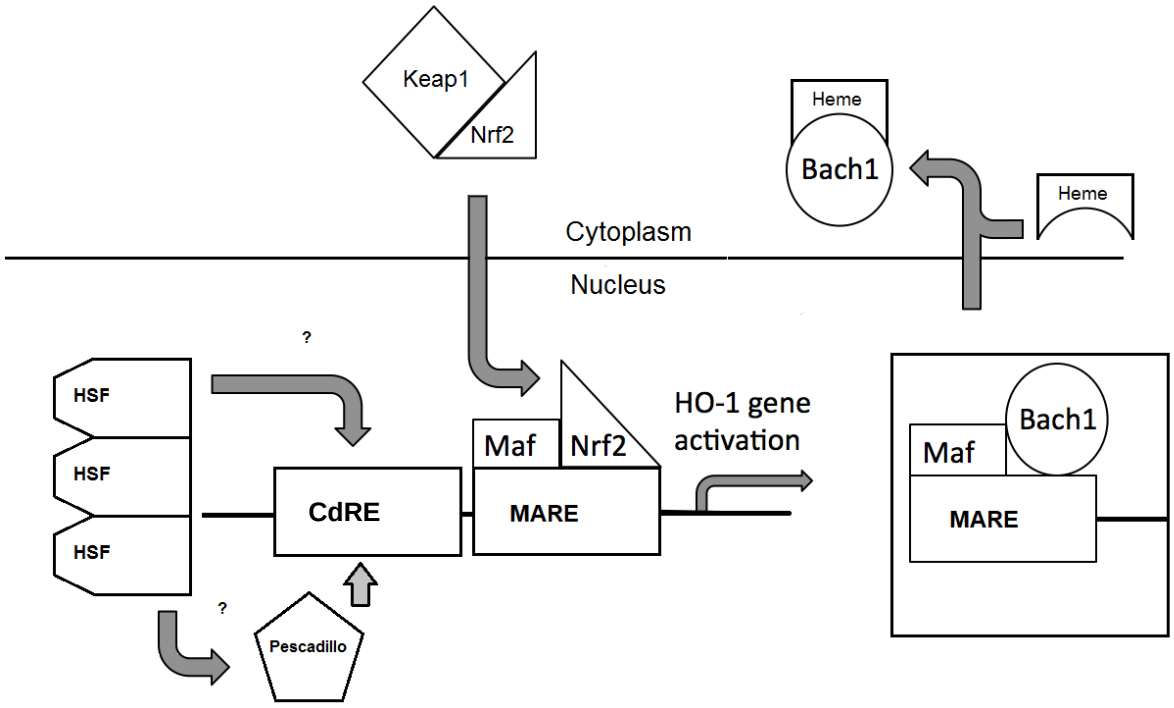
Keap1
Nrf2
Heme
Bach1
Heme
Cytoplasm
Nucleus
?
HSF
HSF
HSF
CdRE
Maf
Nrf2
MARE
HO-1 gene
activation
Bach1
Maf
MARE
?
Pescadillo

in the *ho-1* promoter (Macleod et al., 2009; Stępkowski and Kruszewski 2011). Inhibition of Keap1-Nrf2 binding can occur by electrophilic modification of sulfhydryl groups of cysteine residues in Keap1 (e.g. sulforaphane) or by MAPK phosphorylation of Nrf2 (Zhang and Hannick, 2003; Alam and Cook, 2007; Ryter et al., 2006). Histone deacetylase 6 (HDAC6), a component of the heat shock response machinery was reported to deacetylate p38 MAPK, which then mediated Nrf2-Keap1 disassociation (Kastle et al., 2012). This process was suggested as being the mechanism responsible for HO-1 accumulation in cells treated with proteasomal inhibitors (Kastle et al., 2012; Music et al, 2014). Nrf2 activity was also suppressed by Bach1 (Bric-a-brac and Cap-n-Collar homology), which competed with Nrf2 for binding to the MARE and inhibited *ho-1* gene expression (MacLeod et al., 2009; Ryter et al., 2006). Hemin/heme-induced expression of *ho-1* genes in mammals and zebrafish involved a Bach1-based mechanism (Zenke-Kawasaki et al., 2007; Fuse et al., 2015). Direct binding of heme to Bach1 resulted in the recruitment of an ubiquitin ligase to the Bach-1 heme complex (Zenke-Kawasaki et al., 2007). This results in the degradation of Bach1 and increased Nrf2 binding (Zenke-Kawasaki et al., 2007). Bach1 repression was also inhibited in cells treated with cadmium, which promoted Bach1's export to the nucleus (Suzuki et al., 2003).

As mentioned previously, heat inducibility of *ho-1* genes varied depending on tissue type and organism. Analysis of the *ho-1* gene in human cells revealed a purine-rich region adjacent to the HSE, which is thought to silence the expression of HO-1 in some tissues by an as yet undetermined transcription factor(s) and mechanism (Okinaga et al., 1996). However, it was suggested that even in tissues where HO-1 did not accumulate in response to elevated temperature, heat shock factor 1 (HSF-1) still played a role in *ho-1* gene induction since HSF-1 inhibition reduced *ho-1* gene expression (Alam and Cook, 2007). Moreover, HSF-1 bound to the

ho-1 gene promoter elements, CdRE and HSE, but was not sufficient for cadmium-induced *ho-1* gene expression (Koizumi et al., 2007). Pescadillo, a transcription factor known to interact with the CdRE of the *ho-1* gene promoter, may complex with HSF-1 to mediate cadmium-induced *ho-1* gene expression (Sikorski et al., 2006).

1.3 Mechanisms of HO-1-mediated cytoprotection

It was mentioned previously that HO-1 increased cell survival by inhibiting oxidative damage. HO-1-mediated cytoprotection was suggested to result from the heme breakdown products, CO and bilirubin. At low concentrations, CO was shown to have an anti-inflammatory effect since it inhibited the expression of pro-inflammatory cytokines, TNF-α and IL-1β genes, after exposure to lipopolysaccharide (Otterbein et al., 2000). HO-1-mediated production of CO inhibited apoptosis through its interaction with p38 mitogen-activated kinase (MAPK; Brouard et al., 2000). Furthermore, bilirubin and biliverdin were reported to be potent antioxidants under physiological conditions (Stocker et al., 1987; Morita et al., 1997). For example, bilirubin protected against H_2O_2 -mediated necrotic cell death in HeLa cells and cultured rat neurons (Doré et al., 1999; Baranano et al., 2002). Also, bilirubin was shown to decrease lipid peroxidation of phosphatidylcholine under physiological conditions (Stocker et al., 1987). As biliverdin and bilirubin are amphipathic, they may act as antioxidants in lipid environments.

HO-1 may inhibit apoptosis by degrading free heme (Gozzelino et al., 2010). It has been suggested that intracellular free heme may promote the production of ROS due to the iron found in the heme core, which in turn promoted apoptosis in a TNF-mediated fashion (Gozzelino et al., 2010). It was postulated that degradation of heme by HO-1 should inhibit this pro-apoptotic effect (Gozzelino et al., 2010). This speculative role of HO-1 implies a connection between HO-

1 and the protein degradation machinery since free heme may accumulate in the cell due to the degradation of hemeproteins. This possibility also suggested a role for HO-1 in regulating apoptosis in response to the accumulation and degradation of mitochondrial cytochrome C, a hemeprotein, which acts as a pro-apoptotic signal molecule in the cytosol (Cai et al., 1998).

Cytoprotection by HO-1 against a variety of stressors was shown to be suppressed by the heme oxygenase activity inhibitors, zinc and tin protoporphyrin (Yang et al., 2003; Srisook et al., 2005; Varga et al., 2007; Miyake et al., 2010). For example, ZnPP supressed HO-1-mediated protection against cadmium stress in rat glial cells while the addition of SnPP abrogated protection of mouse T cells from hypoxia by inhibiting HO-1 enzyme activity (Srisook et al., 2005; Dey et al., 2014). Also, both ZnPP and SnPP inhibited HO-1-mediated cytoprotection of rat colons exposed to trinitrobenzene (Varga et al., 2007). ZnPP and SnPP are heme analogs that competitively inhibit HO-1 activity (Vreman et al, 1993; Appleton et al, 1999; Wong et al., 2011; Rahman et al., 2012). Furthermore, while metalloporphyrins can have effects on other enzymes, such as those of the NO synthesis pathway, they are specific for heme oxygenases at concentrations described in the present study (Appleton et al., 1999; Wong et al., 2011; Rahman et al., 2012).

1.4 Inducers of heme oxygenase accumulation

A wide array of stressors was reported to induce HO-1 accumulation in mammalian cultured cells (e.g. macrophage, epithelial and fibroblast) including UV radiation, sodium arsenite, hydrogen peroxide, cadmium, lipopolysaccharide, and hyperoxia. (Keyse and Tyrell, 1989; Camhi et al., 1998; Alam et al., 2000; Brouard et al., 2000). Many of the stresses that induced HO-1 were found to increase the amount of ROS in the cell (cadmium, hyperoxia) or

were themselves ROS, such as hydrogen peroxide (Sarkar et al., 1998; Alam et al., 2000; Hasan and Schafer, 2008). Interestingly, stress-induced HO-1 accumulation enhanced cell survival by inhibiting apoptosis and reducing oxidative damage (Nath et al., 2000; Nath et al., 2001; Dong et al., 2000; Lang et al., 2004). Given the aforementioned findings, HO-1 has been used as a biomarker for oxidative stress in the analysis of various disease states such as hypertension, hepatic steatosis, silicosis and coronary heart disease (Cheng et al., 2005; Chen et al., 2004; Malaguearnera et al., 2005; Sato et al., 2006). Accumulation of HO-1 in response to heat shock was shown in human and rat hepatoma cells as well as in rat brain cells but not in human skin fibroblasts, human macrophages and rat glioma cells (Taketani et al., 1988; Yoshida et al., 1988; Taketani et al., 1989; Keyse and Tyrell, 1989; Mitani et al., 1990; Raju and Maines, 1994). This variability in heat-inducible expression has not been fully explained.

While a great deal of information regarding mammalian HO-1 accumulation and function is available, less is known about HO-1 in poikilothermic vertebrates. However, HO-1 has been used as a biomarker for oxidative stress in fish subjected to environmental toxicants. For example, increased HO-1 accumulation in response to hypoxia, sodium fluoride, cadmium and arsenic was noted in several fish species including zebrafish, goldfish and carp (Lee et al., 1996; Motterlini et al., 2000; Wang et al., 2008; Wang and Gallagher, 2013; Jancsó and Hermesz, 2014; Mukhopadhyay et al., 2015). Also, exposure of European sea bass to sublethal concentrations of a glyphosate-based herbicide resulted in an inhibition of *ho-1* mRNA accumulation in the liver and gills (Prevot-D'Alvise et al., 2013).

1.5 Hemin

Hemin is the chloride salt of heme, an iron-containing metalloporphyrin important to a wide array of biological processes across all kingdoms of life. Heme synthesis is a multi-step enzyme-catalyzed process that occurs in the cytosol, the intermembrane space and the mitochondrial matrix (Heinemann et al., 2008). In animals, the porphyrin ring of heme is synthesized from succinyl CoA and glycine prior to the addition of the iron centre (Heinemann et al., 2008). Heme is associated with carrier proteins *in vivo* since free heme is lipophilic (Khan and Quigley, 2011). Heme import into the cell appears to involve a dual-functional heme/folate import protein (Khan and Quigley, 2011). Several dedicated heme chaperones for intracellular trafficking have been identified in bacteria, although corresponding eukaryotic analogs have not yet been identified (Severance and Hamza, 2009). Free heme, which circulates in the cytosol, was measured to be approximately 20 μM in human erythrocytes (Aich et al., 2016). Increased levels of intracellular free heme was reported to elevate ROS levels and cause lipid peroxidation and oxidative stress-induced DNA damage (Kumar and Bandyopadhyay, 2005; Khan and Quigley, 2011).

Since heme is the substrate for HO-1 enzyme activity, it is not surprising that hemin induces HO-1 accumulation (Alam et al., 1989). In many studies examining the cytoprotective nature of HO-1 induction, hemin was often used as an agent to increase the relative levels of HO-1 prior to a potentially lethal stress (Brouard et al., 2000; Lang et. al., 2004). For example, pretreatment with hemin protected rat kidneys against mercury-induced damage by upregulating HO-1 levels (Yoneya et al., 2000). Also, hemin-mediated cytoprotection against cadmium-induced testes damage and cyclophosphamide-induced cystitis in rats was the result of increased HO-1 accumulation (Fouad et al., 2009; Matsuoka et al., 2007). Finally, hemin was reported to

inhibit protein aggregation *in vitro* (Liu et al, 2014; Hayden et al., 2015; Sonavane et al., 2017). To date this phenomenon has not been demonstrated *in vivo*.

1.6 Baicalein

Baicalein is a flavonoid isolated from *Scutellaria baicalensis* or Baikal skullcap, an Asian plant of the mint family (Li-Weber, 2009). Baicalein was reported to have antioxidant and anti-inflammatory effects and is currently under investigation as a potential antitumour agent and for treatment of cardiac injuries (Li-Weber, 2009, Chen et al., 2006). HO-1 induction by baicalein was reported in a number of cell types and may be responsible for the cytoprotective effects of the compound. Incubation of rat glioma cells with baicalein was shown to induce the accumulation of HO-1, but not HSPs, in a concentration-dependent manner (Chen et al., 2006). In this latter study, the cytoprotective effects of baicalein were abolished by treatment with the HO-1 activity inhibitor, ZnPP. Another study determined that baicalein enhanced the survival of human cardiomyocytes in response to an oxidative stress challenge (Cui et al., 2015). This enhancement was suppressed by RNAi-mediated inhibition of the transcription factor Nrf2 (Cui et al., 2015). Also, baicalein-induced cytoprotection against palmitate lipotoxicity in rat B cells was found to be HO-1 dependent (Kwak et al., 2017). Additionally, a lack of HO-1 involvement was reported in baicalein-mediated survival of pig kidney cells treated with peroxynitrite or cultured mouse neurons subjected to thapsigargin- or brefeldin A-induced apoptosis (Piao et al., 2008; Choi et al., 2010). As reported for hemin, baicalein was found to inhibit protein aggregation *in vitro,* which may also contribute to its cytoprotective abilities (Zhu et al., 2004; Bomhoff et al., 2006; Kostka et al., 2008).

Intriguingly, baicalein was also reported to reduce cell survival in certain studies. For

instance, baicalein treatment decreased cell survival by preventing cell cycle checkpoint progression and inhibiting angiogenesis in xenografted human lung cell tumours (Cathcart et al., 2017). Baicalein was also shown to reduce proliferation of cultured human endothelial cells (Liu et al., 2003). This was believed to occur through a baicalein-vascular endothelial growth factor receptor interaction (Ling et al., 2011). It is likely that baicalein has multiple effects on cellular physiology, with conditions specific to cell type and treatment determining its effect on cell survival.

1.7 Cadmium

Cadmium is a toxic heavy metal introduced into the environment mainly through fossil fuel extraction and mine tailings (Milton et al, 2004; Yusuf, 2007; Boussen et al., 2013; Cullen and Maldonado, 2013) Chronic cadmium exposure was reported to primarily affect the kidneys where it accumulates and causes a decrease in renal function and tissue necrosis (Armenta and Rios, 2007; Nordberg, 2009; Johri et al., 2010; Templeton and Liu, 2010). In kidney, cadmium was found to be particularly toxic to renal epithelial tubular cells. Cadmium was also reported to induce cancers of the kidney, prostate and lung (Waisberg et al., 2003; Joseph, 2009; Templeton and Liu, 2010; Rahimzadeh et al, 2017) Although cadmium is capable of causing DNA damage at high concentrations, it was reported that most cadmium-induced carcinogenesis occurs through the inhibition of DNA repair or oncogene activation (Waalkes, 2003; Mouchet et al., 2007; Joseph, 2009) Cadmium import into cells is mediated by the divalent metal transporter (DMT1), which is also responsible for rat intestinal absorption of cadmium (Talkvist et al., 2001; Park et al., 2002). Zinc transporters, ZIP8 and ZIP14, were also implicated in cadmium uptake in an epithelial cell line derived from mouse kidney proximal tubules (Fujishiro et al., 2012).

Cadmium-mediated induction of HO-1 accumulation was reported in a number of organisms. For example, in rat testes and mouse mammary cells, HO-1 was shown to accumulate in response to cadmium exposure (Alam et al., 1989; Alam et al., 2000). Also, cadmium-induced HO-1 accumulation was detected in zebrafish larvae, chicken liver cells, common carp, mung bean and cabbage leaves (Sardana et al., 1982; Jin et al., 2012; Wang and Gallagher, 2013; Jancsó and Hermesz, 2015; Mahawar et al., 2017). Cadmium is also known to trigger the accumulation of heat shock proteins increased in human kidney, rat liver and rat testicles (Ovelgonne et al., 1995; Somji et al., 2000; Selim et al., 2012). $CdCl_2$ treatment induced the accumulation of HSP24 and HSP70 in chick embryos (Papaconstantinou et al., 2003). Cadmium exposure induced HSP70 accumulation in Chinook salmon embryonic and oyster gill cells (Heikkila et al., 1982; Ivanina et al., 2008) The endoplasmic reticulum chaperone immunoglobulin-binding protein (BiP) accumulated in response to cadmium in chicken hepatocytes and pig renal epithelial cells (Liu et al., 2006; Shao et al., 2014).

1.8 Oxidative Stress

Organisms are constantly challenged by the presence of oxidative molecules in their intracellular environments, which can cause deleterious chemical modifications of DNA, protein and/or lipids. Inefficiencies in oxidative phosphorylation result in the production of superoxide anions, which can induce the formation of reactive anions that are collectively known as reactive oxygen species (ROS; Finkel and Holbrook, 2000; Turrens, 2003; Merksamer et al., 2013). These reactive oxygen species include hydrogen peroxide, hydroxyl radicals, peroxynitrite and oxidized lipids (Niki et al., 1991; Turrens, 2003). ROS production can occur endogenously or be induced or enhanced by the presence of exogenous toxicants including cadmium, sodium

arsenite and mercury (Wiggers et al., 2008; Ruiz-Ramos et al., 2009; Cuypers et al., 2010). The exact nature of the modifications caused by ROS varies but can include oxidation of cysteine thiol groups and/or the peroxidation of lipids (Porter et al., 1995; Tu and Weissman, 2004).

A number of defence mechanisms have evolved to counteract the excessive accumulation of ROS in the cell. For example, superoxide dismutase (SOD) catalyzes the conversion of superoxide to hydrogen peroxide (Turrens, 2003). Hydrogen peroxide is then reduced to water and oxygen by catalase. Peroxiredoxins are a family of six (PRDX1-6) enzymes that reduce peroxides via a reactive cysteine site on the protein (Yuan et al., 2004). ROS production can also be mitigated by the glutathione (GSH) system. Glutathione, also known as (2S)-2-amino-4-{[(1R)-1-[(carboxymethyl)carbamoyl]-2-sulfanylethyl]carbamoyl}butanoic acid, can reduce ROS to non-reactive molecules (Deponte, 2013). After it has reduced a molecule, GSH is converted to glutathione disulphide (GSSG; Deponte, 2013). The GSH pool is then regenerated from GSSG in an NADPH-requiring process. While these systems are generally sufficient in maintaining redox homeostasis, disequilibration can occur. Occasional formation of hydroxy and lipid radicals can have a disproportionately large effect on overall ROS levels resulting from a self-propogating chain reaction of ROS production (Porter et al., 1995). Since ROS also has a role in cell signalling (e.g. hydrogen peroxide activation of cyclic GMP dependent protein kinase or platelet derived growth factor-mediated production of hydrogen peroxide), excess ROS produced for signalling purposes can remain in the wake of a signalling cascade (Ray et al., 2012). Futhermore, a wide array of environmental stressors, such as asbestos, radiation and heavy metals, can result in ROS generation by overwhelming the redox buffering capacity of the cell (Vallyathan and Shi, 1997). When these defence mechanisms are overwhelmed, ROS reacts with other cellular components and can modify DNA, lipids and proteins in a way that impedes

their proper function. In summary, oxidative stress is the condition that arises when the accumulation of ROS begins to have a deleterious effect on the physiology of an organism or cell.

In the process of counteracting oxidative stress, cells may accumulate an excess of antioxidant molecules, which theoretically could also cause cellular damage. Studies examining this phenomenon, called reductive stress, suggest that reductive agents generally exert their effect through dysregulation of antioxidant mechanisms rather than by directly modifying proteins, lipids and DNA (Ghyzczy and Boros, 2001). For example in yeast, the presence of the small redox proteins known as thioredoxins were required for protection against the reducing agent, dithiothreitol (DTT; Trotter and Grant, 2002). In yeast thioredoxin mutants, it was reported that the toxic effects of DTT was due to an over-accumulation of the antioxidant, GSH, which disrupted endoplasmic reticulum function. Recently, reductive stress was detected in animal models of Alzheimer's disease before the onset of cognitive impairment (Lloret et al. 2016).

1.9 Oxidative stress and unfolded proteins

As mentioned above, the deleterious effects of oxidative stress stem, at least in part, from their ability to chemically modify proteins. For example, oxidative modifications can alter protein secondary structure, which may expose hydrophobic regions making them prone to aggregation (Dasuri et al., 2013). This relationship between protein aggregation and oxidative stress was reflected in animal research models of Alzheimer's disease, a condition associated with the accumulation of misfolded protein. For example, an increase in amyloid plaque formation was observed in mice having SOD knockouts as well as in response to an elevation of

ROS generation by NADPH oxidase activity (Li et al., 2004; Bruce-Keller et al., 2011). Additionally, prolonged oxidative stress can result in proteasomal impairment resulting in an inhibition of protein degradation (Aiken et al., 2011). Also, human trabecular meshwork cells cultured under hyperoxic conditions showed impairment in their ability to degrade proline-glutamic acid-serine-threonine (PEST)-enriched green fluorescent protein (GFP) tagged proteins (Caballero et al., 2003). Similarly, a loss of proteolytic activity was found in response to ROS production by paraquat and iron sulphate in cultured human neuroblastoma cells (SH-SY5Y; Ding and Keller, 2001). Thus, oxidative stress may have an impact on misfolded protein accumulation by disrupting protein conformation directly and by reducing the rate at which they are degraded.

Paradoxically, an oxidative environment is also important for proper protein folding. Formation of disulphide bonds in proteins in the ER is an oxidative process. Disulphide bridge formation is catalyzed by the protein disulphide isomerase (PDI)/Ero1p machinery using molecular oxygen as a final electron acceptor, which results in generation of ROS (Tu and Weissman, 2004). Consequently, the redox buffering conferred by GSH:GSSH in the ER lumen tends to favour more oxidizing conditions than the cytosol (Tu and Weissman, 2004). Overexpression of disulphide-rich secretory proteins leads to an increase in the oxidative equilibrium in the ER, but also increases the GSH:GSSH ratio in the cytosol (Delic et al., 2012). Induction of the unfolded protein response (UPR; induction of ER molecular chaperone gene expression in response to an accumulation of unfolded protein) by tunicamycin (N-glycosylation inhibitor) decreases the oxidizing condition of the ER (Delic et al., 2012). This was believed to reduce the rate of protein folding while misfolded proteins were being degraded (Delic et al., 2012). The mechanism causing this decrease in oxidizing conditions triggered by the UPR is

hypothesized to be the result of a corresponding increase in SOD activity (Tan et al., 2009).

The seemingly contradictory roles of oxidizing conditions, being both a cellular stressor and a necessary condition for protein folding, can be reconciled by acknowledging the role of compartmentalization. A more oxidative environment in the ER allows for protein folding to be carried out while preventing the exposure of other cellular compartments to ROS (Go and Jones, 2008; Jones, 2010). This carries a number of implications for the ER membrane. First, it is subjected to higher levels of oxidative stress than the cell in general (Go and Jones, 2008). Secondly, as the interface between the ER lumen and the cytosol its redox potential must be tightly regulated (Go and Jones, 2008).

1.10 Proteostasis

Proteostasis is the maintenance of the synthesis, degradation and conformation of proteins within the cell at a non-deleterious level. Of these processes, the maintenance of conformation can be directly challenged by non-specific stressors such as heat or oxidative stress (Morimoto, 2008). Even in the absence of external stressors, misfolding of proteins can occur due to errors in translation or even as a spontaneous phenomenon (Schubert et al., 2000; Kupfer et al., 2009). Misfolding of soluble proteins may lead to the exposure of a protein's hydrophobic surfaces to the soluble comparments of the cell, which in turn leads to the formation of toxic protein aggregates (Morimoto, 2008). Furthermore, some proteins, such as tau and α-synuclein, may be more prone to aggregation than others (Bucciantini et al., 2002; Stefani and Dobson, 2003; Pawar et al., 2006). Protein aggregates were shown to resist degradation by the ubiquitin proteasome system (UPS; Salomons et al., 2009). Under most conditions, proteins destined for degradation are marked by covalent attachment of multiple ubiquitin molecules through an

enzyme-catalyzed process (Tramutola et al., 2016). These marked proteins are shuttled to the proteasome, a multi-megadalton proteolytic complex that deubiquitinates and then degrades proteins by an ATP-dependent process (Ross et al., 2015). However, as the proteasome can only process linearized polypeptides, protein aggregates are unable to undergo UPS-mediated degradation (Salomons et al., 2009). Maintenance of conformation is therefore of critical importance to proteostasis in general, as its impairment results in an impairment of protein degradation as well.

There are several proposed mechanisms by which protein aggregates cause toxicity. It was suggested that newly formed protein aggregates sequestered proteins including those required for cell survival. This phenomenon was found with aggregates resulting from the expression of exogenous genes introduced into cultured human kidney cells (Olzscha et al., 2011). It has also been hypothesized that as insoluble entities, aggregates interact with cellular membranes, altering their permeability and disrupting intracellular cation concentrations (Stefani and Dobson, 2003). Alternatively the presence of large macromolecular structures like protein aggregates could interfere with molecular trafficking in the crowded cellular environment. Nevertheless, these and other studies have shown the inherent toxicity of protein aggregates and their possible role in various protein conformation diseases including Huntington's disease, Alzheimer's disease and the amyloidoses (Carell and Lomas, 1997; Bayer, 2015).

In situations when the amount of aggregated or unfolded protein exceeds the capacity of the ubiquitin-proteasome machinery to degrade it, the cell partitions aggregated protein into structures called aggresomes, which form proximal to the cell nucleus (Johnson et al, 1998; Taylor et al, 2003; An and Statsyuk, 2015). This accumulation of polyubiquinated proteins is dependent on histone deacetylase 6 (HDAC6) shuttling polyubiquinated protein along

microtubules to the aggresome located at the microtubule organizing complex (MTOC; Kawaguchi et al, 2003; Lee et al., 2010). The aggresome is enclosed by a network of vimentin, an intermediate filament, which is thought to help stabilize the structure (Johnson et al, 1998; Olzmann et al., 2008). Aggresomes are also associated with γ-tubulin, a tubulin isoform found primarily at the MTOC (Oakley, 1992; Mi et al., 2009). Aggresomes, which are ultimately degraded through autophagy, require the presence of proteasomal complexes in order for this mechanism to proceed (Lee et al., 2010; Hao et al., 2013; Nassar et al., 2017). A variety of protein chaperones, such as HSP25, HSP27 and HSP30 have been reported to associate with aggresomes and aggresome-like structures, suggesting a role for small heat shock proteins (sHSPs) in aggresome formation (Ito et al., 2002; Katoh et al., 2004; Goldbaum et al., 2009; Bolhuis and Richter-Landsberg, 2010; Khan et al., 2015).

1.11 Heat shock proteins and the heat shock response

Heat shock proteins are molecular chaperones that are key components in the maintenance of cellular proteostasis. HSPs have been classified into families based on amino acid sequence and include sHSPs, HSP40, HSP60, HSP70, and HSP90 (Morimoto, 2008). They may be strictly inducible, strictly constitutive or constitutive but responsive to additional induction (Morimoto, 1998). HSPs perform a number of roles in maintaining cellular protein homeostasis, such as protein folding, preventing aggregation of unfolded proteins and protein translocation (Balch et al., 2008). SHSPs, which were found to possess a conserved α-crystallin domain, bind unfolded proteins and inhibit the formation of insoluble unfolded protein aggregates before transferring them to ATP-dependent chaperones such as HSP70 for refolding or degradation (Heikkila, 2004; Morimoto, 2008; Mymrikov et al., 2011; Garrido et al., 2012;

Heikkila, 2017).

The heat shock response (HSR) is a near-ubiquitous transcriptional response to stresses that threaten cellular protein homeostasis such as high temperature, heavy metal toxicants and reactive oxygen species (Heikkila, 2004; Voellmy 2004; Morimoto 2008; Heikkila, 2010). More specifically, the HSR, which leads to the expression of *hsp* genes, is activated by the accumulation of unfolded proteins, which interferes with proper protein folding or protein degradation (Westerheide and Morimoto, 2005; Morimoto 2008). Under non-stress conditions, monomeric HSF-1 is normally found in a complex with HSP90 and HDAC6, which renders it inactive (Westerheide and Morimoto, 2005; Morimoto 2008). Stress-induced accumulation of unfolded or misfolded protein results in HSP90 and HDAC6 dissociating from HSF-1, which then, trimerizes, translocates to the nucleus and binds to the HSE (Fig. 2; Voellmy 2004; Morimoto 2008; Kastle et al., 2012)

1.12 *Xenopus laevis*

The South African clawed frog, *Xenopus laevis*, is a well-established model research organism. It has been used extensively in developmental studies since its oocytes and embryos have properties which make them well suited to research. For example, the large size of *Xenopus* oocytes, including their ability to transcribe injected DNA, makes them amenable for microinjection studies (Heikkila et al., 2007). A number of cell lines have been developed, including an immortalized A6 kidney epithelial cell line from the proximal renal tubule (Rafferty, 1969). A6 cells have been used extensively in the study of ion channels by patch clamping for over twenty years (Nelson et al., 1984; Nakagawa et al., 1997; Ma, 2011; Thai et al., 2014). They were used to characterize peroxisomal, assess copper toxicity and cell survival in microgravity

Figure 2: Activation of the heat shock response. Various stresses (yellow lightning bolt) lead to protein unfolding. Accumulation of unfolded protein results in the disassociation of the HSF-1/HDAC6/HSP90 complex. HSF-1 trimerizes, translocates to the nucleus and triggers transcription of stress induced HSPs by binding to the HSE. HSP90 and the stress-induced HSPs then associate with unfolded proteins to inhibit aggregation and promote proper refolding during recovery from stress.

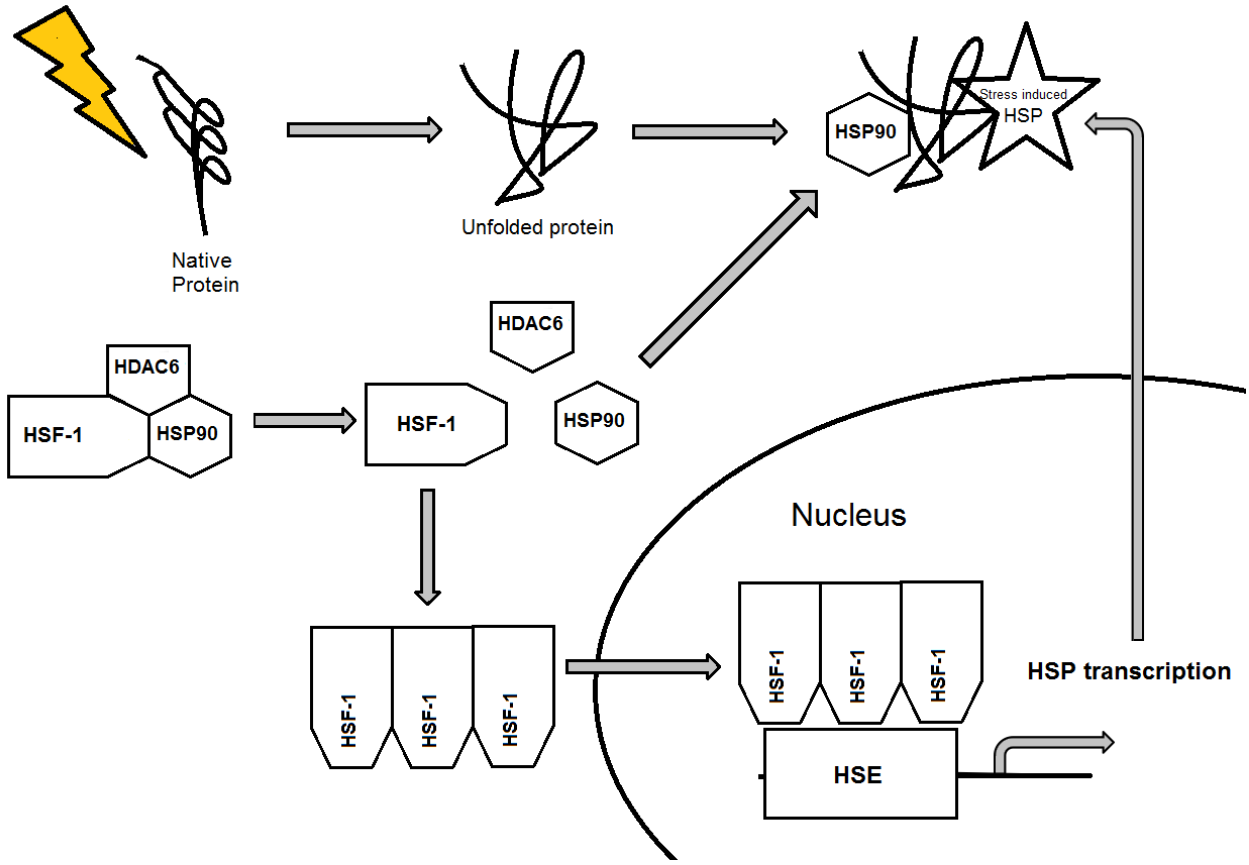
Native
Protein
Unfolded protein
HSP90
Stress induced
HSP
HDAC6
HSF-1
HSP90
HDAC6
HSF-1
HSP90
Nucleus
HSF-1
HSF-1
HSF-1
HSF-1
HSF-1
HSF-1
HSE
HSP transcription

environments (Ikuzawa et al., 2007; Fox et al., 2014; Thit et al., 2015). Finally, as will be outlined below, A6 cells have been used to examine various aspects of HSP gene expression and function (Heikkila, 2010; 2017).

1.12.1 Stress-induced HSP accumulation in *Xenopus* cultured cells

A number of *X. laevis hsp* genes have been sequenced, including *hsp27*, *hsp30*, *hsp47*, *hsp70*, *hsc70* (heat shock cognate 70 gene), and *hsp110* (Heikkila, 2010; 2017). HSP accumulation by heat shock, sodium arsenite, $CdCl_2$, herbimycin A and proteasomal inhibitors was documented and characterized in A6 cells (Darasch et al., 1988; Briant et al., 1997; Woolfson and Heikkila, 2009; Young and Heikkila, 2010; Khamis and Heikkila, 2013). Several A6 cell studies also demonstrated a synergistic action of a mild heat shock plus a chemical stressor (e.g. sodium arsenite, $CdCl_2$ or proteasomal inhibitors) on HSP accumulation (Heikkila, 2010; Young and Heikkila, 2010; Khamis and Heikkila, 2013). Furthermore, it was shown that A6 cells pretreated with a mild heat shock could survive a lethal thermal challenge (Phang et al., 1999; Manwell and Heikkila, 2007). Later studies revealed that thermoresistance could also be conferred by other stressors including sodium arsenite and the proteasomal inhibitors, cucurmin and withaferin A (Young et al., 2009; Khan and Heikkila, 2011; Khan et al., 2012). In A6 cells, HSP-mediated aquisition of thermoresistance likely involves the molecular chaperone properties of HSPs to inhibit the formation of stress-induced toxic protein aggregates (Heikkila, 2010; 2017). For example, HSP30 was found to inhibit the heat-induced aggregation of the client protein, luciferase, and maintain it in a folding-competent state (Fernando and Heikkila, 2000; Abdulle et al., 2002; Fernando et al., 2003). Recently, it was shown that heat shock, $CdCl_2$, sodium arsenite and proteasomal inhibitors induced the formation of aggresome-like inclusion

bodies that were associated with HSP30 (Khan et al., 2015).

1.12.2 Stress-induced HO-1 accumulation in *X. laevis*

In contrast to HSPs, little information is available regarding *X. laevis* HO-1. In 2008, Shi et al. (2008) sequenced *X. laevis* HO-1 and detected the presence of *ho-1* mRNA during early embryogenesis. Also, treatment of adult male *X. laevis* with the endocrine disruptor, 17α-ethinylestradiol, caused decreased levels of *ho-1* and *ho-2* mRNA (Gamshausen et al., 2015). Recently, HO-1 was reported to accumulate in A6 cells subjected to sodium arsenite or $CdCl_2$ treatment in a concentration- and time-dependent manner (Music et al., 2014). In this latter study, HO-1 accumulation was inhibited by addition of actinomycin D or cycloheximide, suggesting de novo transcription. While heat shock did not induce HO-1, mild heat shock was reported to enhance HO-1 accumulation in response to exposure to low concentrations of $CdCl_2$ or sodium arsenite (Music et al., 2014; Shirriff and Heikkila, 2017). Recently, HO-1 accumulation was shown to be upregulated by two sulphur containing plant secondary metabolites namely, benzyl isothiocyanate and phenethyl isothiocyante in *X. laevis* cells (Khamis and Heikkila, 2018). Also, proteasomal inhibitors induced HO-1 accumulation in A6 cells at lower concentrations than reported in mammalian systems (Music et al., 2014). In the aforementioned studies, HO-1 was found to accumulate in the perinuclear region of the cytoplasm, which was consistent with observations of HO-1 being an ER protein (Ryter et al., 2006). In summary, these studies suggest that HO-1 accumulation may be a useful biomarker for toxicants for aquatic poikilothermic vertebrates (Music et al., 2014; Shirriff and Heikkila, 2017).

1.13 Hypothesis and Objectives

Stress-induced HO-1 accumulation remains largely uncharacterized in *X. laevis* and other amphibians. Previously, as mentioned in Section 1.12.3, HO-1 accumulation in A6 cells after treatment with selected stressors was demonstrated, but its ability to confer cytoprotection has not. Furthermore, to the best of my knowledge, there have not been any studies examining the effect of hemin or baicalein on HO-1 accumulation in *Xenopus*. Additional information on HO-1 gene expression and function in amphibians and other aquatic poikilotherms is of importance given the presence of toxic heavy metals, metalloids and other contaminants in their habitats. It is possible that HO-1 accumulation could act as a molecular biomarker of oxidative stress (Music et al., 2014; Shirriff and Heikkila, 2017).

In a broader context, manipulating the accumulation of HO-1 in different human tissues may be of therapeutic value in certain disease states. For example, it was reported that the catalytic by-products of heme have anti-apoptotic and angiogenic effects in tumour cells, which can be diminished by administration of ZnPP, an inhibitor of HO-1 activity. HO-1-mediated cytoprotection assessed by the maintenance of control-like levels of aggregated protein or control-like actin cytoskeletal structure, was found to be of particular importance during acute kidney injury resulting from ischemia, infection or transplant rejection (Shimizu et al., 2000; Blydt-Hansen et al., 2003; Tracz et al., 2007; Nath, 2014). Given that cellular processes are generally conserved through vertebrate evolution, research with *Xenopus* A6 kidney epithelial cells provides a model tissue culture system for understanding the mechanism(s) associated with HO-1-mediated cytoprotection, which may be applicable to human diseases.

Hypothesis: I hypothesize that hemin and baicalein will induce HO-1 accumulation in *X. laevis* A6 cells and that they will also confer cytoprotection against a near-lethal $CdCl_2$ stress challenge. Furthermore, this cytoprotection will be suppressed by HO-1 activity inhibitors.

The main objectives for this doctoral research are as follows:

1. Examine the effect of hemin and baicalein on HO-1 accumulation in *Xenopus*.

In mammalian systems, HO-1 was demonstrated to accumulate in response to hemin by a Bach-1-based mechanism. Investigating whether hemin elicits a similar accumulation in *Xenopus* cells will determine if the cellular response to hemin is conserved in non-mammalian vertebrates and serves as a foundation for future comparative studies of HO-1 using amphibians and other poikilotherms.

2. Determine if HO-1 confers cytoprotection in cultured *Xenopus* cells exposed to near lethal concentrations of $CdCl_2$. HO-1 was found to confer cytoprotection in mammals, but this phenomenon has not been examined in amphibians or other vertebrate poikilotherms. Determination of whether HO-1 has the ability to confer cytoprotection against cadmium in *Xenopus* helps to characterize its physiological role and to emphasize its potential value as a biomarker of oxidative stress in amphibians and other aquatic vertebrates.

2.0 Materials and methods

2.1 Chemicals

Hemin (Sigma-Aldrich, Oakville, ON) was prepared by dissolving it in dimethyl sulfoxide (DMSO; Sigma-Aldrich) to yield a 1.5 mM stock solution. HO-1 enzyme activity inhibitors, tin protoporphyrin (SnPP; Enzo Life Sciences, Farmingdale, NY) and zinc protoporphyrin (ZnPP; Enzo Life Sciences) were dissolved in DMSO to produce 1.5 mM stock solutions. Baicalein (Sigma-Aldrich) was also dissolved in DMSO to produce a 10 mM stock solution. After stocks were made, hemin, ZnPP, SnPP and baicalein were kept wrapped in tin foil to protect from light and stored at -20 °C. $CdCl_2$ (Bioshop, Burlington, ON) was prepared as a 100 mM stock solution in sterile water (Sigma-Aldrich). In experiments with DL-buthionine sulfoximine (BSO; Sigma-Aldrich), a 200 mM stock solution of was freshly prepared before each treatment by dissolving it in sterile water (Sigma-Aldrich). Stocks of actinomycin D (Sigma-Aldrich) were prepared by mixing with DMSO to a final concentration of 2 mg/ml. Cycloheximide (Sigma-Aldrich) stock was prepared in sterile water (Sigma-Aldrich) at a concentration of 10 mM. KNK437 (Sigma-Aldrich) stock was prepared with DMSO at a concentration of 5 mg/ml.

2.2 Culture of *Xenopus laevis* A6 kidney epithelial cells

Xenopus laevis A6 kidney epithelial cells were obtained from the American Type Culture Collection (CCL-102; Rockville, MD). Cells were cultured in T75 cm^2 flasks (VWR, Mississauga, ON) at 22 ºC using 70% L15 (Leibowitz) cell culture media with 10% fetal bovine serum and 1% penicillin/streptomycin (Sigma-Aldrich). Once the cells were confluent, they were rinsed once with 1 ml versene [0.02% (w/v) KCl, (0.8% (w/v) NaCl, 0.02% (w/v) KH_2PO_4,

0.115% (w/v) $NaHPO_4$, 0.02% (w/v) Na_2EDTA] and then again with 2 ml versene followed by treatment with 1 ml of 1X trypsin (Sigma-Aldrich) in Hank's balanced salt solution (HBSS, Sigma-Aldrich) to facilitate cell detachment. Fresh media was then added to resuspend cells and inactivate trypsin followed by transfer of cells to new flasks.

2.3 Cell treatments

Treatments were administered to cells at 90% confluency. In experiments using 10 to 30 μM hemin, 50 to 400 μM baicalein or 25 to 275 μM $CdCl_2$ alone, they were mixed with L-15 media and administered to the cells at the final concentration described. The effect of transcriptional inhibition on HO-1 accumulation involved pretreatment of cells for 30 min with 2 μg/mL actinomycin D (Sigma-Aldrich) at 22 °C before the addition of hemin or baicalein to the cell media. Investigation of the effect of the translational inhibitor, cycloheximide, involved pretreatment of cells with 100 μM cycloheximide (Sigma-Aldrich) for 6 h at 22 °C prior to the addition of hemin or baicalein. In studies determining the effect of HSF1 inhibition on HO-1 accumulation, cells were pretreated for 6 h with 100 μM of the HSF1 inhibitor KNK437 (Sigma-Aldrich; dissolved in DMSO) prior to the addition of hemin or baicalein. Additionally, some flasks of cells were incubated for 4 h with 10 mM BSO at 22 °C followed by supplementation with hemin, baicalein or $CdCl_2$ for 16 h. In experiments examining HO-1 enzyme activity inhibitor effects on cadmium-treated cells, cells were treated with ZnPP or SnPP for 4 h prior to supplementation with 50 μM $CdCl_2$ for 16 h at 22 °C. Finally, cytoprotection studies required the incubation of cells with baicalein or hemin and/or 15 μM SnPP for 4 h prior to supplementation with 275 μM $CdCl_2$ for 16 h, followed by a 4 h recovery in fresh media.

2.4 Protein isolation and quantification

Prior to collection, cells were rinsed once with 2 ml of 65% HBSS and then resuspended in 1 ml 100% HBSS. Cells were transferred to a 1.5 ml microcentrifuge tube (Eppendorf centrifuge; Model No. 5810R; Mississauga, ON) and collected by centrifugation at 14,000 rpm for 1 min and then stored in 1.5 ml microcentrifuge tubes at -80 °C. For protein isolation, cells were lysed using 300 µL of 1% SDS lysis buffer (200 mM sucrose, 2 mM EGTA, 1 mM EDTA, 40 mM NaCl, 30 mM HEPES, pH 7.4, 1% protease inhibitor and 1% SDS) and then pulse sonicated at 10 watts for 30 s on ice (Model 100, Fisher Scientific; Waltham, MA, USA). Cell debris and unlysed cells were separated from the protein isolate by centrifugation at 14,000 rpm for 60 min at 4 °C. Protein content of the supernatant was quantified by the bicinchoninic acid protein quantification assay kit (Pierce, Rockford, IL, USA). Protein standards were made by diluting a bovine serum albumin (BSA; Bioshop) solution with MilliQ water to final concentrations ranging from 0 to 2 mg/mL. Standards and samples were transferred in triplicate to a polystyrene 96-well plate followed by the addition of the assay reagents. The plate was then incubated at 37 °C for 30 min and monitored at 562 nm using a Versamax Tunable microplate reader (Molecular Devices, Sunnyvale, CA, USA) and Softmax Pro software.

2.5 SDS-PAGE and immunoblot analysis

Protein samples were separated by sodium dodecyl-sulphate polyacrylamide gel electrophoresis (SDS-PAGE) using 12% acrylamide gels. Gels were electrophoresed for 10 min at 90 V followed by an increase in voltage to 160 V for the remainder of the procedure. Protein was transferred from acrylamide gels to nitrocellulose membranes using a Trans-Blot Semi-dry transfer system (Bio-Rad, Mississauga, ON) for 25 min at 20 V. Transfer efficiency was assessed

by protein staining with Ponceau S (Sigma-Aldrich). Blots were incubated for 1 h in 5% skim milk (Carnation, Markham ON) in Tris buffered saline (20 mM Tris pH 7.5, 300 mM NaCl) with 0.1% Tween-20 (TBS-T; Sigma-Aldrich) to inhibit non-specific protein binding. The membranes were incubated with rabbit anti-HO-1 antibody (1:500; Enzo Life Sciences; Catalog no. BML-HC3001-100), rabbit anti-*Xenopus* HSP70 (1:350; commercially made against a 16 amino acid C-terminal peptide fragment of *X. laevis* HSP70B; Abgent, San Diego, CA, USA; Gauley et al., 2008), rabbit anti-*Xenopus* HSP30 (1:500; Fernando and Heikkila, 2003), rabbit anti-SOD1, (1:150 ; Genetex, Irvine CA; Catalog no. GTX13498), rabbit anti-Nrf2 (1:200 Abcam, Cambridge MA; Catalog no. 92946), rabbit anti-PRDX5 (1:500; Abcam; Catalog no. 86086) or rabbit anti-actin (1:200; Sigma; Catalog no. A2066) polyclonal antibodies and a mouse anti-α-tubulin monoclonal antibody (1:500; Sigma; Catalog no. T9026) diluted in 5% skim milk solution and left overnight. Membranes were then washed with TBS-T for 15 min and then twice for 10 min each followed by incubation with alkaline phosphatase-conjugated goat-anti-rabbit antibodies (BioRad) in TBS-T with 5% blocking for 1 h at 22 °C. Membranes were rinsed with TBS-T for 15 min followed by two 5 min rinses. Bands were then visualized by incubating blots in alkaline phosphatase detection buffer (100 mM Tris pH 9.5, 100 mM NaCl, 50 mM $MgCl_2$) with 0.3% nitro blue tetrazolium (Roche) and 0.17% 5-bromo-4-chloro-3-idolyl phosphate toluidine salt (Roche).

2.6 Densitometry

Densitometric analysis of immunoblots was performed using Image J software (Version 1.49; National Institute of Health; http://rsb.info.nih.gov/ij/) to quantify band intensity. The band intensity of each sample was expressed as a percentage of the maximum value for HO-1, HSP70,

HSP30 or SOD1 in a particular trial. The band intensities of Nrf2 and PRDX5 were expressed as a *n*–fold increase of the control band intensity. The percentages for a given treatment were averaged across three replicates and graphed. In studies where a consistent Standard error of the mean was indicated as vertical error bars. Significance ($p < 0.05\%$ or $p < 0.1\%$) between control and treatment intensity was determined using one-way ANOVA with Tukey's post hoc test.

2.7 Immunocytochemistry and laser scanning confocal microscopy (LSCM)

Cells for LSCM imaging were grown on flame sterilized base-washed coverslips in Petri dishes (VWR, Catalog no. 351029). Specifically, 22 x 22 mm glass coverslips (VWR; Catalog no. 48366-067) were washed with a base solution [49.5% (v/v) ethanol, 0.22 M NaOH] in small staining jars (Thomas Scientific Apparatus, Philadelphia, PA, USA) for 30 min and then rinsed with distilled water for 3 h. Cells were grown to 50% confluency prior to the addition of treatments to minimize the risk of over-confluency in LSCM images. Treatments were added to media then applied to Petri plates containing coverslips. Supplementation with additional agents was performed by adding the substance to already treated cells in Petri dishes followed by mixing by gentle agitation. Timing and concentration of treatments was as described in section 2.3. Following treatment, coverslips were rinsed with phosphate-buffered saline with magnesium and calcium (PBS; 1.37 M NaCl, 67 mM Na_2HPO_4, 26 mM KCl, 14.7 mM H_2PO_4, 1 mM $CaCl_2$, 0.5 mM $MgCl_2$ pH 7.4). Coverslips were then transferred to small Petri dishes and fixed with 3.7% paraformaldehyde (BDH Inc., Toronto, ON) in PBS for 15 min. Coverslips were washed three times for 5 min each and then permeabilized with 0.3% Triton X-100 (TX-100; Sigma-Aldrich) in PBS for 10 min. Coverslips were washed 3 times with PBS for 2 min each and then incubated in 3.7% BSA in PBS overnight at 4 °C. They were then incubated with a 1:250

dilution of rabbit anti-HO-1 primary antibody (or 1:500 anti-HSP30 or 1:250 anti-α-tubulin) in PBS w/ 3.7% BSA solution for 1 h at 22 °C. After incubation, the coverslips were washed 3 times with PBS and then incubated with a 1:2,000 dilution of fluorescent-conjugated goat anti-rabbit Alexa Fluor 488 secondary antibody (Invitrogen Molecular Probes, Carlsburg, CA) in PBS with 3.7% BSA for 30 min followed by 3 washes with PBS. For actin visualization, coverslips were incubated in PBS with 3.7% BSA containing a 1:60 dilution of rhodamine-tetramethylrhodamine-5-isothiocyanate phalloidin (TRITC; Invitrogen Molecular Probes) for 15 min. After washing, coverslips were allowed to dry and then mounted on glass slides using Vectashield mounting medium (Vector Laboratories, Burlingame CA) with 4, 6-diamidino-2-phenylindole (DAPI). Slides were sealed using clear nail polish and stored at 4 °C until viewed using a Zeiss Axiovert 200 confocal microscope with LSM 510 META software (Carl Zeiss Canada Ltd., Mississauga, ON).

2.8 CellRox Green oxidative stress detection assay

In experiments using CellRox Green, cells were grown on flame sterilized base-washed coverslips in Petri dishes (VWR, Catalog no. 351029). Cells were cultured on glass coverslips for 4 h with either media or media containing 25 μM hemin, 100 μM baicalein, 200 μM $CdCl_2$ or 10 mM BSO at 22 °C. One hour prior to fixation, CellRox Green dye was added to the cell media at a final concentration of 5 μM and kept in the dark. Coverslips were then transferred to small Petri dishes and fixed with 3.7% paraformaldehyde (BDH Inc. Toronto, ON). Coverslips were washed 3 times for 5 min each and then mounted on slides as previously described.

2.9 Proteostat aggregation assay

In experiments using the Proteostat aggresome detection kit (Enzo Life Sciences), cells were grown on flame sterilized base-washed coverslips in Petri dishes. Hemin, baicalein, $CdCl_2$ and the HO-1 enzyme activity inhibitors ZnPP and SnPP were applied as described in the cell treatment section 2.3. In experiments examining HO-1 enzyme activity inhibitor effects on cadmium-treated cells, cells were treated with ZnPP or SnPP for 4 h at 22 °C prior to supplementation with 50 μM $CdCl_2$ for 16 h at 22 °C. For cytoprotection studies, cells were cultured with baicalein or hemin and/or 15 μM SnPP for 4 h at 22 °C prior to supplementation with 275 μM $CdCl_2$ for 16 h, followed by a 4 h recovery in fresh media. Following treatment, coverslips were fixed, permeabilized and incubated in 3.7% BSA in PBS overnight at 4 °C as described above. They were then incubated with a 1:1000 dilution of Proteostat detection reagent in PBS containing 3.7% BSA solution for 1 h at 22 °C. They were then incubated with a 1:250 dilution rabbit anti-HO-1 primary antibody in PBS w/ 3.7% BSA solution for 1 h at 22 °C. Coverslips were washed 3 times with PBS and then incubated with a 1:2,000 dilution of fluorescent-conjugated goat anti-rabbit Alexa Fluor 488 secondary antibody (Invitrogen Molecular Probes) in PBS with 3.7% BSA for 30 min followed by 3 washes with PBS. Coverslips were allowed to dry and then mounted on glass slides as previously described.

2.10 Bioinformatic analysis

A multiple amino acid sequence alignment was performed with *X. laevis* (Genbank accession no NP_001089909.1), *X. tropicalis* (Genbank accession no XP_002934766.1) and *H. sapiens* HO-1 sequences using Clustal Omega (Version O.2.1; https://www.ebi.ac.uk/Tools/msa/clustalo/; Sievers et al., 2011). A multiple amino acid sequence

alignment using Clustal Omega was also carried out using representative sequences from mammals, fish, reptiles and birds. Three dimensional ribbon modelling of *X. laevis* (Genbank accession no NP_001089909.1) and *H. sapiens* HO-1 (Genbank accession no. NP_002124.1) was performed using the RaptorX prediction server. (http://raptorx.uchicago.edu; Källberg et al., 2012). Models were then converted into two-dimensional images using UCSF Chimera v.1.10.2 (https://www.cgl.ucsf.edu/chimera/; Pettersen et al., 2004). Analysis of the *Xenopus laevis ho-1* promoter region was performed using sequence data obtained from Xenbase (J-strain v 9.1; http://www.xenbase.org/, chr4L:107491000..107495999). This region was compared to the upstream region of the *H. sapiens ho-1* gene (NCBI; NC_000022.11). Putative *cis*-acting elements were identified based on corresponding elements found in the human *ho-1* promoter region (Kitamuro et al., 2003). Analysis was performed using the Serial Cloner v.2.6 software (http://serialbasics.free.fr/Serial_Cloner.html).

3.0 Results

3.1 Characterization of the heme oxygenase-1 (HO-1) amino acid sequence in *X. laevis*.

Stress-inducible HO-1 protein accumulation and function has been examined primarily in mammalian model systems including human, mouse, and rat (Alam et al., 2000; Balogun et al, 2003; Chen et al., 2011; Gonzales-Reyes et al., 2013; Detsika et al., 2015). In order to compare the properties of HO-1 in *X. laevis* cells to mammalian HO-1, a series of *in silico* analyses were carried out. Initially, a comparison of the percent identity of *X. laevis* HO-1 amino acid sequence (Genbank accession no. NP_001089909) with HO-1 sequences from an amphibian, *X. tropicalis*, and selected birds, mammals, reptiles, and fish was performed (Table I). While *X. laevis* HO-1 shared 91% identity with *X. tropicalis* HO-1, the percent identity with HO-1 from other animals ranged from 50 to 64%. Also the percent identity of *X. laevis* HO-1 with *H. sapiens* and *X. laevis* HO-2 were 62 and 53%, respectively. This initial analysis was followed by a more detailed comparison of *Xenopus* and *H. sapiens* HO-1 (Fig. 3). Using the well-studied human HO-1 amino acid sequence as a reference, *X. laevis* and *X. tropicalis* HO-1 were determined to have 8 heme-binding pocket residues (K21, T24, H28, Y137, G146, L150, K182, F210; indicated in red), which included an iron-binding histidine (H28; indicated with an arrow). A highly conserved HO-1 signature sequence described in other animal HO-1 proteins was also found in *X. laevis* (Maines and Gibbs, 2005). Fig. 3 also depicts a 14 amino acid sequence in human HO-1 (underlined) that is identical to *X. laevis* HO-1 that was used to generate an anti-HO-1 antibody (Enzo Life Sciences). This antibody was employed in this study to detect *Xenopus* HO-1 accumulation in immunoblot and immunocytochemical analyses.

In a further comparison of *H. sapiens* and *X. laevis* HO-1, three-dimensional ribbon models of these proteins were constructed using RaptorX 3D-dimensional structure prediction to

Table I

A comparison of *Xenopus laevis* HO-1 with selected HO-1 and HO-2 from other organisms.

Percent identity with *Xenopus laevis* HO-1 (NP_001089909.1)	(%)
X. tropicalis HO-1 (XP_002934766.1)	91
C. striatus HO-1 (XP_010195140.1)	64
G. gallus HO-1 (NP_990675.1)	63
A. cygnoides domesticus HO-1 (XP_013036532.1)	63
M. brandtii HO-1 (EPQ19396.1)	62
H. sapiens HO-1 (NP_002124.1)	61
M. musculus HO-1 (NP_037215.1)	59
A. carolensis HO-1 (XP_003220978.2)	61
G. japonicus HO-1 (XP_015265521.1)	60
P. mucrosquamatus HO-1 (XP_015687234.1)	56
D. rerio HO-1 (NP_001120988.1)	54
F. heteroclitus HO-1(XP_012723342.1)	54
C. carpio HO-1(AGI05156.1)	50
H. sapiens HO-2 (BAA04789.1)	62
X. laevis HO-2 (NP_001085675.1)	53

An amino acid sequence comparison of *Xenopus laevis* HO-1 with HO-1 sequences from the amphibian, *Xenopus tropicalis,* and selected birds, mammals, reptiles, and fish as well as HO-2 from *Xenopus laevis* and *Homo sapiens*. Genbank accession numbers are indicated within the brackets.

Figure 3. Alignment of *Xenopus laevis, Xenopus tropicalis* and *Homo sapiens* HO-1 amino acid sequences. Alignment of *X. laevis* (Genbank accession no NP_001089909.1), *X. tropicalis* (Genbank accession no XP_002934766.1) and *H. sapiens* HO-1 (Genbank accession no. NP_002124.1) was performed using Clustal Omega (http://www.ebi.ac.uk/Tools/msa/clustalo/; Sievers et al., 2011). Identical amino acids are denoted by asterisks. Conservative amino acid substitutions are represented by colons and semi-conservative by periods. Deletions are indicated by dashes in the amino acid sequence. Residues associated with the heme-binding pocket are coloured red while the iron-binding histidine is indicated with an arrow. The highly conserved HO-1 signature region is highlighted in grey. Amino acids forming the peptide used to generate the antibody to HO-1 (Enzo Life Sciences) are underlined.

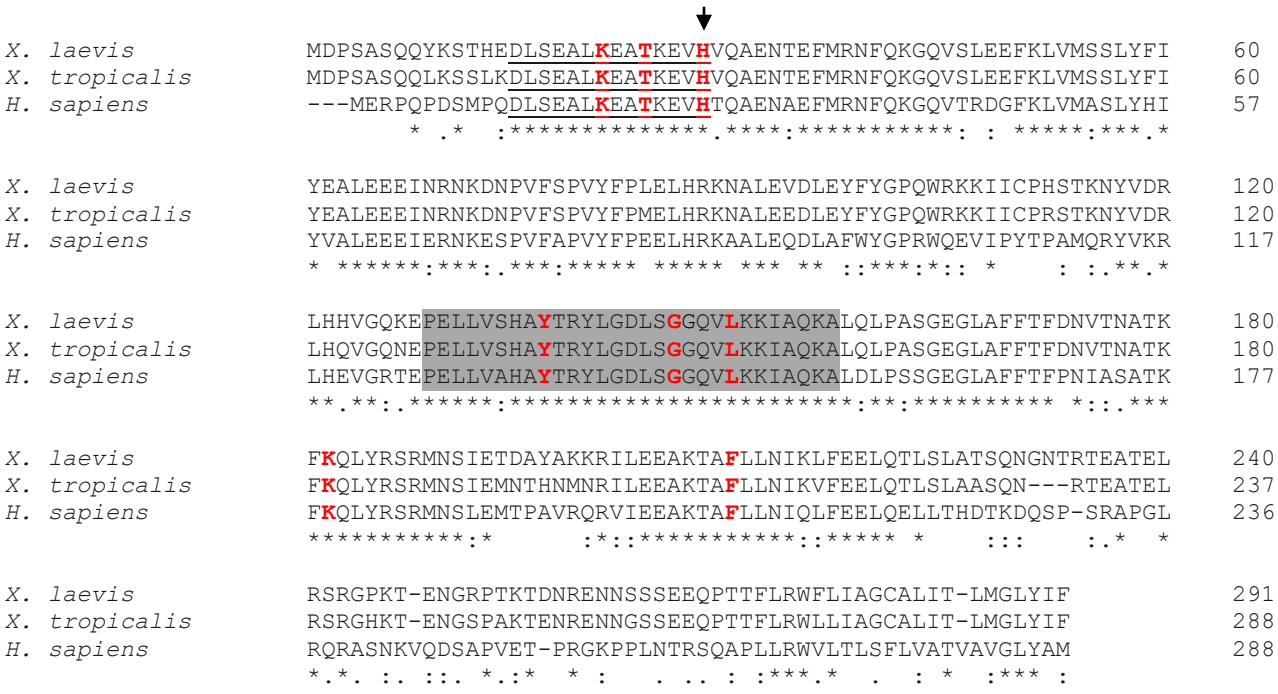
X. laevis MDPSASQQYKSTHEDLSEALKEATKEVHVQAENTEFMRNFQKGQVSLEEFKLVMSSLYFI 60
X. tropicalis MDPSASQQLKSSLKDLSEALKEATKEVHVQAENTEFMRNFQKGQVSLEEFKLVMSSLYFI 60
H. sapiens ---MERPQPDSMPQDLSEALKEATKEVHTQAENAEFMRNFQKGQVTRDGFKLVMASLYHI 57
X. laevis YEALEEEINRNKDNPVFSPVYFPLELHRKNALEVDLEYFYGPQWRKKIICPHSTKNYVDR 120
X. tropicalis YEALEEEINRNKDNPVFSPVYFPMELHRKNALEEDLEYFYGPQWRKKIICPRSTKNYVDR 120
H. sapiens YVALEEEIERNKESPVFAPVYFPEELHRKAALEQDLAFWYGPRWQEVIPYTPAMQRYVKR 117
X. laevis LHHVGQKEPELLVSHAYTRYLGDLSGGQVLKKIAQKALQLPASGEGLAFFTFDNVTNATK 180
X. tropicalis LHQVGQNEPELLVSHAYTRYLGDLSGGQVLKKIAQKALQLPASGEGLAFFTFDNVTNATK 180
H. sapiens LHEVGRTEPELLVAHAYTRYLGDLSGGQVLKKIAQKALDLPSSGEGLAFFTFPNIASATK 177
X. laevis FKQLYRSRMNSIETDAYAKKRILEEAKTAFLLNIKLFEELQTLSLATSQNGNTRTEATEL 240
X. tropicalis FKQLYRSRMNSIEMNTHNMNRILEEAKTAFLLNIKVFEELQTLSLAASQN---RTEATEL 237
H. sapiens FKQLYRSRMNSLEMTPAVRQRVIEEAKTAFLLNIQLFEELQELLTHDTKDQSP-SRAPGL 236
X. laevis RSRGPKT-ENGRPTKTDNRENNSSSEEQPTTFLRWFLIAGCALIT-LMGLYIF 291
X. tropicalis RSRGHKT-ENGSPAKTENRENNGSSEEQPTTFLRWLLIAGCALIT-LMGLYIF 288
H. sapiens RQRASNKVQDSAPVET-PRGKPPLNTRSQAPLLRWVLTLSFLVATVAVGLYAM 288

determine if there were any obvious structural differences between the two proteins (Fig. 4). While the interpretations that can be drawn from 3D structure predictions are limited, the two proteins appear to have similar structural features. Based on earlier structural analysis of HO-1 by Schuller et al. (1999), both human and *X. laevis* HO-1 have a hemin-binding pocket that was formed mainly by an alpha-helix containing the iron-binding histidine (red) and a second kinked alpha-helix present on the other side of the pocket. Both human and *Xenopus* models of HO-1 also show the presence of a membrane anchoring C-terminal helix along with a flexible linker region attached to the globular portion of the HO-1 enzyme.

3.2 Pattern of HO-1 accumulation in cells treated with hemin, baicalein or $CdCl_2$ exposure

The present study examined the effect of different concentrations of hemin, baicalein and $CdCl_2$ on HO-1 accumulation in *X. laevis* A6 cells by immunoblot and subsequent densitometric analysis. As shown in Fig. 5A, maximal levels of HO-1 occurred in cells incubated for 16 h with 25 μM hemin. Densitometric analysis revealed that while control cells had very low levels of HO-1, cells treated with 10, 15, 20 and 30 μM hemin displayed HO-1 levels that were 65%, 83%, 90%, and 94%, respectively, of peak values (Fig. 5B). HSP70 and HSP30 were not detectable at any of the hemin concentrations employed (data not shown). In cells treated with baicalein for 16 h, elevated levels of HO-1 were observed at 50 μM and 100 μM with peak levels at 200 μM while treatment at 400 μM resulted in a reduction to 60% of its peak value (Fig. 6). HSP70 and HSP30 accumulation was not detected in response to baicalein treatment (data not shown). Finally, treatment of cells with 200 μM $CdCl_2$ showed the highest levels of HO-1 accumulation (Fig. 7).

Figure 4. Comparison of *X. laevis* and *H. sapiens* HO-1 structure. The amino acid sequences of *X. laevis* (Genbank accession no NP_001089909.1) and *H. sapiens* HO-1 (Genbank accession no. NP_002124.1) were used to generate three-dimensional ribbon models of the *Xenopus* and human HO-1 protein (http://raptorx.uchicago.edu/StructurePrediction/predict/; Källberg et al., 2012). UCSF Chimera was used to visualize the models. Indicated on the models are residues associated with the heme-binding pocket (orange), the putative iron-binding histidine (red; also part of the heme-binding pocket), residues associated with the C-terminal transmembrane region (yellow), and the putative linker region (green).

Xenopus laevis
HO-1

Homo sapiens
HO-1

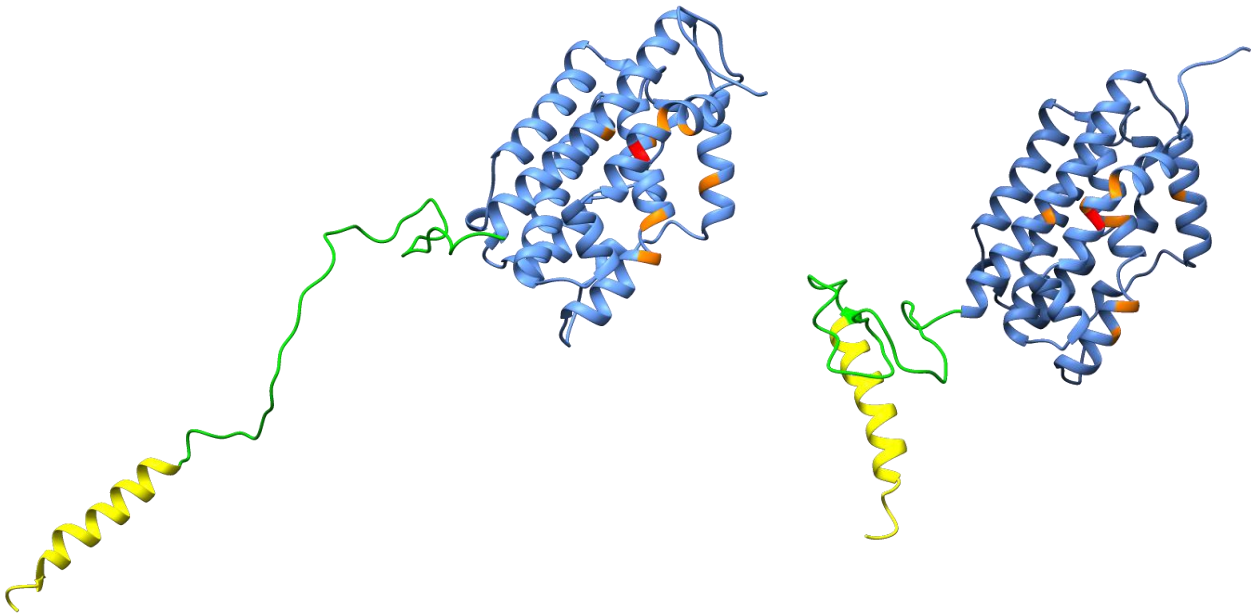

Iron-binding histidine

Heme-binding pocket

Putative linker region

C-Terminal membrane region

Figure 5. Effect of different concentrations of hemin on HO-1 accumulation. A) Cells were maintained, untreated at 22 °C (C) or treated with either 10, 15, 20, 25 or 30 μM of hemin or 50 μM of $CdCl_2$ for 16 h at 22 °C. Proteins were isolated and used to generate an immunoblot using anti-HO-1 and anti-actin antibodies as described in Materials and methods (a representative immunoblot is shown). Bands for HO-1 and actin were detected at 32 kDa and 42 kDa respectively. $CdCl_2$ was used as a positive control since it was previously shown to induce accumulation of HO-1 in A6 cells (Music et al., 2014). B) Densitometric analysis of HO-1 accumulation. The results were expressed as % mean relative density in comparison to the maximum band density obtained for HO-1 (25 μM hemin). Standard error was indicated by the vertical bars. A one-way ANOVA and a Tukey's post-hoc test was used to determine significance ($p < 0.05$), as represented by an asterisk, between control cells and treated cells. These data are representative of 3 separate experiments.

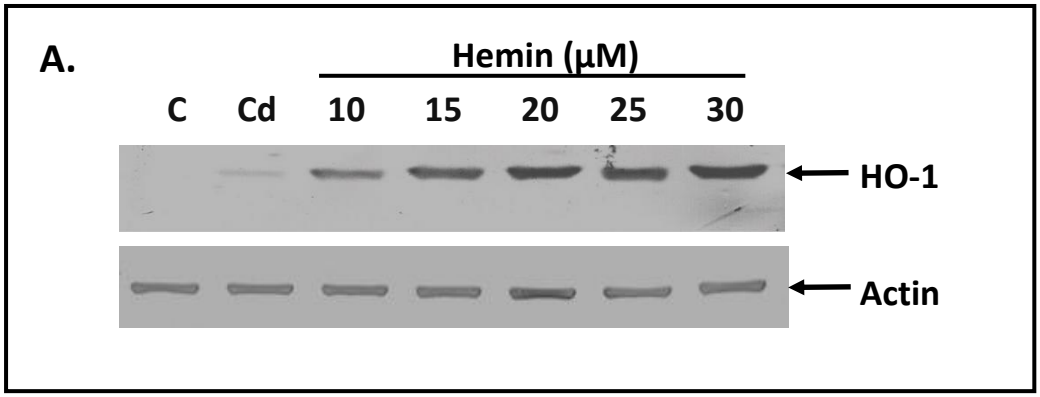
A.
Hemin (μM)
C
Cd
10
15
20
25
30
HO-1
Actin

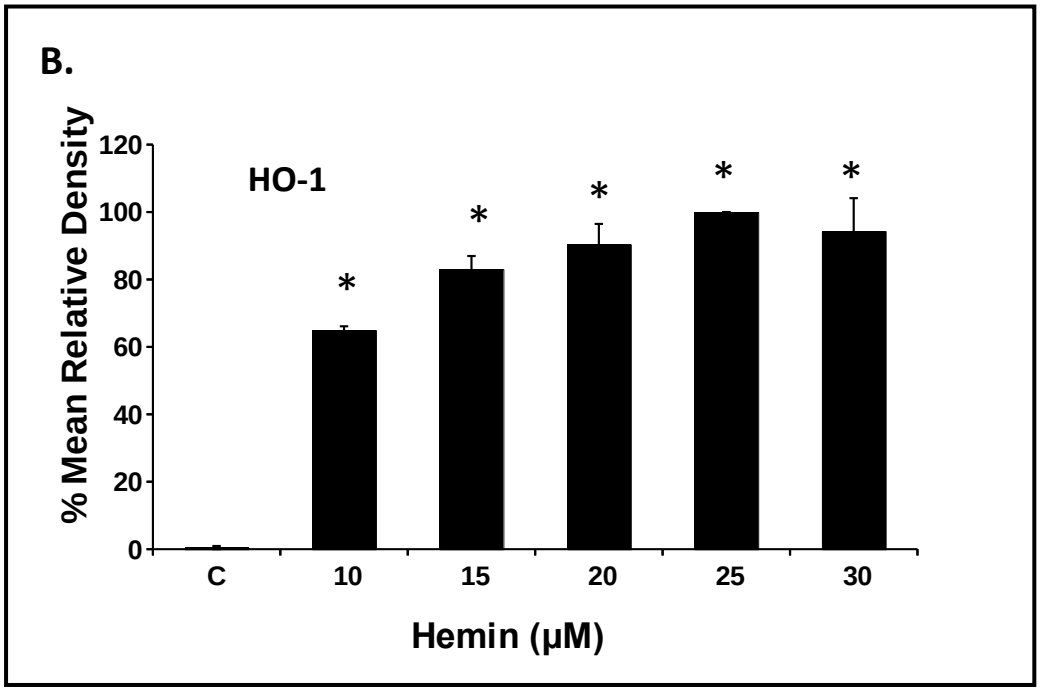
B.
HO-1
% Mean Relative Density
120
100
80
60
40
20
0
C
10
15
20
25
30
Hemin (μM)
*

Figure 6. Concentration-dependent accumulation of HO-1 in response to baicalein treatment. A) Cells were maintained, untreated at 22 °C (C) or treated with 50, 100, 200 or 400 μM of baicalein for 16 h at 22 °C. Immunoblot analysis of isolated proteins employed anti-HO-1 and anti-actin antibodies. B) Densitometric analysis of HO-1 accumulation was performed as described in Materials and methods. The results were expressed as % mean relative density compared to the maximum density (200 μM baicalein) as indicated in the legend of Figure 3. The error bars indicate standard error of the mean while the significance ($p < 0.05$) compared to control was determined by the one-way ANOVA test and Tukey's post-hoc test and represented by an asterisk. These data are representative of 3 separate experiments.

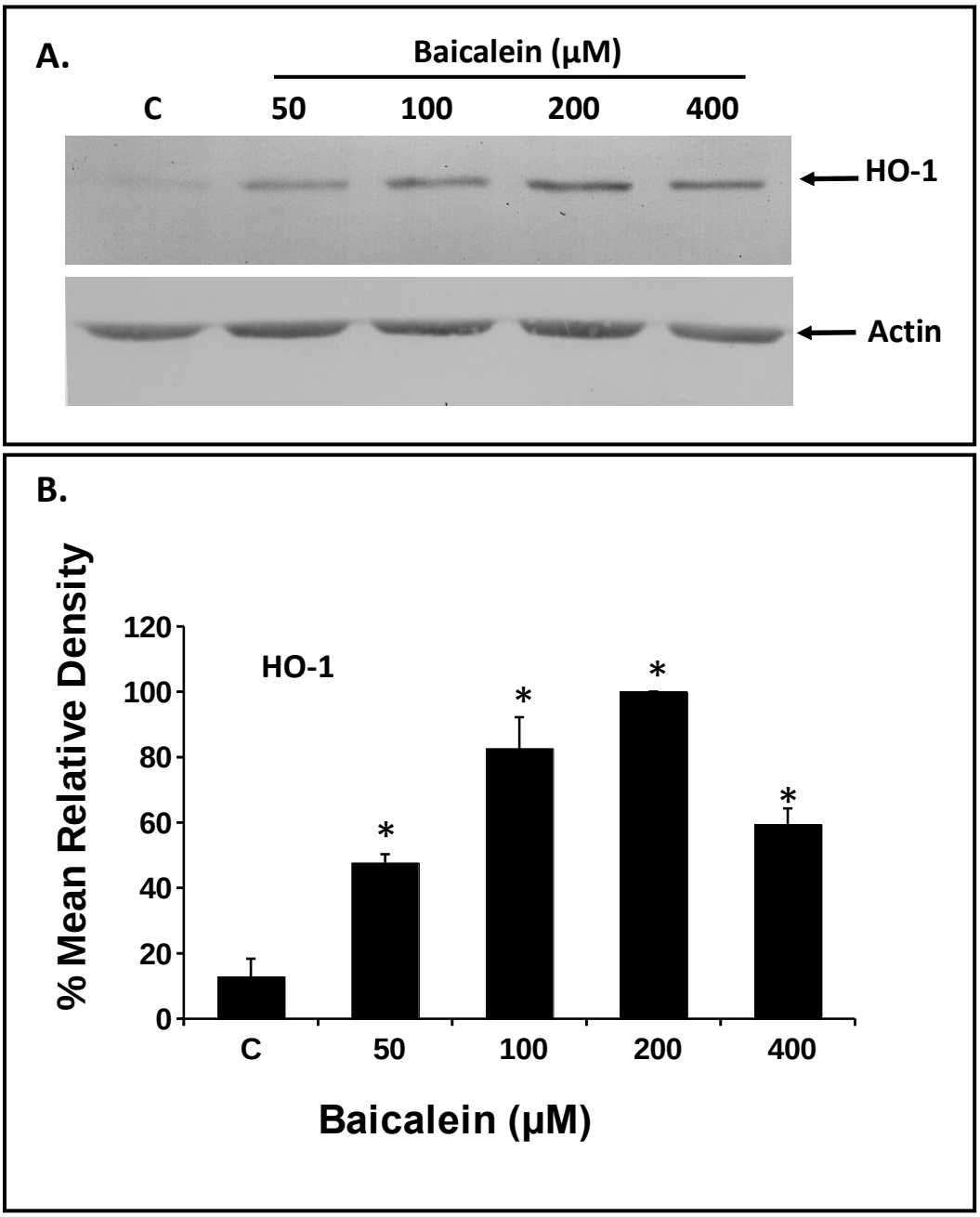
A.
Baicalein (μM)
C
50
100
200
400
HO-1
Actin
B.
% Mean Relative Density
HO-1
120
100
80
60
40
20
0
*
*
*
*
C
50
100
200
400
Baicalein (μM)

Figure 7. Effect of different concentrations of $CdCl_2$ on HO-1, HSP70 and HSP30 accumulation. A) Cells were maintained, untreated at 22 °C (C) or treated with 25, 50, 100 or 200 μM of $CdCl_2$ (Cd) for 16 h at 22 °C. A. Immunoblot analysis was performed as stated in the Materials and methods employing anti-HO-1, anti-HSP70 (detected at 70 kDa), anti-HSP30 (detected at ~24 kDa) and anti-actin antibodies as described in Materials and methods. B) Densitometric analysis of HO-1 (black), HSP70 (grey) and HSP30 (white) accumulation. The results were expressed as % mean relative density of each protein in comparison to the maximum density (HO-1, HSP70 and HSP30 at 200 μM $CdCl_2$). The error bars indicate standard error of the mean while the significance ($p < 0.05$) compared to control was determined by the one-way ANOVA test and Tukey's post-hoc test and represented by an asterisk. These data are representative of 3 separate experiments.

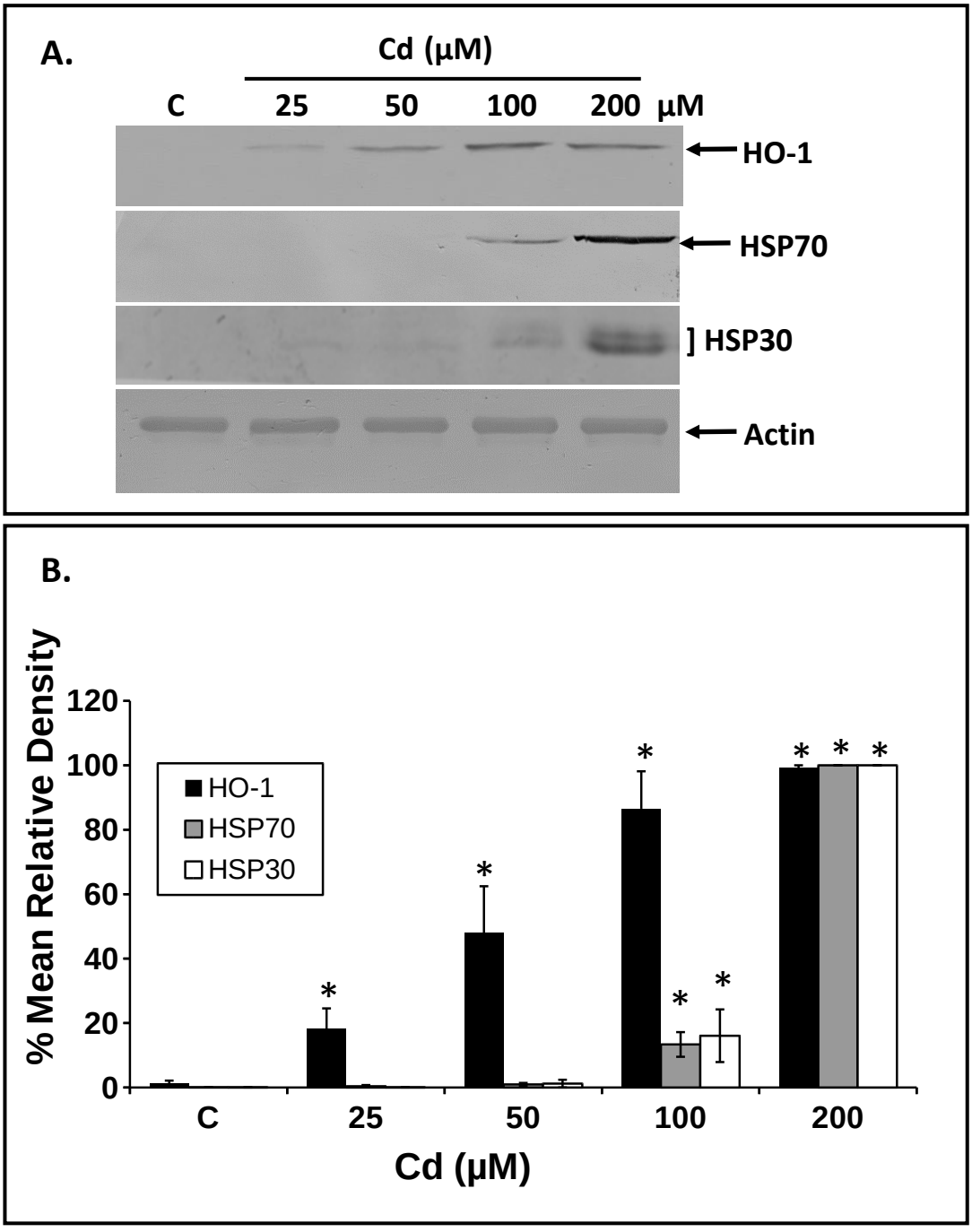
A.
Cd (μM)
C
25
50
100
200 μM
HO-1
HSP70
] HSP30
Actin
B.
% Mean Relative Density
120
100
80
60
40
20
0
HO-1
HSP70
HSP30
C
25
50
100
200
Cd (μM)

Cells treated with 25, 50 or 100 μM $CdCl_2$ resulted in HO-1 levels that were 18%, 48% and 88%, respectively, of peak levels at 200 μM. In contrast to hemin and baicalein, $CdCl_2$ treatment also induced the accumulation of HSP70 and HSP30. Inducible levels of HSP30 and HSP70 were observed with 25 μM and 100 μM $CdCl_2$, respectively, with the highest levels at 200 μM. These findings were consistent with previous studies in our laboratory examining the effect of $CdCl_2$ on HO-1, HSP70 and HSP30 levels in our laboratory (Woolfson and Heikkila, 2009; Khamis and Heikkila, 2013; Music et al., 2014). Finally, the relative levels of actin remained constant in A6 cells treated with different concentrations of hemin, baicalein or $CdCl_2$.

Time course experiments revealed temporal-dependent increases in hemin-, baicalein- and $CdCl_2$ -induced HO-1 accumulation. For example, in cells treated with 25 μM hemin, significant accumulation of HO-1 was detected at 8 h followed by an increase to its peak amount at 12 h (Fig. 8A). Decreased levels of $CdCl_2$ -induced HO-1 accumulation were observed at 16, 24 and 48 h, which had levels of 73%, 40% and 22%, respectively, compared to the peak value at 12 h (Fig. 8B). In cells incubated with 100 μM baicalein, maximum levels of HO-1 were detected at 16 h (Fig. 9A). Relative to peak values of baicalein-induced HO-1, lower amounts were observed at 12 h (48%) and 24 h (51%) time points (Fig. 9B). In 200 μM $CdCl_2$ -treated cells, the highest levels of HO-1, HSP70 and HSP30 were observed at 24 h, the final time point (Fig. 10A). HO-1 and HSP70 were first detected at 8 h having 14% and 42% of peak values, respectively, followed by a further enhancement to 70% and 89%, respectively, at 16 h (Fig. 10B). A statistically significant accumulation of HSP30 (62%) compared to 24 h levels was first detected at 16 h. The levels of actin remained constant in all of the time course experiments with hemin, baicalein and $CdCl_2$.

In recovery experiments, the relative levels of HO-1 were examined in cells treated with

Figure 8. Time course of HO-1 accumulation in response to hemin. A) Cells were maintained at 22 °C for 16 h (C) or were incubated with 25 μM hemin and harvested after 4, 8, 12, 16, 24 or 48 h at 22 °C. Isolated proteins were examined by immunoblot analysis using anti-HO-1 and anti-actin antibodies. B) Densitometric analysis of HO-1 accumulation. The results were expressed as % mean relative density compared to maximum density (12 h time point) as indicated in the legend of Figure 3. The error bars indicate standard error of the mean while the significance ($p < 0.05$) compared to control was determined by the one-way ANOVA test and Tukey's post-hoc test and represented by an asterisk. These data are representative of 3 separate experiments.

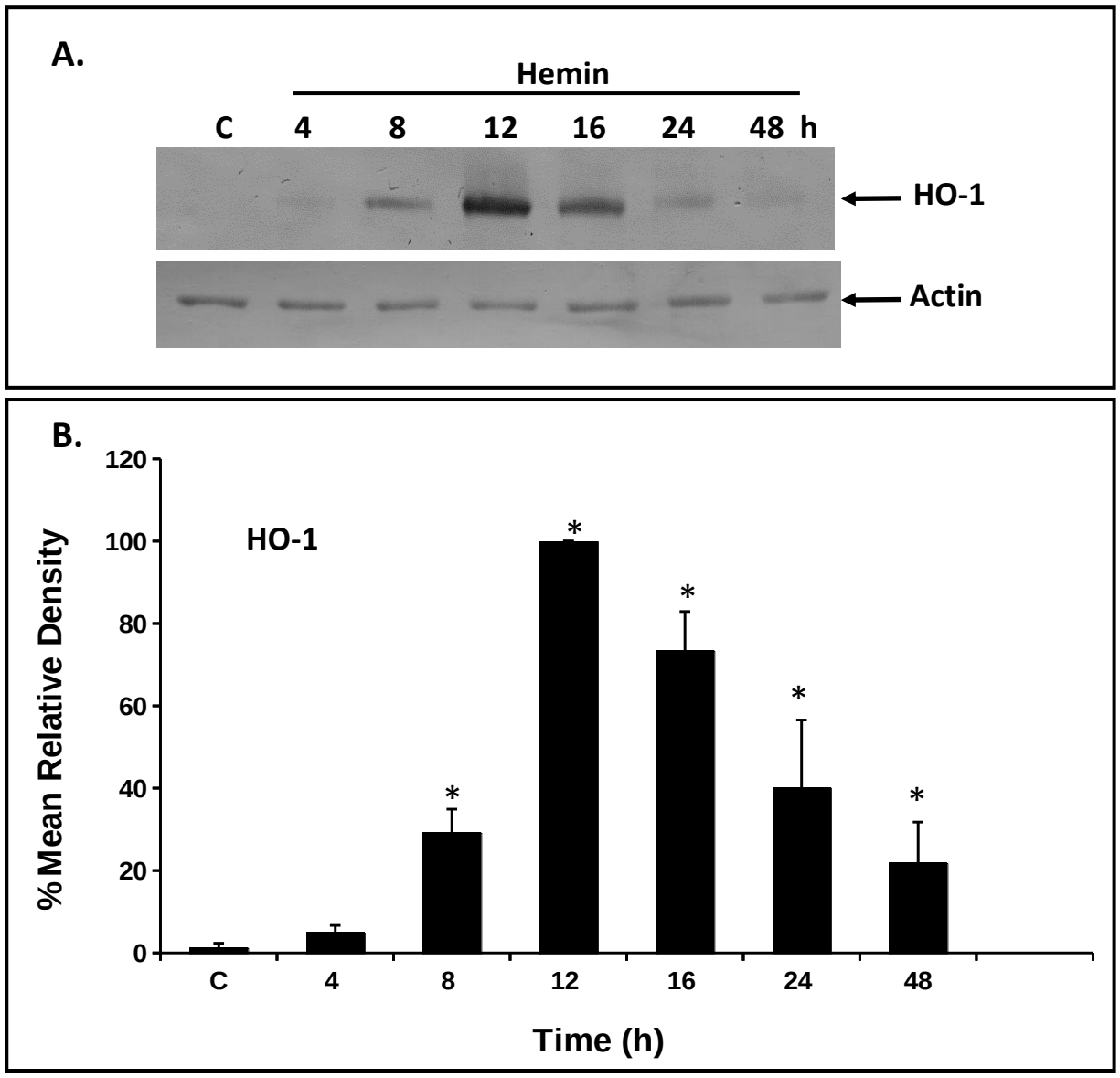
A.
Hemin
C 4 8 12 16 24 48 h
HO-1
Actin
B.
HO-1
% Mean Relative Density
120
100
80
60
40
20
0
C 4 8 12 16 24 48
Time (h)

Figure 9. Temporal pattern of HO-1 accumulation in response to 100 μM baicalein. A) Cells were maintained at 22 °C (C) or were treated with 100 μM baicalein and harvested after 4, 8, 12, 16 or 24 h. Proteins were isolated and assessed by immunoblot analysis using anti-HO-1 and anti-actin antibodies. B) Densitometric analysis of HO-1 accumulation. The results were expressed as % mean relative density compared to maximum density (16 h) as indicated in the legend of Figure 3. The error bars indicate standard error of the mean while the significance ($p < 0.05$) compared to control was determined by the one-way ANOVA test and Tukey's post-hoc test and represented by an asterisk. These data are representative of 3 separate experiments.

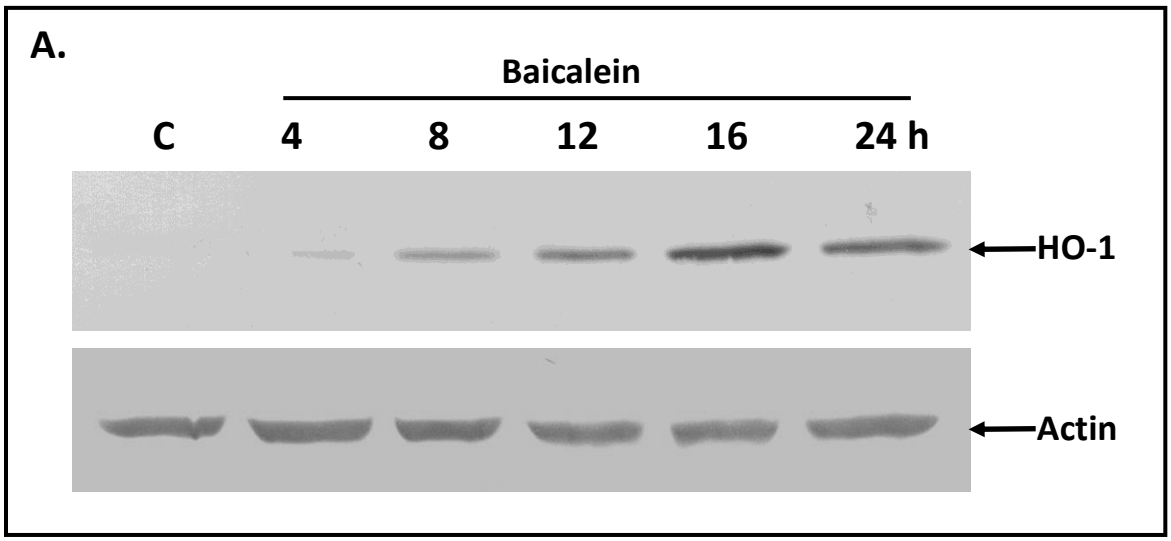
A.
Baicalein
C
4
8
12
16
24 h
HO-1
Actin

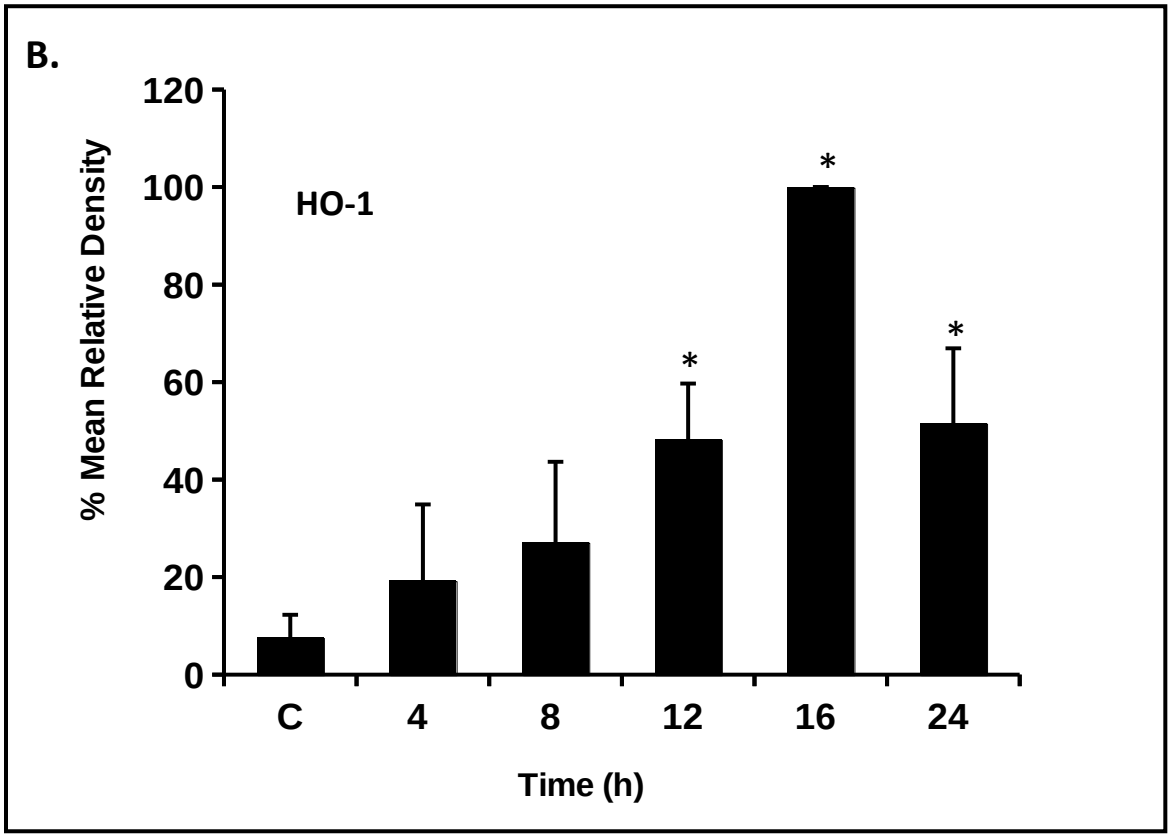
B.
HO-1
% Mean Relative Density
120
100
80
60
40
20
0
C
4
8
12
16
24
Time (h)
*
*
*

Figure 10. Time course of $CdCl_2$-induced HO-1, HSP70 and HSP30 accumulation. A) Cells were either maintained at 22 °C (C) or were treated with 200 μM $CdCl_2$ (Cd) and then harvested after 4, 8, 16 or 24 h. Isolated proteins were subjected to immunoblot analysis as stated in the Materials and methods employing anti-HO-1, anti-HSP70, anti-HSP30 and anti-actin antibodies. B) Densitometric analysis of HO-1 (black), HSP70 (grey) and HSP30 (white) accumulation. The results were expressed as % mean relative density compared to maximum density (HO-1, HSP30 and HSP70 at 24 h). The error bars indicate standard error of the mean while the significance ($p < 0.05$) compared to control was determined by the one-way ANOVA test and Tukey's post-hoc test and represented by an asterisk. These data are representative of 3 separate experiments.

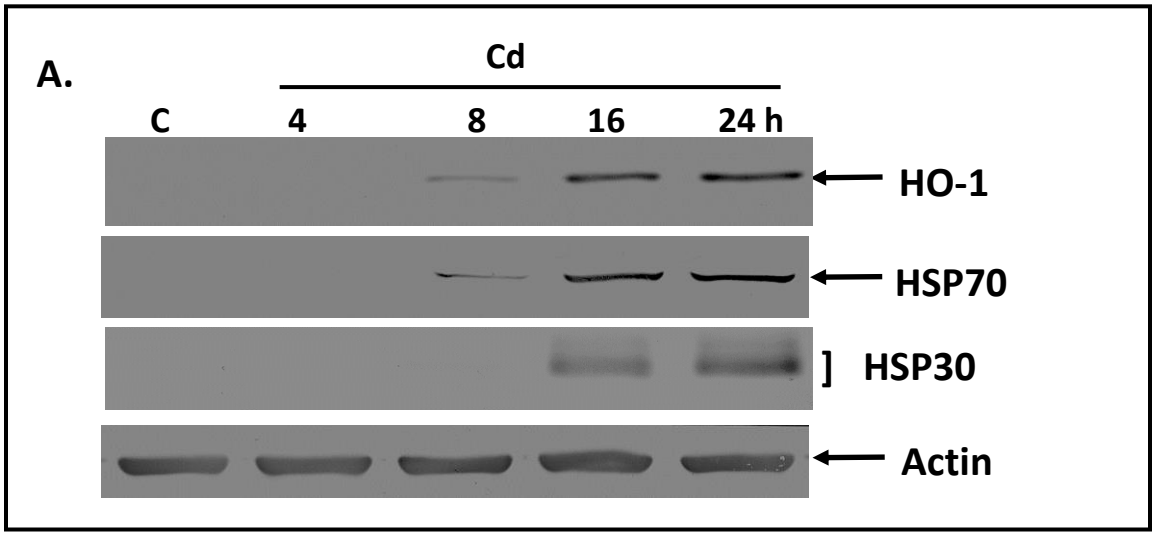
A.
Cd
C
4
8
16
24 h
HO-1
HSP70
] HSP30
Actin

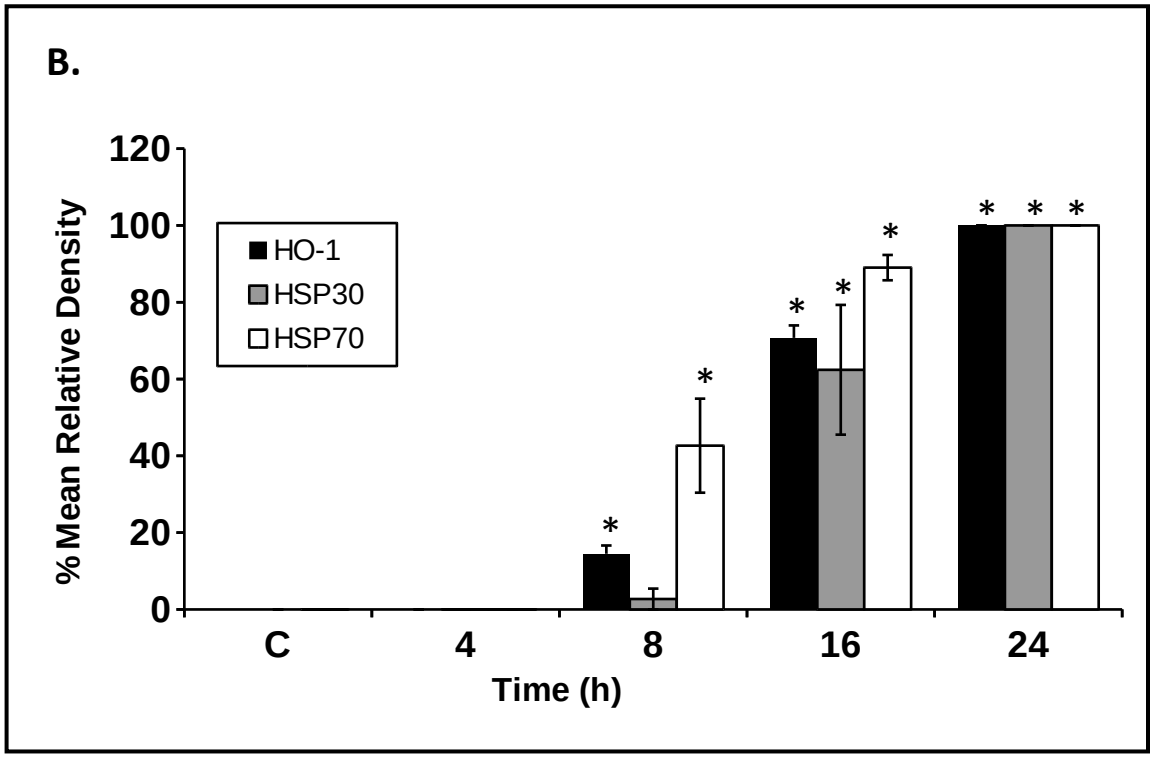
B.
% Mean Relative Density
120
100
80
60
40
20
0
HO-1
HSP30
HSP70
C
4
8
16
24
Time (h)

either 25 μM hemin or 100 μM baicalein for 16 h followed by recovery for up to 72 h in fresh media. As indicated in Fig. 11, the relative levels of hemin-induced HO-1 gradually declined with recovery time to 9% of the levels observed in cells with no recovery. In a similar experiment with baicalein, the relative levels of HO-1 declined to a value of 16% at 72 hcompared to the levels found in baicalein-treated cells with no recovery (Fig. 12). The gradual decreases in HO-1 levels during recovery from hemin or baicalein treatment contrasts with previous studies in our laboratory showing that cells recovering from $CdCl_2$ displayed a spike in HO-1 levels during recovery in fresh media (Music et al., 2014).

3.3 Immunocytochemical analysis of HO-1 and HSP30 localization and actin and tubulin cytoskeletal structure in hemin-, baicalein- and $CdCl_2$-treated cells.

Immunocytochemical analysis was employed to examine the intracellular localization of HO-1 in response to hemin, baicalein and $CdCl_2$ treatment (Fig. 13 to 15). In control cells, the accumulation of HO-1 was either not detectable or present at relatively low levels. After 10 μM hemin treatment, HO-1 was present in the perinuclear region in a punctate pattern with some staining in the nucleus (Fig. 13). Cells treated with 25 μM hemin showed a more intense accumulation of HO-1 but had a similar cell staining pattern to 10 μM hemin. Similar results with respect to HO-1 localization were observed with 100 and 200 μM baicalein as well as 50 and 100 μM $CdCl_2$ (Fig. 14 and 15). Additionally this pattern of perinuclear HO-1 accumulation in a puncate pattern with some staining in the nucleus remained consistent in a series of time course experiments from 8 or 12 h to 24 h of treatment with 25 μM hemin, 100 μM baicalein or 200 μM $CdCl_2$ (Fig. 16-18). While HSP30 was not detected in response to 25 μM hemin or 200 μM baicalein, incubation with 200 μM $CdCl_2$ induced the accumulation of HSP30 in the

Figure 11. HO-1 accumulation during recovery from hemin treatment. A) Cells were maintained at 22 °C for 16 h (C) or were incubated with media containing 25 μM hemin for 16 h, which was then replaced with fresh media. Cells were harvested after incubation in fresh media for 0, 4, 8, 12, 24, 48 or 72 h at 22 °C. Proteins were isolated and examined by immunoblot analysis using anti-HO-1 and anti-actin antibodies. B) Densitometric analysis of HO-1 accumulation. The results were expressed as % mean relative density compared to maximal density (0 h recovery) as indicated in the legend of Figure 3. The error bars indicate standard error of the mean while the significance ($p < 0.05$) compared to control was determined by the one-way ANOVA test and Tukey's post-hoc test and represented by an asterisk. These data are representative of 3 separate experiments.

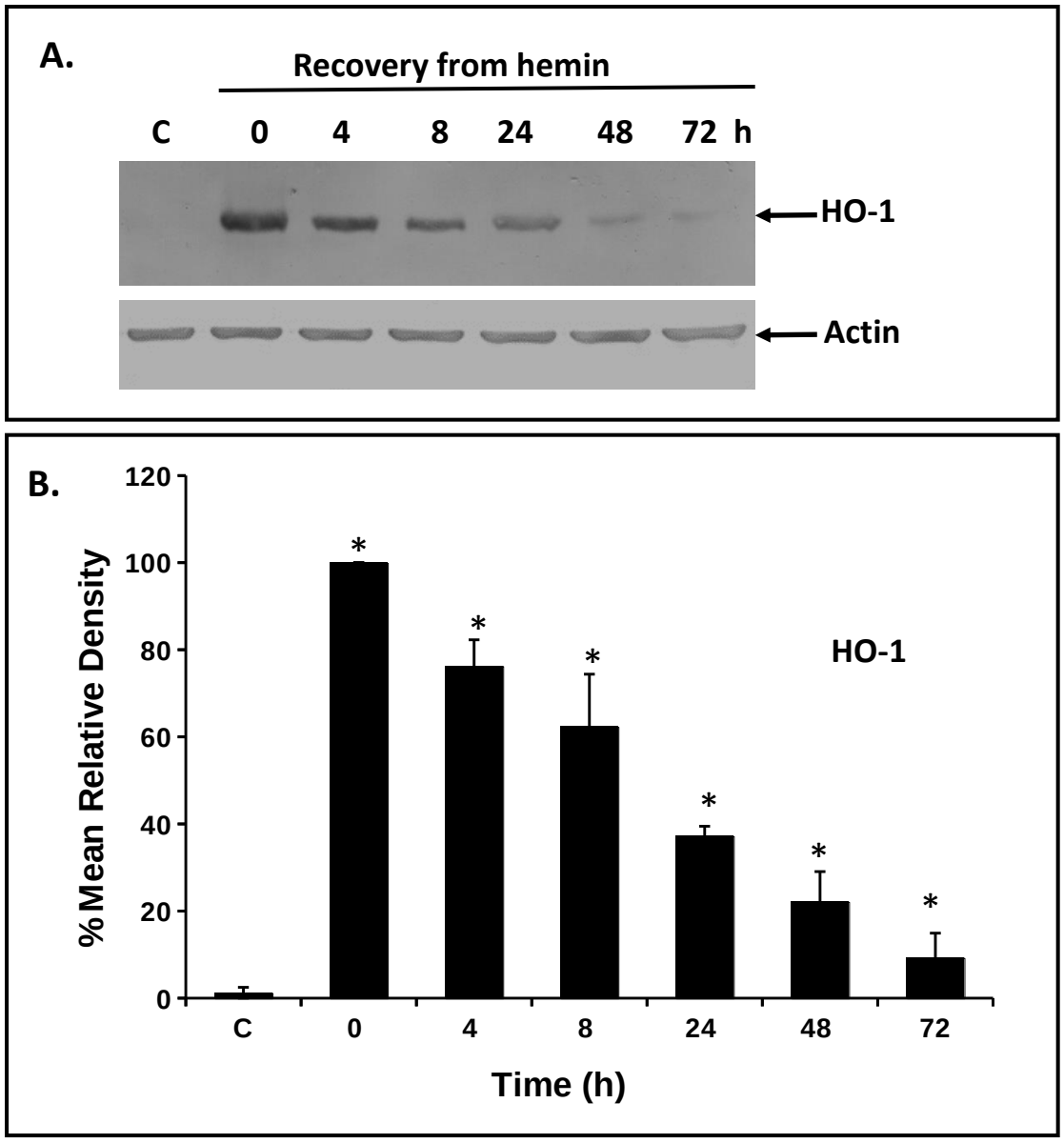
A.
Recovery from hemin
C
0
4
8
24
48
72 h
HO-1
Actin
B.
% Mean Relative Density
120
100
80
60
40
20
0
HO-1
C
0
4
8
24
48
72
Time (h)

Figure 12. Temporal pattern of HO-1 accumulation during recovery from baicalein treatment. A) Cells were maintained at 22 °C for 16 h (C) or incubated with media containing 100 μM baicalein for 16 h followed by replacement with fresh media and incubated at 22 °C. Cells were harvested after 0, 24, 48 or 72 h of recovery. Immunoblot analysis using anti-HO-1 and anti-actin antibodies was conducted on isolated proteins. B) Densitometric analysis of HO-1 accumulation. The results were expressed as % mean relative density (0 h recovery) as indicated in the legend of Figure 3. The error bars indicate standard error of the mean while the significance ($p < 0.05$) compared to control was determined by the one-way ANOVA test and Tukey's post-hoc test and represented by an asterisk. These data are representative of 3 separate experiments

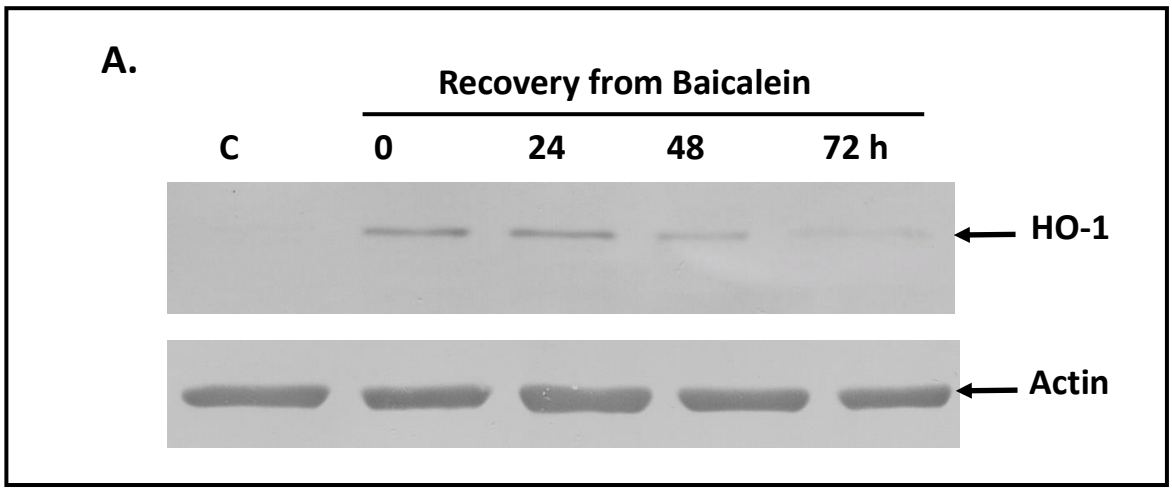
A.
Recovery from Baicalein
C
0
24
48
72 h
HO-1
Actin

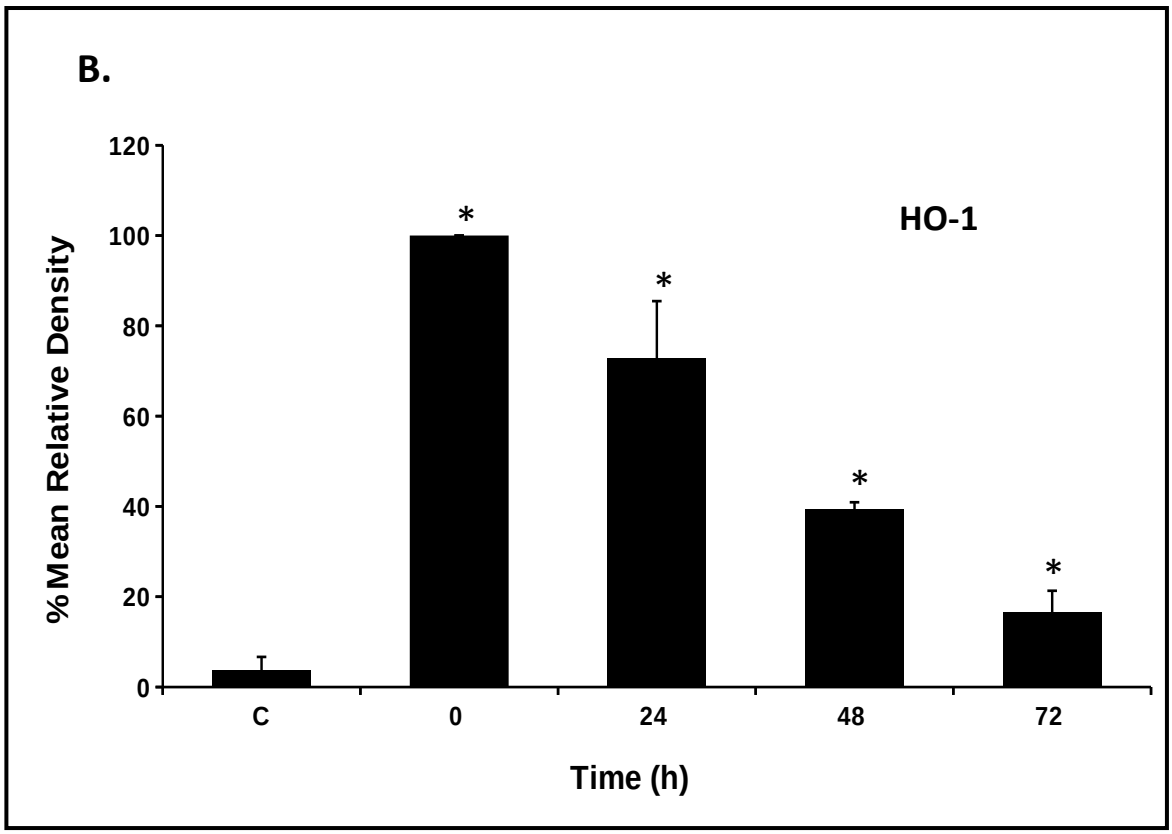
B.
HO-1
% Mean Relative Density
120
100
80
60
40
20
0
*
*
*
*
C
0
24
48
72
Time (h)

Figure 13. Localization of HO-1 in cells treated with hemin. Cells were cultured on glass coverslips for 16 h at 22 °C with either media (C) or media containing 10 or 25 μM hemin (HM). Nuclei and actin filaments were stained directly using DAPI (blue) and rhodamine phalloidin (red), respectively. HO-1 was detected with an anti-HO-1 antibody and the secondary antibody conjugate, Alexa-488 fluorophore (green). White 10 μm scale bars are indicated in the lower right corner of each panel. From left to right are columns showing actin, HO-1 and merged detection channels These results are representative of at least 3 separate experiments.

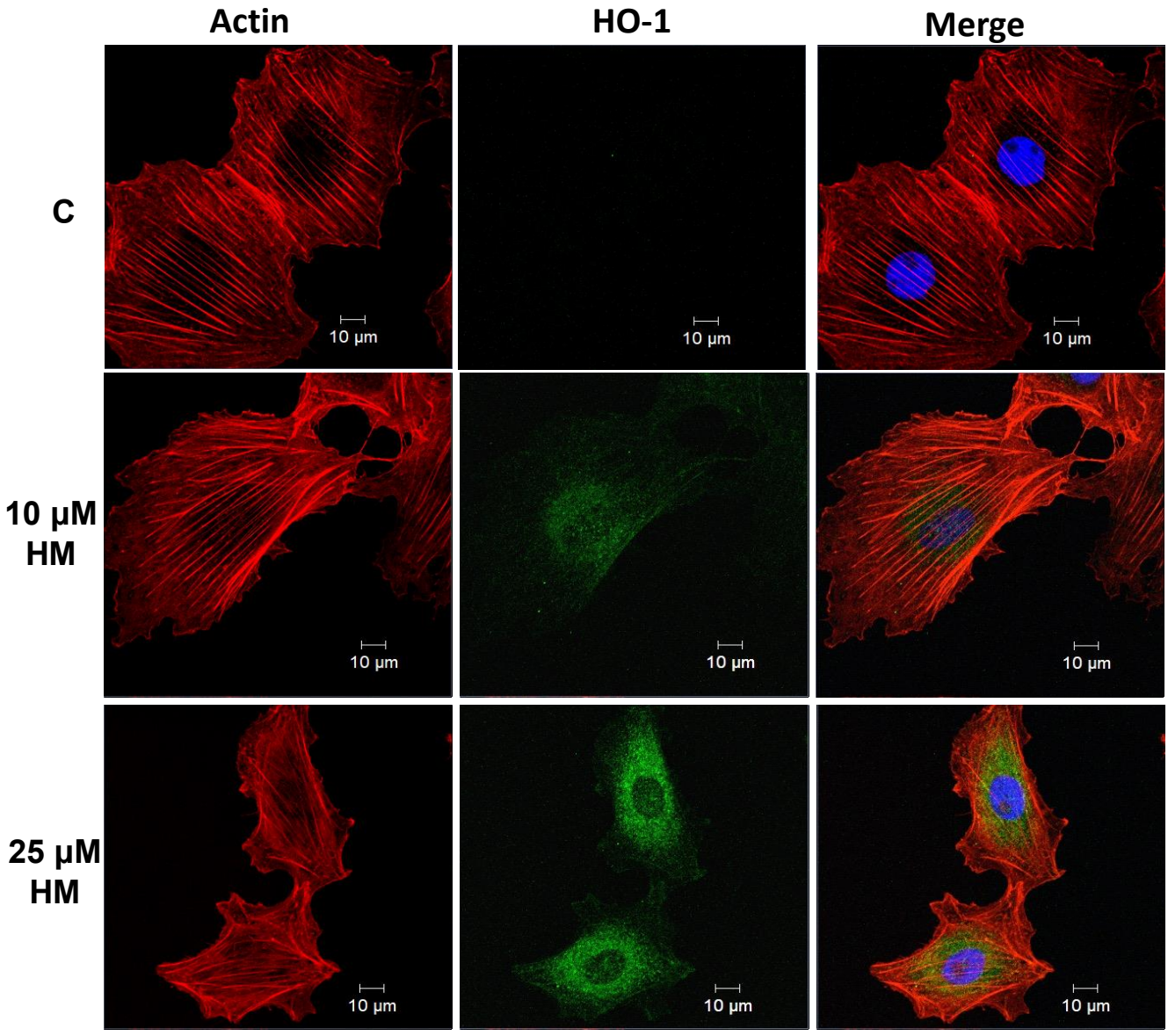
Actin
HO-1
Merge
C
10 µM HM
25 µM HM
10 µm

Figure 14. Accumulation and distribution of HO-1 in baicalein-treated cells. Cells were cultured on glass coverslips for 16 h at 22 °C with either media (C) or media containing 100 or 200 μM baicalein (BC). Nuclei and actin filaments were stained directly using DAPI (blue) and rhodamine phalloidin (red), respectively. HO-1 was detected with an anti-HO-1 antibody and the secondary antibody conjugate, Alexa-488 fluorophore (green). White 10 μm scale bars are indicated in the lower right corner of each panel. These results are representative of at least 3 separate experiments.

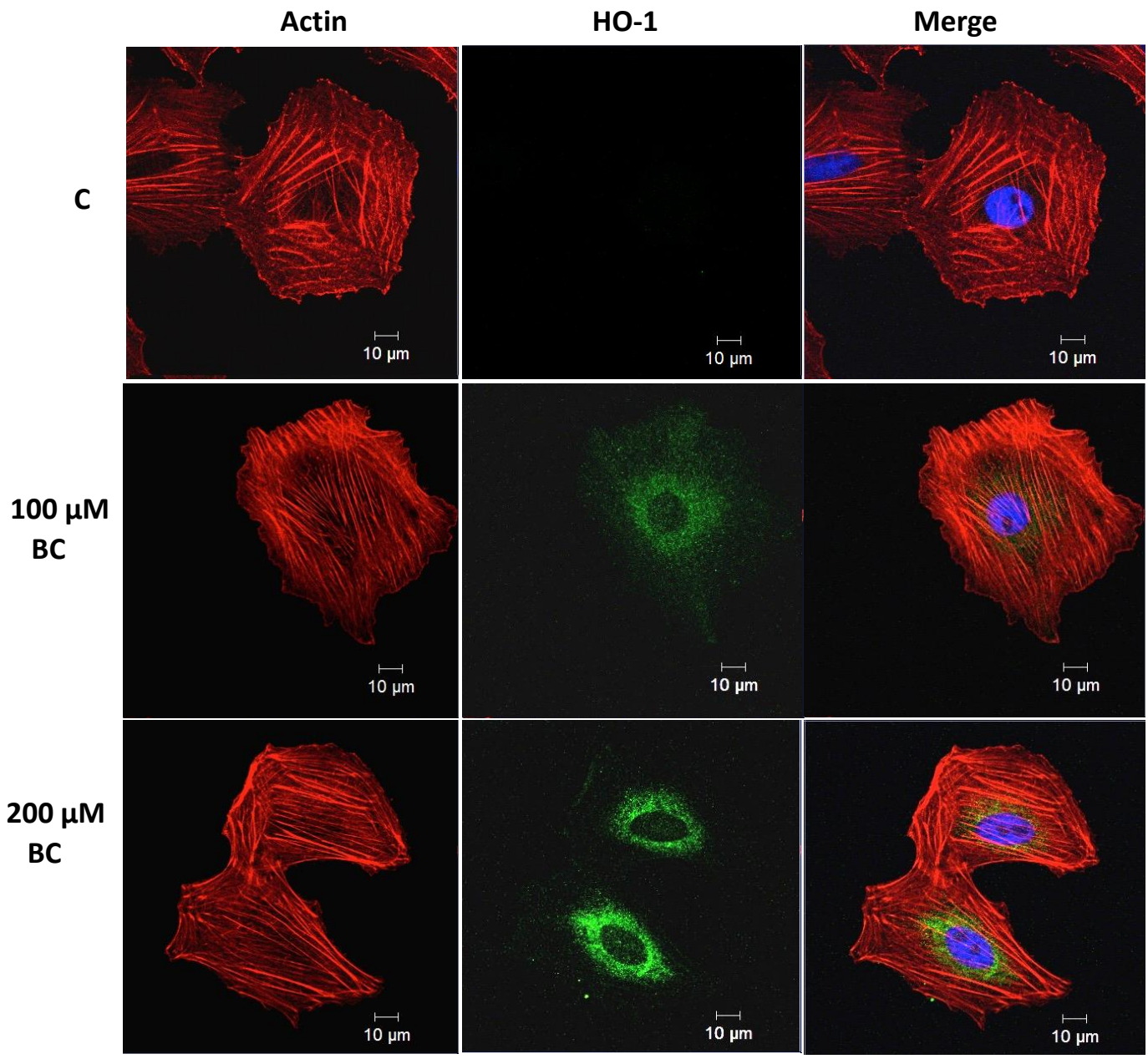
Actin
HO-1
Merge
C
100 µM BC
200 µM BC
10 µm

Figure 15. HO-1 localization in cells treated with $CdCl_2$. Cells were cultured on glass coverslips for 16 h at 22 °C with either media (C) or media containing 50 or 100 μM $CdCl_2$ (Cd). Nuclei and actin filaments were stained directly using DAPI (blue) and rhodamine phalloidin (red), respectively. HO-1 was detected with the anti-HO-1 antibody and the secondary antibody conjugate, Alexa-488 fluorophore (green). White 10 μm scale bars are indicated in the lower right corner of each panel. These results are representative of at least 3 separate experiments.

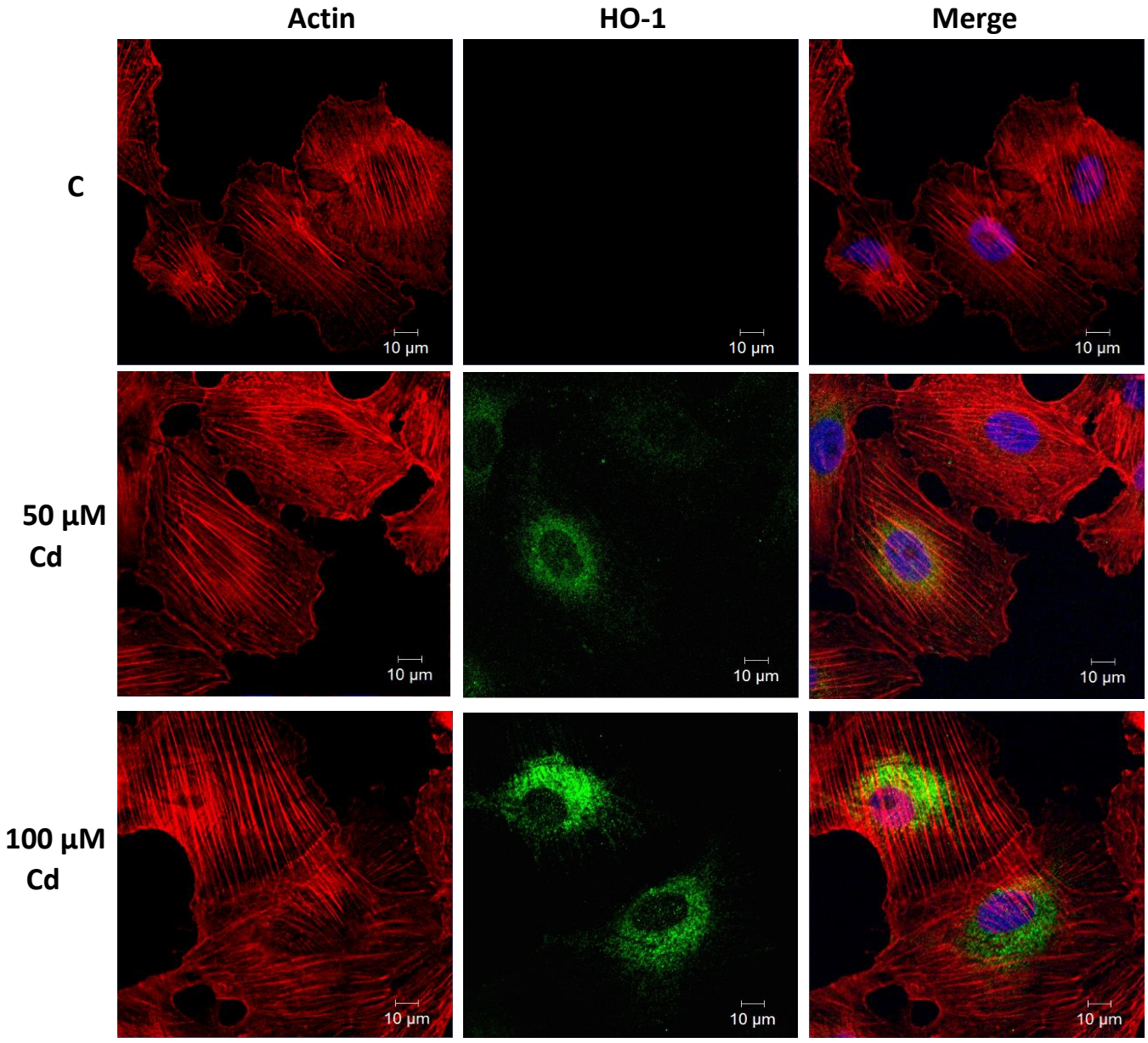
Actin
HO-1
Merge
C
50 µM Cd
100 µM Cd
10 µm

Figure 16. Time course of HO-1 localization in cells treated with hemin. Cells were cultured on glass coverslips for 16 h at 22 °C with either media (C) or media containing 25 μM hemin for 12, 16 or 24 h. HO-1 was detected with an anti-HO-1 antibody and the secondary antibody conjugate, Alexa-488 fluorophore (green). Actin filaments were stained with rhodamine phalloidin (red) and nuclei using DAPI (blue). White 10 μm scale bars are indicated in the lower right corner of each panel. These results are representative of at least 3 separate experiments.

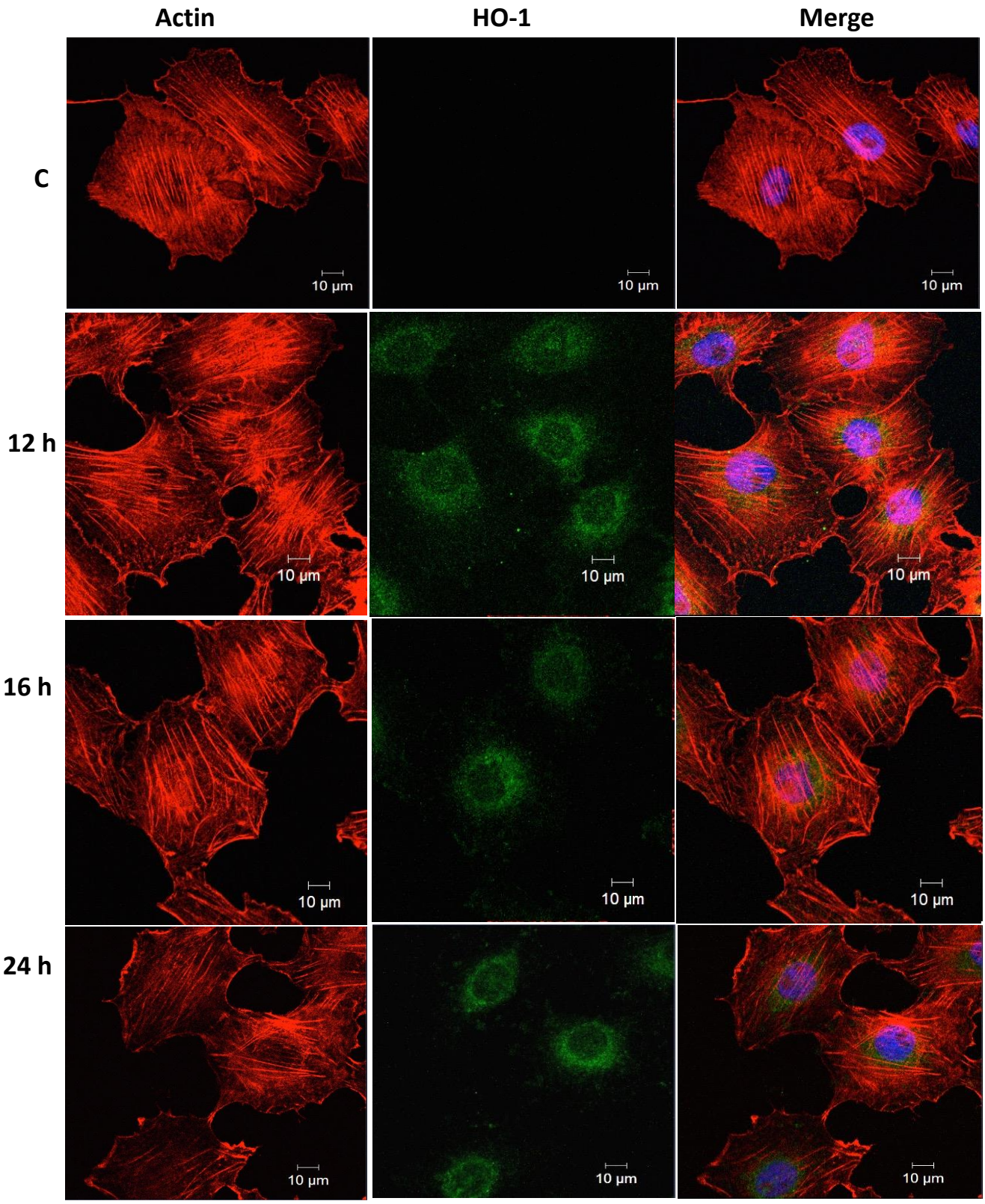
Actin
HO-1
Merge
C
12 h
16 h
24 h
10 μm

Figure 17. Temporal pattern of HO-1 localization in cells treated with baicalein. Cells were cultured on glass coverslips for 16 h at 22 °C with either media (C) or media containing 100 μM baicalein for 12, 16 or 24 h. HO-1 was detected with an anti-HO-1 antibody and the secondary antibody conjugate, Alexa-488 fluorophore (green). Actin filaments were stained with rhodamine phalloidin (red) and nuclei using DAPI (blue). White 10 μm scale bars are indicated in the lower right corner of each panel. These results are representative of at least 3 separate experiments.

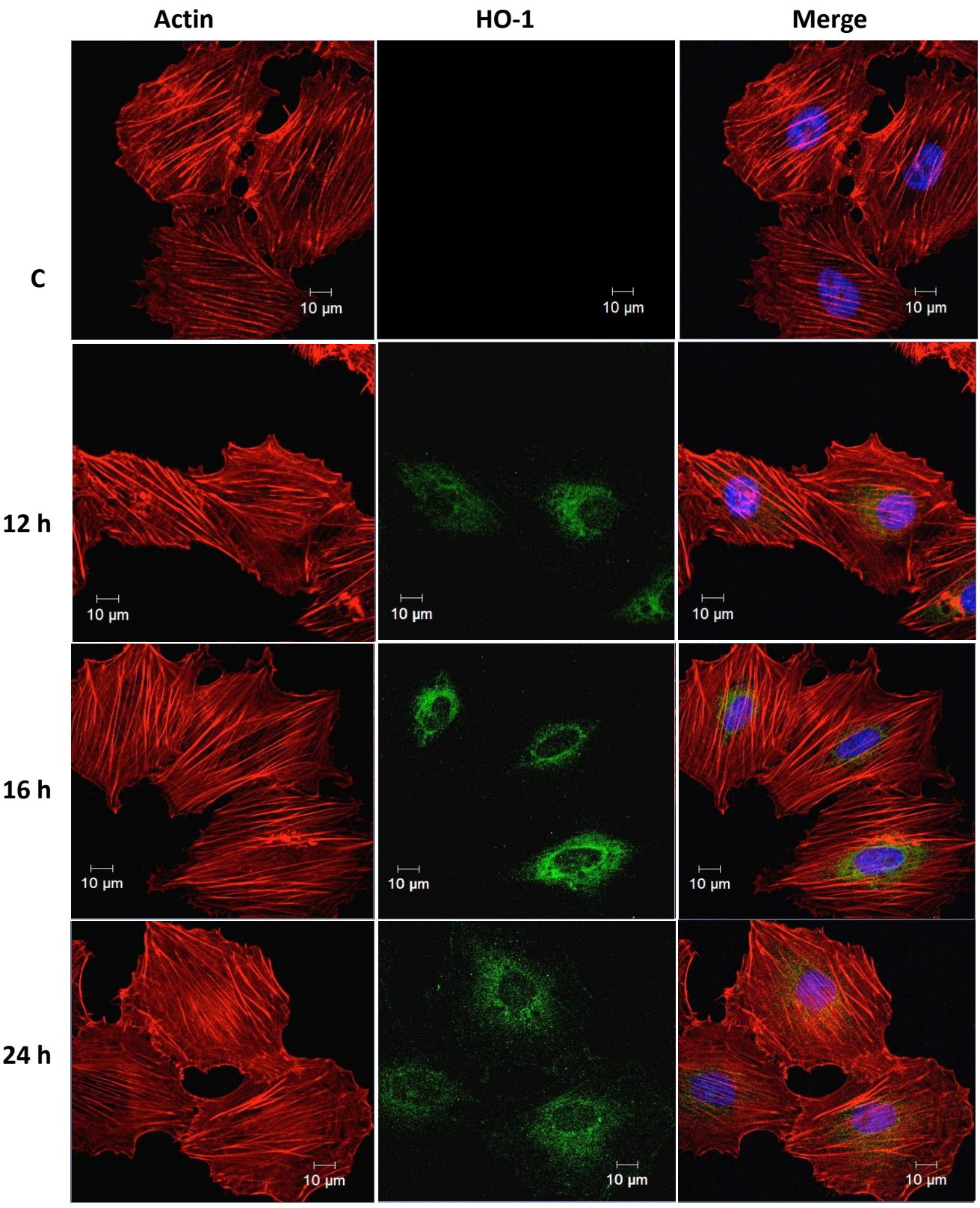
Actin
HO-1
Merge
C
12 h
16 h
24 h
10 μm

Figure 18. Time course of HO-1 localization in cells treated with $CdCl_2$. Cells were cultured on glass coverslips for 16 h at 22 °C with either media (C) or media containing 200 μM $CdCl_2$ for 8, 16 or 24 h. HO-1 was detected with an anti-HO-1 antibody and the secondary antibody conjugate, Alexa-488 fluorophore (green). Rhodamine phalloidin (red) and DAPI (blue) were used to stain actin filaments and nuclei directly. White 10 μm scale bars are indicated in the lower right corner of each panel. These results are representative of at least 3 separate experiments.

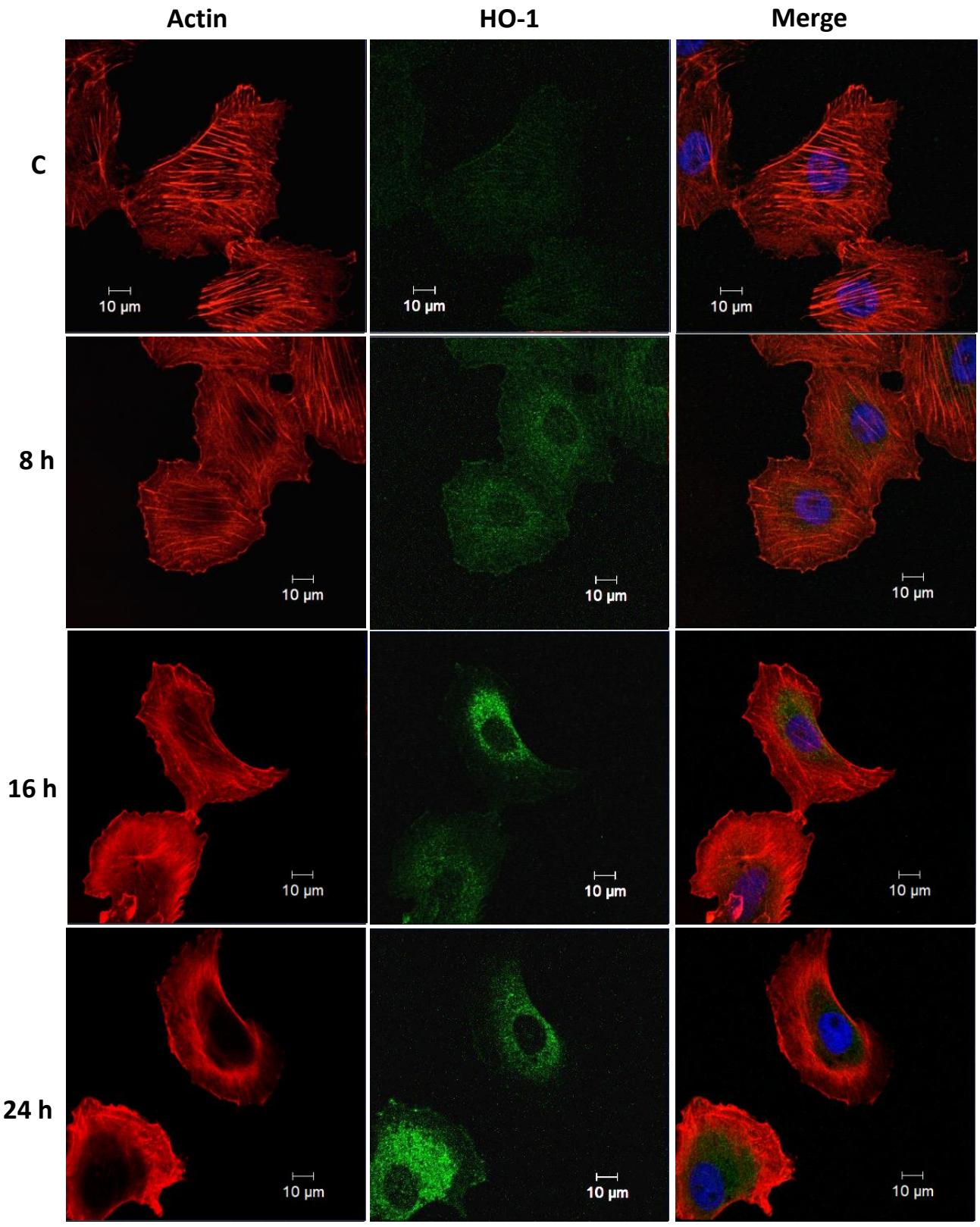
Actin
HO-1
Merge
C
8 h
16 h
24 h
10 µm

perinuclear region in a granular fashion with some larger staining structures (indicated with white arrows; Fig. 19).

Actin stress fibres, as detected using phalloidin staining, were generally control-like inexperiments using 10 μM hemin or 100 μM baicalein, although a slight disorganization of actin filaments was observed with higher concentrations of these agents including 25 μM hemin and 200 μM baicalein (Fig. 13, 19). Actin fibres were also control-like in cells treated with $CdCl_2$ concentrations of 100 μM or less (Fig 15). However, treatment of cells with concentrations of 200 μM $CdCl_2$ resulted in disorganization of actin fibres and membrane ruffling after 12 h (Fig. 19, 20). Compared to control cells, the microtubule structure, as detected by anti-α-tubulin antibody staining, was not markedly affected by 25 μM hemin or by 200 μM baicalein treatment. In contrast, treatment of cells with 200 μM $CdCl_2$ resulted in some microtubule network disorganization including a coalescence of anti-α-tubulin antibody staining fibres (Fig. 20).

3.4. Effect of transcriptional and translational inhibitors on hemin- and baicalein-induced HO-1 accumulation.

Hemin- and baicalein-induced HO-1 accumulation in A6 cells was the result of de novo transcription and translation (Fig. 21). Treatment with 2 or 5 μg/mL of the transcriptional inhibitor, actinomycin D, suppressed the 25 μM hemin- or 200 μM baicalein-induced accumulation of HO-1 to near control levels with no marked effect on actin levels. Furthermore, treatment of cells with 100 μM of the translational inhibitor, cycloheximide, prevented hemin- and baicalein-induced accumulation of HO-1. Previous studies in our laboratory have demonstrated that $CdCl_2$-induced accumulation of HO-1 was inhibited by actinomycin D or cycloheximide treatment (Music et al., 2014).

Figure 19. Effect of hemin, baicalein or $CdCl_2$ on HSP30 localization of HSP30. Cells were cultured on glass coverslips for 16 h at 22 °C. Cells were left untreated (C) or incubated with 25 μM hemin (HM) 200 μM baicalein (BC) or 200 μM $CdCl_2$ (Cd). Rabbit anti-HSP30 antibody and an anti-rabbit antibody conjugated to an Alexa-488 fluorophore were used to detect HSP30 (green). Nuclei and actin filaments were stained directly using DAPI (blue) and rhodamine phalloidin (red), respectively. Large anti-HSP30 staining structures in the perinuclear region are indicated with a white arrow. White 10 μm scale bars are indicated in the lower right of each panel. These results are representative of at least 3 separate experiments.

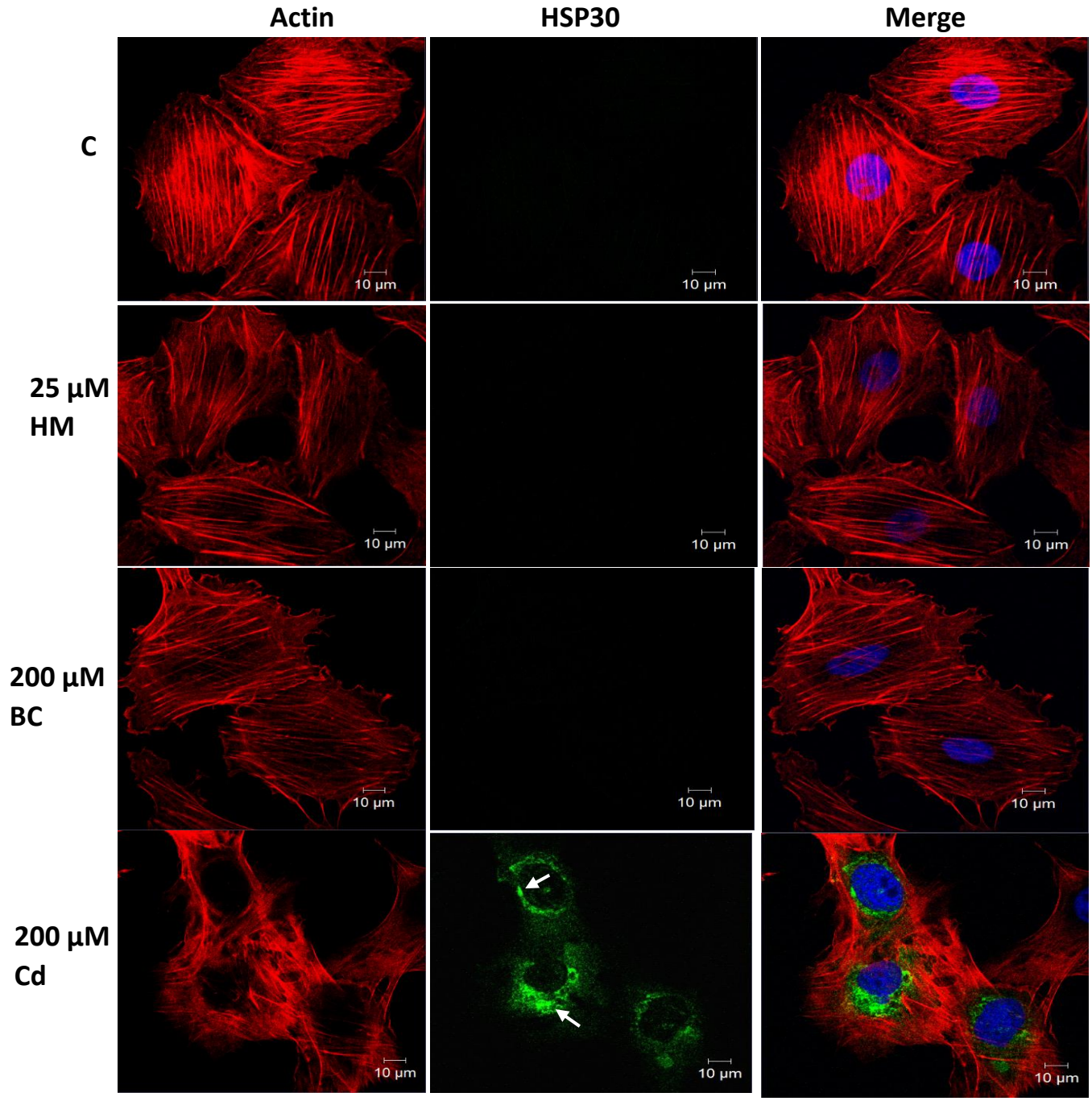
Actin
HSP30
Merge
C
25 µM HM
200 µM BC
200 µM Cd
10 µm

Figure 20. Effect of hemin, baicalein or $CdCl_2$ treatment on the actin and tubulin cytoskeleton. Cells were cultured on glass coverslips for 16 h at 22 °C. Cells were left untreated (C) or incubated with 25 μM hemin (HM) 200 μM baicalein (BC) or 200 μM $CdCl_2$ (Cd). Alpha-tubulin was detected using a mouse anti-α-tubulin antibody and an anti-mouse antibody conjugated to an Alexa-488 fluorophore (green). Actin filaments were stained directly using rhodamine phalloidin (red) while nuclei were stained with DAPI (blue). White 10 μm scale bars are indicated in the lower right of each panel. These results are representative of at least 3 separate trials.

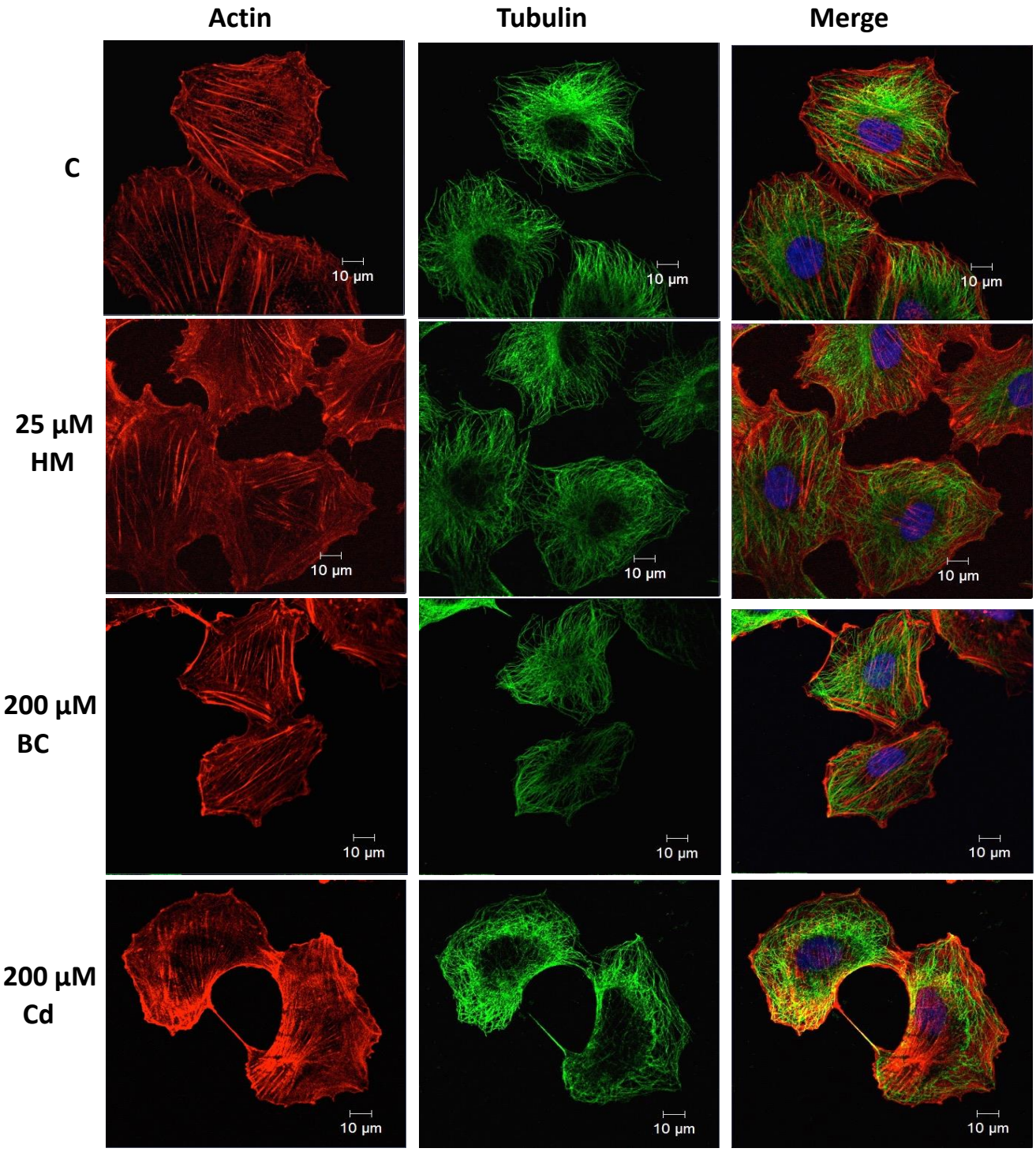
Actin
Tubulin
Merge
C
25 µM HM
200 µM BC
200 µM Cd
10 µm

Figure 21. Effect of actinomycin D and cycloheximide on hemin- and baicalein-induced HO-1 accumulation. A) Cells were maintained at 22 °C (C) or were treated with or without 2 or 5 μg/ml actinomycin D for 30 min prior to supplementation with 25 μM hemin or 200 μM baicalein for 16 h at 22 °C and then harvested. B) Cells were maintained at 22 °C (C) or were treated with or without a 6 h pretreatment using 100 μM cycloheximide followed by supplementation with 25 μM hemin or 200 μM baicalein for 16 h. After the different sets of treatments, proteins were isolated and subjected to immunoblot analysis using anti-HO-1 and anti-actin antibodies. These data are representative of 2 separate experiments.

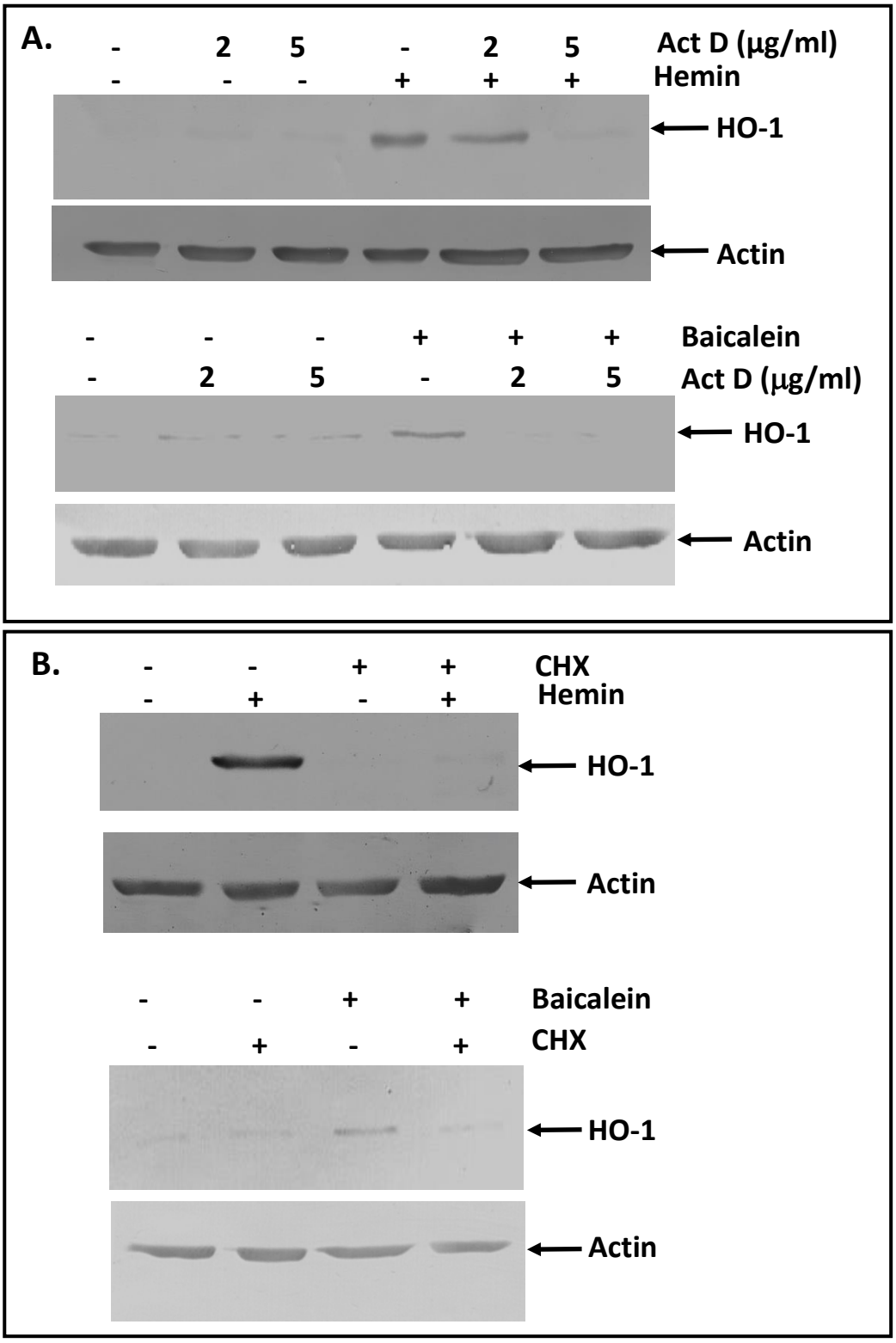
A.
- 2 5 - 2 5 Act D (μg/ml)
- - - + + + Hemin
HO-1
Actin
- - - + + + Baicalein
- 2 5 - 2 5 Act D (μg/ml)
HO-1
Actin
B.
- - + + CHX
- + - + Hemin
HO-1
Actin
- - + + Baicalein
- + - + CHX
HO-1
Actin

3.5. Identification of Nrf2 and HSF1 transcription factor binding sites in the 5' regulatory region of the *X. laevis ho-1* gene

In order to help identify possible mechanisms that may be responsible for triggering HO-1 accumulation in response to hemin or baicalein treatment of A6 cells, putative transcription factor binding sites in the 5' regulatory region of *X. laevis ho-1* gene were identified using Xenbase online sequence data and the Serial Cloner sequence analysis tool (Fig. 22). Two potential maf recognition elements (MARE), MARE (1) and MARE (2) were located at -1788 and -2589, respectively, upstream of the HO-1 transcriptional start site. MARE (1) also had an adjacent cadmium-responsive element (CdRE) at -1807. Finally, a heat shock element (HSE) was found at position -613 that had a 100% identity to the HSE consensus sequence (Amin et al., 1988).

3.6 Effect of hemin, baicalein and $CdCl_2$ on Nrf-2 levels in A6 cells

Since hemin-, baicalein- or $CdCl_2$-induced HO-1 accumulation may be mediated, at least in part by Nrf-2, the levels of this transcription factor in response to each of these agents was examined by immunoblot analysis (Fig. 23). In cells incubated with 25 μM hemin, no significant changes in Nrf-2 levels were detected over a 24 h period (Fig. 23A and B). In contrast, a significant increase in Nrf-2 accumulation was detected in 100 μM baicalein-treated cells at 8 h, reaching 1.8-fold at 16 h (Fig. 23D). Similarly, treatment with $CdCl_2$ resulted in significantly increased amounts of Nrf-2 accumulation at 16 h, with increased levels at 24 h, which were 1.8-fold greater than control levels (Fig. 23F).

Figure 22. Nrf-2 and HSF1 transcription factor binding sites in the *Xenopus laevis ho-1* gene promoter region. This schematic of the upstream region of a *Xenopus laevis ho-1* gene was generated using sequence data obtained from Xenbase (J-strain v 9.1; http://www.xenbase.org/, chr4L:107491000..107495999). Putative transcription factor binding sites are represented as boxes. The distance from the transcriptional start site to the 5' and 3' ends of each binding site are denoted at the ends of each box. Percent identity to corresponding elements in the upstream region of the *Homo sapiens* HO-1 gene are included in brackets beside each box (Kitamuro et al., 2003).

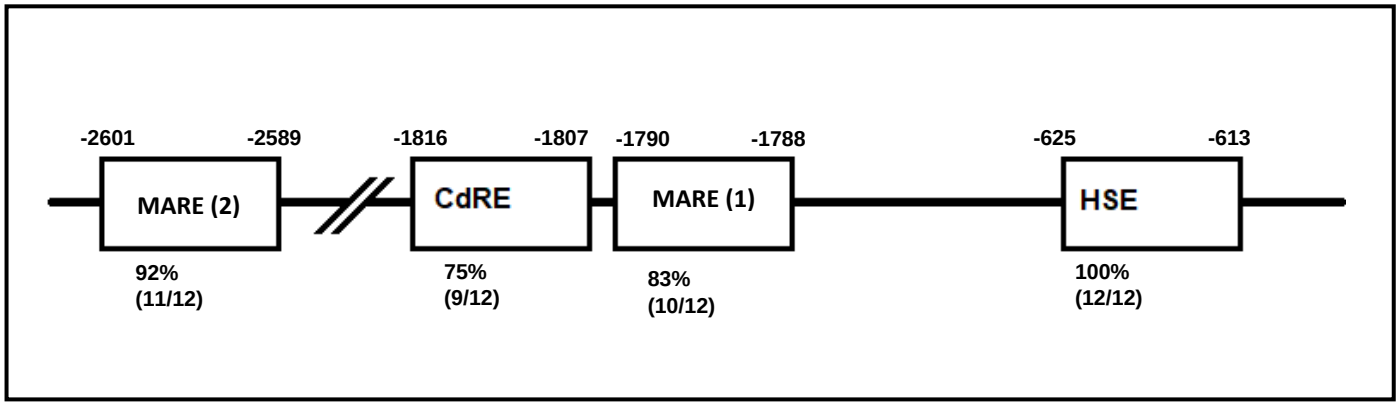
-2601
-2589
-1816
-1807
-1790
-1788
-625
-613
MARE (2)
CdRE
MARE (1)
HSE
92%
(11/12)
75%
(9/12)
83%
(10/12)
100%
(12/12)

Figure 23. Effect of hemin, baicalein, and $CdCl_2$ on Nrf-2 accumulation. A) Cells were maintained at 22 °C for 16 h (C) or were incubated with 25 μM hemin (A, B), 100 μM baicalein (C, D) or 200 μM $CdCl_2$ (E, F) and harvested after 4, 8, 16 or 24 h at 22 °C. Isolated proteins were analysed by immunoblot using anti-Nrf-2 and anti-actin antibodies. Densitometric analysis of Nrf-2 (detected at 66 kDa) accumulation in response to the 3 stressors were carried out. The results are expressed as the fold increase relative to the density of the control response. The error bars indicate standard error of the mean while the significance ($p < 0.05$) compared to control was determined by the one-way ANOVA test and Tukey's post-hoc test and represented by an asterisk. These data are representative of 3 separate experiments.

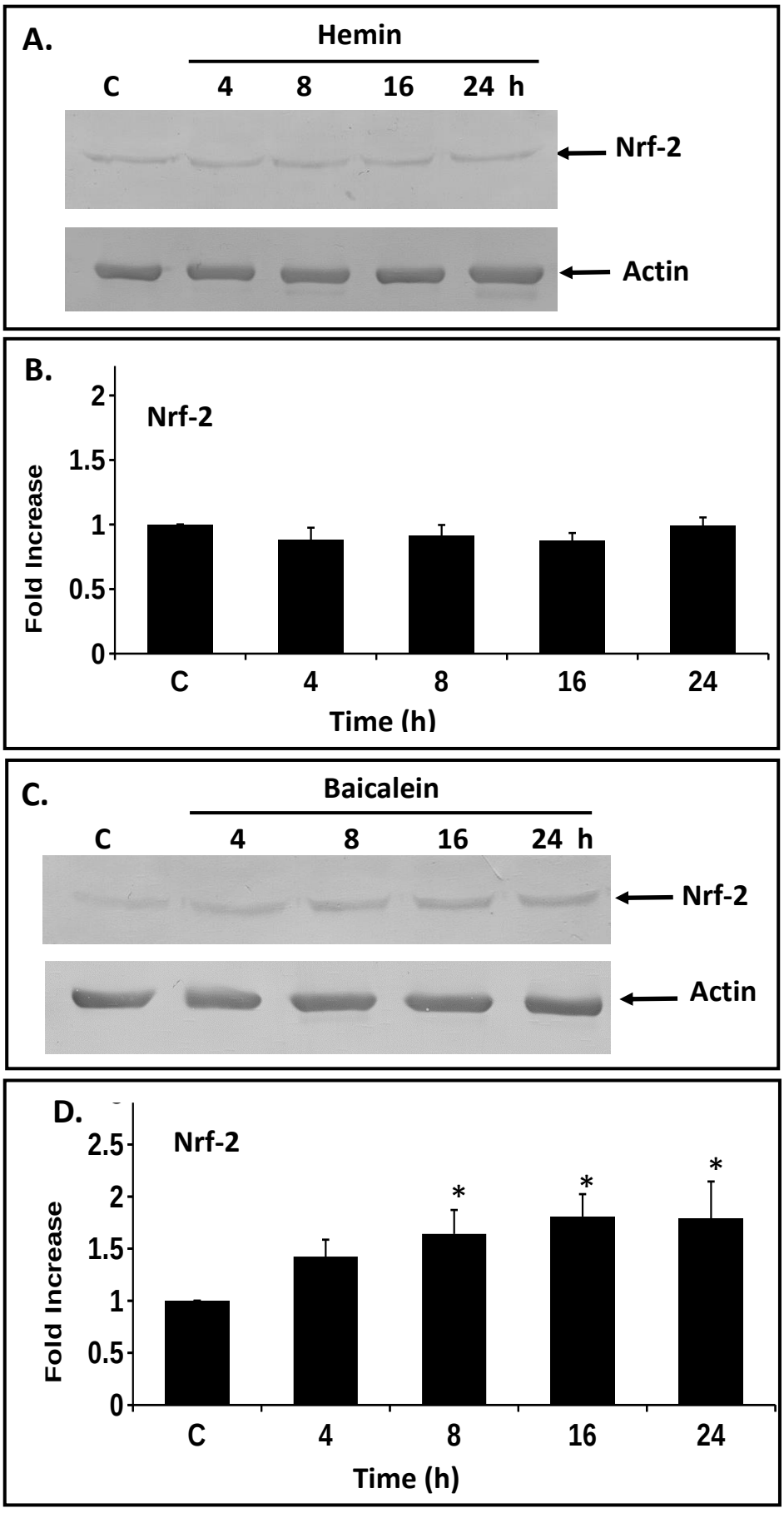
A.
Hemin
C
4
8
16
24 h
Nrf-2
Actin
B.
Nrf-2
Fold Increase
2
1.5
1
0.5
0
C
4
8
16
24
Time (h)
C.
Baicalein
C
4
8
16
24 h
Nrf-2
Actin
D.
Nrf-2
Fold Increase
2.5
2
1.5
1
0.5
0
*
*
*
C
4
8
16
24
Time (h)

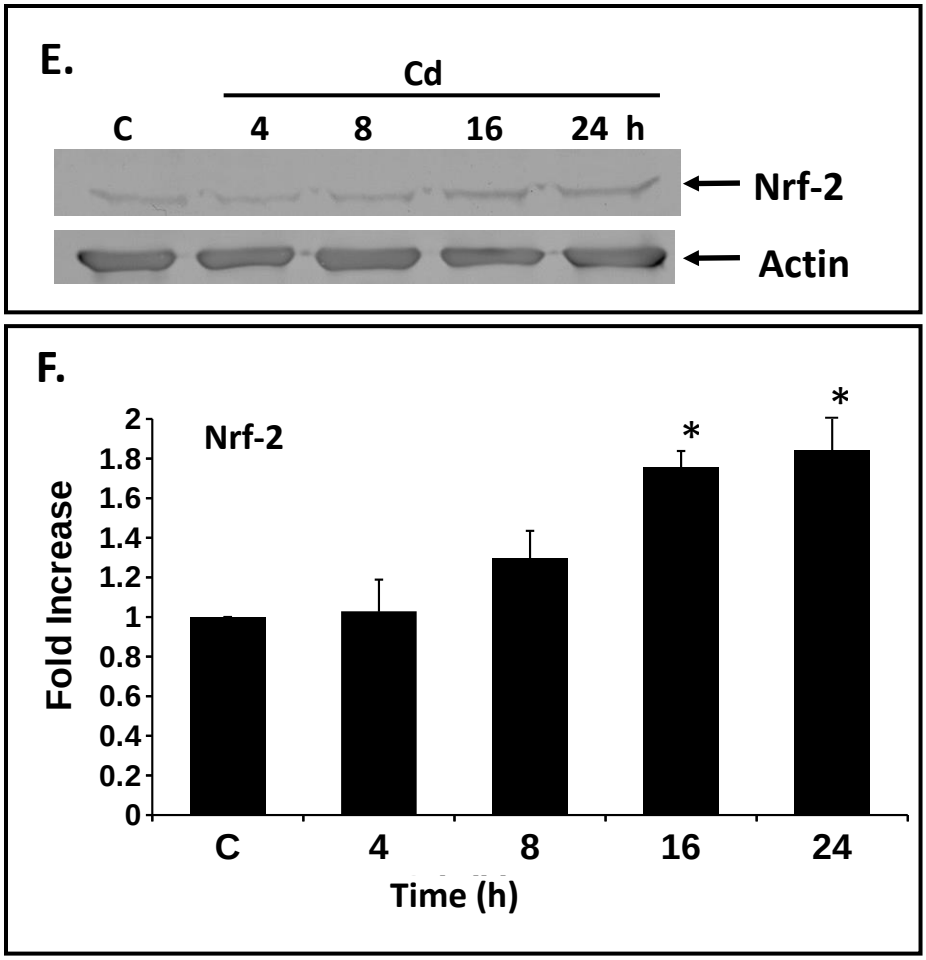
E.
Cd
C
4
8
16
24 h
Nrf-2
Actin
F.
Nrf-2
Fold Increase
2
1.8
1.6
1.4
1.2
1
0.8
0.6
0.4
0.2
0
*
*
C
4
8
16
24
Time (h)

3.7 Effect of an HSF1 inhibitor, KNK437, on hemin-, baicalein- and $CdCl_2$-induced HO-1 accumulation.

Given the finding of an HSE consensus sequence in the 5' regulatory region of the *X. laevis ho-1* gene, it was possible that HSF-1 may be involved in HO-1 induction by hemin, baicalein or $CdCl_2$. Therefore, the effect of 100 μM KNK437, an inhibitor of HSF-1 activity, on HO-1 levels induced by the 3 stressors was investigated (Fig. 24). In previous studies, KNK437 treatment of *X. laevis* A6 cells inhibited HSP70 and/or HSP30 accumulation induced by a number of stressors including heat shock, sodium arsenite, $CdCl_2$, proteasomal inhibitors, and curcumin (Manwell and Heikkila, 2007; Voyer and Heikkila, 2008; Woolfson and Heikkila, 2009; Young and Heikkila, 2010; Khan and Heikkila, 2011; Khamis and Heikkila, 2013). This concentration of KNK437 was reported to inhibit *hsp* gene expression by inhibiting HSF1-HSE binding activity in mammalian and *Xenopus* cultured cells with no detectable effect on cell viability (Ohnishi et al., 2004; Manwell and Heikkila, 2007; Heikkila, 2017). Additionally, similar effects of HSP inhibition were reported after treatment of human endothelial or glioma cells with either KNK437 or siRNA directed against *hsf1* mRNA (Ding et al., 2012; Liu et al., 2012). In the present study, treatment of cells with 100 μM KNK437 resulted in a decrease in hemin-, baicalein- or $CdCl_2$-induced HO-1 accumulation to very low or undetectable levels. Furthermore, KNK437 pretreatment also prevented $CdCl_2$-induced HSP70 accumulation.

3.8 Effect of hemin, baicalein and $CdCl_2$ on PRDX5 accumulation

The peroxiredoxin 5 *(prdx5)* gene, which contains an Nrf2 binding site in its promoter region, encodes an antioxidant enzyme determined to be ROS stress-inducible in certain cell types (Yuan et al., 2004; Nguyên-Nhu et al., 2007). As shown in Fig. 25, levels of PRDX5 were

Figure 24. Effect of HSF1 inhibitor, KNK437, on hemin-, baicalein- or $CdCl_2$-induced HO-1 accumulation. Cells were either maintained at 22 °C (C) or were treated with or without a 6 h pretreatment of 100μM KNK437 followed by supplementation with either 25 μM hemin, 100 μM baicalein or 200 μM $CdCl_2$ for 16 h. Proteins were isolated and analysed by immunoblot using anti-HO-1, anti-HSP70 and anti-actin antibodies. These data are representative of 3 separate experiments.

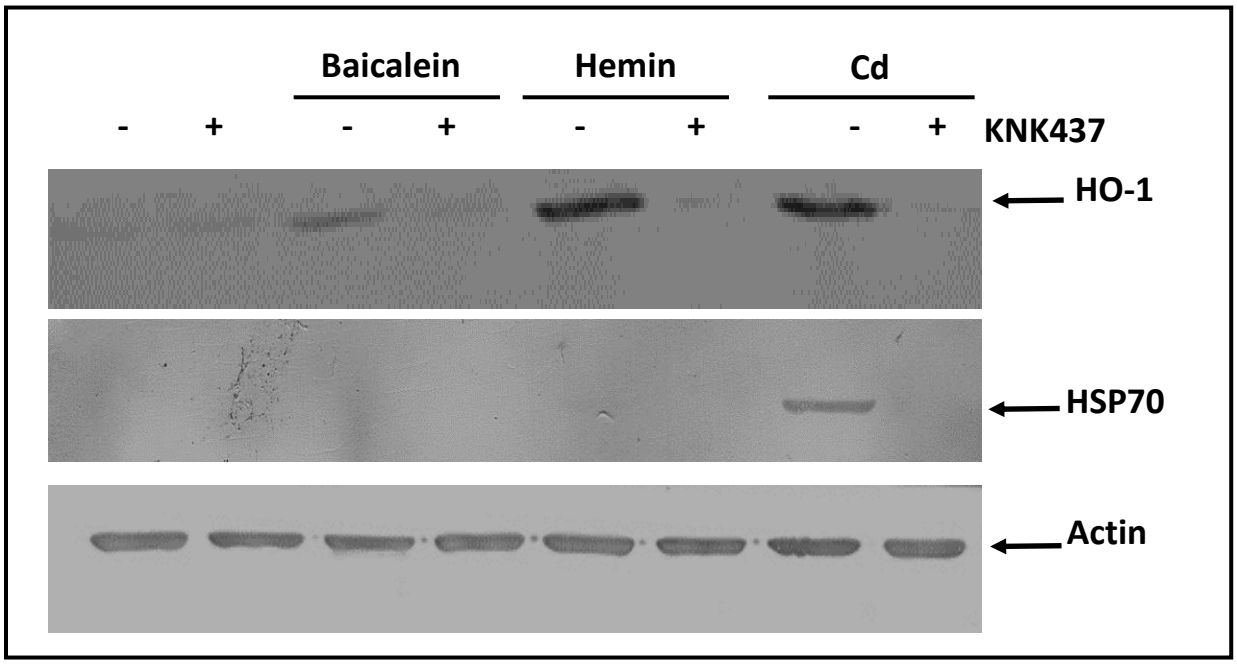
Baicalein
Hemin
Cd
- + - + - + - +
KNK437
HO-1
HSP70
Actin

Figure 25. Effect of hemin, baicalein, and $CdCl_2$ on PRDX-5 accumulation. Cells were maintained at 22 °C for 16 h (Control; C) or were incubated with 25 μM hemin (A, B), 100 μM baicalein (C, D) or 200 μM $CdCl_2$ (E, F) and harvested after 4, 8, 16 or 24 h at 22 °C. Isolated proteins were analysed by immunoblot using anti-PRDX-5 (detected at 20 kDa) and anti-actin antibodies. B) Densitometric analysis of PRDX-5 accumulation. The results are expressed as the fold increase of the intensity of the control response. The error bars indicate standard error of the mean while the significance compared to control was determined by the one-way ANOVA test and Tukey's post-hoc test and represented by an asterisk ($p < 0.05$) or triangle ($p < 0.1$). These data are representative of 3 separate experiments.

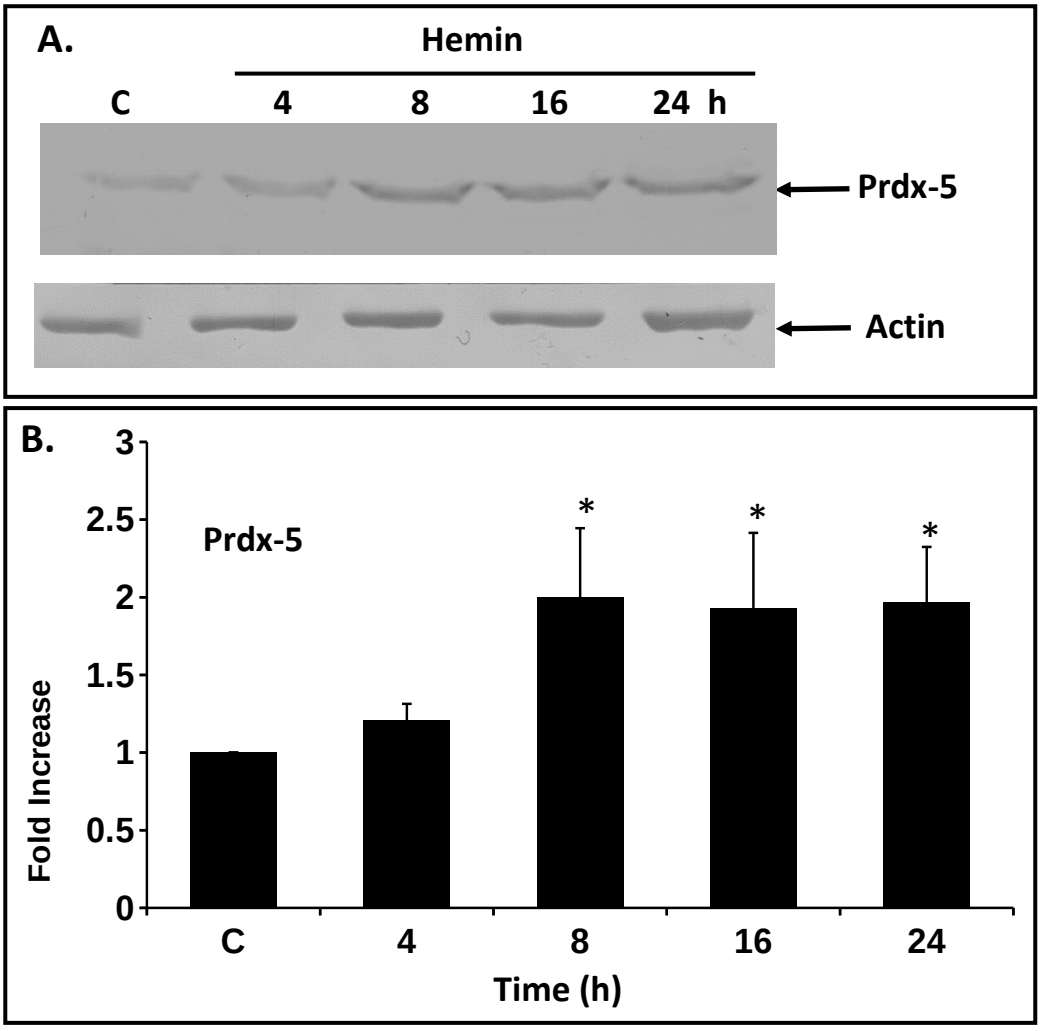
A.
Hemin
C
4
8
16
24 h
Prdx-5
Actin
B.
Prdx-5
Fold Increase
3
2.5
2
1.5
1
0.5
0
*
*
*
C
4
8
16
24
Time (h)

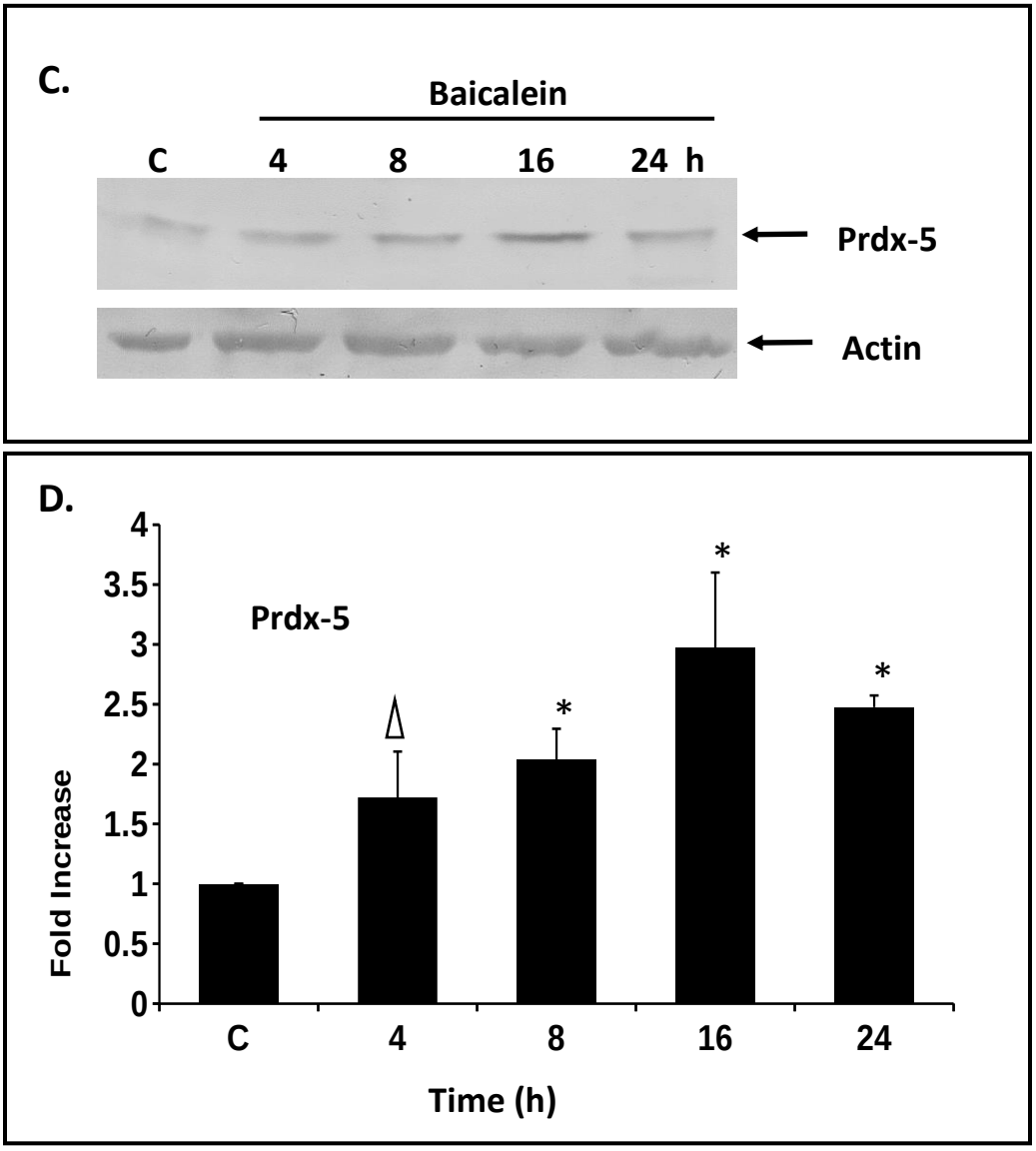
C.
Baicalein
C
4
8
16
24 h
Prdx-5
Actin
D.
Prdx-5
Fold Increase
4
3.5
3
2.5
2
1.5
1
0.5
0
*
*
*
C
4
8
16
24
Time (h)

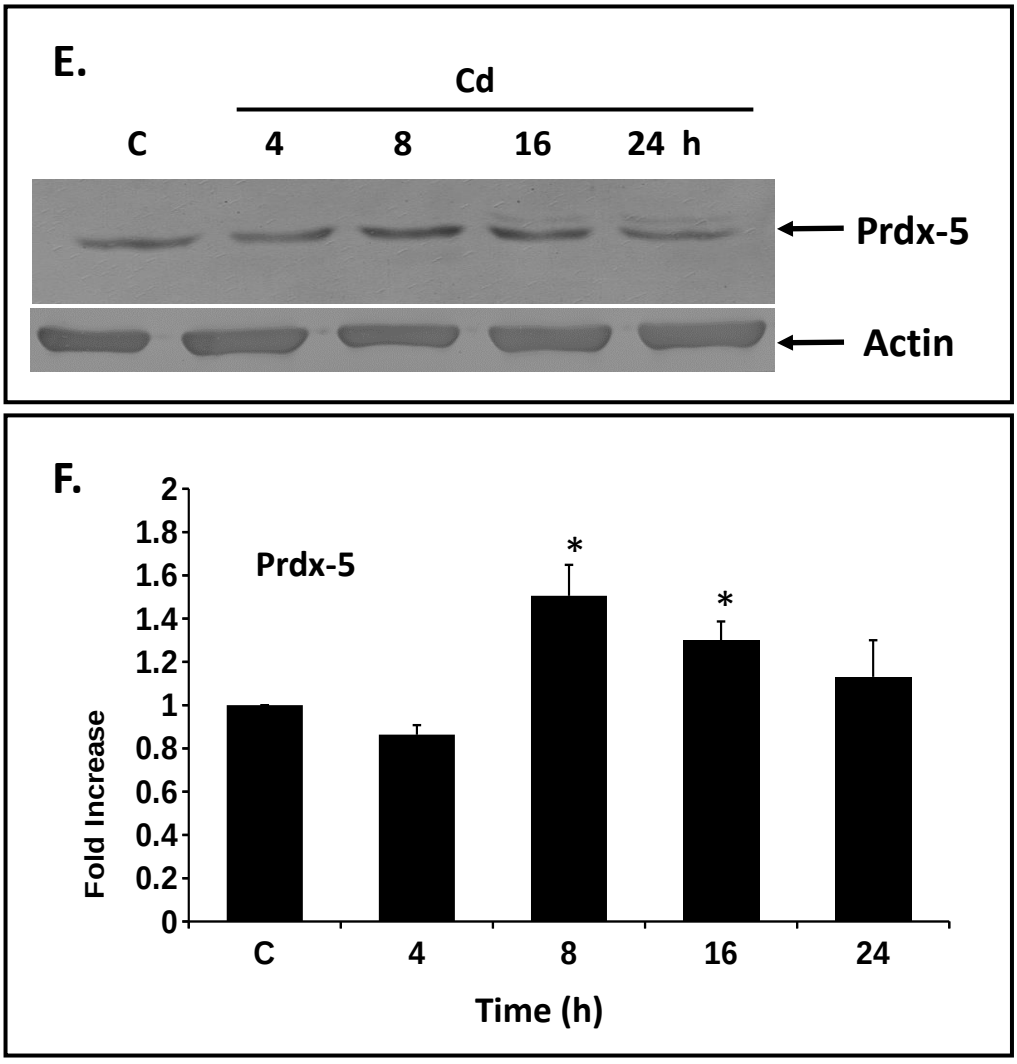
E.
Cd
C
4
8
16
24 h
Prdx-5
Actin
F.
Prdx-5
Fold Increase
2
1.8
1.6
1.4
1.2
1
0.8
0.6
0.4
0.2
0
*
*
C
4
8
16
24
Time (h)

examined in A6 cells treated with 25 μM hemin, 100 μM baicalein or 200 μM $CdCl_2$ (Fig. 25). A constitutive amount of PRDX5 was observed in control cells. Relative to control, hemin treatment enhanced PRDX5 by 2-fold at 8 h, 1.9-fold at 12 h and 2-fold at 24 h. The levels of PRDX5 in baicalein-treated cells increased to 2-fold at 8 h reaching a maximum of 3-fold at 16 h followed by a decrease to 2.4-fold at 24 h. Finally, the relative levels of PRDX5 in $CdCl_2$-treated cells increased by 1.5-fold at 8 h, decreased to 1.3-fold at 16 h and then to near control-like levels at 24 h.

3.9 Detection of ROS generation in hemin, baicalein and $CdCl_2$ treated cells

Since both HO-1 and PRDX5 have roles in counteracting oxidative stress (Nath et al., 2000; Yuan et al., 2004), the next phase of this study examined the effect of hemin, baicalein and $CdCl_2$ on ROS generation in A6 cells using CellROX green. CellROX green is a molecular probe that fluoresces and moves into the nucleus in the presence of elevated levels of ROS. As shown in Fig. 26, minimal fluorescence was detected in control cells and in cells treated with 25 μM hemin for 4 h. A slight increase in fluorescence was observed with 200 μM baicalein relative to control. However, the strongest CellROX fluorescence level of the 3 stressors was observed with $CdCl_2$-treated cells. The most pronounced fluorescence was found in cells treated with the glutathione synthesis inhibitor, buthionine sulfoxamine (BSO), which was used as a positive control.

3.10 Effect of buthionine sulfoxamine (BSO) treatment on hemin, baicalein and $CdCl_2$-induced HO-1 accumulation

The next part of this study determined if hemin-, baicalein- or $CdCl_2$-induced HO-1.

Figure 26. Effect of hemin, baicalein and $CdCl_2$ on ROS accumulation in A6 cells. Cells were cultured on glass coverslips for 4 h with either media (C) or media containing 25 μM hemin (HM), 100 μM baicalein (BC), 200 μM $CdCl_2$ (Cd) or 10 mM BSO. ROS generation was detected using the CellROX Green reagent (green). Nuclei were stained using DAPI (blue). White 10 μm scale bars are indicated in the lower right corner of each panel. These results are representative of at least 3 separate experiments.

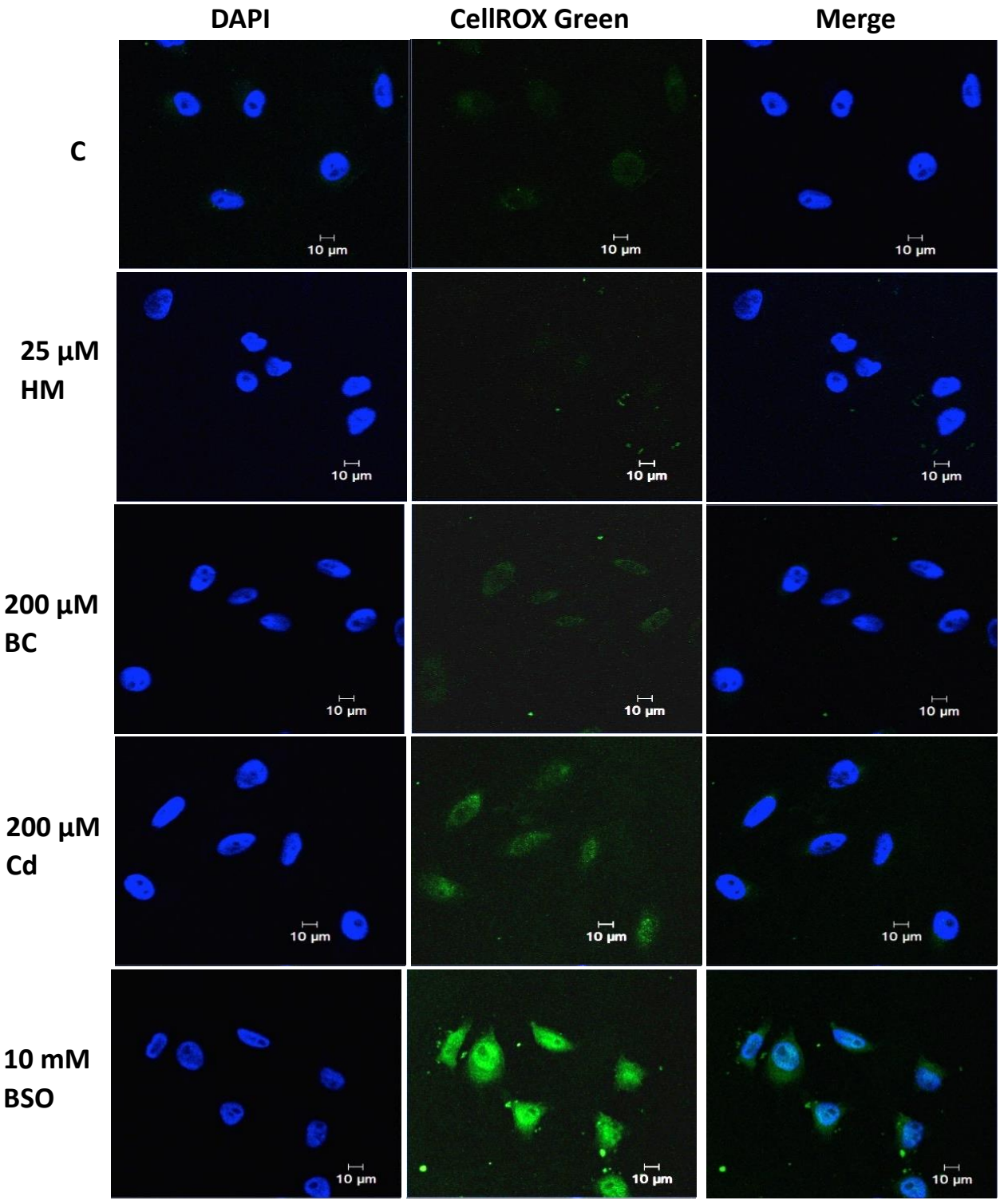
DAPI
CellROX Green
Merge
C
25 µM HM
200 µM BC
200 µM Cd
10 mM BSO
10 µm

accumulation could be altered by the oxidative stressor, BSO. In these experiment, cells were pretreated with 10 mM BSO for 4 h prior to the addition of 15 μM hemin, 100 μM baicalein or 50 μM $CdCl_2$ for 16 h. Immunoblot analysis was used to detect HO-1 and the ROS-inducible enzyme, superoxide dismutase 1 (SOD1). BSO treatment did not induce elevated levels of HO-1 but did induce SOD1 accumulation (Fig. 27). Also 15 μM hemin treatment enhanced both HO-1 and SOD1 levels compared to control. However, treatment with BSO prior to supplementation with hemin did not induce levels of HO-1 or SOD1 that were greater than found with hemin alone. While exposure of cells to 100 μM baicalein induced elevated levels of both HO-1 and SOD1, BSO and baicalein treatment did not affect the amount of HO-1 but did reduce the levels of SOD1 to control levels (Fig. 28). Finally, treatment of A6 cells with 25 μM $CdCl_2$ induced elevated levels of both HO-1 and SOD1 relative to control (Fig. 29). However, in contrast to hemin and baicalein, treatment of cells with BSO prior to augmentation with $CdCl_2$ enhanced the relative levels of HO-1 compared to BSO or $CdCl_2$ alone. In this latter treatment regimen, SOD1 levels were comparable to those found in cells treated with BSO or $CdCl_2$ alone.

3.11 Effect of hemin, baicalein and $CdCl_2$ on the accumulation of aggregated protein and aggresome-like structures

In the previous experiments, it was found that treatment of A6 cells with either 25 μM hemin, 100 μM baicalein or 200 μM $CdCl_2$ enhanced the relative levels of SOD1 and PRDX5. Furthermore, CELLROX analyses determined that $CdCl_2$ and to a lesser extent, baicalein, increased the presence of ROS in these cells. Also, other studies reported that reactive oxygen species have the potential to alter protein structure, which could possibly lead to their aggregation (Aiken et al., 2011; Dasuri et al., 2013). Therefore, the next set of experiments.

Figure 27. Effect of BSO treatment on hemin-induced HO-1 and SOD1 accumulation. A) Cells were maintained at 22 °C for 16 h (C) or were incubated with or without a 4 h treatment with 10 mM BSO followed by supplementation with 15 μM hemin for 16 h. Isolated proteins were examined by immunoblot analysis using anti-HO-1, anti-SOD1 (detected at 15 kDa) and anti-actin antibodies. B) Densitometric analysis of HO-1 or SOD1 accumulation. The results were expressed as % mean relative density compared to the maximum density (10 mM BSO and 15 μM hemin for both HO-1 and SOD1) as indicated in the legend of Figure 3. The error bars indicate standard error of the mean while the significance ($p < 0.05$) compared to control was determined by the one-way ANOVA test and Tukey's post-hoc test and represented by an asterisk. These data are representative of 3 separate experiments.

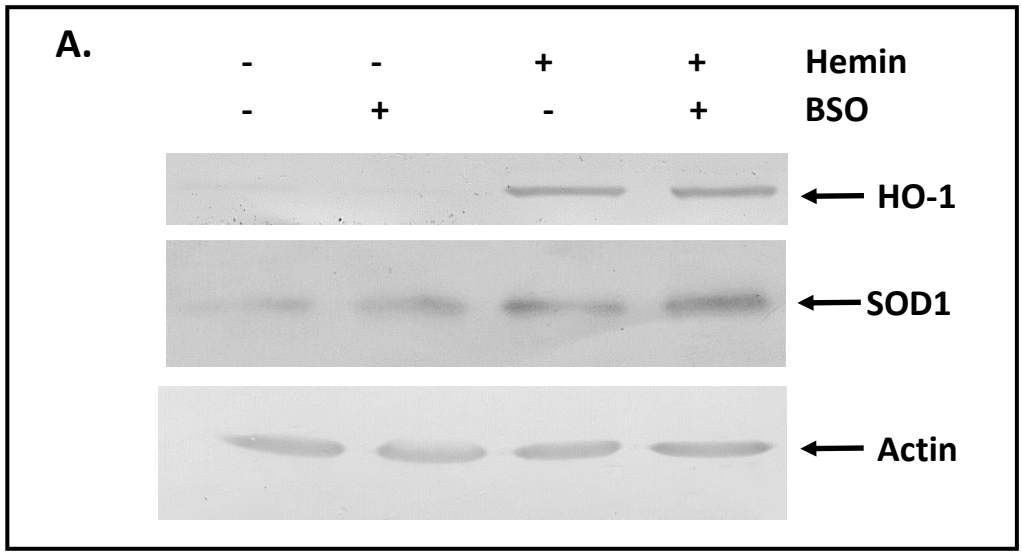
A.
- - + + Hemin
- + - + BSO
HO-1
SOD1
Actin

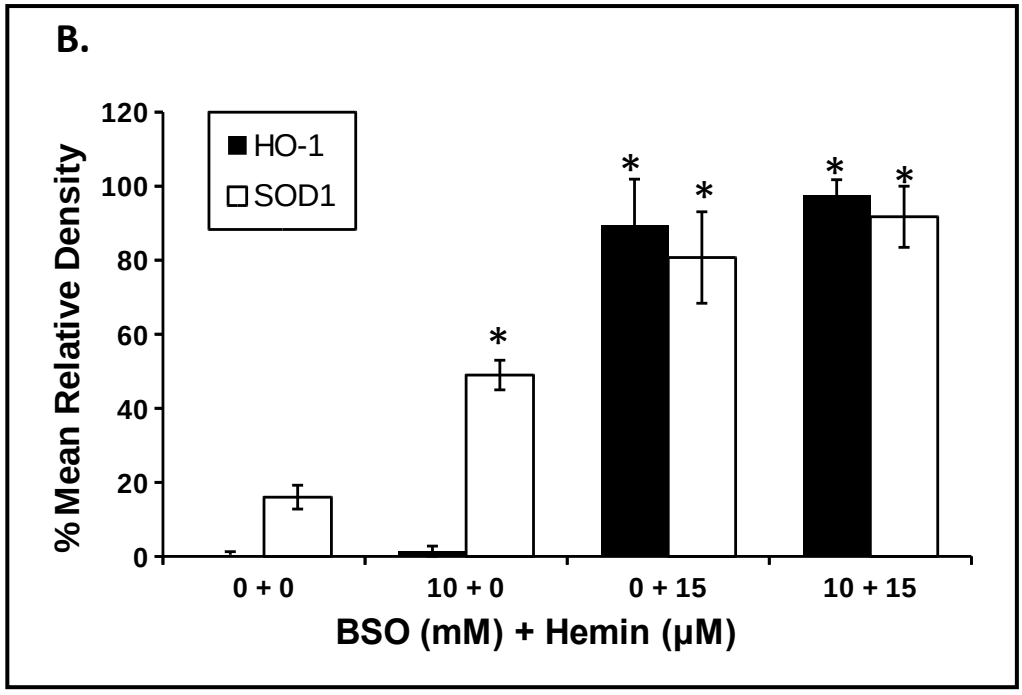
B.
% Mean Relative Density
120
100
80
60
40
20
0
HO-1
SOD1
*
0 + 0
10 + 0
0 + 15
10 + 15
BSO (mM) + Hemin (μM)

Figure 28. Influence of BSO treatment on baicalein-induced HO-1 and SOD1 accumulation. A) Cells were maintained at 22 °C for 16 h (C) or were incubated with or without a 4 h treatment with 10 mM BSO followed by augmentation with 100 μM baicalein for 16 h. Isolated proteins were assessed by immunoblot analysis using anti-HO-1, anti-SOD1 and anti-actin antibodies. B) Densitometric analysis of HO-1 or SOD1 accumulation. The results were expressed as % mean relative density compared to maximum density (10 mM BSO for HO-1 and 100 μM baicalein for HO-1) as indicated in the legend of Figure 3. The error bars indicate standard error of the mean while the significance ($p < 0.05$) compared to control was determined by the one-way ANOVA test and Tukey's post-hoc test and represented by an asterisk. These data are representative of 3 separate experiments.

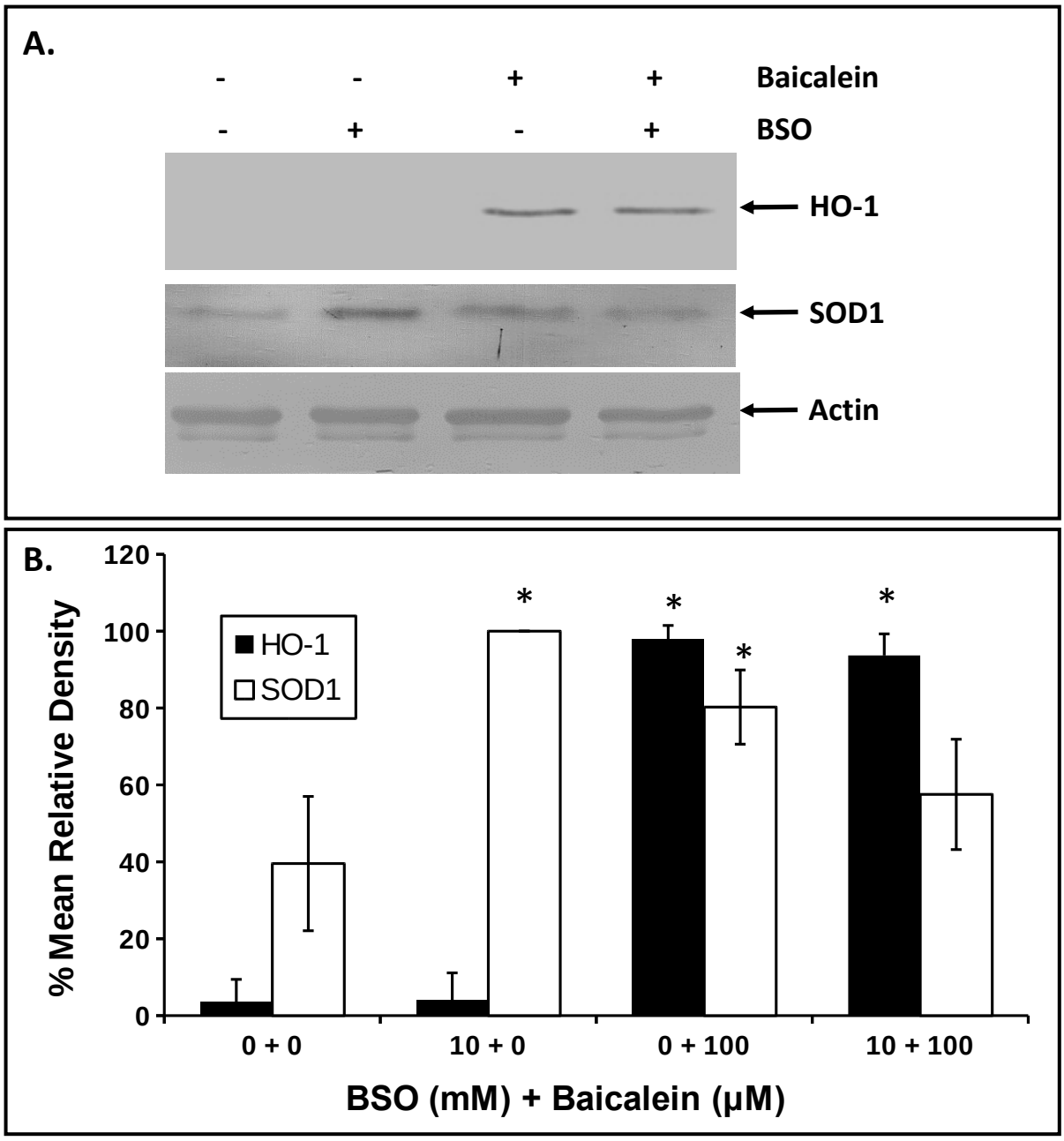
A.
- - + + Baicalein
- + - + BSO
HO-1
SOD1
Actin
B.
% Mean Relative Density
120
100
80
60
40
20
0
HO-1
SOD1
*
*
*
*
0 + 0
10 + 0
0 + 100
10 + 100
BSO (mM) + Baicalein (μM)

Figure 29. Effect of BSO treatment on $CdCl_2$-induced HO-1 and SOD1 accumulation. A) Cells were maintained at 22 °C for 16 h (C) or were incubated with or without a 4 h treatment with 10 mM BSO followed by supplementation with 25 μM $CdCl_2$ for 16 h. Isolated proteins were examined by immunoblot analysis using anti-HO-1, anti-SOD1 and anti-actin antibodies. B) Densitometric analysis of HO-1 or SOD1 accumulation. The results were expressed as % mean relative density compared to maximum density (10 mM BSO plus 25 μM baicalein for HO-1 and SOD1) as indicated in the legend of Figure 3. The error bars indicate standard error of the mean while the significance ($p < 0.05$) compared to control was determined by the one-way ANOVA test and Tukey's post-hoc test and represented by an asterisk. These data are representative of 3 separate experiments.

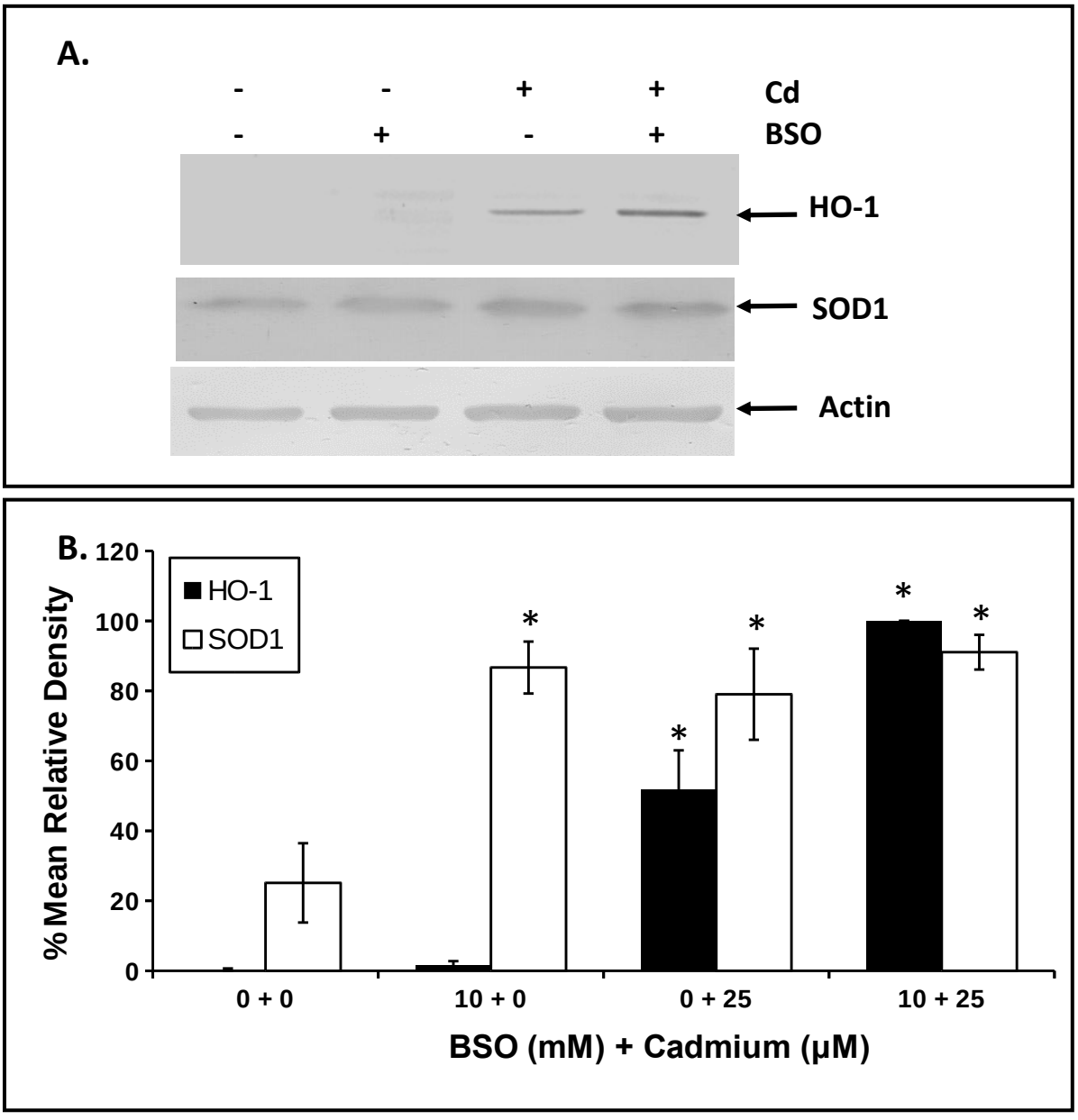
A.
- - + + Cd
- + - + BSO
HO-1
SOD1
Actin
B.
HO-1
SOD1
% Mean Relative Density
120
100
80
60
40
20
0
0 + 0
10 + 0
0 + 25
10 + 25
BSO (mM) + Cadmium (μM)
*

employed a Proteostat dye to investigate the presence of aggregated protein or aggresome-like structures in A6 cells treated with hemin, baicalein or $CdCl_2$ (Khan et al., 2015; Shirriff and Heikkila, 2017; Khamis and Heikkila, 2018). As demonstrated in Fig. 30, Proteostat staining was minimal in control cells as well as in cells treated with 25 μM hemin or 200 μM baicalein. However, incubation with 200 μM $CdCl_2$ resulted in the accumulation of aggregated protein primarily in the perinuclear region in a granular fashion. Large aggresome-like structures, as indicated by white arrows, were also detected in 200 μM $CdCl_2$-treated cells. $CdCl_2$-induced aggresome-like structures were previously reported in *X. laevis* A6 cells and human embryonic kidney cells (Song et al., 2008; Khan et al., 2015). Finally, the microtubular structure, as detected by an anti-α-tubulin antibody, in hemin- and baicalein-treated cells resembled control cells whereas microtubules in $CdCl_2$-treated cells displayed areas of disorganization.

3.12 Effect of HO-1 enzyme activity inhibitors, SnPP and ZnPP, on the accumulation HO-1 in $CdCl_2$-treated A6 cells.

This study also examined the effect of inhibiting HO-1 enzyme activity on $CdCl_2$-induced accumulation of HO-1. Two inhibitors of HO-1 enzyme activity, zinc protoporphyrin (ZnPP) and tin protoporphyrin (SnPP), were employed (Drummond and Kappas 1981; Srisook et al., 2005). Initial analyses determined that treatment of cells with 5 or 7.5 μM ZnPP induced a slight enhancement of HO-1 levels compared to control whereas treatment with 5, 15 or 25 μM had no effect (Fig. 31). The presence of either 5 μM ZnPP or 15 μM SnPP enhanced $CdCl_2$-induced accumulation of HO-1 compared to 50 μM $CdCl_2$ alone (Fig. 32). Densitometric analysis determined that the relative level of HO-1 found with SnPP alone was comparable to control levels. Also, HO-1 levels in cells treated with 50 μM $CdCl_2$ was present at 45% of maximum

Figure 30. Effect of hemin, baicalein and $CdCl_2$ on the accumulation of aggregated protein and aggresome-like structures. Cells were cultured on glass coverslips for 16 h at 22 °C. Cells were left untreated (C) or incubated with 25 μM hemin (HM), 200 μM baicalein (BC) or 200 μM $CdCl_2$ (Cd). Alpha-tubulin was detected using a mouse anti-α-tubulin antibody and an anti-mouse antibody conjugated to an Alexa-488 fluorophore (green). Aggregated protein and aggresome-like structures were detected using the Proteostat dye (red). Nuclei are stained with DAPI (blue). White arrows indicate the presence of aggresome-like structures. White 10 μm scale bars are indicated in the lower right of each panel. These data are representative of 3 separate experiments.

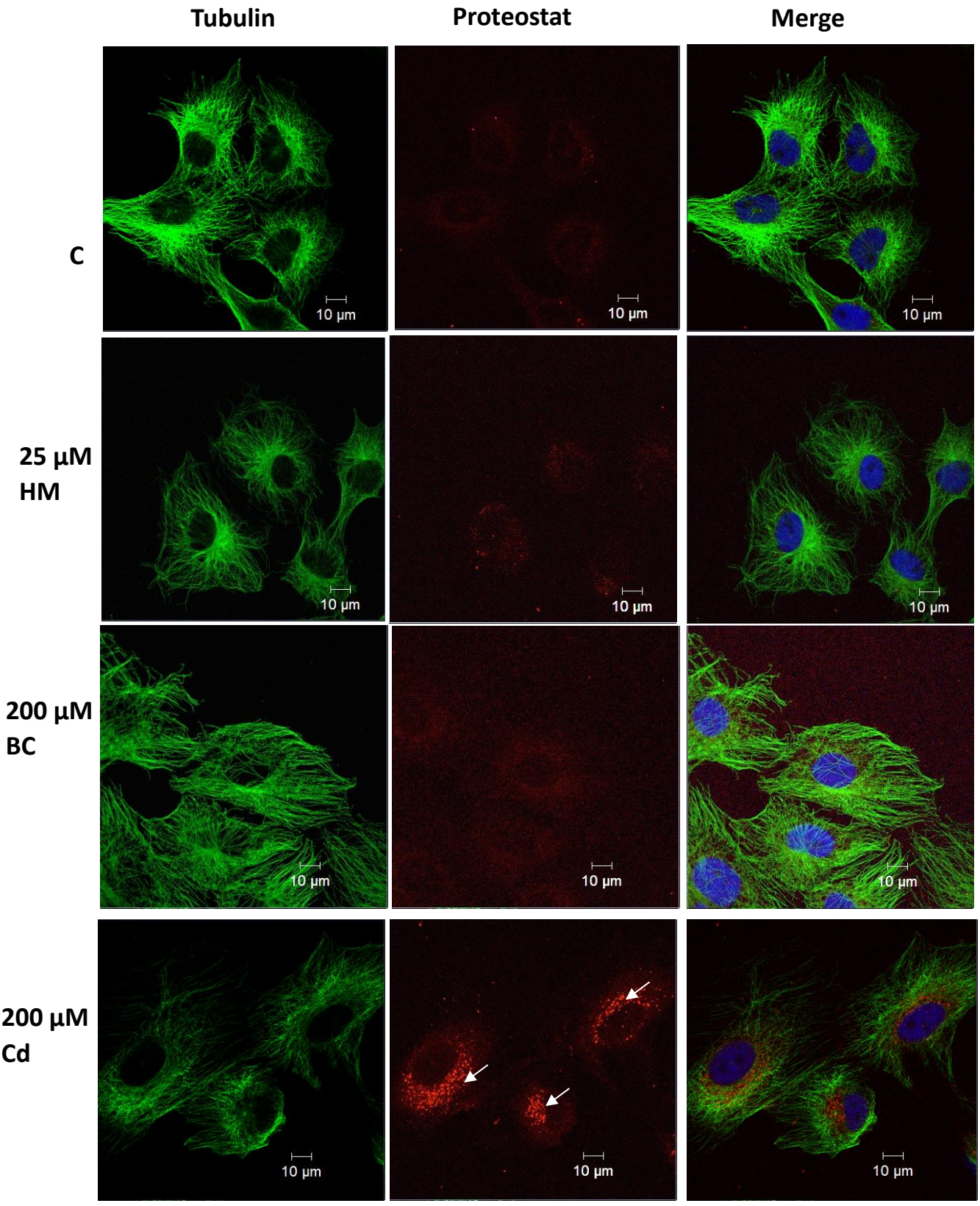
Tubulin
Proteostat
Merge
C
25 µM HM
200 µM BC
200 µM Cd
10 µm

Figure 31. Effect of ZnPP and SnPP on HO-1 accumulation. A) Cells were maintained at 22 °C (C) or treated with 2.5, 5, or 7.5 μM of ZnPP or 5, 15, or 25 μM of SnPP or 25 μM hemin for 16 h at 22 °C. Hemin was used as a positive control since it induced accumulation of HO-1. Immunoblot analysis of isolated proteins employed anti-HO-1 and anti-actin antibodies. B) Densitometric analysis of HO-1 accumulation. The results were expressed as % mean relative density as indicated in the legend of Figure 3. The error bars indicate standard error of the mean while the significance ($p < 0.05$) compared to control was determined by the one-way ANOVA test and Tukey's post-hoc test and represented by an asterisk. These data are representative of 3 separate experiments.

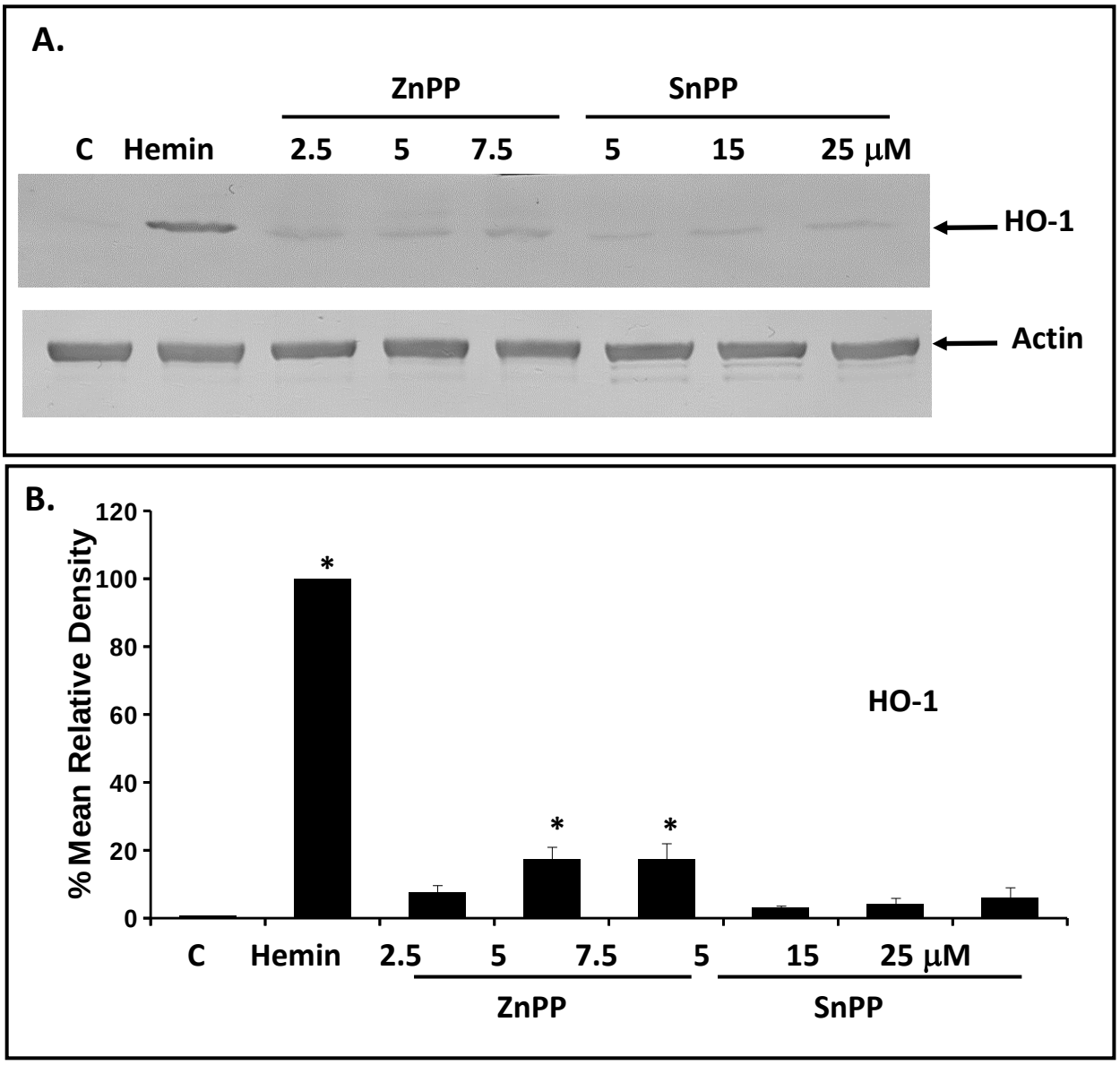
A.
ZnPP
SnPP
C
Hemin
2.5
5
7.5
5
15
25 μM
HO-1
Actin
B.
% Mean Relative Density
120
100
80
60
40
20
0
*
*
*
HO-1
C
Hemin
2.5
5
7.5
5
15
25 μM
ZnPP
SnPP

Figure 32. Effect of ZnPP or SnPP treatment on 50 μM $CdCl_2$-induced HO-1 and HSP70 accumulation. A) Cells were maintained at 22 °C (C) or treated with or without a 5 μM ZnPP or 15 μM SnPP 4 h treatment prior to supplementation with 50 μM $CdCl_2$ for 16 h at 22 °C. Immunoblot analysis of isolated proteins employed anti-HO-1, anti HSP70 and anti-actin antibodies. B) Densitometric analysis of HO-1 (black bars) and HSP70 (grey bars) accumulation. The results were expressed as % mean relative density as indicated in the legend of Figure 3. The error bars indicate standard error of the mean while the significance ($p < 0.05$) compared to control was determined by the one-way ANOVA test and Tukey's post-hoc test and represented by an asterisk. These data are representative of 3 separate experiments.

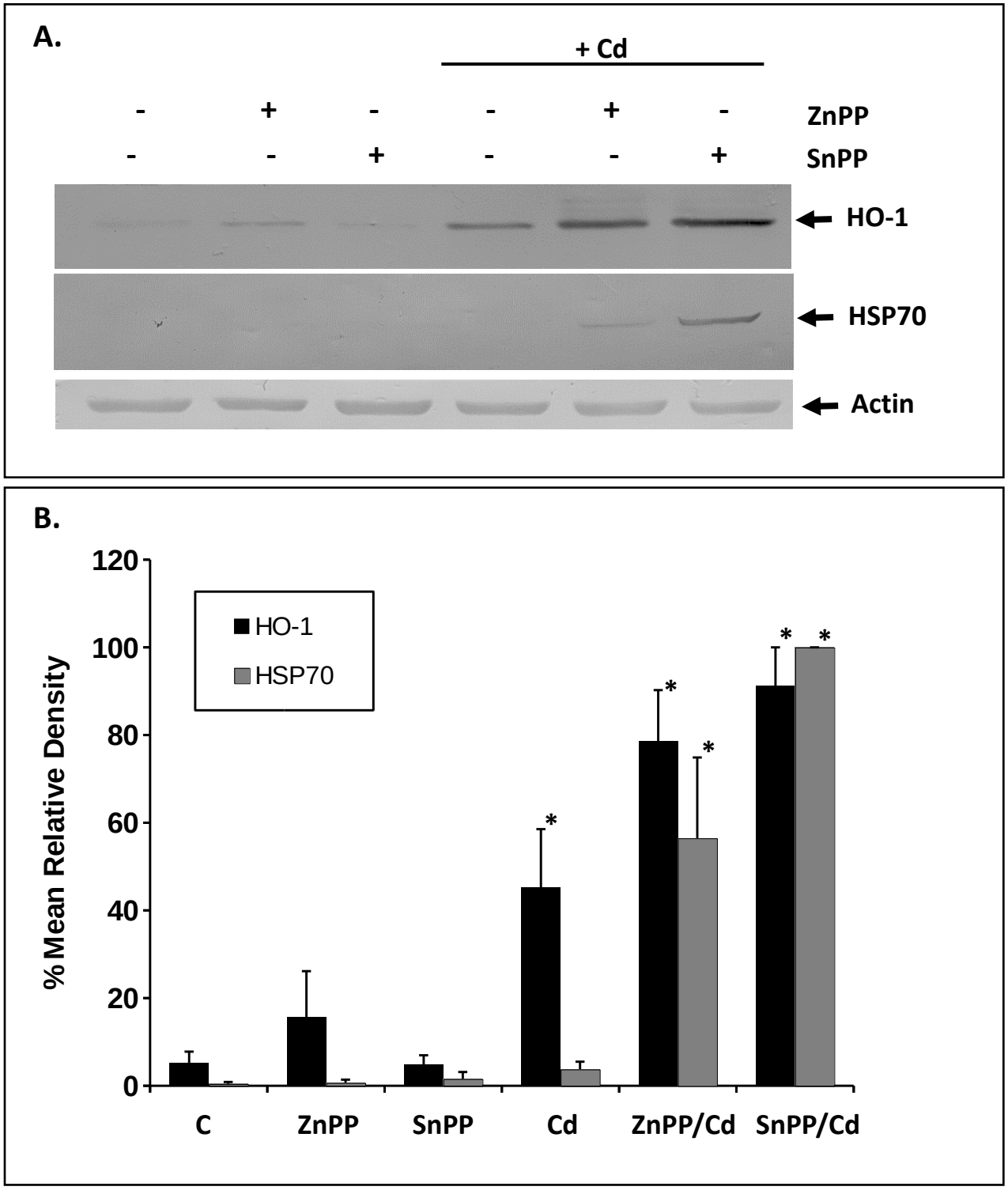
A.
+ Cd
- + - - + - ZnPP
- - + - - + SnPP
HO-1
HSP70
Actin
B.
% Mean Relative Density
120
100
80
60
40
20
0
HO-1
HSP70
*
C
ZnPP
SnPP
Cd
ZnPP/Cd
SnPP/Cd

levels whereas the mean relative density of SnPP plus $CdCl_2$ was 90%. Finally, while the HO-1 enzyme activity inhibitors did not induce detectable HSP70 accumulation and 50 μM $CdCl_2$ induced only a slight increase in HSP70 levels relative to control, treatment with either ZnPP or SnPP plus $CdCl_2$ resulted in mean relative density values of 56% and 100%, respectively.

3.13 Effect of HO-1 enzyme activity inhibitors on $CdCl_2$-induced HO-1 localization, actin and tubulin cytoskeletal structure and the presence of aggregated protein.

Since treatment of A6 cells with HO-1 enzyme activity inhibitors enhanced $CdCl_2$-induced HO-1 and HSP70 accumulation, it was of interest to determine whether ZnPP or SnPP had an effect on $CdCl_2$-induced HO-1 localization, cytoskeletal structure and the production of aggregated protein. As revealed in Fig. 33, treatment with either 5 μM ZnPP or 15 μM SnPP prior to augmentation with 100 μM $CdCl_2$ enhanced the accumulation of HO-1 in the perinuclear region with some staining in the nucleus compared to cells incubated with $CdCl_2$ or the HO-1 enzyme activity inhibitors alone. As shown in Fig. 33 and 34, actin stress fibres and the pattern of microtubules in cells treated with ZnPP, SnPP or 100 μM $CdCl_2$ resembled those of control cells. In cells treated with either ZnPP or SnPP prior to supplementation with $CdCl_2$, there was noticeable membrane ruffling and disorganization of the actin cytoskeleton. The effect of ZnPP plus $CdCl_2$ exposure on the microtubule network was characterized by a reduction in anti-α-tubulin antibody staining in the perinuclear region and a mesh-like appearance throughout the cytoplasm compared to control cells. In cells treated with SnPP prior to the addition of $CdCl_2$, tubulin filaments appeared to be more tangled or intertwined than found in control.

The HO-1 enzyme activity inhibitors also enhanced the 100 μM $CdCl_2$-induced accumulation of aggregated protein in $CdCl_2$ treated cells. As indicated in Fig. 35, cells treated

Figure 33. Effect of ZnPP or SnPP treatment on $CdCl_2$-induced HO-1 localization. Cells were cultured on glass coverslips for 16 h at 22 °C. Cells were left untreated (C) or incubated with 100 μM $CdCl_2$ (Cd) for 16 h. In other experiments, cells were treated for 4 h with either 5 μM ZnPP (panel A) or 15 μM SnPP (panel B) and then supplemented with 100 μM $CdCl_2$ for 16 h. Nuclei and actin filaments were stained directly using DAPI (blue) and rhodamine phalloidin (red), respectively. HO-1 was detected with an anti-HO-1 antibody and the secondary antibody conjugate, Alexa-488 fluorophore (green). White 10 μm scale bars are indicated in the lower right of each panel. These data are representative of 3 separate trials.

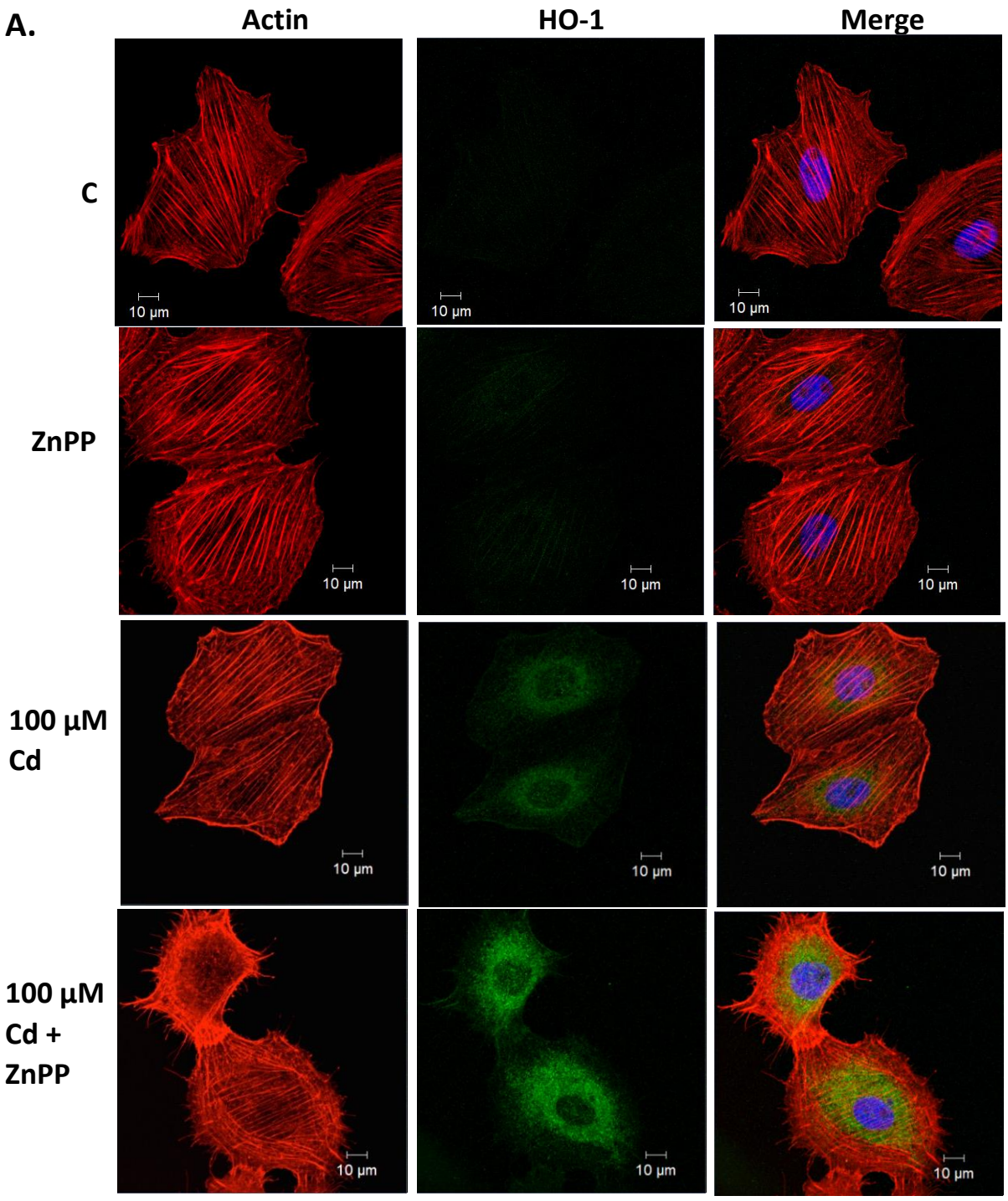
A.
Actin
HO-1
Merge
C
ZnPP
100 µM Cd
100 µM Cd + ZnPP
10 µm

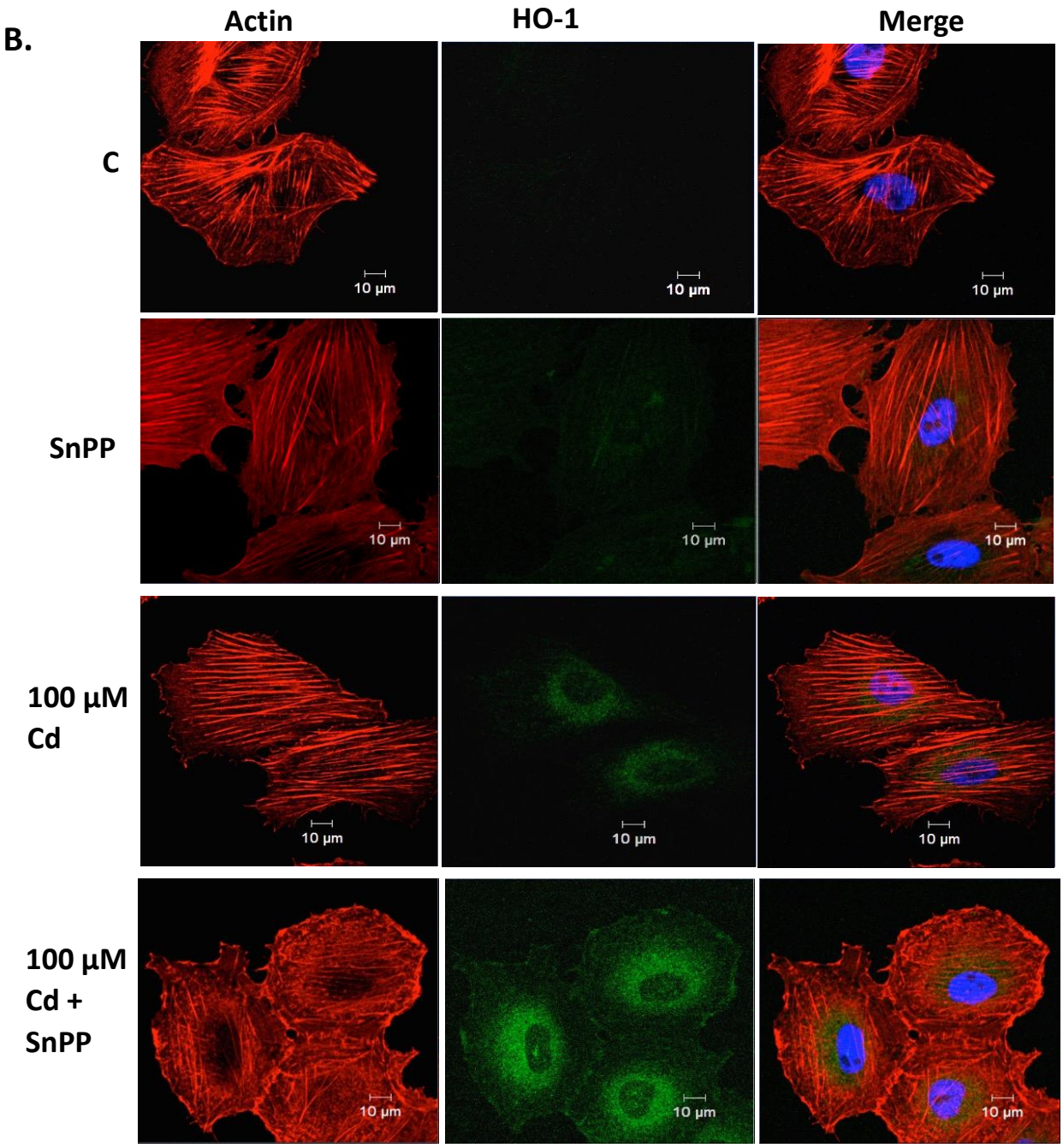
B.
Actin
HO-1
Merge
C
SnPP
100 µM Cd
100 µM Cd + SnPP
10 µm

Figure 34. Effect of ZnPP or SnPP treatment on actin and tubulin organization. Cells were cultured on glass coverslips for 16 h at 22 °C. Cells were left untreated (C) or incubated with 100 μM $CdCl_2$ (Cd) for 16 h. In other experiments, cells were treated for 4 h with either 5 μM ZnPP (panel A) or 15 μM SnPP (panel B) and then supplemented with 100 μM $CdCl_2$ for 16 h. Nuclei and actin filaments were stained directly using DAPI (blue) and rhodamine phalloidin (red), respectively. Alpha-tubulin was detected using a mouse anti-α-tubulin antibody and an anti-mouse antibody conjugated to an Alexa-488 fluorophore (green). White 10 μm scale bars are indicated in the lower right of each panel. These data are representative of 3 separate experiments.

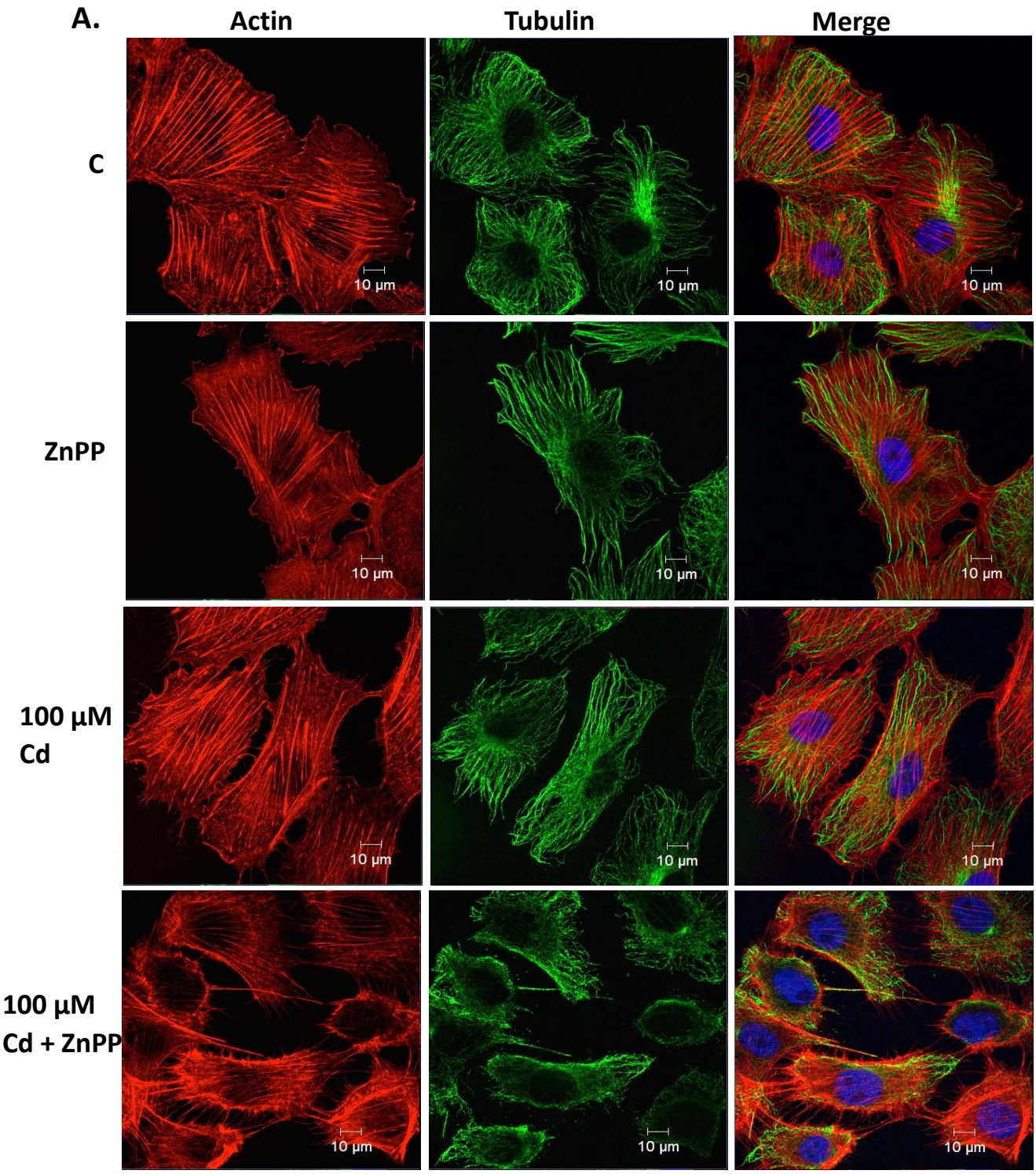
A.
Actin
Tubulin
Merge
C
ZnPP
100 µM Cd
100 µM Cd + ZnPP
10 µm

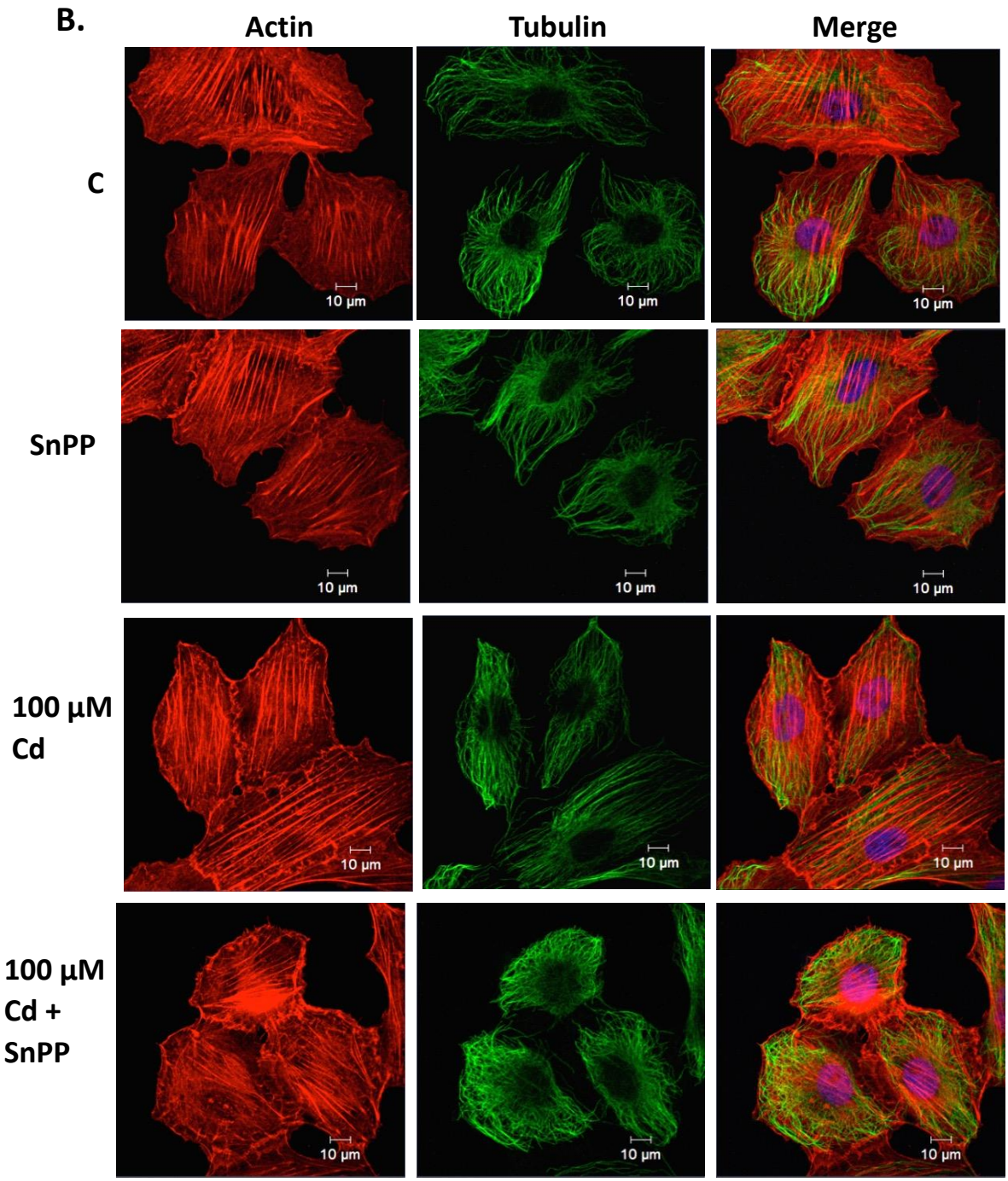
B.
Actin
Tubulin
Merge
C
SnPP
100 µM Cd
100 µM Cd + SnPP
10 µm

Figure 35. Effect of ZnPP or SnPP treatment on $CdCl_2$-induced aggregated protein and aggresome-like structure formation. Cells were left untreated (C) or incubated with 100 μM $CdCl_2$ (Cd) for 16 h. In other experiments, cells were treated for 4 h with either 5 μM ZnPP or 15 μM SnPP and then supplemented with 100 μM $CdCl_2$ for 16 h. Alpha-tubulin was detected using a mouse anti-α-tubulin antibody and an anti-mouse antibody conjugated to an Alexa-488 fluorophore (green). Aggregated protein and aggresome-like structures were detected using the Proteostat dye (red).Nuclei are stained with DAPI (blue). White arrows indicate the presence of aggresome-like structures. White 10 μm scale bars are indicated in the lower right of each panel. These data are representative of 3 separate trials

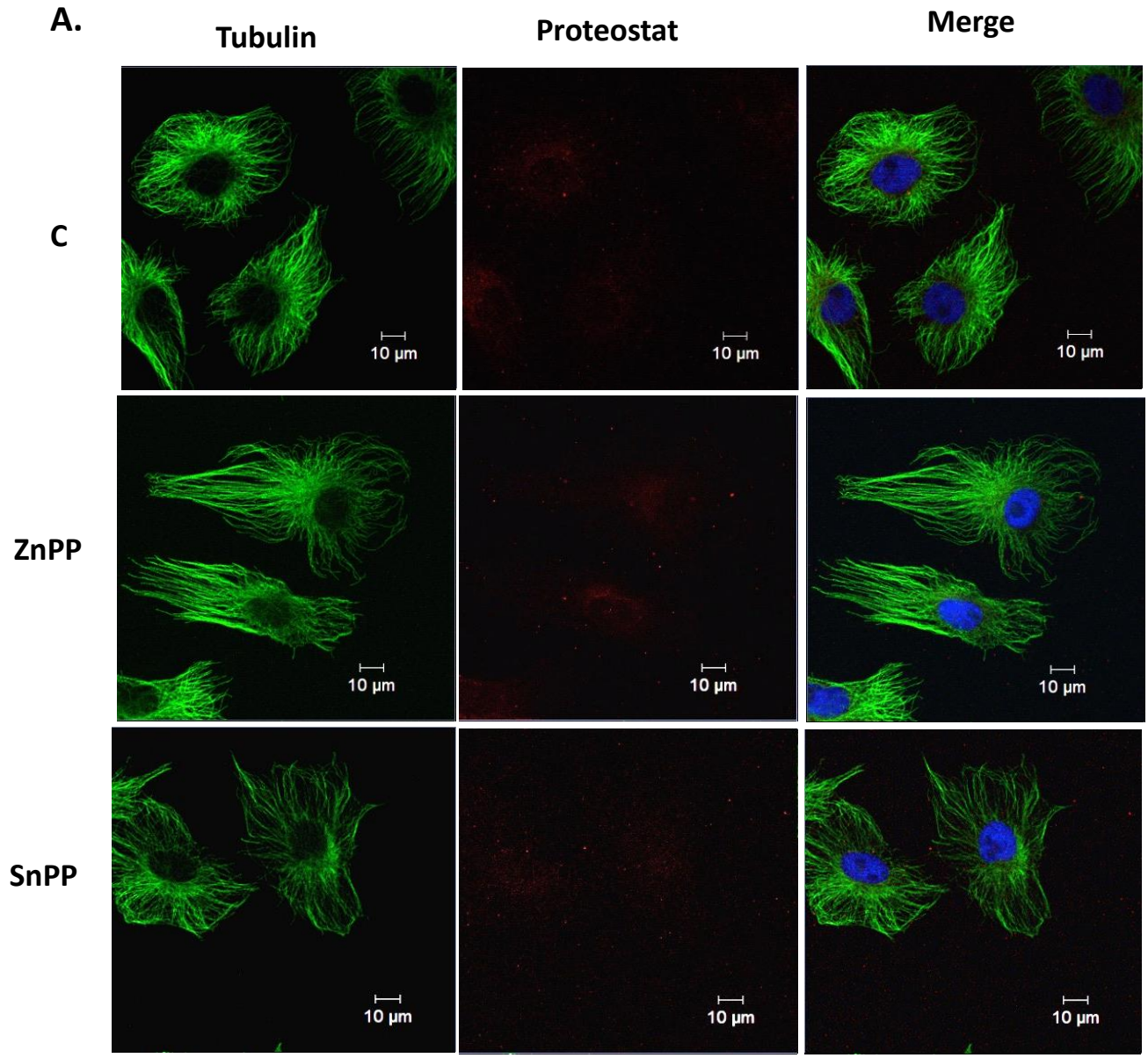
A.
Tubulin
Proteostat
Merge
C
ZnPP
SnPP
10 µm

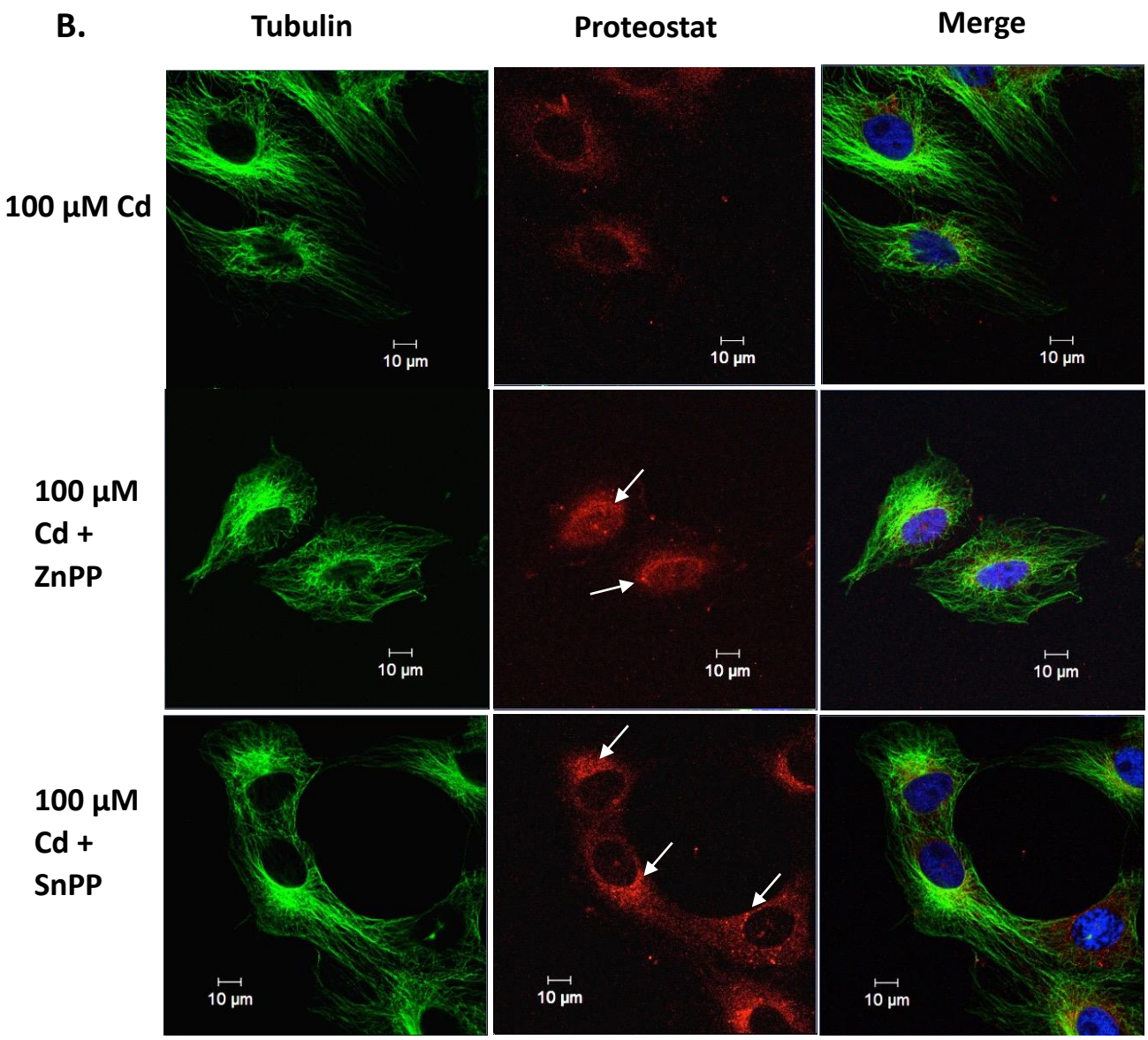
B.
Tubulin
Proteostat
Merge
100 µM Cd
100 µM Cd + ZnPP
100 µM Cd + SnPP
10 µm

with 5 μM ZnPP or 15 μM SnPP resulted in minimal accumulation of aggregated protein that was similar to control cells as determined by Proteostat dye staining. An increase in aggregated protein in the perinuclear region was detected in cells treated with 100 μM $CdCl_2$. However, this accumulation of aggregated protein was enhanced in cells treated with ZnPP or SnPP prior to supplementation with $CdCl_2$. Furthermore, these cells were characterized by the presence of larger, aggresome-like staining structures, as indicated by white arrows.

3.14 Effect of hemin and baicalein treatment on $CdCl_2$-induced changes to actin cytoskeletal structure and the accumulation of aggregated protein.

Previous studies reported that treatment of cells with hemin or baicalein have the potential to ameliorate the deleterious effects of potentially toxic conditions including $CdCl_2$ exposure (Salahudeen et al., 2001; Gozzelino et al., 2010; Cui et al., 2015). Furthermore, studies in mammalian cells have shown that pretreatment with hemin also protected cells against injurious levels of $CdCl_2$ (Srisook et al., 2005; Fouad et al., 2009). The next section of the present study investigated the ability of low levels of hemin or baicalein to protect A6 cells from relatively high concentrations of $CdCl_2$ (Fig. 36 & 37). Initial experiments examined the effect of a 4 h 10 μM hemin treatment followed by supplementation with 275 μM $CdCl_2$ for 16 h and a subsequent 4 h recovery in fresh media on actin cytoskeleton and HO-1 accumulation. As revealed in Fig. 36, treatment of cells with 10 μM hemin for 16 h had no discernable effect on the actin cytoskeleton whereas exposure of cells to 275 μM $CdCl_2$ resulted in actin cytoskeletal disorganization, cell rounding and membrane ruffling. However, treatment of cells with hemin prior to the addition of $CdCl_2$ resulted in the presence of control-like actin stress fibres although some membrane ruffling persisted at the cell periphery. The addition of 15 μM SnPP to hemin-

Figure 36. Effect of treatment with hemin and/or SnPP on Cd-induced HO-1 localization and actin organization. Cells were left untreated (C) or incubated with 275 μM $CdCl_2$ (Cd) for 16 h at 22 °C. In other experiments cells were treated for 4 h with 10 μM hemin (HM) and/or 15 μM SnPP prior to being supplemented with 275 μM $CdCl_2$. Nuclei and actin filaments were stained directly using DAPI (blue) and rhodamine phalloidin (red), respectively. HO-1 was detected with an anti-HO-1 antibody and the secondary antibody conjugate, Alexa-488 fluorophore (green). White 10 μm scale bars are indicated in the lower right of each panel. These data are representative of 3 separate experiments.

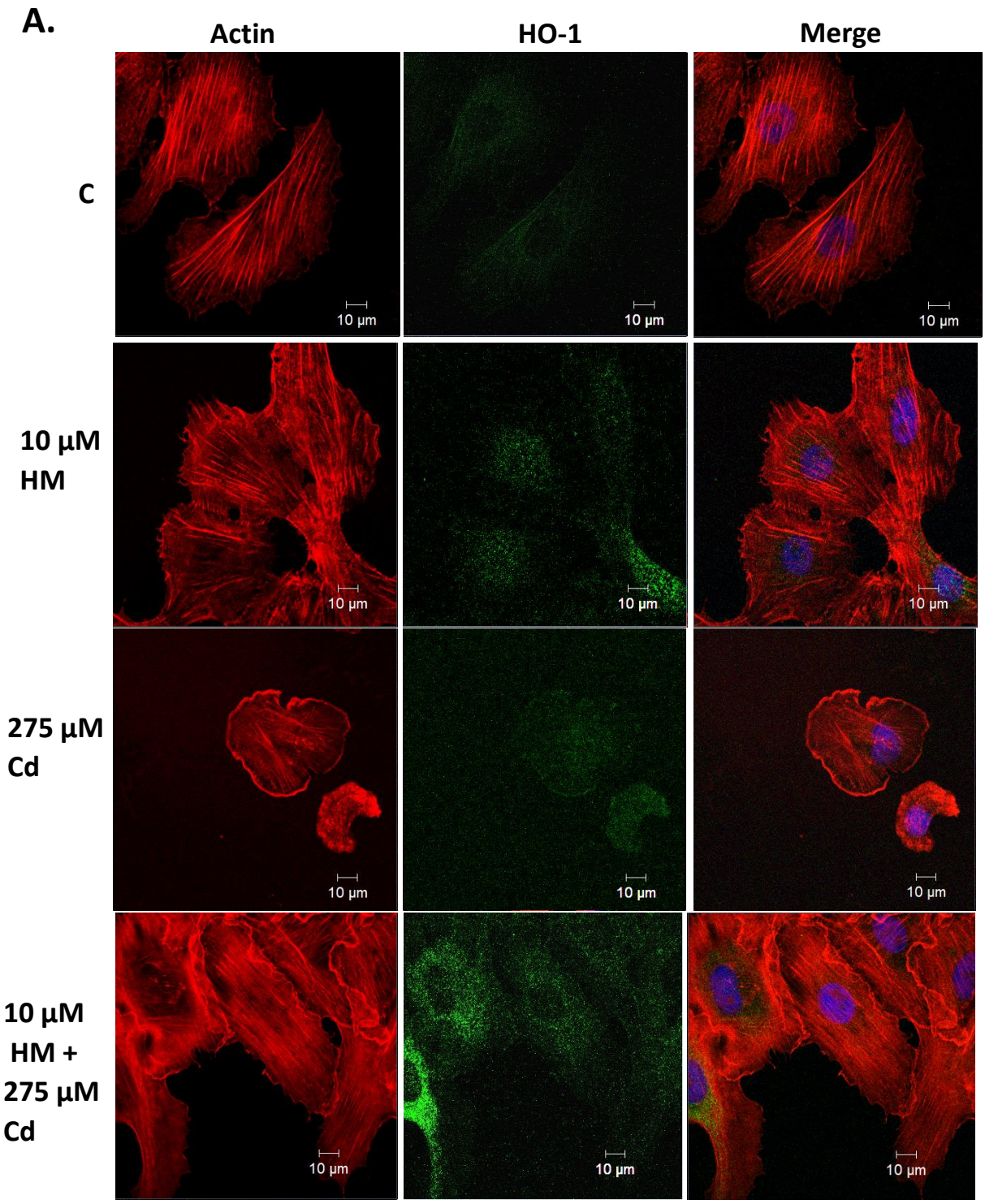
A.
Actin
HO-1
Merge
C
10 µM HM
275 µM Cd
10 µM HM + 275 µM Cd
10 µm

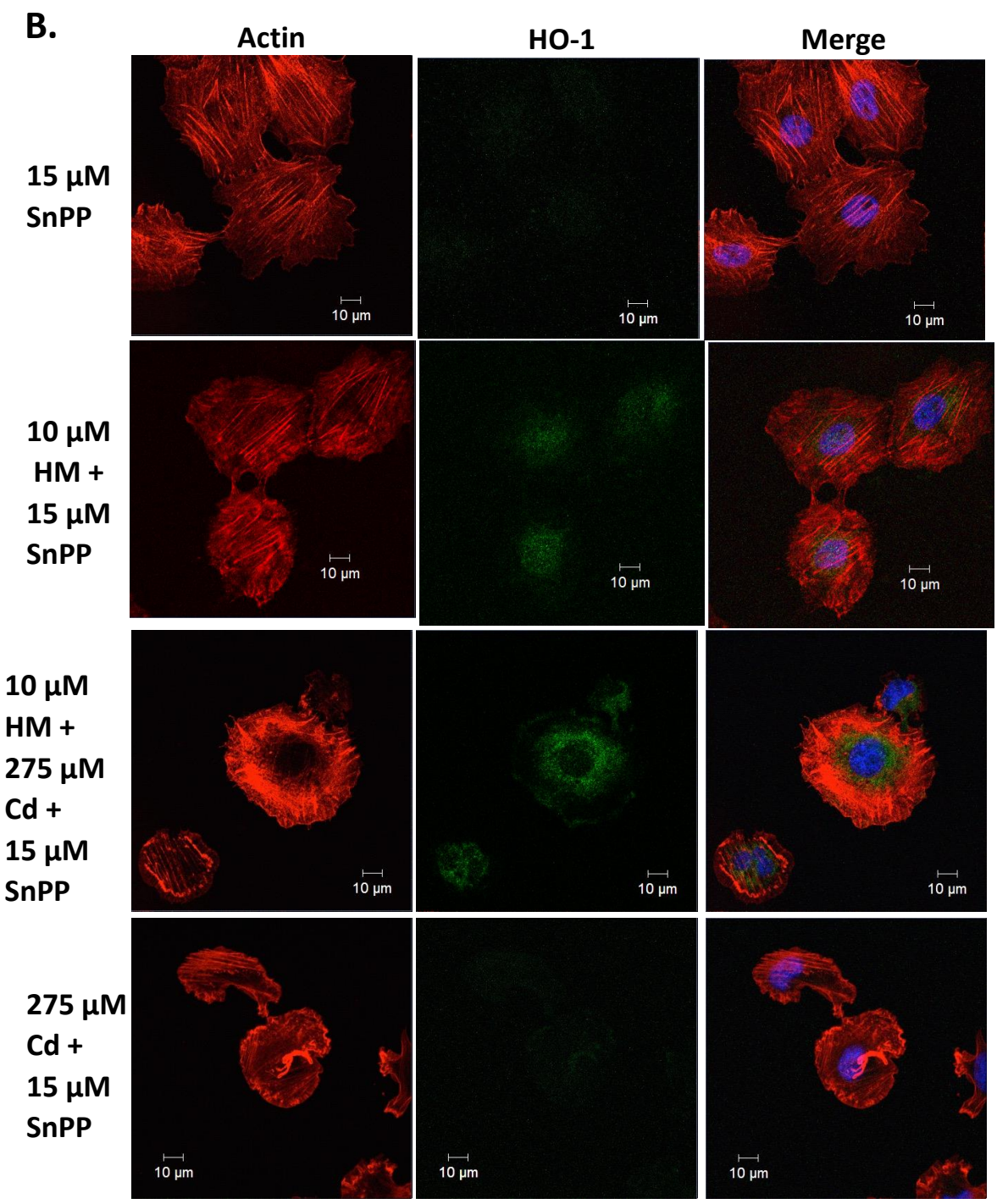
B.
Actin
HO-1
Merge
15 µM SnPP
10 µM HM + 15 µM SnPP
10 µM HM + 275 µM Cd + 15 µM SnPP
275 µM Cd + 15 µM SnPP
10 µm

Figure 37. Effect of treatment with baicalein and/or SnPP on Cd-induced HO-1 localization and actin organization. Cells were left untreated (C) or incubated for 16 h with 275 μM $CdCl_2$ (Cd) followed by a 4 h recovery in fresh media. In other experiments, cells were treated for 4 h with 50 μM baicalein (BC) and/or 15 μM SnPP before supplementation with 275 μM $CdCl_2$ followed by a 4 h recovery in fresh media. Nuclei and actin filaments were stained directly using DAPI (blue) and rhodamine phalloidin (red), respectively. HO-1 was detected with an anti-HO-1 antibody and the secondary antibody conjugate, Alexa-488 fluorophore (green). White 10 μm scale bars are indicated in the lower right of each panel. These data are representative of 3 separate trials.

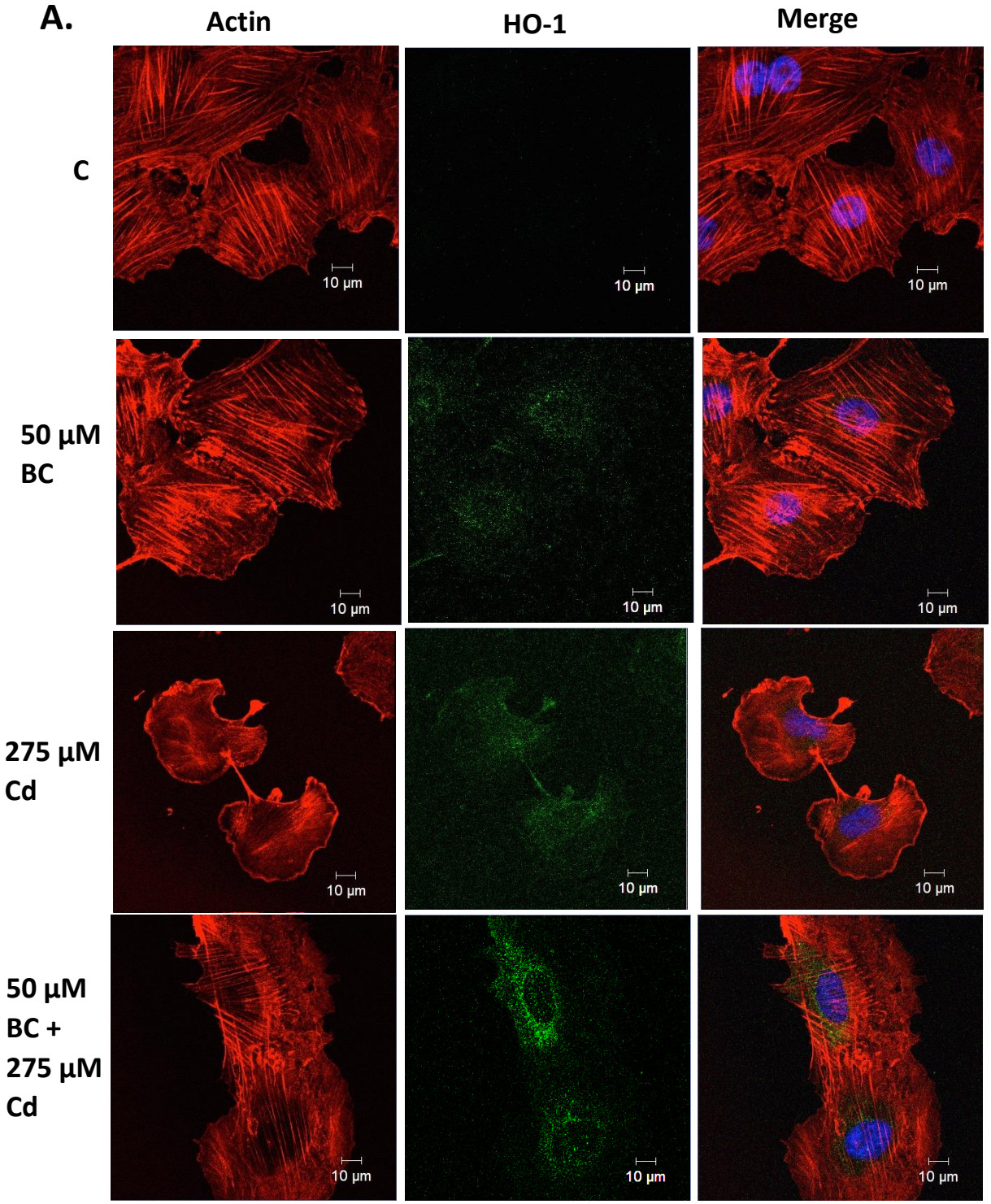
A.
Actin
HO-1
Merge
C
50 µM BC
275 µM Cd
50 µM BC + 275 µM Cd
10 µm

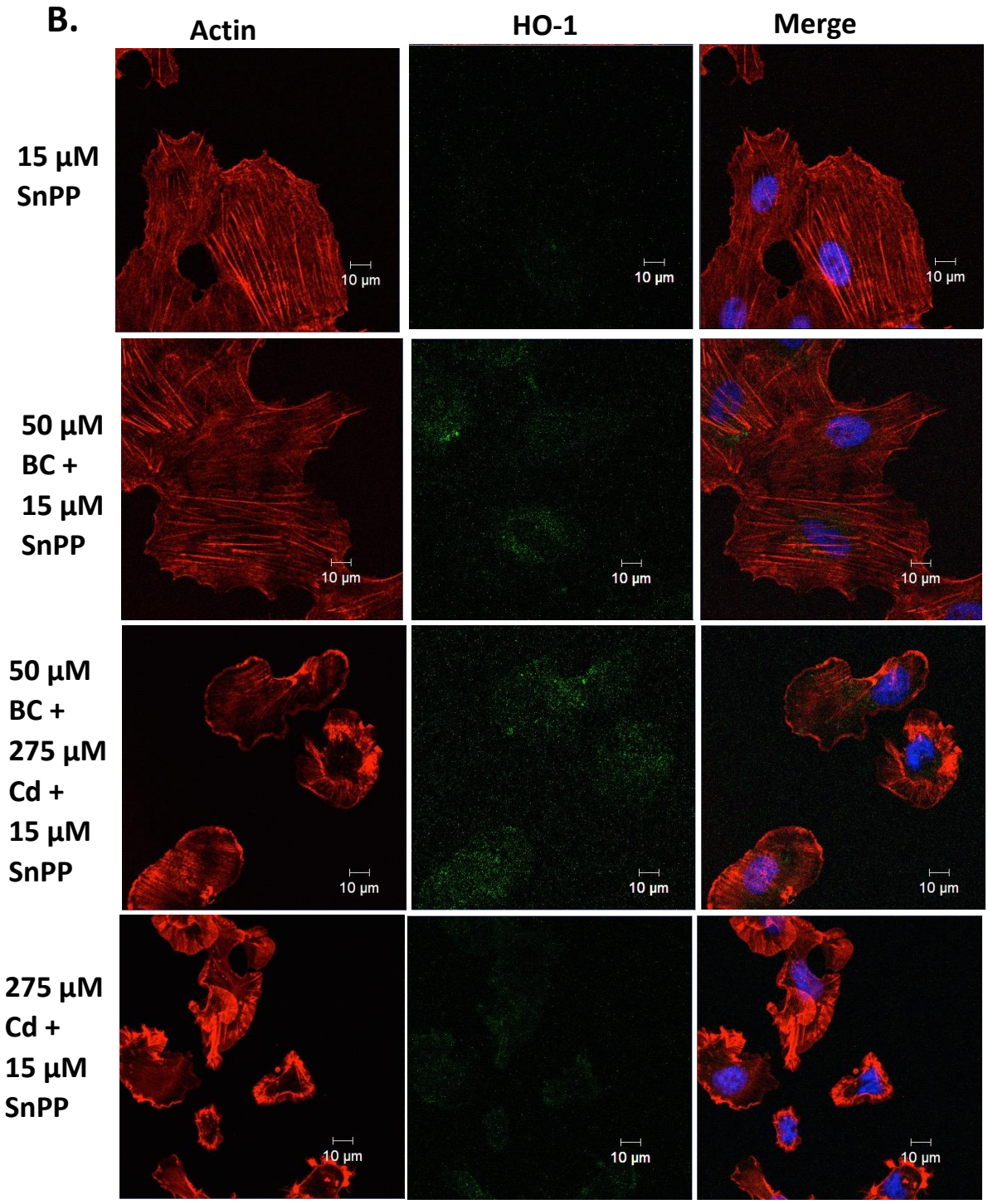
B.
Actin
HO-1
Merge
15 µM SnPP
50 µM BC + 15 µM SnPP
50 µM BC + 275 µM Cd + 15 µM SnPP
275 µM Cd + 15 µM SnPP
10 µm

treated cells resulted in a pattern of actin distribution similar to that found with hemin alone. Cells treated with $CdCl_2$ and SnPP without hemin also showed a severe disruption of the actin cytoskeleton. As shown in Fig. 37, exposure of cells to 50 μM baicalein prior to augmentation with 275 μM $CdCl_2$ resulted in the presence of actin stress fibres and a cell shape that was similar to control although some membrane ruffling was detected. Exposure of cells to SnPP and hemin treatment followed by the addition of $CdCl_2$ also resulted in an actin cytoskeleton that was similar to $CdCl_2$ alone, including cell rounding, membrane ruffling and cytoskeletal collapse. Additionally, abundant amounts of HO-1 were observed in the perinuclear region of cells pretreated with hemin or baicalein prior to the addition of $CdCl_2$ in contrast to lower levels of HO-1 found with hemin, $CdCl_2$ or SnPP alone (Fig. 36 and 37).

The effect of hemin or baicalein treatment prior to the addition of $CdCl_2$ on the levels of aggregated protein accumulation are shown in Fig. 38 and 39. Treatment of cells with 275 μM $CdCl_2$ resulted in the perinuclear accumulation of aggregated protein as well as the presence of large aggresome-like staining structures. Exposure of cells to 10 μM hemin or 50 μM baicalein followed by supplementation with $CdCl_2$ resulted in diminished amounts of both diffuse and perinuclear aggregated protein and aggresome-like staining structures. However, if cells were treated with SnPP and hemin or baicalein prior to the addition of $CdCl_2$, aggregated protein and aggresome-like structures were observed. In an examination of microtubule structure, treatment with 275 μM $CdCl_2$ resulted in some disorganization and intertwining of microtubules. This effect was mitigated in cells treated with hemin prior to $CdCl_2$ addition as they had more elongated, parallel microtubules compared to $CdCl_2$ alone. In cells that were treated with SnPP and hemin prior to supplementation with $CdCl_2$, the microtubules had a mesh-like appearance.

Figure 38. Effect of treatment with hemin and/or SnPP on Cd-induced aggregated protein and microtubular network. Cells were left untreated (C) or incubated with 275 μM $CdCl_2$ (Cd) for 16 h. Other treatments included incubation of cells with 10 μM hemin (HM) and/or 15 μM SnPP for 4 h prior to supplementation with 275 μM $CdCl_2$ for 16 h followed by a 4 h recovery in fresh media. Alpha-tubulin was detected using a mouse anti-α-tubulin antibody and an anti-mouse antibody conjugated to an Alexa-488 fluorophore (green). Aggregated protein and aggresome-like structures was detected by use of the Proteostat dye (red).Nuclei are stained with DAPI (blue). White arrows indicate the presence of aggresome-like structures. White 10 μm scale bars are indicated in the lower right of each panel. These data are representative of 3 separate experiments.

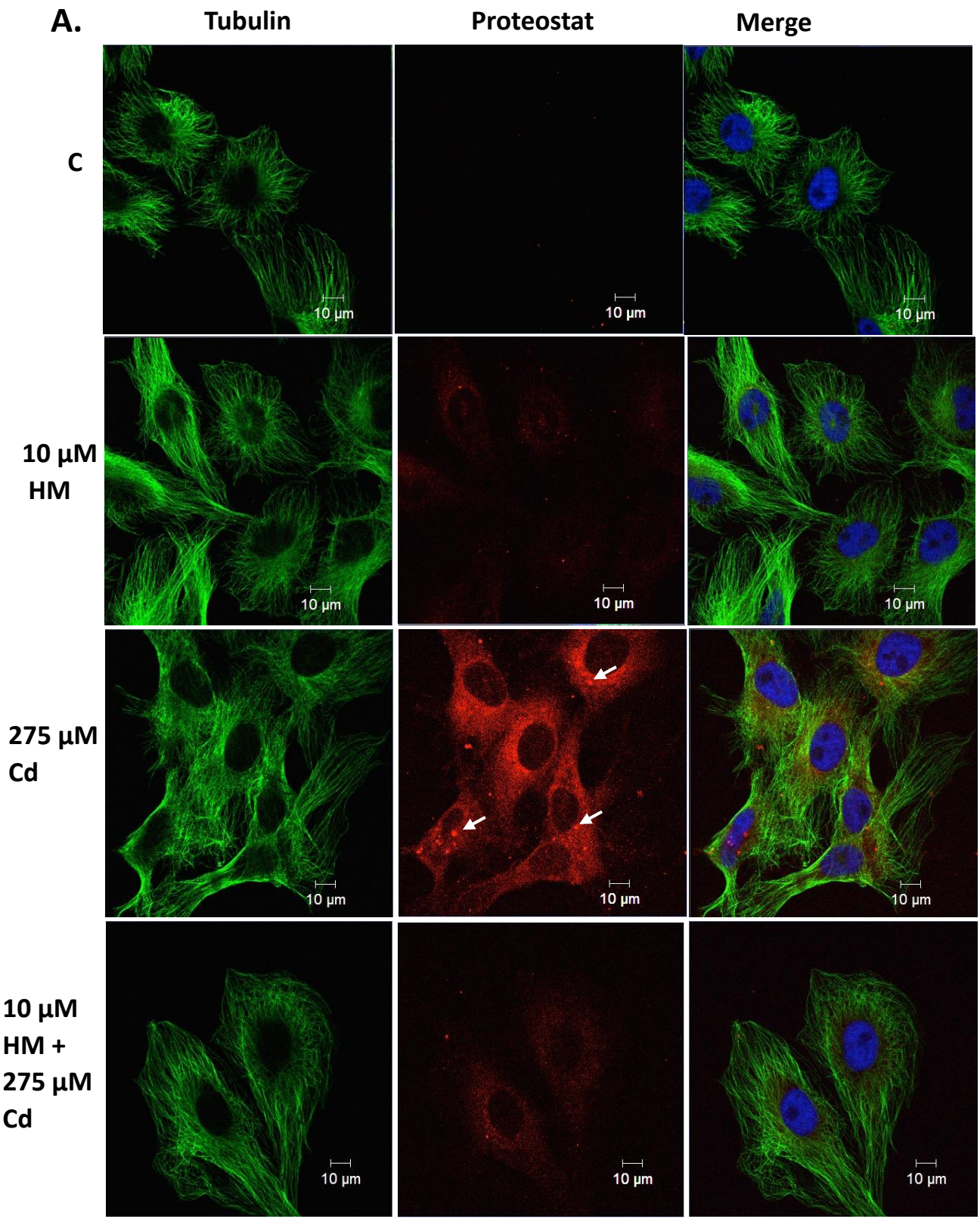
A.
Tubulin
Proteostat
Merge
C
10 µM HM
275 µM Cd
10 µM HM + 275 µM Cd
10 µm

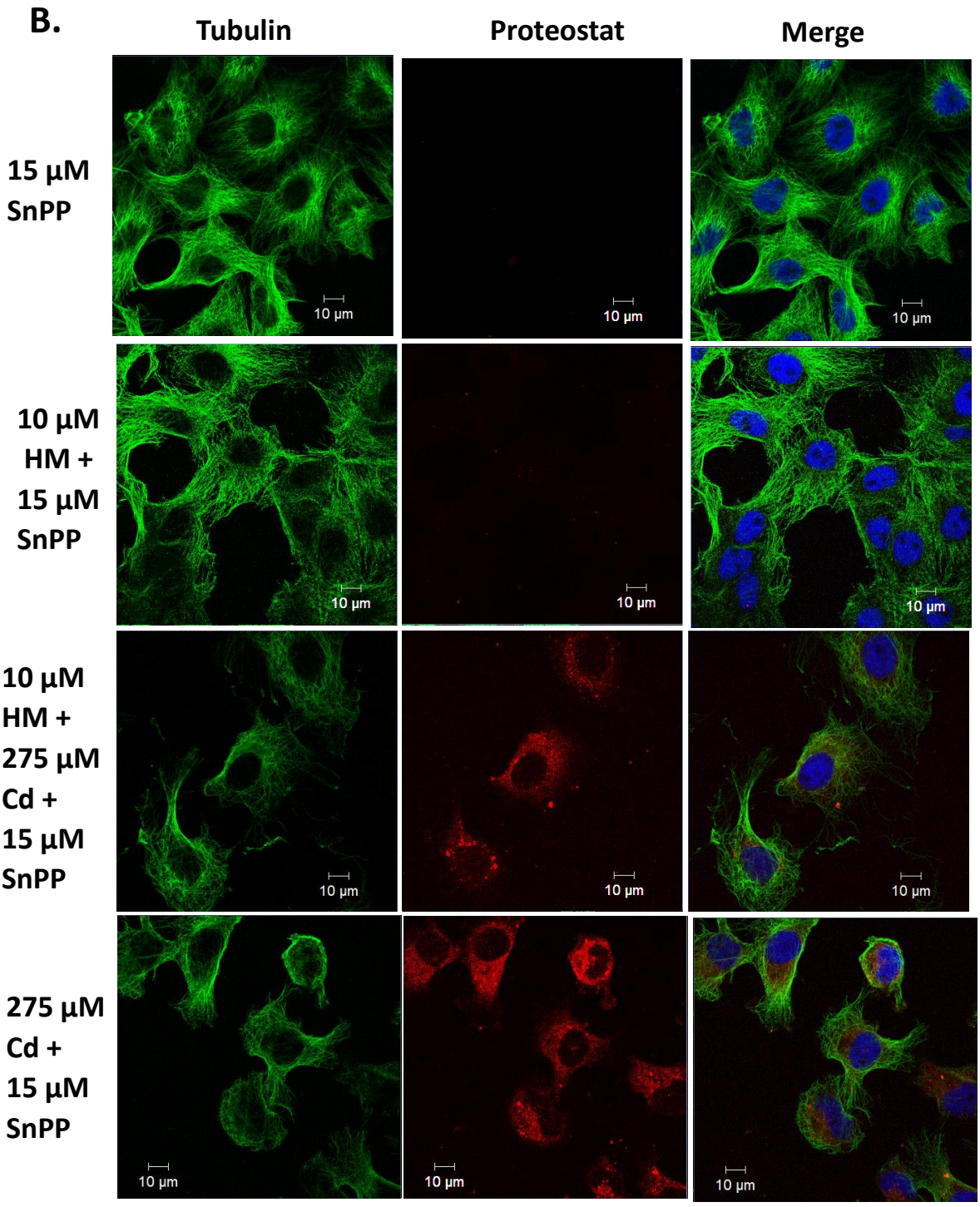
B.
Tubulin
Proteostat
Merge
15 µM SnPP
10 µM HM + 15 µM SnPP
10 µM HM + 275 µM Cd + 15 µM SnPP
275 µM Cd + 15 µM SnPP
10 µm

Figure 39. Effect of treatment with baicalein and/or SnPP on Cd-induced aggregated protein and microtubular network. Cells were left untreated (C) or incubated with 275 μM $CdCl_2$ (Cd) for 16 h. Other treatments included incubation of cells with 50 μM baicalein (BC) and/or 15 μM SnPP for 4 h prior to supplementation with 275 μM $CdCl_2$ for 16 h followed by a 4 h recovery in fresh media. Alpha-tubulin was detected using a mouse anti-α-tubulin antibody and an anti-mouse antibody conjugated to an Alexa-488 fluorophore (green). Aggregated protein and aggresome-like structures were detected using the Proteostat dye (red). Nuclei are stained with DAPI (blue). White arrows indicate aggresome-like structures. White 10 μm scale bars are indicated in the lower right of each panel. These data are representative of 3 separate trials.

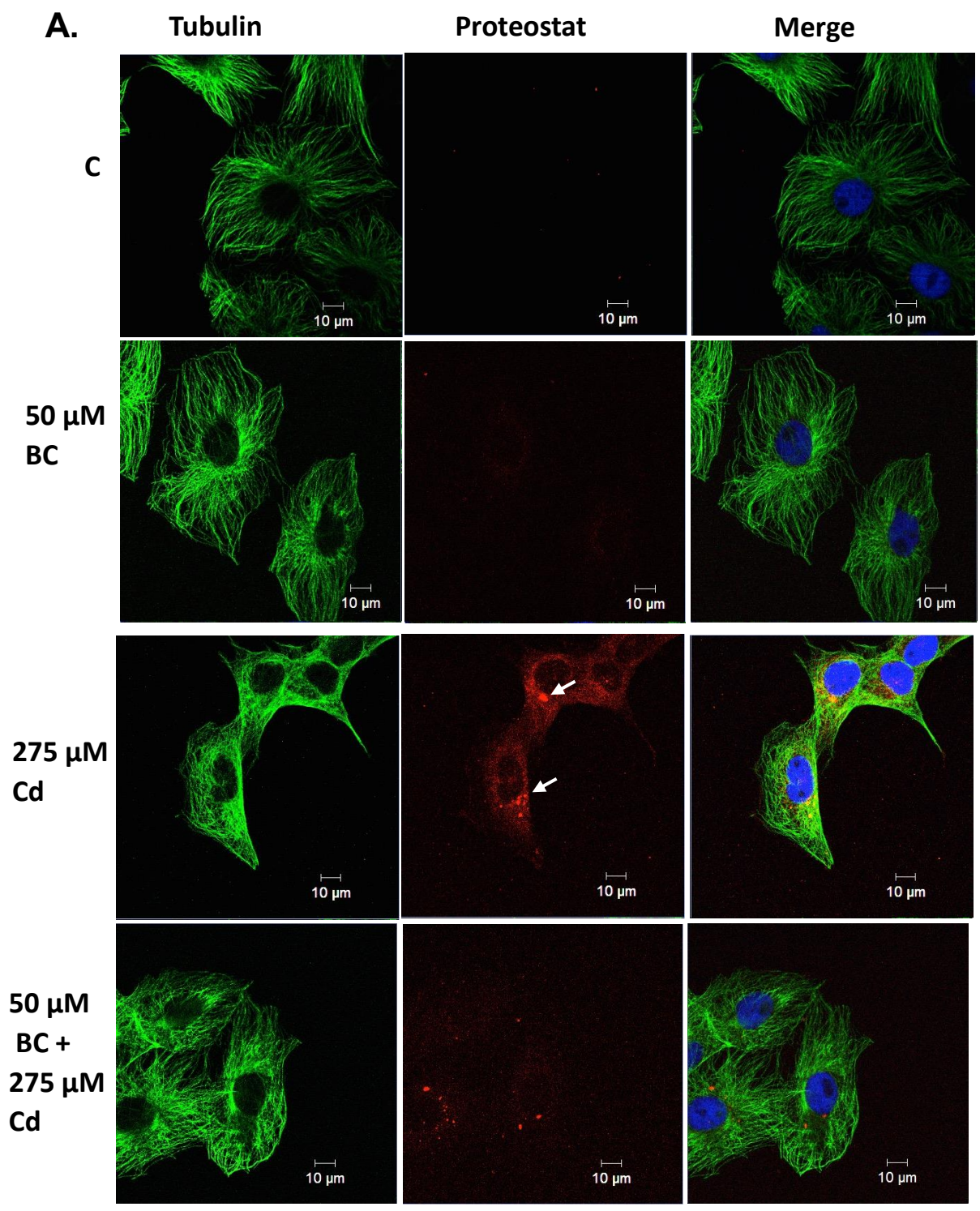
A.
Tubulin
Proteostat
Merge
C
50 µM BC
275 µM Cd
50 µM BC + 275 µM Cd
10 µm

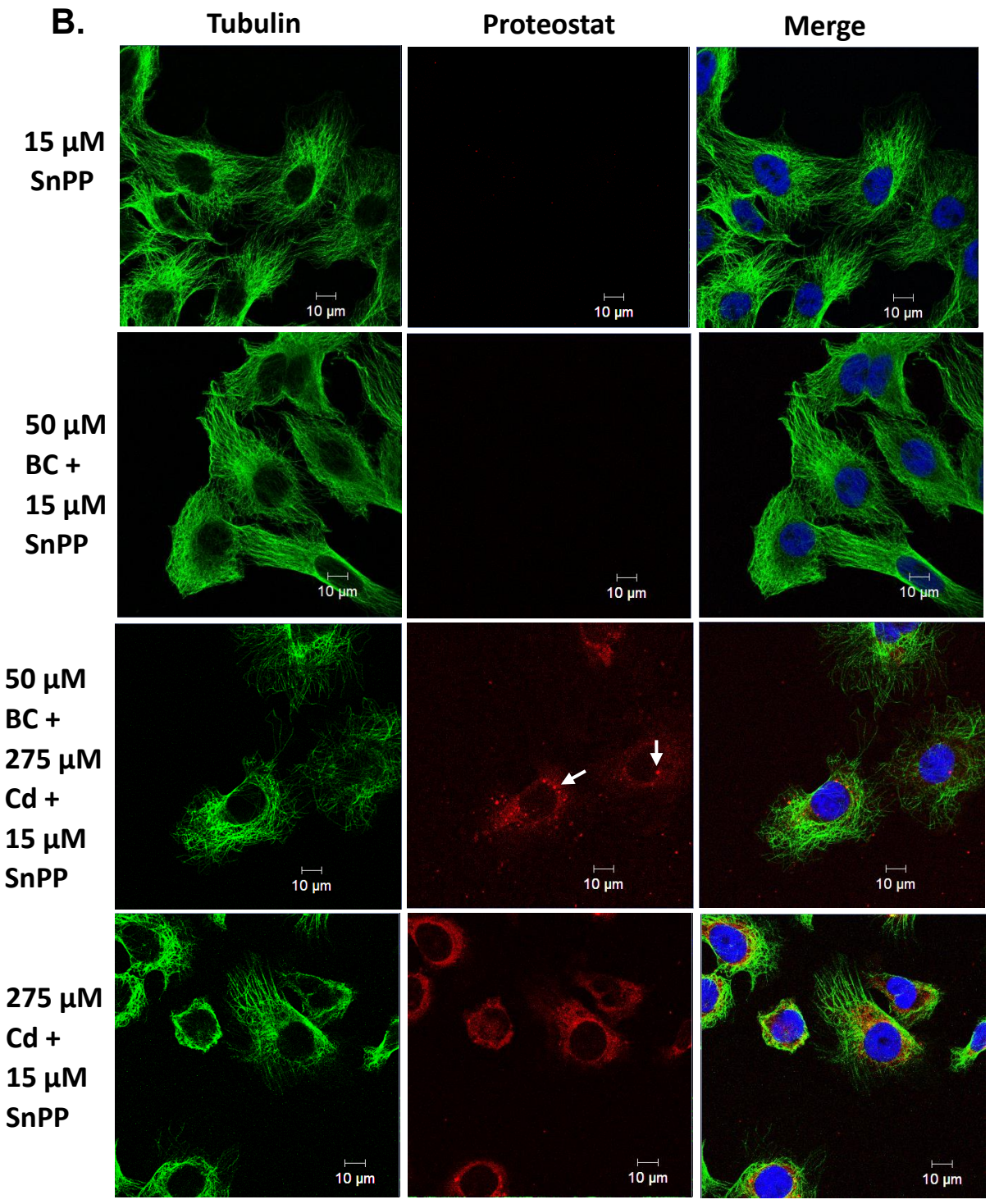
B.
Tubulin
Proteostat
Merge
15 µM SnPP
50 µM BC + 15 µM SnPP
50 µM BC + 275 µM Cd + 15 µM SnPP
275 µM Cd + 15 µM SnPP
10 µm

3.15 Effect of hemin, baicalein and SnPP treatment on the localization of $CdCl_2$-induced HSP30 and aggregated protein accumulation.

Previously, our laboratory reported that $CdCl_2$-induced aggresome-like structures that co-localized with the small HSP, HSP30 (Khan et al., 2015). Given these earlier results, HSP30 localization was examined in the current study (Fig. 40). In cells treated with $CdCl_2$ alone, HSP30 accumulated in a punctate pattern with larger staining structures, as indicated by the white arrows. These larger anti-HSP30 antibody stained structures co-localized with the aggresome-like structures (detected by the Proteostat dye), given their yellow colour in the merged channel. This finding was verified by means of Z-stack analysis (data not shown). In cells treated with hemin prior to supplementation with $CdCl_2$, the amount of aggregated protein was reduced compared to $CdCl_2$ alone whereas the amount of HSP30 accumulation in some cells was elevated and had a more diffuse pattern of cytoplasmic distribution and fewer larger structures. Addition of SnPP plus hemin prior to $CdCl_2$ treatment resulted in cells having a pattern of HSP30 accumulation that resembled $CdCl_2$ alone. The accumulation of HSP30 and aggregated protein was also investigated in cells that were treated with baicalein and $CdCl_2$ (Fig. 41). Treatment with baicalein followed by supplementation with $CdCl_2$ reduced the intensity of Proteostat dye staining as well as the lower number of larger-aggresome structures compared to what was found in $CdCl_2$-treated cells. However, HSP30 levels were elevated in baicalein and $CdCl_2$-supplemented cells compared to cells treated with $CdCl_2$ alone. As with hemin treatment, exposure of cells to baicalein resulted in a diffuse cytoplasmic pattern of HSP30 accumulation with enrichment in the perinuclear region and fewer aggresome-like structures, compared to $CdCl_2$ treatment alone, that co-localized with HSP30 as determined by Z-stack analysis (data not shown). Finally, the addition of SnPP plus baicalein prior to $CdCl_2$ treatment in A6 cells resulted

Figure 40. Effect of treatment with hemin and SnPP on Cd-induced HSP30 and aggregated protein and aggresome-like structures. Cells were left untreated (C) or incubated with 275 μM $CdCl_2$ (Cd) for 16 h. Other treatments included incubation of cells with 10 μM hemin (HM) and/or 15 μM SnPP for 4 h prior to supplementation with 275 μM $CdCl_2$ for 16 h followed by a 4 h recovery in fresh media. Rabbit anti-HSP30 antibody and an anti-rabbit antibody conjugated to an Alexa-488 fluorophore were used to detect HSP30 (green). Aggregated protein and aggresome-like structures (white arrows) was detected by means of the Proteostat dye (red). Nuclei are stained with DAPI (blue). White 10 μm scale bars are indicated in the lower right of each panel. These data are representative of 3 separate experiments.

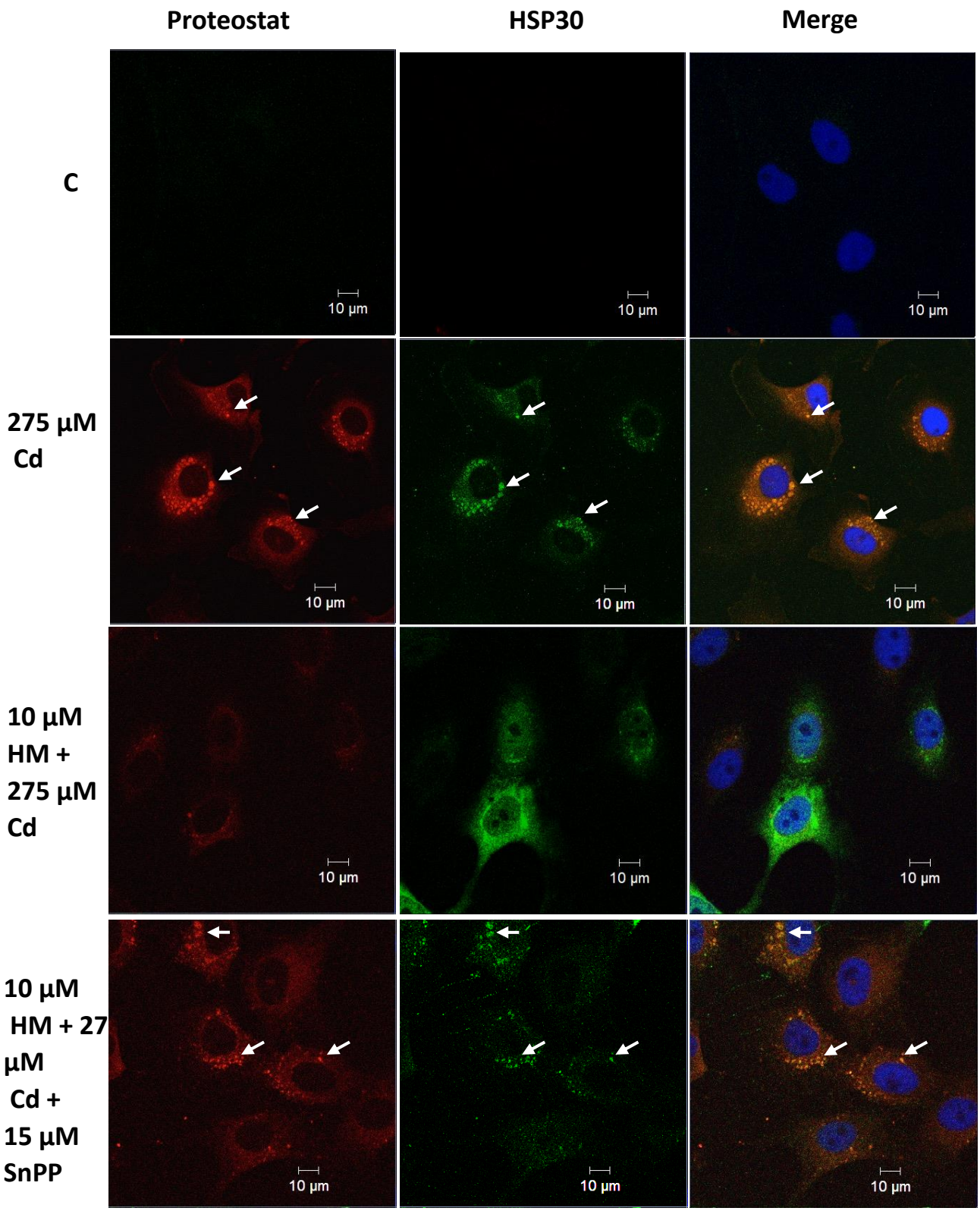
Proteostat
HSP30
Merge
C
275 µM Cd
10 µM HM + 275 µM Cd
10 µM HM + 27 µM Cd + 15 µM SnPP
10 µm

Figure 41. Effect of treatment with baicalein and SnPP on Cd-induced HSP30 and aggregated protein and aggresome-like structure accumulation. Cells were left untreated (C) or incubated with 275 μM $CdCl_2$ (Cd) for 16 h. Other treatments included incubation of cells with 50 μM baicalein (BC) and/or 15 μM SnPP for 4 h prior to supplementation with 275 μM $CdCl_2$ for 16 h followed by a 4 h recovery in fresh media. Rabbit anti-HSP30 antibody and an anti-rabbit antibody conjugated to an Alexa-488 fluorophore were used to detect HSP30 (green). Aggregated protein and aggresome-like structures were detected using Proteostat dye (red). Nuclei are stained with DAPI (blue). White arrows indicate aggresome-like structures. White 10 μm scale bars are indicated in the lower right of each panel. These data are representative of 3 separate trials.

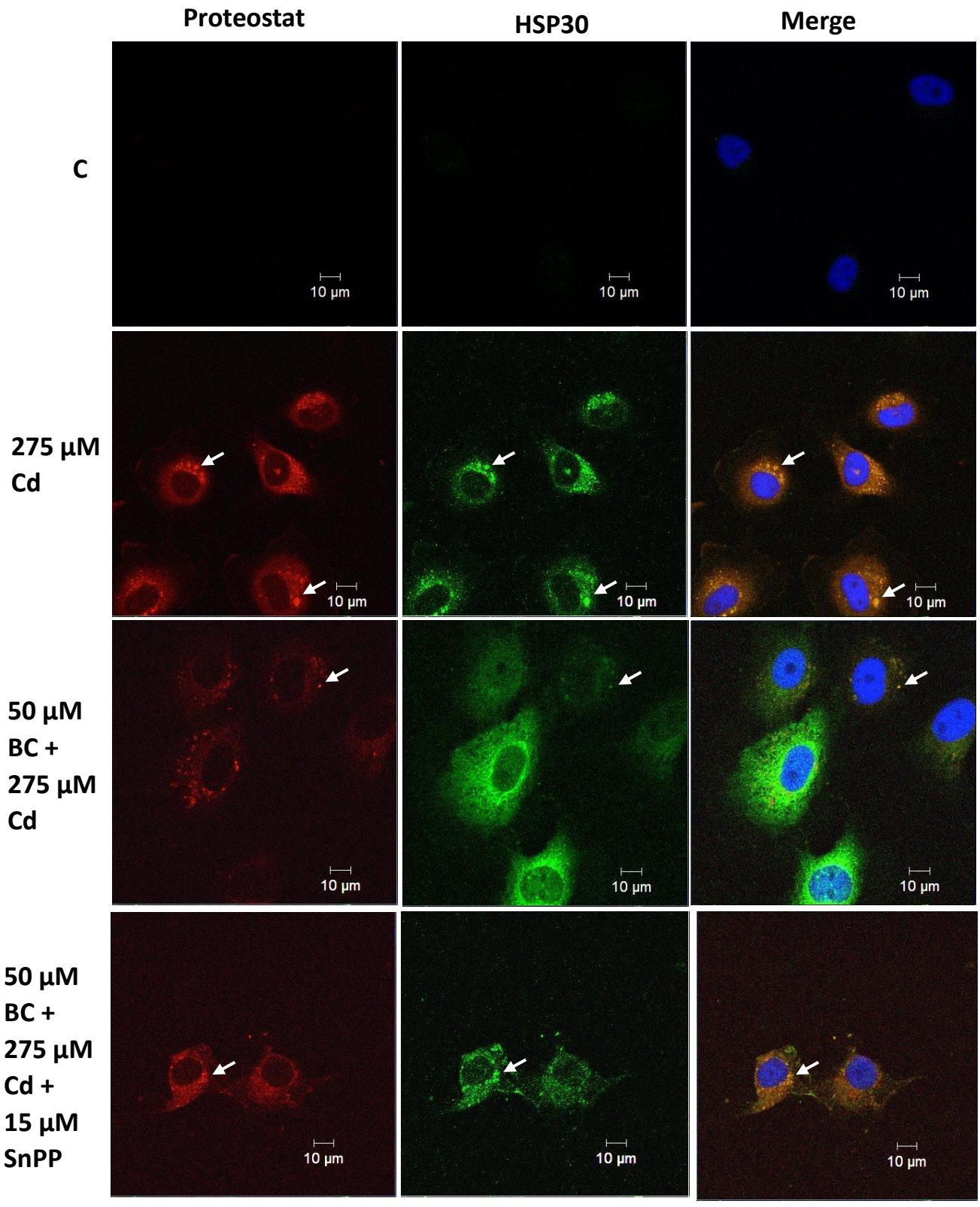
Proteostat
HSP30
Merge
C
275 µM Cd
50 µM BC + 275 µM Cd
50 µM BC + 275 µM Cd + 15 µM SnPP
10 µm

in a pattern of HSP30 accumulation, which resembled that of $CdCl_2$ alone.

4.0 Discussion

This study has described for the first time, in *Xenopus laevis*, the effects of hemin and baicalein on HO-1 accumulation. Furthermore, hemin and baicalein treatment of A6 kidney epithelial cells conferred cytoprotection against a $CdCl_2$ stress challenge, which was assessed by the maintenance of the actin cytoskeleton and an inhibition in the accumulation of aggregated protein and aggresome-like structures. HO-1 enzyme activity inhibitor treatment determined that HO-1 accumulation was vital in cytoprotection in response to $CdCl_2$ treatment.

Analysis of the *X. laevis* HO-1 amino acid sequence determined that it shared 91% sequence identity with *X. tropicalis* HO-1 but only 50 to 64% identity with bird, fish, reptile, and mammalian HO-1 or constitutive human or *X. laevis* HO-2. In general, the present findings were in agreement with previous studies of *X. laevis* HO-1 amino acid sequence (Music et al., 2014). However, a more detailed comparison of the amino acid sequence alignment of *X. laevis* and *H. sapiens* HO-1 amino acid sequences revealed a 100% shared identity in residues that were important for heme binding including a histidine involved in iron binding, which is essential for its catalytic function (Schuller et al., 1999). Another highly conserved feature of *Xenopus* and human HO-1 is a 24 amino acid HO-1 signature domain starting at P189 in *Xenopus* (Maines and Gibbs, 2005). In this region, *X. laevis* and *H. sapiens* sequence identity was 95% (23 out of 24 amino acids). Conservation was lower in other regions of HO-1, specifically near the N- and C-terminus and the flexible linker region. It was reported that goldfish HO-1 had a similar pattern of conservation, with high amino acid identity with other species in the core catalytic region and greater variability in the N-terminal, C-terminal helix and the flexible linker regions (Wang et al., 2008). Computer model predictions of *X. laevis* and *H. sapiens* HO-1 indicated that both proteins have similar secondary structure in the heme-binding site region. Furthermore, the similarity

between the computer models suggested that the non-conserved regions of *X. laevis* HO-1 were not radically different from *H. sapiens* as to affect the overall theoretical structure of the protein. This finding suggested that the *X. laevis* and human HO-1 may have a similar catalytic mechanism.

Initial immunoblot studies determined that hemin-induced HO-1 accumulation in A6 cells was concentration- and time-dependent. For example, hemin induced elevated HO-1 levels compared to control at 10 μM hemin with a peak at 25 μM. Also, continuous treatment of cells with 25 μM hemin induced transient accumulation of HO-1, which peaked at 12 h followed by a gradual reduction from 16 to 48 h. In other studies, hemin concentrations ranging from 2.5 to 20 μM were employed to induce the accumulation of *ho-1* mRNA or encoded protein in rat glioma, human kidney and HeLa cells as well as in human monocytes (Shibahara, 1987; Masuya et al., 1998; Salahudeen et al., 2001; Lang et al., 2004). In human monocytes, hemin-induced accumulation of HO-1 mRNA was dose-dependent while the accumulation of HO-1 protein was transient showing elevated levels at 12 h, maximal amounts at 24 h followed by a reduction at 48 h (Lang et al., 2004).

Baicalein-induced HO-1 accumulation in A6 cells was also dose-dependent with detectable amounts at 50 μM and peak levels at 200 μM. As found with hemin, continuous baicalein treatment also induced a transient increase in HO-1 levels with maximal amounts at 16 h and reduced levels at 24 h. In rat C6 glial cells, a dose-dependent increase in HO-1 was reported after baicalein treatment using concentrations ranging from 25 to 200 μM (Chen et al., 2006). Choi et al. (2016) also reported a time-dependent accumulation in response to baicalein in glial cells from 1 to 6 h (their final time point). Dose-dependent (12.5 to 200 μM) and time-dependent (4 to 12 h) increases in baicalein-induced HO-1 accumulation were also reported with

mouse macrophages and rat adrenal pheochromocytoma cells (Lin et al., 2007; Zhang et al., 2012). The results of the present research in *X. laevis* cells indicate that treatment with hemin or baicalein induced a dose- and temperature-dependent accumulation of HO-1 as reported in mammalian cultured cells.

Additionally, this study determined that $CdCl_2$-induced HO-1 accumulation occurred in a concentration- and time-dependent manner in A6 cells. For example, treatment with 25 μM $CdCl_2$ was sufficient to cause a detectable increase in the amount of HO-1, with maximum accumulation observed after treatment with 200 μM $CdCl_2$. Accumulation of HO-1 was detectable at 8 h of treatment with 200 μM $CdCl_2$ before reaching its maximum level at 24 h. These results are supported by previous analyses in our laboratory regarding $CdCl_2$-induced enhancement of HO-1 in A6 cells (Music et al., 2014). Induction of HO-1 by cadmium has been documented across a wide range of organisms. In Atlantic cod cell cultures, an increase in HO-1 accumulation occurred after 24 h of treatment with 100 μM $CdCl_2$ (Søfteland et al., 2010). In mouse hepatoma cells, HO-1 mRNA was detected after 4 h of treatment with 2.5 μM $CdCl_2$ while in chicken liver cells, an increase in heme oxygenase activity was detected after administration of 2 μM $CdCl_2$ (Sardana et al., 1982; Alam et al., 1989). Also, HO-1 mRNA was detected in human leukemia cells treated with 10 μM $CdCl_2$ after 8 h (Taketani et al., 1989). Finally, an increase in HO-1 mRNA occurred in soybean root nodules 48 h after exposure to 200 μM $CdCl_2$ (Balestrasse et al., 2008). The present study found that $CdCl_2$ treatment of *X. laevis* cells also induced the accumulation of HSP70 and HSP30. Studies in our laboratory reported that $CdCl_2$ was capable of inducing the heat shock response in A6 cells leading to the accumulation of HSP30 and HSP70 (Woolfson and Heikkila, 2009; Khamis and Heikkila, 2013; Khan et al., 2015; Shirriff and Heikkila, 2017). Furthermore, previous findings indicated that treatment with

the HSF1 inhibitor, KNK437, inhibited $CdCl_2$-induced HSP30 and HSP70 accumulation (Voyer and Heikkila, 2008; Khamis and Heikkila, 201). It was suggested that $CdCl_2$ treatment of cells can cause an increase in unfolded proteins through either oxidative damage or by the formation of polydentate coordination complexes with the protein backbone (Galazyn-Sidorczuk et al., 2009; Tamás et al., 2014). The accumulation of unfolded protein then acts as a trigger for HSF1 activation leading to the expression of *hsp* genes in an attempt to counteract the formation of toxic protein aggregates (Westerheide and Morimoto, 2005; Morimoto 2008).

The inhibition of hemin- or baicalein-induced HO-1 accumulation in response to actinomycin D or cycloheximide treatment indicated that HO-1 accumulation was the consequence of *de novo* transcription and translation. Analysis of the promoter region upstream of the *X. laevis ho-1* transcriptional start site revealed key *cis*-acting promoter elements that may be involved in stress-induced *ho-1* gene expression. As in humans and mice, the *X. laevis ho-1* promoter possesses multiple MARE sequences, suggesting the involvement of the transcription factors, Nrf-2/Keap1 and Bach1 in *ho-1* gene expression. Previous reports from our laboratory speculated that $CdCl_2$ induction of HO-1 was due to the generation of ROS and disruption of Nrf-2/Keap1 association causing Nrf-2 stabilization (Fig. 42; Music et al., 2014). However, hemin- or baicalein-induced accumulation may rely on an alternate mechanism. As shown in this study, hemin treatment did not promote an increase in Nrf-2 levels. In other organisms, it was reported that heme was capable of directly binding to the repressor protein, Bach1, which caused it to detach from the MARE site, thus permitting the binding of Nrf-2. Therefore, it is likely that hemin treatment of A6 cells resulted in an inhibition of Bach1 repression and that constitutive levels of Nrf-2 were sufficient to bind to the MARE site and cause HO-1 transcription (Fig. 42). While baicalein treatment of A6 cells resulted in increased Nrf-2 levels, this treatment induced

Figure 42. Induction of *ho-1* gene expression induction by hemin, baicalein or cadmium. A) Treatment with hemin increases intracellular heme levels (1). Increased heme binds to Bach1 (2), causing its export from the nucleus and degradation (3). This frees the MARE element and permits binding by low levels of Nrf2 (4). While HSF involvement in hemin-induced HO-1 accumulation was indicated by KNK437 experiments, the exact mechanism of HSF involvement remains undetermined although it may bind to the HSE or to CdRE either alone or bound to Pescadillo (5). B) Baicalein disrupts Nrf2-Keap1 interactions by binding to Keap1 (1). This results in increased Nrf2 stabilization and accumulation (2) permitting it to bind to MARE and initiating *ho-1* gene expression (3). As stated earlier, partial inhibition of Bach1 repression by endogenous heme is sufficient to allow for HO-1 expression (4). HSF may be involved in baicalein-induced HO-1 accumulation as mentioned above (5). C) Cadmium, either through increased ROS generation or modification of cysteine residues of Keap1 (1), disrupts the Keap1-Nrf2 interaction (2). This results in an increase in Nrf2 stabilization and accumulation allowing it to bind to MARE resulting in *ho-1* gene expression (3). Partial inhibition of Bach1 repression by endogenous heme is sufficient to allow *ho-1* gene expression (4). HSF involvement in ho-1 gene expression may occur via binding to HSE or to CdRE alone or complexed with Pescadillo (5). Cadmium exposure also causes an increase in unfolded proteins either directly or via ROS generation (6). Unfolded protein accumulation results in HSF activation (7) and the *hsp* gene expression (8).

A.

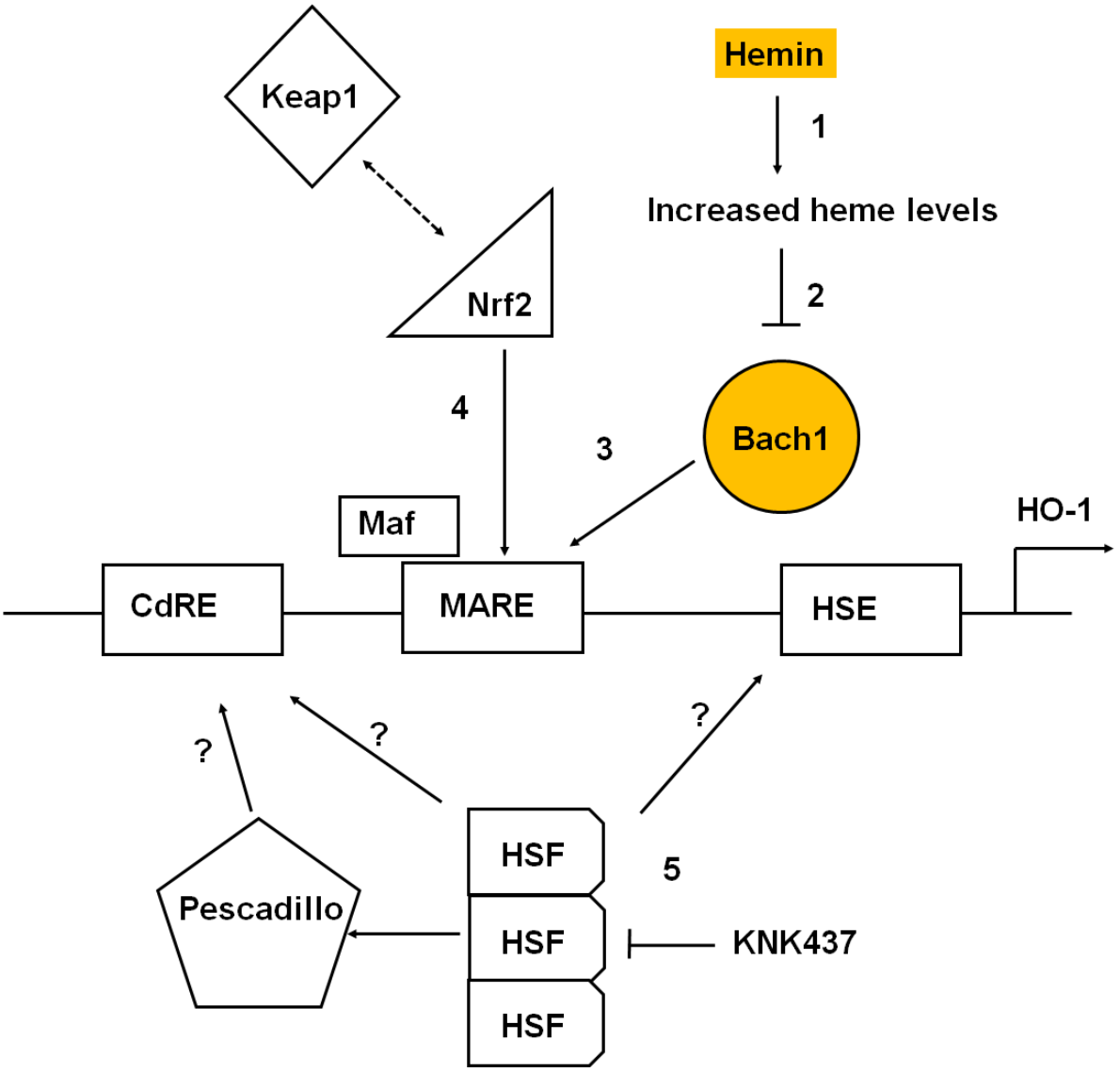
Keap1
Hemin
1
Increased heme levels
2
Nrf2
4
3
Bach1
Maf
HO-1
CdRE
MARE
HSE
?
?
?
HSF
5
Pescadillo
HSF
KNK437
HSF

B.

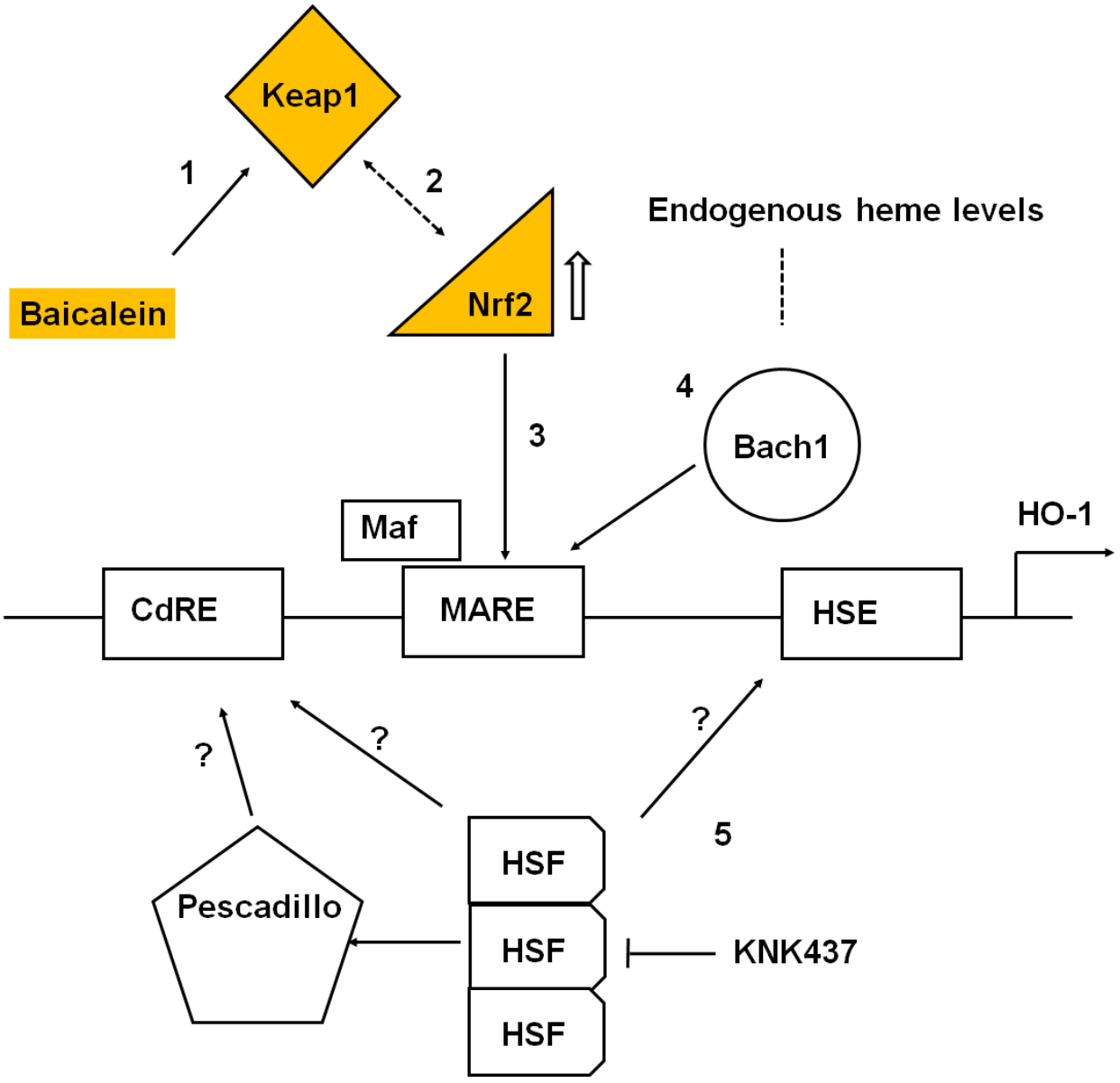
Keap1
1
2
Endogenous heme levels
Baicalein
Nrf2
3
4
Bach1
Maf
HO-1
CdRE
MARE
HSE
?
?
?
5
HSF
HSF
HSF
Pescadillo
KNK437

C.

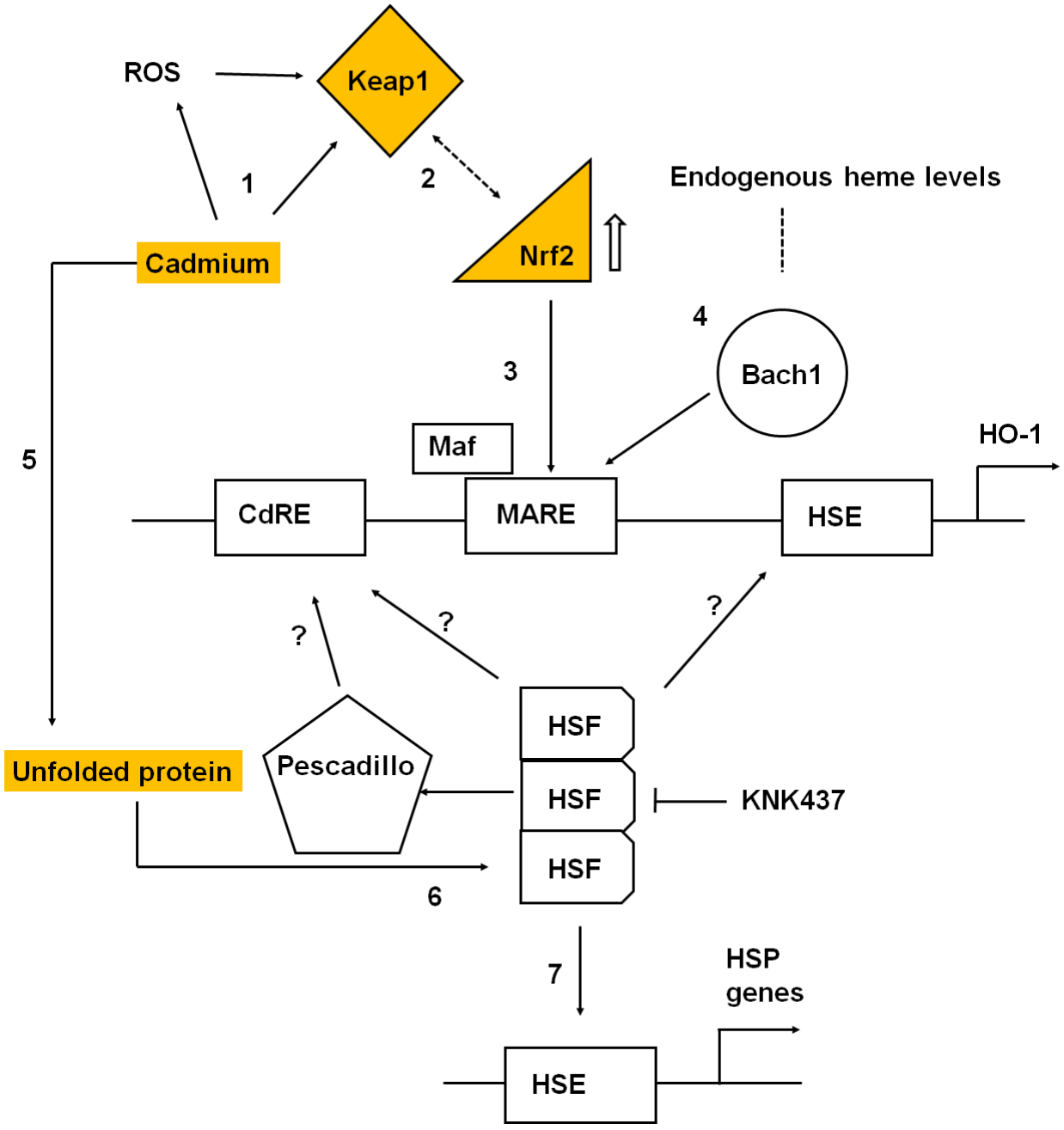
ROS
Keap1
1
2
Endogenous heme levels
Cadmium
Nrf2
4
3
Bach1
Maf
HO-1
5
CdRE
MARE
HSE
?
?
?
HSF
Pescadillo
HSF
KNK437
Unfolded protein
HSF
6
7
HSP
genes
HSE

only a slight increase in ROS levels compared to $CdCl_2$ treatment. Other studies suggested that baicalein may directly modify cysteine residues on Keap-1 causing its disassociation from Nrf-2 resulting in increased Nrf-2 stabilization (Zhang et al., 2012, Cui et al., 2015). This explanation is consistent with the present study, in which baicalein treatment increased Nrf-2 levels and a mild level of oxidative stress (Fig. 42). However, further studies will be required to verify this possible mechanism.

In *X. laevis* cells, the HSF1 DNA binding inhibitor, KNK437, inhibited the accumulation of HO-1 in response to hemin, baicalein or $CdCl_2$ treatment. Furthermore, DNA sequence analysis determined that the promoter region of the *X. laevis ho-1* gene has CdRE and HSE elements. As mentioned in the introduction, these elements were capable of binding HSF1 although these events were not sufficient by themselves to induce *ho-1* gene expression in HeLa cells (Koizumi et al., 2007). Also, the possibility that HSF1 activation by hemin or baicalein was necessary for HO-1 accumulation was not supported by the finding that treatment with these agents did not induce a detectable increase in either HSP70 or HSP30. Also, earlier studies reported that HO-1 accumulation was not heat shock-inducible in *X. laevis* A6 cells and in a variety of human cell lines, including alveolar macrophages, hepatoma, glioma, fibroblast and others (Yoshida et al., 1988; Keyse and Tyrrell, 1989; Taketani et al., 1989; Mitani et al., 1990; Okinaga et al., 1996; Music et al., 2014). It has been suggested that the involvement of HSF1 in HO-1 induction may be indirect, possibly acting in conjunction with another transcription factor, such as pescadillo (Sikorski et al., 2006). In this latter study, pescadillo interacted with the CdRE in the *ho-1* promoter and that overexpression of pescadillo increased HO-1 accumulation in human kidney cells. The possibility of pescadillo and HSF1 acting in concert was proposed in a study that identified HSF1/CdRE binding involvement in *ho-1* gene expression but noted that

HSF1 activation alone was not sufficient to result in transcription of CdRE containing genes (Koizumi, 2007). Another possibility was the involvement of an alternative HSF family member in HO-1 activation. It was reported that hemin treatment resulted in an increase in HSF2 binding to promoter regions in human leukemia cells (Sistonen et al., 1992). Further studies using leukemia cells showed by means of chromatin immunoprecipitation that HSF2 binding was activated by hemin but not heat shock (Trinklein et al., 2004). It has also been shown that HSF2 can interact with HSEs as a heterooligomer with HSF1 (Östling et al., 2007). Thus, it is possible that KNK437 may have an inhibitory effect on HSF2 or that it can inhibit HSF1-HSF2 complexes by acting on HSF1. Further research on the effects of hemin and baicalein on HSF1, HSF2 and possible interacting partners like pescadillo is necessary to fully understand HO-1 induction in response to hemin, baicalein or $CdCl_2$.

The subcellular localization of HO-1 in hemin-, baicalein- and $CdCl_2$-treated A6 cells was consistently perinuclear in a punctate pattern. Previously, our laboratory found a similar perinuclear localization of HO-1 in A6 cells treated with $CdCl_2$, sodium arsenite, MG132 or isothiocyanates (Music et al, 2014; Khamis and Heikkila, 2018). The present finding was also in agreement with mammalian studies, which reported that HO-1, which lacks an ER target sequence, was anchored to the ER by a C-terminal transmembrane region such that it faced the cytosol (Yoshida and Sato, 1989; Gottlieb et al., 2012). In some A6 cells, it was determined that hemin, baicalein or $CdCl_2$ treatment resulted in HO-1 accumulation in the nucleus. The appearance of HO-1 in nuclei was reported in a number of mammalian tumour cells or in cells subjected to hypoxia stress (Converso et al., 2006; Slebos et al., 2007; Lin et al., 2007; Gandini et al., 2012; Namba et al., 2014). Studies in mammalian cells determined that HO-1 could be cleaved from its ER anchor and undergo translocation to the nucleus (Lin et al., 2007; Sacca et

al., 2007). Finally, the punctate pattern of hemin-, baicalein- or $CdCl_2$-induced HO-1 accumulation in A6 cells may be the result of HO-1 oligomerization. This possibility is based on studies that have shown that NADPH cytochrome P450 reductase can inhibit nuclear translocation and promote the formation of HO-1 into higher order complexes containing biliverdin reductase (Huber et al., 2009; Linnenbaum et al., 2012).

The next phase of this study examined whether hemin, baicalein or $CdCl_2$ treatment induced oxidative stress in A6 cells by examining the levels of PRDX5 and ROS. PRDX5 levels were detected constitutively in A6 kidney epithelial cells, which agrees with previous studies showing that the *prdx5* gene was robustly expressed in the proto-nephric region in developing *X. laevis* embryos (Shafer et al., 2011). In A6 cells, hemin treatment enhanced PRDX5 accumulation relative to control. Studies in mammalian systems indicated that the *prdx5* gene promoter possesses a MARE sequence suggesting that its expression may occur by means of Bach1 repression as noted above (Nguyen-Nhu et al., 2007). In contrast to PRDX5, hemin treatment did not result in enhanced ROS levels compared to control. This latter finding was unusual, as free heme is generally thought to be a strong inducer of oxidative stress (Kumar and Bandyopadhyay, 2005). It is possible that this assay, which is designed for mammalian cells, may not be sensitive enough to detect hemin-induced ROS levels in *Xenopus* cells or that HO-1 induction by hemin occurs at concentrations that are lower than those required to induce elevated levels of ROS. In contrast to hemin, baicalein enhanced ROS and PRDX5 levels compared to control. Prior studies have shown that 25 to 250 μM baicalein treatment can upregulate ROS levels in osteosarcoma, human leukemia, lung and bladder cancer cells (Wang et al., 2004; Ye et al., 2015; Kim et al., 2016; Choi et al., 2016). While baicalein is thought to function as an antioxidant molecule outside the cell, it was suggested that its ability to induce antioxidant

enzyme expression may partly be a consequence of it upsetting redox regulation *in vivo* in addition to its more direct effects on Nrf2 (Lin et al., 2007). Baicalein and $CdCl_2$ treatment of A6 cells also increased PRDX5 accumulation, likely due to their ability to stabilize Nrf2. Finally, $CdCl_2$ treatment of A6 cells resulted in robust ROS levels compared to hemin or baicalein. In support of this finding, cadmium-induced ROS formation was detected in rat tissue lysates by means of spin-trapping and electron spin resonance studies (Liu et al., 2009). Furthermore, cadmium caused an increase in lipid peroxidation, an indicator of ROS activity, in *R. decussatus* gill tissue (Geret et al., 2002). ROS formation in response to cadmium was also reported in freshwater turtle plasma, mouse neurons and chicken testes (Song et al., 2017; Huo et al., 2018; Moyano et al., 2018).

In experiments measuring oxidative stress using the CellRox detection assay, it was found that the highest level of ROS compared to control was generated by the positive control, BSO. BSO is an inhibitor of glutathione synthesis that was found to deplete glutathione in rat hepatocytes and *X. laevis* gametes (Kannan et al., 1996; Xu et al., 2003; Tong et al., 2015). Also, Xu et al. (2003) reported that $CdCl_2$ treatment of rat hepatocytes depleted glutathione levels resulting in enhanced ROS levels. In the present study, while BSO supplementation did not augment hemin- or baicalein-induced HO-1 accumulation, BSO enhanced HO-1 accumulation in $CdCl_2$-treated cells. In my research, SOD1 was also examined since its gene promoter contains a MARE element and previous studies reported that it was induced by cadmium exposure in rat hepatoma cells, zebrafish gills and mouse liver (Yoo et al., 1999; Liu et al., 2015; Yin et al., 2018). In A6 cells, BSO alone induced SOD1 accumulation, as did hemin, baicalein and $CdCl_2$ while supplementation with BSO did not enhance stress-induced SOD1 levels. In a study examining the effects of cadmium and BSO in rat hepatocytes, it was noted that increases in the

expression of antioxidant genes caused by each of these agents, individually, were of comparable magnitude (Hsiao and Stapleton, 2009). It was suggested in this latter paper that both cadmium and BSO exerted their influence through glutathione depletion and the resultant activation of Nrf2. If this was the case in A6 cells then it suggests that ROS and Nrf2 activation, alone, were not sufficient for HO-1 induction since BSO induced SOD1 but not HO-1. Secondly, it suggested that the Nrf2 pathway that was activated by BSO was not further potentiated by hemin, baicalein or $CdCl_2$, since SOD1 accumulation in response to these agents was not enhanced by BSO supplementation. Since $CdCl_2$-induced HO-1 accumulation was enhanced by BSO, it indicates that HO-1 induction may not be mediated exclusively by Nrf2 and that another, as yet unidentified, pathway may be involved. Interestingly, it was reported that BSO enhanced the cadmium-induced accumulation of proteins important for proteostasis (Abe et al., 1994; Galan et al., 2001; Shirriff and Heikkila, 2017).

Since $CdCl_2$ treatment induced HO-1 accumulation, SnPP and ZnPP were used to determine if inhibition of HO-1 enzyme activity had an effect on HO-1 levels in A6 cells treated with 50 μM $CdCl_2$. Immunoblot analysis determined that ZnPP weakly induced HO-1 levels compared to control or the positive control, hemin exposure. Also, SnPP did not induce significant levels of HO-1 accumulation. However, both inhibitors strongly enhanced $CdCl_2$ mediated accumulation of HO-1 as well as HSP70. Immunocytochemical analysis also showed that there was a strong enhancement in HO-1 staining in cells treated with SnPP or ZnPP and cadmium compared to those treated with cadmium alone. It was reported that HO-1 induction by metalloporphyrins is via activation of upstream MARE sites, suggesting involvement of the proteins of the Nrf2/Bach1 pathway (Kwok, 2013). However the weak induction of HO-1 by ZnPP and the lack of significant induction by SnPP, as well as the absence of detectable

induction of HSP70 by either of the enzyme activity inhibitors indicates that this mechanism may not be responsible for the enhancement of cadmium induced HO-1 and HSP70 accumulation. Alternatively, it could be an indication that HO-1 enzyme activity inhibition enhances the deleterious effects of cadmium treatment/stress.

In order to observe the effects of HO-1 enzyme activity inhibitors on the morphology of cadmium-treated cells, immunocytochemical methods were used to monitor the actin cytoskeleton. Previous studies have shown that treatment of cells with $CdCl_2$ or oxidative stress can cause actin fragmentation and depolymerisation (Huot et al., 1996; Wang et al., 1996; Woolfson and Heikkila, 2009) The disruption of the actin cytoskeleton by cadmium appears to be dependent on the action of gelsolin, which is thought to be activated as a consequence of apoptosis triggered by $CdCl_2$ (Apostalova et al., 2005; Liu and Templeton, 2010). While the HO-1 enzyme activity inhibitors or 100 μM $CdCl_2$ had a control-like actin cytoskeleton, $CdCl_2$ in combination with ZnPP and SnPP resulted in a severe disturbance of the actin cytoskeletal network. Disorganization of tubulin also occurred in cells treated with both cadmium and ZnPP or SnPP. This was possibly due to enhancement of cadmium-mediated damage to proteins or it may be a reflection of gross changes in cell morphology due to disruption of the cytoskeletal actin network (Galazyn-Sidorczuk et al., 2009; Tamás et al., 2014).

Studies in our laboratory determined that treatment of A6 cells with $CdCl_2$ induced the accumulation of aggregated protein and the formation of aggresome-like structures (Khan et al., 2015; Shirriff and Heikkila, 2017). Since ZnPP and SnPP treatment each accentuated $CdCl_2$-induced actin cytoskeletal disruption of A6 cells, a Proteostat dye was employed to monitor the effect of these combined treatments on aggregated protein and aggresome-like structure formation. Interestingly, the HO-1 enzyme activity inhibitors increased the production of

aggregated protein and aggresome-like structures induced by $CdCl_2$. These findings suggested that endogenous HO-1 enzyme activity may be required to mitigate the effects of $CdCl_2$ toxicity. Suppression of HO-1 by these enzyme activity inhibitors was reported to enhance the toxic effects of cadmium in other cell types. For example, caspase-3 activity and ROS production in cadmium-treated liver cells were significantly enhanced by the addition of SnPP (Lawal et al., 2015). In human renal tubule cells, SnPP-induced HO-1 enzyme activity inhibition suppressed hemin-mediated protection against cadmium damage (Yang et al., 2003). Additionally, the inhibition of HO-1 enzyme activity by ZnPP and/or SnPP was reported to enhance the toxicity of other stressors as well. For example, HO-1 enzyme activity inhibition by ZnPP enhanced the cytotoxicity of the chemotherapeutic agent, gemcitabine, in human prostate cells (Miyake et al., 2010). Finally, both ZnPP and SnPP each enhanced colonic damage suffered by rats in response to trinitrobenzene treatment (Varga et al., 2007).

In contrast to ZnPP and SnPP, HO-1 accumulation inducers, hemin and baicalein, were reported to protect animal model systems against oxidative stress and inflammatory tissue injuries (Yoneya et al., 2000; Chen et al., 2008; Liu et al., 2010; Jung and Lee, 2014; Choi et al., 2016). For example, hemin conferred cytoprotection against hydrogen peroxide treatment of human tracheal epithelial cells, serum depletion of human monocytes and cold stress in human tubular epithelial cells (Yamada et al., 1998; Salahudeen et al., 2001; Lang et al, 2004). Also, baicalein treatment inhibited oxidative stress-induced apoptosis in rat glial cells, mouse macrophages and human melanocytes (Chen et al., 2006; Lin et al., 2007; Liu et al., 2012). However, there is very little information available on the possible cytoprotective effects of HO-1 accumulation against potentially lethal concentrations of cadmium in animal cells. In the present study, treatment of A6 cells with 275 μM $CdCl_2$ resulted in highly disorganized actin

cytoskeletons and irregular cell boundaries. However, treatment with hemin or baicalein mitigated the effects of $CdCl_2$ on actin cytoskeletal structure. In previous studies, hemin treatment was shown to protect rats against cadmium-induced testicular damage (Fouad et al., 2009). In this latter study, co-treatment of cells with the HO-1 enzyme activity inhibitor, SnPP, suppressed the protection conferred by hemin. This finding suggested that the cytoprotection conferred by hemin may be mediated by HO-1. This connection between HO-1 and cytoprotection against cadmium-induced damage was reported in rat glial cells in which HO-1, induced by NO, inhibited the toxic effects of $CdCl_2$-induced oxidative stress (Srisook et al., 2005). Previously, it was reported that cadmium-mediated disruption of actin stress fibres was a consequence of pro-apoptotic mechanisms mediated by p38 MAPK activation (Apostalova et al., 2005; Liu and Templeton, 2010). Also, it was found that HO-1-mediated production of CO inhibited apoptosis, also through a p38 MAPK based mechanism (Brouard et al., 2000). Thus, it is possible that the pro-apoptotic effects of cadmium and the anti-apoptotic effects of CO production by HO-1 are integrated at the level of p38 MAPK phosphorylation.

Incubation of A6 cells with 275 μM $CdCl_2$ also induced the accumulation of aggregated protein and aggresome-like structures compared to control. However, cotreatment with hemin or baicalein resulted in fewer Proteostat dye and anti-HSP30 antibody stained aggresome-like structures compared to $CdCl_2$ treatment alone. Furthermore, the addition of the HO-1 enzyme activity inhibitor, SnPP, suppressed the effect of hemin or baicalein treatment. This result suggested that HO-1 enzyme activity induced by hemin or baicalein may be involved in suppressing the proteotoxic stress exerted by $CdCl_2$. As stated earlier, cadmium-induced protein unfolding was the result of oxidative stress and interaction of cadmium ions with the protein backbone and thiol-containing residues (Galazyn-Sidorczuk et al., 2009; Tamás et al., 2014).

Additionally, HO-1 enzyme activity may counteract cadmium-induced oxidative stress through the production of bilirubin. Bilirubin was reported to act directly as an antioxidant in human endothelial cells (Ziberna et al., 2015). Also, bilirubin was reported to reduce superoxide production in rat kidneys through its inhibitory action on NADPH oxidase (Fuji et al., 2010). Previous studies reported that hemin-induced HO-1 enzyme activity or HO-1 overexpression resulted in enhanced ferritin accumulation (Gonzales et al., 2002; Lanceta et al., 2013). While ferritin is an iron-binding protein, it can bind to other metal cations including cadmium (Hegenauer, 1979; Flora and Pauchari, 2010). Thus, excess ferritin may sequester cadmium and mitigate its effects on protein unfolding. Hemin and baicalein may also inhibit protein aggregation independent of HO-1 activation. Both hemin and baicalein were reported to inhibit protein aggregation directly. For example, hemin was shown to non-specifically inhibit *in vitro* amyloid fibril-type aggregation of a wide variety of proteins, including alpha-synuclein, alcohol dehydrogenase, catalase, gamma-s-crystallin and beta-amyloid as well as being capable of disaggregating pre-existing fibrils (Liu et al, 2014; Hayden et al., 2015; Sonavane et al., 2017). Baicalein was reported to have a similar activity with respect to inhibiting the aggregation of various proteins in vitro including alpha-synuclein, 1SS-alpha-lacalbumin and lysozyme (Zhu et al., 2004; Bomhoff et al., 2006; Kostka et al., 2007). Finally, it was found to reduce alpha-synuclein fibril formation in mouse neuroblastoma cells (Jiang et al., 2010). Therefore, it is possible that hemin and baicalein may have a direct effect on inhibiting protein aggregation as well as an indirect effect by activating the expression of *ho-1* genes.

It has been noted that amphibians are well suited to serve as sentinel species in monitoring ecological health as they are particularly sensitive to a variety of toxicants including heavy metals and endocrine disruptors (Berzins and Bundy, 2002; Kloas and Lutz, 2006;

Burggren & Warburton, 2007). The present study has revealed a number of biomarkers including HO-1, HSPs and aggregated protein that accumulated in response to cadmium treatment. Other studies have also used the *Xenopus* system in a similar fashion to examine the effect of other environmental toxicants including perfluoroalkylated substances and dioxins (Lavine et al., 2005; Gorrochategui et al., 2016). The use of the biomarkers, which was explored in the current study, may be of value to the analysis of the effects of toxicants on other poikilotherms. It is important to develop these types of biomarkers not only to monitor the health of ecosystems but also in enconomic ventures such as fish farming.

In the present study, it was determined that Nrf2-regulated proteins, namely HO-1, PRDX5, and SOD1, displayed differential accumulation in A6 cells in response to treatments with different agents. It is likely that different sets of stress proteins accumulate in response to different stressors in spite of having similar regulatory elements. In the future, a more comprehensive understanding of stress pathways would allow for more accurate associations to be made between specific environmental stressors and the induction of specific stress proteins. Performing initial analyses in a model poikilothermic tissue culture system reduces the need to collect large numbers of animals, especially those from a vulnerable declining population.

Future directions

Given the findings of this thesis, future studies could examine a number of possible mechanisms in more detail. For example, this research demonstrated that two HO-1-inducing agents, hemin and baicalein, conferred cytoprotection in A6 cells subjected to a potentially lethal concentration of $CdCl_2$. Administration of the HO-1 enzyme activity inhibitor, SnPP, suppressed this cytoprotective effect. This suggested that cytoprotection was a consequence of HO-1 enzyme

activity. This finding should be verified by inhibiting HO-1 accumulation using either RNAi or antisense morpholino oligonucleotides (Xia et al., 2007; Tandon et al., 2012). Conversely, it would be of interest to determine whether HO-1 accumulation induced by overexpression of *ho-1* gene expression in transfected cells was capable of inducing cytoprotection against high concentrations of $CdCl_2$.

The present study also demonstrated that HO-1 accumulation by hemin, baicalein or $CdCl_2$ were inhibited by the HSF1 inhibitor, KNK437. In future, this analysis should directly inhibit HSF1 and/or HSF2 by means of RNAi or morpholino technology to determine if these transcription factors were involved in *ho-1* gene expression.

This study suggested that HO-1 activity protected A6 cells against oxidative stress by producing bilirubin, which subsequently acted as an antioxidant molecule (Fuji et al., 2010; Ziberna et al., 2015). One of the interesting properties of bilirubin is its amphipathicity, having both hydrophilic and hydrophobic protein domains (Tazuma and Holzbach, 1986). While there are numerous cellular defences against oxidative stress (e.g. catalase, SOD enzymes, the glutathione system, thioredoxins, peroxiredoxins, etc.) few of them would be capable of acting directly in a lipid environment. Oxidative stress generally causes peroxidation of membrane lipids (Turrens et al., 2003). Bilirubin is one of a few antioxidant defence mechanisms that could function within a biological membrane. If this is the case, then it is possible that HO-1 inducers are more effective at inhibiting lipid peroxidation than other ROS scavenging agents. The effectiveness of hemin and baicalein at inhibiting lipid peroxidation could be compared to the ROS scavenger dimethylthiourea and polyethylene glycol-superoxide dismutase by using a malondialdehyde assay (Kinugawa et al., 2000; Grotto et al, 2009; Sun, 2010; Kim et al., 2015).

Finally, in addition to the prevention of oxidative stress, the enzyme activity of HO-1

may also be associated with the prevention of apoptosis in $CdCl_2$-treated A6 cells. While the morphology of the actin cytoskeleton in cadmium-treated A6 cells was consistent with apoptotic cells. However, it was impossible to conclude whether there was an increase in apoptosis by phalloidin staining alone (Bottone et al., 2013). Therefore, it would be useful to determine the proportion of cadmium-treated A6 cells that underwent apoptosis compared to those which were supplemented with heme or baicalein. Numerous quantitative assays for detecting apoptosis exist including annexin V staining combined with flow cytometry or caspase activation assays (Archana et al., 2013).

References

Abdulle, R., Mohindra, A., Fernando, P., Heikkila, J.J. 2002. *Xenopus* small heat shock proteins, Hsp30C and Hsp30D, maintain heat- and chemically-denatured luciferase in a folding-competent state. Cell Stress Chaperones. 7, 6-16.

Abe, T., Konishi, T., Katoh, T., Hirano, H., Matsukuma, K., Kashimura, M., Higashi, K. 1994. Induction of heat shock 70 mRNA by cadmium is mediated by glutathione suppressive and non-suppressive triggers. Biochim. Biophys. Acta. 120, 29-36.

Aich, A., Freundlich, M., Vekilov. 2015. The free heme concentration in healthy human erythrocytes. Blood Cells Mol. Dis. 55, 402–409.

Aiken, C.T., Kaake, R.M., Wang, X., Huang, L. 2011. Oxidative stress-mediated regulation of proteasome complexes. Mol. Cell. Proteomics. 10, 006924.

Alam, J. and Cook, J. 2007. How many transcription factors does it take to turn on the heme oxygenase-1 gene? Am. J. Respir. Cell. Mol. Biol. 36, 166-174.

Alam, J., Shibahara, S., Smith, A. 1989. Transcriptional activation of the heme oxygenase gene by heme and cadmium in mouse hepatoma cells. J Biol Chem. 264, 6371-6375.

Alam, J., Wicks, C., Stewart, D., Gong, P., Touchard, C., Otterbein, S., Choi, A.M.K., Burow, M.E., and Tou, J. 2000. Mechanism of heme oxygenase-1 gene activation by cadmium in MCF-7 mammary epithelial cells, role of p38 kinase and Nrf2 transcription factor. J. Biol. Chem. 275, 27694-27702.

An, H., Statsyuk, A., 2015. An inhibitor of ubiquitin conjugation and aggresome formation. Chem. Sci. 6, 5235-5245.

Apostolova, M.D., Christova, T., Templeton, D.M. 2006. Involvement of gelsolin in cadmium-induced disruption of the mesangial cell cytoskeleton. Toxicol. Sci. 89, 465-474.

Appleton, S.D., Chretien, M.L., McLaughlin, B.E., Vreman, H.J., Stevenson, D.K., Brien, J.F., Nakatsu, K., Maurice, D.H., Marks, G.S. 1999. Selective inhibition of heme oxygenase, without inhibition of nitric oxide synthase or soluble guanylyl cyclase, by metalloporphyrins at low concentrations. Drug Metab. Dispos. 27, 1214–1219

Archana, M., Bastian, Yogesh, T.L., Kumaraswamy, K.L. Various methods available for detection of apoptotic cells- A review. Indian J. Cancer. 50, 274-283.

Balch W.E., Morimoto R.I., Dillin A., Kelly J.W. 2008. Adapting proteostasis for disease intervention. Science. 319, 916-9.

Balestrasse, K.B., Noriega, G.O., Batlle, A., Tomaro, M.L. 2006. Heme oxygenase activity and oxidative stress signalling in soybean leaves. Plant Sci. 170, 339-346.

Balogun, E., Hoque, M., Gong, P., Killeen, E., Green, C.J. Foresti, R., Alam, J., and Motterlini, R. 2003. Curcumin activates the haem oxygenase-1 gene via regulation of Nrf2 and the antioxidant-responsive element. Biochem. J. 371, 887-895.

Baranano, D.E., Rao, M., Ferris, C.D., Snyder, S.H. 2002. Biliverdin reductase: a major physiologic cytoprotectant. Proc. Natl. Acad. Sci. 99, 16093-16098.

Bayer, T.A. 2015. Proteinopathies, a core concept for understanding and ultimately treating degenerative disorders? Eur. Neuropsychopharmacol. 25, 713-724.

Berzins, D.W., Bundy, K.J. 2002. Bioaccumulation of lead in Xenopus laevis tadpoles from water and sediment. Environ. Int. 28, 69-77.

Blydt-Hansen, T.D., Katori, M., Lassman, C., Ke, B., Coito, A.J., Iyer, S., Buelow, R., Ettenger, R., Busuttil, R.W., Kupiec-Weglinski, J.W. 2003. Gene transfer-induced local heme oxygenase-1 overexpression protects rat kidney transplants from ischemia/reperfusion injury. J. Am. Soc. Nephrol. 14, 745-754.

Bolhuis, S., Richter-Landsberg, C., 2010. Effect of proteasome inhibition by MG-132 on HSP27 oligomerization, phosphorylation, and aggresome formation in the OLN-93 oligodendroglia cell line. J. Neurochem. 114, 960-971.

Bomhoff, G., Sloan, K., McLain, C., Gogol, E.P., Fisher, M.T. 2006. The effects of the flavonoid baicalein and osmolytes on the Mg 2+ accelerated aggregation/fibrillation of carboxymethylated bovine 1SS-alpha-lactalbumin. Arch. Biochem. Biophys. 453, 75-86.

Boussen, S., Soubrand, M., Bril, H., Ouerfelli, K., Abdeljaouad, S. 2013. Transfer of lead, zinc and cadmium from mine tailings to wheat in carbonated Mediterranean (Northern Tunisia) soils. Geoderma. 192, 227-236.

Briant, D., Ohan, N., Heikkila, J.J. 1997. Effect of herbimycin A on hsp30 and hsp70 heat shock protein gene expression in *Xenopus* cultured cells. Biochem. Cell Biol.75, 777-782.

Brouard, S., Otterbein, L.E., Anrather J, Tobiasch, E., Bach, F.H., Choi, A.M., Soares, M.P. 2000. Carbon monoxide generated by heme oxygenase 1 suppresses endothelial cell apoptosis. J. Exp. Med. 192, 1015-1026.

Bruce-Keller,A.J., Gupta,S., Knight,A.G., Beckett,T.L., McMullen,J.M., Davis, P.R. 2011.Cognitive impairment in humanized APPxPS1 mice is linked to Abeta(1–42) and NOX activation. Neurobiol. Dis. 44, 317–326.

Bucciantini, M., Giannoni, E., Chiti, F., Baroni, F., Formigli, L., Zurdo, J., Taddei, N., Ramponi, G., Dobson, C.M., Stefani, M. 2002. Inherent toxicity of aggregates implies a common

mechanism for protein misfolding diseases. Nature. 416, 507-511.

Burggren, W. W., Warburton, S. 2007. Amphibians as animal models for laboratory research in physiology. ILAR. J. 48, 260-269.

Caballero, M., Liton, P.B., Epstein, D.L., Gonzalez, P. 2003.Proteasome inhibition by chronic oxidative stress in human trabecular meshwork cells. Biochem. Biophys. Res. Commun. 308, 346-352.

Cai, J., Yang, J. and Jones, D. P. 1998. Mitochondrial control of apoptosis: the role of cytochrome c. Biochim. Biophys. Acta. 1366, 139-149.

Camhi, S. L., J. Alam, G. W. Wiegand, B. Y. Chin, A. M. K. Choi. 1998. Transcriptional activation of the HO-1 gene by lipopolysaccharide is mediated by 5′ distal enhancers: role of reactive oxygen intermediates and AP-1. Am. J. Respir. Cell Mol. Biol. 18, 226-234.

Carrell, R.W., Lomas, D.A. 1997. Conformational disease. Lancet. 350, 134–138.

Cathcart, M.C., Useckaite, Z., Drakeford, C., Semik, V., Lysaght, J., Gately, K., O'Byrne, K.J., Pidgeon, G.P. 2016. Anti-cancer effects of baicalein in non-small cell lung cancer in-vitro and in-vivo. BMC. Cancer. 16, 707.

Chen Y.C., Chow J.M., Lin C.W., Wu C.Y., Shen S.C. 2006. Baicalein inhibition of oxidative-stress-induced apoptosis via modulation of ERKs activation and induction of HO-1 gene expression in rat glioma cells C6. Toxicol. Appl. Pharmacol. 216, 263-273.

Chen, J.S., Huang, P.H., Wang, C.H., Lin, F.Y., Tsai, H.Y., Wu, T.C., Lin, S.J., Chen, J.W. 2011. Nrf-2 mediated heme oxygenase-1 expression, an antioxidant-independent mechanism, contributes to anti-atherogenesis and vascular protective effects of Ginkgo biloba extract. Atherosclerosis. 214, 301-309.

Chen, S.F., Hsu, C.W., Huang, W.H., Wang, J.Y. 2008. Post-injury baicalein improves histological and functional outcomes and reduces inflammatory cytokines after experimental traumatic brain injury. Br. J. Pharmacol. 155, 1279-1296.

Chen, S.M., Li, Y.G., Wang, D.M. 2005. Study on changes of heme oxygenase-1 expression in patients with coronary heart disease. Clin. Cardiol. 28, 197-201.

Cheng, P.Y., Chen, J.J., Yen, M.H. 2004. The expression of heme oxygenase-1 and inducible nitric oxide synthase in aorta during the development of hypertension in spontaneously hypertensive rats. Am. J. Hypertens. 17, 1127-34.

Choi, E.O., Park, C., Hwang, H.J., Hong, S.H., Kim, G.Y., Cho, E.J., Kim, W.J., Choi, Y.H. 2016. Baicalein induces apoptosis via ROS-dependent activation of caspases in human bladder cancer 5637 cells. Int J Oncol. 49, 1009-1018.

Choi, J.H., Choi, A.Y., Yoon, H., Choe, W., Yoon, K.S., Ha, J., Yeo, E.J., Kang, I. 2010. Baicalein protects HT22 murine hippocampal neuronal cells against endoplasmic reticulum stress-induced apoptosis through inhibition of reactive oxygen species production and CHOP induction. Exp. Mol. Med. 42, 811-822.

Converso, D.P., Taillé, C., Carreras, M.C., Jaitovich, A. Poderoso, J.J., Boczkowski, J. 2006. HO-1 is located in liver mitochondria and modulates mitochondrial heme content and metabolism. FASEB J. 20, 1236-1238.

Cui, G., Luk, S.C., Li, R.A., Chan, K.K., Lei, S.W., Wang, L., Shen, H., Leung, G.P., Lee, S.M. 2015. Cytoprotection of baicalein against oxidative stress-induced cardiomyocytes injury through the Nrf2/Keap1 pathway. J. Cardiovasc. Pharmacol. 65, 39-46.

Cullen, J. T., Maldonado, M. T. 2013. Biogeochemistry of cadmium and its release to the environment. Met. Ions Life Sci. 11, 31-62.

Cuypers, A., Plusquin, M., Remans, T., Jozefczak, M., Keunen, E., Gielen, H., Opdenakker, K., Nair, A.R., Munters, E., Artois, T.J., Nawrot, T., Vangronsveld, J., Smeets, K. 2010. Cadmium stress: an oxidative challenge. Biometals. 23, 927-40.

Darasch, S., Mosser D.D., Bols, N.C., Heikkila, J.J. 1988. Heat shock gene expression in *Xenopus laevis* cells in response to heat shock and sodium arsenite treatments. Cell Biol. 66, 862-868.

Dasuri, K., Zhang, L., Keller, J.N. 2013. Oxidative stress, neurodegeneration, and the balance of protein degradation and protein synthesis. Free Radic. Biol. Med. 62, 170-185.

Delic, M., Rebnegger, C., Wanka, F., Puxbaum, V., Haberhauer-Troyer, C., Hann, S., Köllensperger, G., Mattanovich, D., Gasser, B. 2012. Oxidative protein folding and unfolded protein response elicit differing redox regulation in endoplasmic reticulum and cytosol of yeast. Free Radic. Biol. Med. 52, 2000-12.

Deponte, M. 2013. Glutathione catalysis and the reaction mechanisms of glutathione-dependent enzymes. Biochim. Biophys. Acta. 1830, 3217-66.

Detsika, M.G., Duann, P., Lianos, E.A. 2015. HO-1 expression control in the rat glomerulus. Biochem. Biophys. Res. Commun. 460, 786-792.

Dey, M., Chang, A.L., Wainwright, D.A., Ahmed, A.U., Han, Y., Balyasnikova, I.V., Lesniak, M.S. 2014. Heme oxygenase-1 protects regulatory T cells from hypoxiainduced cellular stress in an experimental mouse brain tumor model. J. Neuroimmunol. 266. 33–42.

Ding, Q., Keller, J.N. 2001. Proteasome inhibition in oxidative stress neurotoxicity: implications for heat shock proteins. J. Neurochem. 77, 1010-7.

Ding, Y., Song, N., Liu, C., He, T., Zhuo, W., He, X., Chen, Y., Song, X., Fu, Y., Luo, Y. 2012.

Heat shock cognate 70 regulates the translocation and angiogenic function of nucleolin. Arterioscler. Thromb. Vasc. Biol. 32, e126-134.

Dong, Z., Lavrovsky, Y., Venkatachalam, M. A. and Roy, A. K. 2000. Heme oxygenase-1 in tissue pathology. The yin and yang. Am. J. Pathol. 156, 1488.

Doré, S., Takahashi, M., Ferris, C.D., Zakhary, R., Hester, L.D., Guastella, D., Snyder, S.H. 1999. Bilirubin, formed by activation of heme oxygenase-2, protects neurons against oxidative stress injury. Proc. Natl. Acad. Sci. 96, 2445-2450.

Drummond, G.S., Kappas, A. 1981. Prevention of neonatal hyperbilirubinemia by tin protoporphyrin IX, a potent competitive inhibitor of heme oxidation. Proc. Natl. Acad. Sci. U S A. 78, 6466-6470.

Fernando, P., Heikkila, J.J. 2000. Functional characterization of *Xenopus* small heat shock protein, Hsp30C: the carboxyl end is required for stability and chaperone activity. Cell Stress Chaperones. 5, 148-159.

Fernando, P., Megeney, L.A., Heikkila, J.J. 2003. Phosphorylation-dependent structural alterations in the small hsp30 chaperone are associated with cellular recovery. Exp. Cell. Res. 286, 175-185.

Ferris, C.D., Jaffrey, S.R., Sawa, A., Takahashi, M., Brady, S.D., Barrow, R.K., Tysoe, S.A., Wolosker, H., Baranano, D.E., Dore, S., Poss, K.D., Snyder, S.H., 1999. Haem oxygenase-1 prevents cell death by regulating cellular iron. Nat. Cell. Biol. 1, 152-157.

Finkel, T., Holbrook, N.J. 2000. Oxidants, oxidative stress and the biology of aging. Nature. 408, 239-47.

Flora, S.J., Pachauri, V. 2010. Chelation in metal intoxication. Int. J. Environ. Res. Public Health. 7, 2745-2788.

Fouad, A.A., Qureshi, H.A., Al-Sultan, A.I., Yacoubi, M.T., Ali AA. 2009. Protective effect of hemin against cadmium-induced testicular damage in rats. Toxicology. 257, 153-60.

Fox M.A., Nieuwesteeg M.A., Willson J.A., Cepeda M., Damjanovski S. 2014. Knockdown of Pex11β reveals its pivotal role in regulating peroxisomal genes, numbers, and ROS levels in *Xenopus laevis* A6 cells. In. Vitro. Cell. Dev. Biol. Anim. 50, 340-9.

Fuji, M., Inoguchi, T., Sasaki, S., Maeda, Y., Zheng, J., Kobayashi, K., Takayanagi, R. 2010. Bilirubin and biliverdin protect rodents against diabetic nephropathy by downregulating NAD(P)H oxidase. Kidney. Int. 78, 905-919.

Fujishiro, H., Yano, Y., Takada, Y., Tanihara, M., and Himeno, S. 2012. Roles of ZIP8, ZIP14, and DMT1 in transport of cadmium and manganese in mouse kidney proximal tubule cells. Metallomics : Integrated Biometal Science. 4, 700–8.

Fuse, Y., Nakajima, H., Nakajima-Takagi, Y., Nakajima, O., Kobayashi, M. 2015. Heme-mediated inhibition of Bach1 regulates the liver specificity and transience of the Nrf2-dependent induction of zebrafish heme oxygenase 1. Genes Cells. 20, 590-600.

Galan, A., Troyano, A., Vilaboa, N.E., Fernandez, C., de Blas, E., Aller, P. 2001. Modulation of the stress response during apoptosis and necrosis induction in cadmium-treated U-937 human promonocytic cells. Biochim. Biophys. Acta. 1538, 38-46.

Galazyn-Sidorczuk, M., Brzoska, M.M., Jurczuk, M., Moniuszko-Jakoniuk, J., 2009. Oxidative damage to proteins and DNA in rats exposed to cadmium and/or ethanol. Chem. Biol. Interac. 180, 31-38.

Gandini, N.A., Fermento, M.E., Salomón, D.G., Blasco, J., Patel, V., Gutkind, J.S., Molinolo, A.A., Facchinetti, and M.M., and Curino, A.C. 2012. Nuclear localization of heme oxygenase-1 is associated with tumor progression of head and neck squamous cell carcinomas. Exp. Mol. Pathol. 93, 237-245.

Garmshausen, J., Kloas, W., Hoffmann, F. 2015. 17α-Ethinylestradiol can disrupt hemoglobin catabolism in amphibians. Comp. Biochem. Physiol. C. Toxicol. Pharmacol. 171, 34-40.

Garrido, C., Paul, C., Seigneuric, R., Kampinga, H.H. 2012. The small heat shock proteins family, the long forgotten chaperones. Int J Biochem Cell. Biol. Review. 44, 1588-1592.

Geret, F., Serafim, A., Barreira, L., Bebianno, M.J. 2002. Effect of cadmium on antioxidant enzyme activities and lipid peroxidation in the gills of the clam Ruditapes decussatus. Biomarkers. 7, 242-256.

Ghyczy, M., Boros, M. 2001. Electrophilic methyl groups present in the diet ameliorate pathological states induced by reductive and oxidative stress: a hypothesis. Br. J. Nutr. 85, 409-14.

Go, Y.M., Jones, D.P. 2008. Redox compartmentalization in eukaryotic cells. Biochim. Biophys. Acta. 1780, 1273–1290.

Goldbaum, O., Riedel, M., Stahnke, T., Richter-Landsberg, C., 2009. The small heat shock protein HSP25 protects astrocytes against stress induced by proteasomal inhibition. Glia. 57, 1566-1577.

Gonzales, S., Erario, M.A., Tomaro, M.L. 2002. Heme oxygenase-1 induction and dependent increase in ferritin. A protective antioxidant stratagem in hemin-treated rat brain. Dev. Neurosci. 24, 161-168.

González-Reyes, S., Guzmán-Beltrán, S., Medina-Campos, O.N., and Pedraza-Chaverri, J. 2013. Curcumin pretreatment induces Nrf2 and an antioxidant response and prevents 107 hemin-induced toxicity in primary cultures of cerebellar granule neurons of rats. Oxid. Med. Cell

Longev. doi: 10.1155/2013/801418.

Gorrochategui, E., Lacorte, S., Tauler, R., Martin, F.L., 2016. Perfluoroalkylated substance effects in Xenopus laevis A6 kidney epithelial cells determined by ATR-FTIR spectroscopy and chemometric analysis. Chem. Res. Toxicol. 29, 924-932.

Gottlieb, Y., Truman, M., Cohen, L.A., Leichtmann-Bardoogo, Y., Meyron-Holtz, E.G. 2012. Endoplasmic reticulum anchored heme-oxygenase 1 faces the cytosol. Haematologica. 97, 1489-1493.

Gozzelino., R, Jeney, V., Soares, M.P. 2010. Mechanisms of cell protection by heme oxygenase-1. Annu. Rev. Pharmacol. Toxicol. 50, 323-54.

Grotto, D., Santa Maria, L., Valentini, J. 2009. Importance of the lipid peroxidation biomarkers and methodological aspects FOR malondialdehyde quantification. Quimica Nova. 32, 169–174.

Hao, R., Nanduri, P., Rao, Y., Panichelli, R.S., Ito, A., Yoshida, M., Yaho, T.-P., 2013. Proteasomes activate aggresome disassembly and clearance by producing unanchored ubiquitin chains. Mol. Cell. 51, 819-828.

Hasan R.N., Schafer, A.I. 2008. Hemin upregulates Egr-1 expression in vascular smooth muscle cells via reactive oxygen species ERK-1/2-Elk-1 and NF-kappaB. Circ. Res. 102, 42-50.

Hayashi S., Omata Y., Sakamoto H., Higashimoto Y., Hara T., Sagara Y., Noguchi M. 2004 Characterization of rat heme oxygenase-3 gene. Implication of processed pseudogenes derived from heme oxygenase-2 gene. Gene. 336, 241-50.

Hayden, E.Y., Kaur, P., Williams, T.L., Matsui, H., Yeh, S.R., Rousseau, D.L. 2015. Heme stabilization of α-Synuclein oligomers during amyloid fibril formation. Biochemistry. 54, 4599-4610.

Hayden, E.Y., Kaur, P., Williams, T.L., Matsui, H., Yeh, S.R., Rousseau, D.L. 2015. Heme Stabilization of α-Synuclein Oligomers during Amyloid Fibril Formation. Biochemistry. 54, 4599-4610.

Hegenauer, J., Saltman, P., Hatlen, L. 1979. Removal of cadmium(II) from crystallized ferritin. Biochem J. 177, 693-695.

Heikkila J.J., Kaldis A., Morrow G., Tanguay R.M. 2007. The use of the *Xenopus* oocyte as a model system to analyze the expression and function of eukaryotic heat shock proteins. Biotechnol. Adv. 25, 385-95.

Heikkila, J.J. 2004. Regulation and function of small heat shock protein genes during amphibian development.J. Cell. Biol. Chem. 93, 672-680.

Heikkila, J.J. 2010. Heat shock protein gene expression and function in amphibian model

systems. Comp. Biochem. Physiol. A. Mol. Integr. Physiol. 156, 19-33.

Heikkila, J.J. 2017. The expression and function of hsp30-like small heat shock protein genes in amphibians, birds, fish, and reptiles. Comp. Biochem. Physiol. A. Mol. Integr. Physiol. 203, 179-192.

Heikkila, J.J., Schultz, G.A., Iatrou, K., Gedamu, L. 1982. Expression of a set of fish genes following heat or metal ion exposure. J. Biol. Chem. 257, 12000-12005.

Heinemann, I.U., Jahn, M., Jahn, D. 2008. The biochemistry of heme biosynthesis. Arch. Biochem. Biophys. 474, 238-51.

Hsiao, C.J., Stapleton, S.R. 2009. Early sensing and gene expression profiling under a low dose of cadmium exposure. Biochimie. 91, 329-343.

Huber, III, W.J. Scruggs, B.A., Backes, W.L. 2009. C-terminal membrane spanning region of human heme oxygenase-1 mediates a time-dependent complex formation with cytochrome P450 reductase. Biochemistry 48, 190-197.

Huo, J., Dong, A., Niu, X., Dong, A., Lee, S., Ma, C., Wang L.. 2018. Effects of cadmium on oxidative stress activities in plasma of freshwater turtle *Chinemys reevesii*. Environ. Sci. Pollut. Res. Int. doi: 10.1007/s11356-017-1139-z

Huot, J., Houle, F., Spitz, D.R., Landry, J. 1996. HSP27 phosphorylation-mediated resistance against actin fragmentation and cell death induced by oxidative stress. Cancer Res. 56, 273-279.

Hwang, H.W., Lee, J.R., Chou, K.Y., Suen, C.S., Hwang, M.J., Chen, C., Shieh, R.C., Chau, L.Y. 2009. Oligomerization is crucial for the stability and function of heme oxygenase-1 in the endoplasmic reticulum. J. Biol. Chem. 284, 22672–22679.

Ikuzawa, M., Akiduki, S., Asashima, M. 2007. Gene expression profile of *Xenopus* A6 cells cultured under random positioning machine shows downregulation of ion transporter genes and inhibition of dome formation. Adv. Space Res. 40, 1694-1702.

Ito, H., Kamei, K., Iwamoto, I., Inaguma, Y., Garcia-Mata, R., Sztul, E., Kato, K., 2002. Inhibition of the proteasome induces accumulation, phosphorylation, and recruitment of HSP27 and alphaβ-crystallin to aggresomes. J. Biochem. 131, 593-603.

Ivanina AV1, Cherkasov, A.S., Sokolova, I.M. 2008. Effects of cadmium on cellular protein and glutathione synthesis and expression of stress proteins in eastern oysters, *Crassostrea virginica* Gmelin. J. Exp. Biol. 211, 577-586.

Jancsó, Z., Hermesz, E. 2015. Impact of acute arsenic and cadmium exposure on the expression of two haeme oxygenase genes and other antioxidant markers in common carp (*Cyprinus carpio*). J. Appl. Toxicol. 35, 310-8.

Jiang, M., Porat-Shliom, Y., Pei, Z., Cheng, Y., Xiang, L., Sommers, K., Li, Q., Gillardon, F., Hengerer, B., Berlinicke, C., Smith, WW., Zack, D.J., Poirier, M.A., Ross, C.A., Duan, W. 2010. Baicalein reduces E46K alpha-synuclein aggregation in vitro and protects cells against E46K alpha-synuclein toxicity in cell models of familiar Parkinsonism. J. Neurochem. 114, 419-429.

Jin, Q.J., Yuan, X.X., Cui, W.T., Han, B., Feng, J.F., Xu, S., Shen, W.B. 2012. Isolation and characterization of a heme oxygenase-1 gene from Chinese cabbage. Mol. Biotechnol. 50, 18-17.

Johnston, J.A., Ward, C.L., Kopito, R.R. 1998. Aggresomes: a cellular response to misfolded proteins. J. Cell Biol. 143, 1883-1898.

Johri, N., Jacquillet, G., Unwin, R. Heavy metal poisoning: the effects of cadmium on the kidney. Biometals. 23, 783-792.

Jones, D.P., Go, Y.M. 2010. Redox compartmentalization and cellular stress. Diabetes Obes. Metab. 12, 116–125.

Joseph, P. 2009. Mechanisms of cadmium carcinogenesis. Toxicol. Appl. Pharmacol. 238, 272-279.

Jung, E.B., Lee, C.S. 2014. Baicalein attenuates proteasome inhibition-induced apoptosis by suppressing the activation of the mitochondrial pathway and the caspase-8- and Bid-dependent pathways. Eur. J. Pharmacol. 730, 116-124.

Kannan, R., Yi, J. R., Tang, D., Zlokovic, B. V., Kaplowitz, N. 1996. Identification of a novel, sodium-dependent, reduced glutathione transporter in the rat lens epithelium. Investig. Ophthalmol. Vis. Sci. 37, 2269-2275.

Kastle,M.,Woschee, E.,Grune, T., 2012. Histone deacetylase 6 (HDAC6) plays a crucial role in p38MAPK-dependent induction of heme oxygenase-1 (HO-1) in response to proteasome inhibition. Free Radic. Biol. Med. 53, 2092–2101.

Katoh, Y., Fujimoto, M., Nakamura, K., Inouye, S., Sugahara, K., Izu, H., Nakai, A., 2004. Hsp25, a member of the Hsp30 family, promotes inclusion formation in response to stress. FEBS Lett. 565, 28-32.

Kawaguchi, Y., Kovacs, J. J., McLaurin, A., Vance, J. M., Ito, A., Yao, T. P. 2003. The deacetylase HDAC6 regulates aggresome formation and cell viability in response to misfolded protein stress. Cell. 115, 727-738.

Khamis, I., Heikkila, J.J. 2013. Enhanced HSP30 and HSP70 accumulation in *Xenopus* cells subjected to concurrent sodium arsenite and cadmium chloride stress. Comp. Biochem. Physiol. C. Toxicol. Pharmacol. 158, 165-172.

Khamis, I., Heikkila, J.J. 2018. Effect of isothiocyanates, BITC and PEITC, on stress protein accumulation, protein aggregation and aggresome-like structure formation in *Xenopus* A6 kidney

epithelial cells. Comp. Biochem. Physiol. C Toxicol. Pharmacol. 204, 1-13.

Khan S., Khamis I., Heikkila J.J., 2015. The small heat shock protein, HSP30, is associated with aggresome-like inclusion bodies in proteasomal inhibitor-, arsenite-, and cadmium-treated *Xenopus* kidney cells. Comp. Biochem. Physiol. A. Mol. Integr. Physiol. 189, 130-40.

Khan, A.A., Quigley, J.G. 2011. Control of intracellular heme levels: Heme transporters and Heme oxygenases. Biochim. Biophys. Acta. 1813, 668–682.

Khan, S., Heikkila, J.J. 2011. Curcumin-induced inhibition of proteasomal activity, enhanced HSP accumulation and the acquisition of thermotolerance in *Xenopus laevis* A6 cells. Comp. Biochem. Physiol. A. Mol. Integr. Physiol. 158, 566-576.

Khan, S., Rammeloo, A.W., and Heikkila, J.J. 2012. Withaferin A induces proteasome inhibition, endoplasmic reticulum stress, the heat shock response and acquisition of thermotolerance. PLOS ONE. 7, e50547.

Kim, E.J., Lee, H.J., Lee, J., Youm, H.W., Lee, J.R., Suh, C.S., Kim, S.H. The beneficial effects of polyethylene glycol-superoxide dismutase on ovarian tissue culture and transplantation. J. Assist Reprod. Genet. 32, 1561-1569.

Kim, H.J., Park, C., Han, M.H., Hong, S.H., Kim, G.Y., Hong, S.H., Kim, N.D., Choi, Y.H. 2016.Baicalein induces caspase-dependent apoptosis associated with the generation of ROS and the activation of AMPK in human lung carcinoma A549 Cells. Drug Dev. Res.77, 73-86.

Kinugawa, S., Tsutsui, H., Hayashidani, S., Ide, T., Suematsu, N., Satoh, S., Utsumi, H., Takeshita, A. 2000. Treatment with dimethylthiourea prevents left ventricular remodeling and failure after experimental myocardial infarction in mice: role of oxidative stress. Circ. Res. 87, 392-398.

Kloas, W., Lutz, I. 2006. Amphibians as model to study endocrine disrupters. J. Chromatogr. A. 1130, 16-27.

Koizumi, S., Gong, P., Suzuki, K.,Murata, M., 2007. Cadmium-responsive element of the human heme oxygenase-1 gene mediates heat shock factor 1-dependent transcriptional activation. J. Biol. Chem. 282, 8715–8723.

Kostka, M., Högen, T., Danzer, K.M., Levin, J., Habeck, M., Wirth, A., Wagner, R., Glabe, C.G., Finger, S., Heinzelmann, U., Garidel, P., Duan, W., Ross, C.A., Kretzschmar, H., Giese, A. 2008. Single particle characterization of iron-induced pore-forming alpha-synuclein oligomers. J. Biol. Chem. 283, 10992-11003.

Kothary, R.K., Candido, E.P.M. 1982.Induction of a novel set of polypeptides by heat shock or sodium arsenite in cultured cells of rainbow trout, *Salmo gairdnerii*. Can J Biochem. 60, 347-55.
Kumar, S., Bandyopadhyay, U. 2005. Free heme toxicity and its detoxification systems in human. Toxicol. Lett. 157, 175-188.

Kumar, S., Bandyopadhyay, U. 2005. Free heme toxicity and its detoxification systems in human. Toxicol. Lett. 157, 175–188.

Kupfer, L., Hinrichs, W., Groschup, M.H. 2009. Prion protein misfolding. Curr. Mol. Med. 9, 826–835.

Kwak, H.J., Yang, D., Hwang, Y., Jun, H.S., Cheon, H.G. 2017. Baicalein protects rat insulinoma INS-1 cells from palmitate-induced lipotoxicity by inducing HO-1. PLoS One. 12, e0176432.

Kwok, S.C. 2013. Zinc Protoporphyrin upregulates heme oxygenase-1 in PC-3 cells via the stress response pathway. Int. J. Cell Biol. 2013, 162094.

Lanceta, L., Li, C., Choi, A.M., Eaton, J.W. 2013. Haem oxygenase-1 overexpression alters intracellular iron distribution. Biochem. J. 449, 189-194.

Lang, D., Reuter, S, Buzescu, T., August, C., Heidenreich, S. 2004. Heme-induced heme oxygenase-1 (HO-1) in human monocytes inhibits apoptosis despite caspase-3 up-regulation. Int. Immunol. 17, 155-65.

Lavine, J.A., Rowatt, A.J., Klimova, T., Whitington, A.J., Dengler, E., Beck, C., Powell, W.H. 2005. Aryl hydrocarbon receptors in the frog Xenopus laevis: two AhR1 paralogs exhibit low affinity for 2,3,7,8-tetrachlorodibenzo-p-dioxin (TCDD). Toxicol. Sci. 88, 60-72.

Lawal, A.O., Marnewick, J.L., Ellis, E.M. 2015. Heme oxygenase-1 attenuates cadmium-induced mitochondrial-caspase 3-dependent apoptosis in human hepatoma cell line. BMC Pharmacol. Toxicol. 16, 41.

Lee, J.Y., Koga, H., Kawaguchi, Y., Tang, W., Wong, E., Gao, Y.S., Pandey, U.B., Kaushik, S., Tresse, E., Lu, J., Taylor, J.P., Cuervo, A.M., Yao, T.P. 2010. HDAC6 controls autophagosome maturation essential for ubiquitin-selective quality-control autophagy. EMBO J. 29, 969-980.

Lee, P.J., Alam, J., Wiegand, G.W., Choi, A.M.K. 1996. Overexpression of heme oygenase-1 in human pulmonary epithelial cells results in cell growth arrest and increased resistance to hyperoxia. Proc. Natl. Acad. Sci. 93, 10393-10398.

Li-Weber M. 2009. New therapeutic aspects of flavones: the anticancer properties of Scutellaria and its main active constituents Wogonin, Baicalein and Baicalin. Cancer Treat. Rev. 35, 57-68.

Li,F. Calingasan, N.Y., Yu,F., Mauck, W.M., Toidze, M., Almeida, C.G. 2004. Increased plaque burden in brains of APP mutant MnSOD hetero-zygous knockout mice. 2004. J. Neurochem. 89, 1308–1312.

Lin, H.Y., Shen, S.C., Lin, C.W., Yang, L.Y., Chen, Y.C. 2007. Baicalein inhibition of hydrogen peroxide-induced apoptosis via ROS-dependent heme oxygenase 1 gene expression. Biochim. Biophys. Acta. 1773, 1073-1086.

Ling, Y., Chen, Y., Chen, P., Hui, H., Song, X., Lu, Z., Li, C., Lu, N., Guo, Q. 2011. Baicalein potently suppresses angiogenesis induced by vascular endothelial growth factor through the p53/Rb signaling pathway leading to G1/S cell cycle arrest. Exp. Biol. Med. (Maywood). 236, 851-858.

Linnenbaum, M., Busker, M., Kraehling, J.R., Behrends, S. 2012. Heme oxygenase isoforms differ in their subcellular trafficking during hypoxia and are differentially modulated by cytochrome P450 reductase. PLOS ONE. 7, e35483.

Liu, C., Wu, J., Xu, K., Cai, F., Gu, J., Ma, L., Chen, J. 2010. Neuroprotection by baicalein in ischemic brain injury involves PTEN/AKT pathway. J Neurochem. 112, 1500-1512.

Liu, F., Inageda, K., Nishitai, G., Matsuoka, M. 2006. Cadmium induces the expression of Grp78, an endoplasmic reticulum molecular chaperone, in LLC-PK1 renal epithelial cells. Enviro. Heal. Per. , 859-864.

Liu, J., Qu, W., Kadiiska, M.B. 2009. Role of oxidative stress in cadmium toxicity and carcinogenesis. Toxicol. Appl. Pharmacol. 238, 209-214.

Liu, J.J., Huang, T.S., Cheng, W.F., Lu, F.J. 2003. Baicalein and baicalin are potent inhibitors of angiogenesis: Inhibition of endothelial cell proliferation, migration and differentiation. Int. J. Cancer. 106, 559-565.

Liu, L., Tao, R., Huang, J., He, X., Qu, L., Jin, Y., Zhang, S., Fu, Z. 2015. Hepatic oxidative stress and inflammatory responses with cadmium exposure in male mice. Environ. Toxicol. Pharmacol. 39, 229-236.

Liu, Y., Carver, J.A., Ho, L.H., Elias, A.K., Musgrave, I.F., Pukala, T.L. 2014. Hemin as a generic and potent protein misfolding inhibitor. Biochem. Biophys. Res. Commun. 454, 295-300.

Liu, Y., Templeton, D.M. 2010. Role of the cytoskeleton in Cd2+-induced death of mouse mesangial cells. Can. J. Physiol. Pharmacol. 88, 341-352.

Liu, Y., Zheng, T., Zhao, S., Liu, H., Han, D., Zhen, Y., Xu, D., Wang, Y., Yang, H., Zhang, G., Wang, C., Wu, J., Ye, Y. 2012. Inhibition of heat shock protein response enhances PS341-mediated glioma cell death. Ann. Surg. Oncol. 19, 421-429.

Lloret, A., Fuchsberger, T., Giraldo, E., Vina, J. 2016. Reductive stress: a new concept in Alzheimer's disease. Curr. Alzheimer Res. 13, 206-211.

Lynes, E. M., Bui, M., Yap, M. C., Benson, M. D., Schneider, B., Ellgaard, L., Simmen, T. 2012. Palmitoylated TMX and calnexin target to the mitochondria-associated membrane. EMBO J. 31, 457–470.

Ma, HP. 2011. Hydrogen peroxide stimulates the epithelial sodium channel through a

phosphatidylinositide 3-kinase-dependent pathway. J. Biol. Chem. 286, 32444-53.

MacLeod AK, McMahon M, Plummer SM, Higgins LG, Penning TM, Igarashi K, Hayes JD. 2009. Characterization of the cancer chemopreventive NRF2-dependent gene battery in human keratinocytes, demonstration that the KEAP1-NRF2 pathway, and not the BACH1-NRF2 pathway, controls cytoprotection against electrophiles as well as redox-cycling compounds. Carcinogenesis. 30, 1571-80

Mahawar, L, Kumar, R, Shekhawat, G.S. 2017. Evaluation of heme oxygenase 1 (HO 1) in Cd and Ni induced cytotoxicity and crosstalk with ROS quenching enzymes in two to four leaf stage seedlings of Vigna radiata. Protoplasma. 254, 1-19.

Maines, M.D., Gibbs, P.E. 2005. 30 some years of heme oxygenase: from a "molecular wrecking ball" to a "mesmerizing" trigger of cellular events. Biochem. Biophys. Res. Commun. 338, 568-577.

Malaguarnera, L., Madeddu, R., Palio, E., Arena, N., Malaguarnera, M. 2005. Heme oxygenase-1 levels and oxidative stress-related parameters in non-alcoholic fatty liver disease patients. J. Hepatol. 42, 585-91.

Manwell, L.A., Heikkila, J.J. 2007. Examination of KNK437- and quercetin-mediated inhibition of heat shock-induced heat shock gene expression in *Xenopus laevis* cultured cells. Comp. Biochem. Physiol. 148, 521-530.

Masuya, Y., Hioki, K., Tokunuga, R., Taketani, S. 1998. Involvement of the tyrosine phosphorylation pathway in induction of human heme oxygenase-1 by hemin, sodium arsenite and cadmium chloride. Journal of Biological Chemistry. 633, 628–633.

Matsuoka, Y., Masuda, H., Yokoyama, M., Kihara, K. 2007. Protective effects of heme oxygenase-1 against cyclophosphamide-induced haemorrhagic cystitis in rats. BJU. Int. 100, 1402-1408.

McCoubrey, W.K. Jr., Huang, T.J., Maines, M.D. 1997. Isolation and characterization of a cDNA from the rat brain that encodes hemoprotein heme oxygenase-3. Eur. J. Biochem. 247, 725-32.

Mendelson, K.G., Contois, L.R., Tevosian, S.G., Davis, R.J., Paulson, K.E. 1996. Independent regulation of JNK/p38 mitogen-activated protein kinases by metabolic oxidative stress in the liver. Proc. Natl. Acad. Sci. U.S.A. 93, 12908-13.

Mendez-Armenta, M., Rios, C. 2007. Cadmium neurotoxicity. Environ. Toxicol. Pharmacol. 23, 350-358.

Merksamer, P.I., Liu, Y., He, W., Hirschey, M.D., Chen, D., Verdin, E., 2013. The sirtuins, oxidative stress and aging: an emerging link. Aging. 5, 144-50

Mi, L., Gan, N., Chung, F.L. 2009. Aggresome-like structure induced by isothiocyanates is novel

proteasome-dependent degradation machinery. Biochem. Biophys. Res. Commun. 388, 456-462.

Milton, A., Cooke, J.A., Johnson, M.S. 2004. A comparison of cadmium in ecosystems on metalliferous mine tailings in Wales and Ireland. Water Air Soil Pollut. 153, 157-172.

Mitani, K., Fujita, H., Sassa, S., Kappas, A., 1990. Activation of heme oxygenase and heat shock protein 70 genes by stress in human hepatoma cells. Biochem. Biophys. Res.Commun. 166, 1429–1434.

Miyake M., Fujimoto K., Anai S., Ohnishi, S., Nakai, Y., Inoue, T., Matsumara, Y., Tomioka, A., Ikeda, T., Okajma, E., Tanaka, N., Hirao, Y. 2010. Inhibition of heme oxygenase-1 enhances the cytotoxic effect of gemcitabine in urothelial cancer cells. Anticancer Res. 30, 2145-2152.

Morimoto, R.I. 1998. Regulation of the heat shock transcriptional response, Cross talk between a family of heat shock factors, molecular chaperones, and negative regulators. Genes Dev. 12, 3788-3796.

Morimoto, R.I. 2008. Proteotoxic stress and inducible chaperone networks in neurodegenerative disease and aging. Genes Dev. 22, 1427-1438.

Morita, T., Mitsialis, S.A., Koike, H., Liu, Y., Kourembanas, S. 1997. Carbon monoxide controls the proliferation of hypoxic smooth muscle cells. J. Biol. Chem. 272, 32804–32809.

Motterlini, R., Foresti, R., Bassi, R., Calabrese, V., Clark, J.E., Green, C.J. 2000 Endothelial heme oxygenase-1 induction by hypoxia. Modulation by inducible nitric-oxide synthase and S-nitrosothiols. J. Biol. Chem. 275, 13613-20.

Mouchet, F., Baudrimont, M., Gonzalez, P., Cuenot, Y., Bourdineaud, J.P., Boudou, A., and Gauthier, L. 2006. Genotoxic and stress inductive potential of cadmium in *Xenopus laevis* larvae. Aquat. Toxicol. 78, 157-166.

Moyano, P., de Frias, M., Lobo, M., Anadon, M.J., Sola, E., Pelayo, A., Díaz, M.J., Frejo, M.T., Del Pino, J. 2018. Cadmium induced ROS alters M1 and M3 receptors, leading to SN56 cholinergic neuronal loss, through AChE variants disruption. Toxicology. 394, 54-62.

Mukhopadhyay, D., Srivastava, R., Chattopadhyay, A. 2015. Sodium fluoride generates ROS and alters transcription of genes for xenobiotic metabolizing enzymes in adult zebrafish (*Danio rerio*) liver: expression pattern of Nrf2/Keap1 (INrf2). Toxicol. Mech. Methods. 25, 364-73.

Müller RM, Taguchi H, Shibahara S. 1987. Nucleotide sequence and organization of the rat heme oxygenase gene. J. Biol. Chem. 62, 6795-802.

Music, E., Khan, S., Khamis, I., Heikkila, J.J. 2014. Accumulation of heme oxygenase-1 (HSP32) in *Xenopus laevis* A6 kidney epithelial cells treated with sodium arsenite, cadmium chloride or proteasomal inhibitors. Comp. Biochem. Physiol. C. Toxicol, Pharmacol. 166C, 75-87.

Mymrikov, E.V, Seit-Nebi, A.S., Gusev, N.B. 2011. Large potentials of small heat shock proteins. Physiol. Rev. 91, 1123-59.

Nakagawa, N., Mori, M., Tamaki, N., Okada, Y., 1997. Non-selective cation conductance in a *Xenopus* renal epithelial line. Kobe. J. Med. Sci. 43, 179-89.

Namba, F., Go, H., Murphy, J.A., La, P., Yang, G., Sengupta, S., Fernando, A.P., Yohannes, M., Biswas, C., Wehrli, S.L. and Dennery, P.A. 2014. Expression level and subcellular localization of heme oxygenase-1 modulates its cytoprotective properties in response to lung injury: a mouse model. PLOS ONE. 9, e90936.

Nassar, M., Samaha, H., Ghabriel, M., Yehia, M., Taha, H., Salem, S., Shaaban, K., Omar, M., Ahmed, N., El-Naggar, S. 2017. LC3A Silencing hinders aggresome vimentin cage clearance in primary choroid plexus carcinoma. Sci. Rep. 7, 8022-8030.

Nath, K.A. 2014. Heme oxygenase-1 and acute kidney injury. Curr. Opin. Nephrol. Hypertens. 23, 17-24.

Nath, K.A., Grande, J.P., Haggard, J.J., Croatt, A.J., Katusic, Z.S., Solovey, A., Hebbel, R.P. 2001. Oxidative stress and induction of heme oxygenase-1 in the kidney in sickle cell disease. Am. J. Pathol. 158, 893-903.

Nath, K.A., Haggard, J.J., Croatt, A.J., Grande, J.P., Poss, K.D., Alam, J. 2000. The indispensability of heme oxygenase-1 in protecting against acute heme protein-induced toxicity in vivo. Am. J. Path. 156(5), 1527-1535.

Nelson, D.J., Tang, J.M., Palmer, L.G. 1984. Single-channel recordings of apical membrane chloride conductance in A6 epithelial cells. J. Membr. Biol. 80, 81-9.

Nguyên-Nhu, N.T., Berck, J., Clippe, A., Duconseille, E., Cherif, H., Boone, C., Van der Eecken, V., Bernard, A., Banmeyer, I., Knoops, B. 2007. Human peroxiredoxin 5 gene organization, initial characterization of its promoter and identification of alternative forms of mRNA. Biochim. Biophys. Acta. 1769, 472-483.

Niki, E., Yamamoto, Y., Komuro, E., Sato, K. 1991. Membrane damage due to lipid oxidation. Am. J. Clin. Nutr. 53, 201-205.

Nordberg, G. F. 2009. Historical perspectives on cadmium toxicology. Toxicology and Applied Pharmacology, 238, 192–200.

Oakley, B.R. 1992. y-Tubulin: the microtubule organizer? Trends Cell Biol. 2, 1-5.

Ohnishi, K., Takahashi, A., Yokota, S., Ohnishi, T., 2004. Effects of a heat shock protein inhibitor KNK437 on heat sensitivity and heat tolerance in human squamous cell carcinoma cell lines differing in p53 status. Int. J. Radiat. Biol. 80, 607–614.

Okinaga, S.,Takahashi, K.,Takeda, K.,Yoshizawa, M.,Fujita, H.,Sasaki, H.,Shibahara, S., 1996.Regulation of human heme oxygenase-1 gene expression under thermal stress. Blood 87, 5074–5084.

Olzmann, J.A., Li, L., Chin, L.S., 2008. Aggresome formation and neurodegenerative diseases: therapeutic implications. Curr. Med. Chem. 15, 47-60.

Olzscha, H., Schermann, S.M., Woerner, A.C., Pinkert, S., Hecht, M.H., Tartaglia, G.G., Vendruscolo, M., Hayer-Hart, M., Hart, F.U., Vabulas, R.M. 2011. Amyloid-like aggregates sequester numerous metastable proteins with essential cellular functions. Cell. 7, 67-78.

Ortiz de Montellano, PR. 2000. The mechanism of heme oxygenase. Curr. Opin. Chem. Biol. 4, 221-7.

Ostling, P., Björk, J.K., Roos-Mattjus, P., Mezger, V., Sistonen, L. 2007. Heat shock factor 2 (HSF2) contributes to inducible expression of hsp genes through interplay with HSF1. Biol. Chem. 282, 7077-7086.

Otterbein L.E,, Bach, F,H,, Alam, J., Soares, M., Tao Lu, H/, Wysk, M/, Davis, R.J., Flavell, R.A., Choi, A.M. 2000. Carbon monoxide has anti-inflammatory effects involving the mitogen-activated protein kinase pathway. Nat. Med. 6, 422-8.

Ovelgönne, J.H., Bitorina, M., and Van Wijk, R. 1995. Stressor-specific activation of heat shock genes in H35 rat hepatoma cells. Toxicol. Appl. Pharmacol. 135, 100-109.

Papaconstantinou, A.D., Brown, K.M., Noren, B.T., McAlister, T., Fisher, B.R., Goering, P.L. 2003. Mercury, cadmium, and arsenite enhance heat shock protein synthesis in chick embryos prior to embryotoxicity. Birth Defects Res. B. Dev. Reprod. Toxicol. 68, 456-464.

Park, J., Liu, A.Y. 2001. JNK phosphorylates the HSF1 transcriptional activation domain: role of JNK in the regulation of the heat shock response. J. Cell Biochem. 82, 326-38.

Park, J.D., Cherrington, N.J., Klaassen, C.D. 2002. Intestinal absorption of cadmium is associated with divalent metal transporter 1 in rats. Toxicol. Sci. 68, 288-294.

Pawar, A.P., Dubay, K.F., Zurdo, J., Chiti, F., Vendruscolo, M., Dobson, C.M. 2005. Prediction of "aggregation-prone" and "aggregation-susceptible" regions in proteins associated with neurodegenerative diseases. J. Mol. Biol. 350, 379-92.

Phang, D., Joyce, E.M., Heikkila, J.J. 1999. Heat shock-induced acquisition of thermotolerance at the levels of cell survival and translation in *Xenopus* A6 kidney epithelial cells. Biochem. Cell. Biol. 77, 141-51.

Piao, X.L., Cho, E.J., Jang, M.H. 2008. Cytoprotective effect of baicalein against peroxynitrite-induced toxicity in LLC-PK(1) cells. Food Chem. Toxicol. 46, 1576-1581.

Platt, J.L., Nath, K.A. 1998. Heme oxygenase, protective gene or Trojan horse? Nat. Med. 12(4),1392-1396.

Porter, N.A., Caldwell, S.E., Mills, K.A. 1995. Mechanisms of free radical oxidation of unsaturated lipids. Lipids. 30, 277-90.

Prevot-D'Alvise. N., Richard, S., Coupé, S., Bunet, R., Grillasca, J.P. 2013. Acute toxicity of a commercial glyphosate formulation on European sea bass juveniles (Dicentrarchus labrax L.): gene expressions of heme oxygenase-1 (ho-1), acetylcholinesterase (AChE) and aromatases (cyp19a and cyp19b). Cell. Mol. Biol. 31, 59.

Rafferty, K.A. 1969. Mass culture of amphibian cells: Methods and observations concerning stability of cell type. In: Mizell, M. Biology of amphibian tumors. pp. 58-81. Berlin: Springer Verlag.

Rahimzadeh, R.M., Rahimzadeh, R.M., Kazemi, S., Moghadamnia, A.A. 2017. Cadmium toxicity and treatment: An update. Caspian J. Intern. Med. 8, 135-145.

Rahman, M.N., Vukomanovic, D., Vlahakis, J.Z., Szarek, W.A., Nakatsu, K., Jia, Z. 2013. Structural insights into human heme oxygenase-1 inhibition by potent and selective azole-based compounds. J. R. Soc. Interface. 10, 20120697

Raju, V.S., Maines, M.D., 1994. Coordinated expression and mechanism of induction of HSP32 (heme oxygenase-1) mRNA by hyperthermia in rat organs. Biochim. Biophys. Acta 1217, 273–280.

Ray, P.D., Huang, B.W., Tsuji, Y. 2012. Reactive oxygen pecies (ROS) homeostasis and redox regulation in cellular signaling. Cell Signal. 24, 981-90.

Ross, J.M., Olson, L., Coppotelli, G., 2015. Mitochondrial and the ubiquitin proteasome system dysfunction in ageing and disease: two sides of the same coin? Int. J. Mol. Sci. 16, 19458-19476.

Ruiz-Ramos, R., Lopez-Carrillo, L., Rios-Perez, A.D., De Vizcaya-Ruíz, A., Cebrian, M.E. 2009. Sodium arsenite induces ROS generation, DNA oxidative damage, HO-1 and c-Myc proteins, NF-kappaB activation and cell proliferation in human breast cancer MCF-7 cells. Mutat. Res. 674, 109-115.

Ryter, S.W., Alam, J., and Choi, A.M. 2006. Heme oxygenase-1/carbon monoxide, from basic science to therapeutic applications. Physiol. Rev. 86, 583-650.

Sacca, P., Meiss, R., Casas, G., Mazza, O., Calvo, J.C., Navone, N., Vazquez, E. 2007. Nuclear translocation of haeme oxygenase-1 is associated to prostate cancer. Br. J. Cancer. 97, 1683–1689.

Salahudeen, A.A., Jenkins, J.K., Huang, H., Ndebele, K., Salahudeen, A.K. 2001.

Overexpression of heme oxygenase protects renal tubular cells against cold storage injury: studies using hemin induction and HO-1 gene transfer. Transplantation. 72, 1498-1504.

Salomons, F.A., Menéndez-Benito, V., Böttcher, C., McCray, B.A., Taylor, J.P., Dantuma, N.P. 2009. Selective accumulation of aggregation-prone proteasome substrates in response to proteotoxic stress. Mol. Cell. Biol. 29, 1774-1785.

Sardana, M.K., Sassa, S., and Kappas, A. 1982. Metal ion-mediated regulation of heme oxygenase induction in cultured avian liver cells. J. Biol. Chem. 257, 4806-4811

Sarkar S, Yadav P, Bhatnagar D. 1998. Lipid peroxidative damage on cadmium exposure and alterations in antioxidant system in rat erythrocytes: a study with relation to time. BioMetals. 11, 153–157.

Sato, T., Takeno, M., Honma, K., Yamauchi, H., Saito, Y., Sasaki, T., Morikubo, H., Nagashima, Y., Takagi, S., Yamanaka, K., Kaneko, T., Ishigatsubo, Y. 2006. Heme oxygenase-1, a potential biomarker of chronic silicosis, attenuates silica-induced lung injury. Am. J. Respir. Crit. Care Med. 174, 906-914.

Schubert, U., Antón, L.C., Gibbs, J., Norbury, C.C., Yewdell, J.W., Bennink, J.R. 2000. Rapid degradation of a large fraction of newly synthesized proteins by proteasomes. Nature. 404, 770-774.

Selim, M.E., Rashed el, H.A., Aleisa, N.A., Daghestani, M.H. 2012. The protection role of heat shock protein 70 (HSP-70) in the testes of cadmium-exposed rats. Bioinformation. 8, 58-64.

Severance, S., Hamza, I. 2009. Trafficking of heme and porphyrins in metazoa. Chem. Rev. 109, 4596–4616.

Shafer, M.E., Willson, J.A., Damjanovski, S. 2011. Expression analysis of the peroxiredoxin gene family during early development in *Xenopus laevis*. Gene Expr. Patterns. 11, 511-516.

Shao, C. C., Li, N., Zhang, Z. W., Su, J., Li, S., Li, J. L., Xu, S. W. 2014. Cadmium supplement triggers endoplasmic reticulum stress response and cytotoxicity in primary chicken hepatocytes. Ecotoxicol. Environ. Saf. 106, 109-114.

Shi, J.,Mei,W.,Yang, J., 2008. Heme metabolism enzymes are dynamically expressed during *Xenopus* embryonic development. Biol. Cell. 32, 259–263.

Shibahara, S., Yoshida, T., and Kikuchi, G. 1978. Induction of heme oxygenase by hemin in cultured pig alveolar macrophages. Arch. Biochem. Biophys. 188, 243-250.

Shimizu, H., Takahashi, T., Suzuki, T., Yamasaki, A., Fujiwara, T., Odaka, Y., Hirakawa, M., Fujita, H., Akagi, R. 2000. Protective effect of heme oxygenase induction in ischemic acute renal failure. Crit. Care Med. 28, 809-817.

Shirriff, C.S., Heikkila, J.J. 2017. Characterization of cadmium chloride-induced BiP accumulation in *Xenopus laevis* A6 kidney epithelial cells. Comp. Biochem. Physiol. C. Toxicol. Pharmacol. 191, 117-128.

Sikorski EM, Uo T, Morrison RS, Agarwal A. 2006. Pescadillo interacts with the cadmium response element of the human heme oxygenase-1 promoter in renal epithelial cells. J Biol Chem. 281:24423-30.

Sistonen, L., Sarge, K.D., Phillips, B., Abravaya, K., Morimoto, R.I. 1992. Activation of heat shock factor 2 during hemin-induced differentiation of human erythroleukemia cells. Mol. Cell Biol. 12, 4104-4111.

Slebos, D.J., Ryter, S.W., van der Toorn, M., Liu, F., Guo, F., Baty, C.J., Karlsson, J.M., Watkins, S.C., Kim, H.P., Wang, X., Lee. J.S., Postma, D.S., Kauffman, H.F., Choi, A.M. 2007. Mitochondrial localization and function of heme oxygenase-1 in cigarette smoke-induced cell death. Am. J. Respir. Cell. Mol. Biol. 36, 409-417.

Søfteland, L., Holen, E., and Olsvik, P.A. 2010. Toxicological application of primary hepatocyte cell cultures of Atlantic cod (*Gadus morhua*)—effects of BNF, PCDD and Cd. Comp. Biochem. Physiol. C Toxicol. Pharmacol. 151, 401-411.

Somji, S., Todd, J.H., Sens, M.A., Garrett, S.H., Sens, D.A. 2000. Expression of heat shock protein 60 in human proximal tubule cells exposed to heat, sodium arsenite and CdCl(2). Toxicol. Lett. 115, 127-136.

Sonavane, S., Haider, S.Z., Kumar, A., Ahmad, B. 2017. Hemin is able to disaggregate lysozyme amyloid fibrils into monomers. Biochim. Biophys. Acta. 1861, 1315-1325.

Song, C., Xiao, Z., Nagashima, K., Li, C. C. H., Lockett, S. J., Dai, R. M., Wang, Q. 2008. The heavy metal cadmium induces valosin-containing protein (VCP)-mediated aggresome formation. Toxicol. Appl. Pharmacol. 228, 351-363.

Song, Y., Zhang, R., Wang, H., Yan, Y., Ming, G. 2017. Protective effect of *Agaricus blazei* polysaccharide against cadmium-induced damage on the testis of chicken. Biol. Trace Elem. Res. doi: 10.1007/s12011-017-1196-7.

Srisook K., Jung, N.H., Kim, B.R., Cha, S.H., Kim, H.S., Cha, Y.N. 2005. Heme oxygenase-1-mediated partial cytoprotective effect by NO on cadmium-induced cytotoxicity in C6 rat glioma cells. Toxicol. In Vitro. 19. 31-39.

Stefani, M., Dobson, C.M. 2003. Protein aggregation and aggregate toxicity: new insights into protein folding, misfolding diseases and biological evolution. J. Mol. Med. 81, 678-699.

Stępkowski, T.M., Kruszewski, M.K. 2011. Molecular cross-talk between the NRF2/KEAP1 signaling pathway, autophagy, and apoptosis. Free Radic. Biol. Med. 50,1186-95.

Stocker, R., Yamamoto, Y., McDonagh A.F., Glazer, A.N., Ames, B.N. 1987. Bilirubin is an antioxidant of possible physiological importance. Science. 235, 1043-6.

Sun, C., Fu, J., Chen, J., Jiang, L., Pan, Y. 2010. On-line HPLC method for screening of antioxidants against superoxide anion radical from complex mixtures. J. Sep. Sci. 33, 1018-1023.

Suzuki, H.,Tashiro, S.,Sun, J.,Doi, H.,Satomi, S.,Igarashi, K., 2003. Cadmium induces nuclear export of Bach1, a transcriptional repressor of heme oxygenase-1 gene. J. Biol. Chem. 278, 49246–49253.

Taketani, S., Kohno, H., Yoshinaga, T., Tokunaga, R. 1988. Induction of heme oxygenase in rat hepatoma cells by exposure to heavy metals and hyperthermia. Biochem. Int. 17, 665-72.

Taketani. S., Kohno, H., Yoshinaga, T., Tokunaga, R. 1989. The human 32-kDa stress protein induced by exposure to arsenite and cadmium ions is heme oxygenase. FEBS Lett. 245, 173-6.

Tallkvist, J., Bowlus, C.L., Lönnerdal, B. 2001. DMT1 gene expression and cadmium absorption in human absorptive enterocytes. Toxicol Lett. 122, 171-177.

Tamás, M.J., Sharma, S.K., Ibstedt, S., Jacobson, T., Christen, P. 2014. Heavy metals and metalloids as a cause for protein misfolding and aggregation. Biomolecules. 4, 252-267.

Tan, S.X., Teo, M., Lam, Y.T., Dawes, I.W., Perrone, G.G. Cu, Zn superoxide dismutase and NADP(H) homeostasis are required for tolerance of endoplasmic reticulum stress. Mol. Bio. Cell. 20, 1493-1508.

Tandon, P., Showell, C., Christine, K., Conlon, FL. 2012. Morpholino injection in *Xenopus*. Methods Mol. Biol. 843, 29-46.

Taylor, J.P., Tanaka, F., Robitschek, J., Sandoval, C.M., Taye, A., Markovic-Plese, S., Fischbeck, K.H. Aggresomes protect cells by enhancing the degradation of toxic polyglutamine-containing protein. Hum. Mol. Genet. 12, 749-57.

Tazuma, S., Holzbach R.T. 1987. Transport of conjugated bilirubin and other organic anions in bile: Relation to biliary lipid structures. Proc. Natl. Acad. Sci. 84, 2052-2056

Templeton, D.M., Liu, Y. 2010. Multiple roles of cadmium in cell death and survival. Chem. Biol. Interact. 188, 267-275.

Tenhunen, R., Marver, H.S., Schmid, R. 1968. The enzymatic conversion of heme to bilirubin by microsomal heme oxygenase. Proc. Natl. Acad. Sci. 61, 748–755.

Thai, T.L., Yu, L., Eaton, D.C., Duke, B.J., Al-Khalili, O., Lam, H.Y., Ma, H., Bao, H.F. Basolateral P2X4 channels stimulate ENaC activity in *Xenopus* cortical collecting duct A6 cells. Am. J. Physiol. Renal. 307, F806-13.

Thit A., Selck H., Bjerregaard H.F. 2015. Toxic mechanisms of copper oxide nanoparticles in epithelial kidney cells. Toxicol. In Vitro. 29, 1053-9.

Tong, X., Lopez, W., Ramachandran, J., Ayad, W. A., Liu, Y., Lopez-Rodriguez, A., Contreras, J. E. 2015. Glutathione release through connexin hemichannels: Implications for chemical modification of pores permeable to large molecules. The Journal of General Physiology, 146, 245-254.

Tracz, M.J., Alam, J., Nath, K.A. 2007. Physiology and pathophysiology of heme: implications for kidney disease. J. Am. Soc. Nephrol. 18, 414-420.

Tramutola, A, Di Domenico, F., Barone, E., Perluigi, M., Butterfield, D.A. 2016. It is all about (U)biquitin: Role of altered ubiquitin. Oxid. Med. Cell Longev. 7, 1-12.

Trinklein, N.D., Chen, W.C., Kingston, R.E., Myers, R.M. 2004. Transcriptional regulation and binding of heat shock factor 1 and heat shock factor 2 to 32 human heat shock genes during thermal stress and differentiation. Cell Stress Chaperones. 9, 21-28.

Trotter, E.W., Grant, C.M., 2002. Thioredoxins are required for protection against a reductive stress in the yeast *Saccharomyces cerevisiae*. Mol. Micro. 46, 869-878.

Tu, P.T., Weissman, J.S. 2004. Oxidative protein folding in eukaryotes: mechanisms and consequences. J. Cell Bio. 164, 341-346.

Turrens, J.F. 2003. Mitochondrial formation of reactive oxygen species. J. Physiol. 552, 335-44.
Vallyathan, V., Shi, X. 1997. The role of oxygen free radicals in occupational and environmental lung diseases. Environ. Health Perspect. 105, 165-77.

Varga, C., Laszlo, F., Fritz, P., Cavicchi, M., Lamarque, D., Horvath, K., Posa, A., Berko, A., Whittle, B.J.R. 2007. Modulation by heme and zinc protoporphyrin of colonic heme oxygenase-1 and experimental inflammatory bowel disease in the rat. Eur. J. Pharmacol. 561. 164-171.

Voellmy, R. 2004. On mechanisms that control heat shock transcription factor activity in metazoan cells. Cell Stress Chaperones. 9, 122-133.

Voyer, J., Heikkila, J.J. 2008. Comparison of the effect of heat shock factor inhibitor, KNK437, on heat shock- and chemical stress-induced hsp30 gene expression in *Xenopus laevis* A6 cells. Comp. Biochem. Physiol. A Mol. Integr. Physiol. 151, 253-261.

Vreman, H.J., Ekstrand, B.C., Stevenson, D.K. 1993. Selection of metalloporphyrin heme oxygenase inhibitors based on potency and photoreactivity. Pediatr. Res. 33, 195–200.

Waalkes, M.P. 2003. Cadmium carcinogenesis. Mut. Res. 533, 107-120.

Waisberg, M., Joseph, P., Hale, B., Beyersmann, D. 2003. Molecular and cellular mechanisms of cadmium carcinogenesis. Toxicology. 192, 95–117.

Wang L., Gallagher, E.P. 2013. Role of Nrf2 antioxidant defense in mitigating cadmium-induced oxidative stress in the olfactory system of zebrafish. Toxicol. Appl. Pharmacol. 266, 177-86.

Wang, D., Zhong, X.P., Qiao, Z.X., Gui, J.F. 2008. Inductive transcription and protective role of fish heme oxygenase-1 under hypoxic stress. J. Exp. Biol. 211, 2700-6.

Wang, J., Yu, Y., Hashimoto, F., Sakata, Y., Fujii, M., Hou, D.X. 2004. Baicalein induces apoptosis through ROS-mediated mitochondrial dysfunction pathway in HL-60 cells. Int. J. Mol. Med. 14, 627-632.

Wang, Z., Chin, T.A., Templeton, D.M. 1996. Calcium-independent effects of cadmium on actin assembly in mesangial and vascular smooth muscle cells. Cell Motil. Cytoskeleton. 33, 208-222.

Westerheide, S.D., Morimoto, R.I. 2005. Heat shock response modulators as therapeutic tools for diseases of protein conformation. J. Biol. Chem. 280, 33097-100.

Wiggers, G.A., Peçanha, F.M., Briones, A.M., Pérez-Girón, J.V., Miguel, M., Vassallo, D.V., Cachofeiro, V., Alonso, M.J., Salaices, M. 2008. Low mercury concentrations cause oxidative stress and endothelial dysfunction in conductance and resistance arteries. Am. J. Physiol. Heart Circ. Physiol. 295, 1033-1043.

Wong, R.J., Vreman, H.J., Shulz, S., Kalish, F.S., Pierce, N.W., Stevenson, D.K. 2011. In vitro inhibition of heme oxygenase isoenzymes by metalloporphyrins. J. Perinatol. 31, S35-S41.

Woolfson, J.P., Heikkila, J.J. 2009. Examination of cadmium-induced expression of the small heat shock protein gene, hsp30 in *Xenopus laevis* A6 kidney epithelial cells. Comp. Biochem. Physiol. A. 152, 91-99.

Xia, Z.W., Li, C.E., Jin, Y.X., Shi, Y., Xu, L.Q., Zhong, W.W., Li, Y.Z., Yu, S.C., Zhang, Z.L. 2007. Reduction of bilirubin by targeting human heme oxygenase-1 through siRNA. Exp. Biol. Med. 232, 495-502.

Xu, J., Maki, D., Stapleton, S.R. 2003. Mediation of cadmium-induced oxidative damage and glucose-6-phosphate dehydrogenase expression through glutathione depletion. J. Biochem. Mol. Toxicol. 17, 67-75.

Yamada, N., Yamaya, M., Okinaga, S., Lie, R., Suzuki, T., Nakayama, K., Takeda, A., Yamaguchi, T., Itoyama, Y., Sekizawa, K., Sasaki, H. 1999. Protective effects of heme oxygenase-1 against oxidant-induced injury in the cultured human tracheal epithelium. Am. J. Respir. Cell Mol. Biol. 21, 428-435.

Ye, F., Wang, H., Zhang, L., Zou, Y., Han, H., Huang J. 2015. Baicalein induces human osteosarcoma cell line MG-63 apoptosis via ROS-induced BNIP3 expression. Tumour Biol. 36, 4731-4740.

Yin, J., Wang, A.P., Li, W.F., Shi, R., Jin, H.T., Wei, J.F. 2018. Time-response characteristic and potential biomarker identification of heavy metal induced toxicity in zebrafish. Fish Shellfish Immunol. 72, 309-317.

Yoneya, R., Ozasa, H., Nagashima, Y., Koike, Y., Teraoka, H., Hagiwara, K., Horikawa, S. 2000. Hemin pretreatment ameliorates aspects of the nephropathy induced by mercuric chloride in the rat. Toxicol. Lett. 116, 223-229.

Yoo, H.Y., Chang, M.S., Rho, H.M. 1999. Heavy metal-mediated activation of the rat Cu/Zn superoxide dismutase gene via a metal-responsive element. Mol. Gen. Genet. 262, 310-313.

Yoshida, T., Biro, P., Cohen, T.,Muller, R.M., Shibahara, S., 1988. Human heme oxygenase cDNA and induction of its mRNA by hemin. Eur. J. Biochem. 171, 457–461.

Yoshida, T., Sato, M. 1989. Posttranslational and direct integration of heme oxygenase into microsomes. Biochem. Biophys. Res. Commun. 163, 1086-1092.

Young, J.T., Heikkila, J.J. 2010. Proteasome inhibition induces hsp30 and hsp70 gene expression as well as the acquisition of thermotolerance in *Xenopus laevis* A6 cells. Cell Stress Chaperones. 15, 323-334.

Yuan, J., Murrell, G.A., Trickett, A., Landtmeters, M., Knoops, B., Wang M.X. 2004. Overexpression of antioxidant enzyme peroxiredoxin 5 protects human tendon cells against apoptosis and loss of cellular function during oxidative stress. Biochim. Biophys. Acta. 1693, 37-45.

Yusuf, K.A. 2007. Sequential extractions of lead, copper, cadmium, and zinc in soils near Ojota waste site. J. Agron. 6, 331-337.

Zenke-Kawasaki, Y., Dohi, Y., Katoh, Y., Ikura, T., Ikura, M., Asahara, T., Tokunaga, F., Iwai, K., Igarashi, K. 2007. Heme induces ubiquitination and degradation of the transcription factor Bach1. Mol. Cell Biol. 27, 6962-71.

Zhang, D.D., Hannink, M. 2003. Distinct cysteine residues in Keap1 are required for Keap1-dependent ubiquitination of Nrf2 and for stabilization of Nrf2 by chemopreventive agents and oxidative stress. Mol. Cell Biol. 23, 8137-51.

Zhang, Z., Cui, W., Li, G., Yuan, S., Xu, D., Hoi, M.P., Lin, Z., Dou, J., Han, Y., Lee, S.M. 2012. Baicalein protects against 6-OHDA-induced neurotoxicity through activation of Keap1/Nrf2/HO-1 and involving PKCα and PI3K/AKT signaling pathways. J. Agric. Food Chem. 60, 8171-8182.

Zhu, M., Rajamani, S., Kaylor, J., Han, S., Zhouh, F., Fink, A.L. 2004. The flavanoid baicalein inhibits fibrillation of alpha-synuclein and disaggregates existing fibrils. J. Biol. Chem. 279, 26846-26857.

Ziberna, L., Martelanc, M., Franko, M., Passamonti, S. 2016. Bilirubin is an endogenous antioxidant in human vascular endothelial cells. Sci. Rep. 6, 29240.